The dynamic behaviour of pump gates in the Afsluitdijk

Application of semi-analytical fluid-structure interaction models

O. C. Tieleman

TU Delft

Delft
University of
Technology

Challenge the future

The dynamic behaviour of pump gates in the Afsluitdijk

Application of semi-analytical fluid-structure interaction models

by

O. C. Tieleman

in partial fulfillment of the requirements for the degree of

Master of Science
in Civil Engineering

at the Delft University of Technology.

Graduation committee

Prof. dr. ir. S. N. Jonkman	Delft University of Technology
Dr. ir. R. J. Labeur	Delft University of Technology
Prof. dr. ir. A. V. Metrikine	Delft University of Technology
Ir. W. F. Molenaar	Delft University of Technology
Ir. A. Tsouvalas	Delft University of Technology

TU Delft
Delft
University of
Technology

Preface

This thesis report is the result of the final project to complete my master degree in Hydraulic Engineering at Delft University of Technology. I would like to thank my committee members from the university. Their varying fields of expertise and guidance have made it possible to continuously learn from the process towards the end result of this thesis. Further, I thank ir. P. van der Ven and his colleagues from Deltares for their time and input.

Special thanks to my parents for their support and providing me with the opportunities to achieve my goals. Finally, I thank Annebelle for being at my side these years.

<div align="right">

Orson Tieleman

Delft, February 2015

</div>

Abstract

As part of the Afsluitdijk project the discharge capacity, which is currently facilitated by two sluice complexes, is increased to cope with future sea level rise. It was decided to realise this by an innovative solution: the pump gate. The steel lifting gates, each containing three pumps, will be implemented in the existing sluice complex in phases, expecting a total of thirteen by the year 2050. This concept provides the possibility of pumping when necessary without hampering the discharge capacity during gravity flow, in which case the gates are lifted. The gates were designed to withstand quasi-static loads. Mainly due to the presence of the pumps, which have a high weight and require limited vibrations, the dynamic behaviour of the gate may lead to more strict design requirements. Two reference designs are investigated: the regular, and flood defence pump gate. The latter is designed to act as part of the primary flood defence, and is therefore significantly more robust. The analysis of the pump gate is limited to three components: the gate structure with its supports, pumps, and fluid.

Standard expressions for the hydrodynamic pressures do not apply to the pump gate and surrounding fluid, mainly due to the three-dimensional vibration shape of the gate and the presence of the pumps. General methods or numeric models to quantify vibrations are not readily available for a continuous system with interacting gate, pumps, and fluid. In this thesis, a method is developed to determine the dynamic behaviour of gate-fluid systems confined by sluices. This method is based on a frequency domain semi-analytical coupled modal analysis, able to directly solve the behaviour of gate and fluid for the linearized equations.

Several fluid schematizations are found in literature taking surface waves, compressibility, or neither into consideration. The validity of these schematizations was investigated for a wide range of water depths and excitation frequencies. Distinct regions, shown in figure 1, were found in which these physical processes do or do not have an effect on the hydrodynamic mass. The so-called 'transition region' is characterised by the absence of both compressibility and surface wave effects. The hydrodynamic mass is therefore frequency-independent in this region and no hydrodynamic damping is present.

The response of the pump gate reference designs is quantified by a three-dimensional plate model, based on previously described method. Both designs have considerably higher eigenfrequencies than those corresponding to regular wave excitation. For the Den Oever case, the quasi-static approach therefore suffices when considering wave loads. This is not the case for excitations originating from the pumps, which relate to a wider and higher frequency range. As a consequence of the preliminary design phase, exact pump specifications are not available. Results are therefore based on a pump envelope of possible excitations and presented as risks. These apply to the Den Oever gate designs, but are also relevant to the pump gate concept in general.
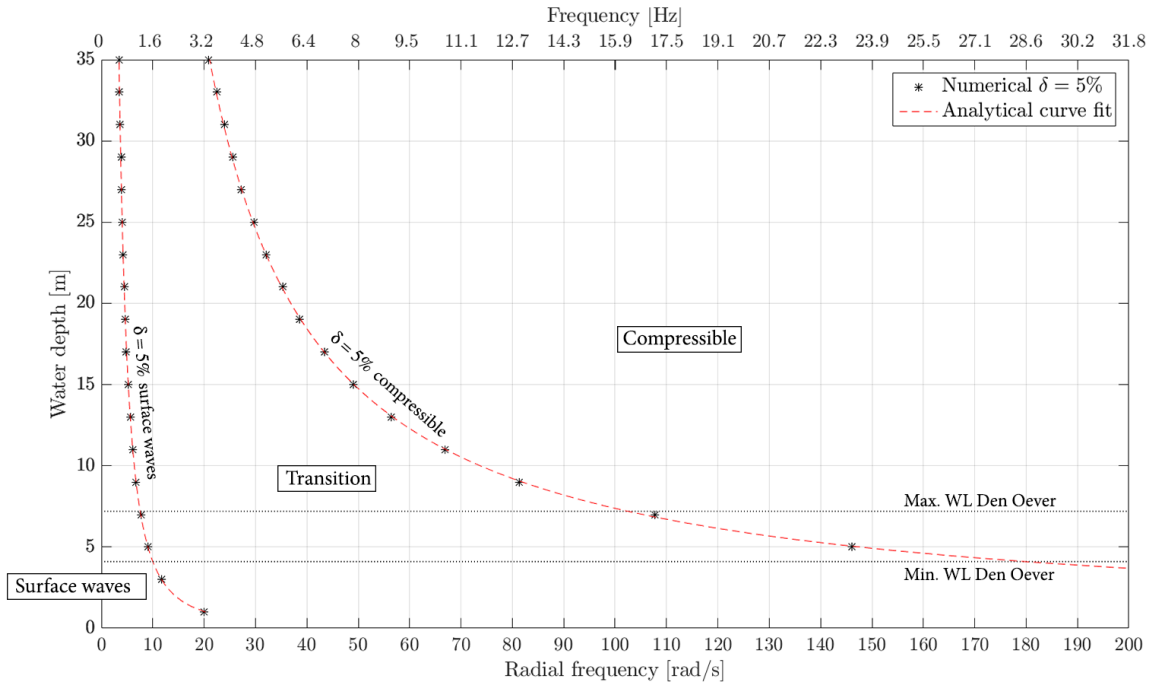
Figure 1: Frequency and water depth regions for which surface waves and compressibility play a role for a two-dimensional fluid system.

Three response amplitudes were quantified: the gate's deflection, pump vibration velocity and the resulting fluid pressures. Furthermore, based on the amplification of the static deflection an estimation of the maximum stresses is made. For both designs maximum deflections were less than a millimetre, which is negligible considering the dimensions of the gate. This is explained by the relatively small amplitude of the pump excitation forces compared to the total of static loads. Nevertheless, a significant deflection amplification (dynamic/static) is found. When internal stresses are amplified similarly, a risk of fatigue and even direct failure exists for the regular pump gate design. The more robust flood defence pump gate design reduces stresses to acceptable levels. Vibration velocities of the pumps were compared to ISO limits for non-rotating pump parts. For the regular design at several frequencies these limits were exceeded. The robust design is able to limit these velocities considerably.

Most concerning is the magnitude of the pressure fluctuations in the fluid. For the regular design, pressure head amplitudes at the suction side up to 0.5 metre were found. This leads to an increased risk of cavitation, and therewith damage and a reduced efficiency. Furthermore, total head fluctuations over both sides of the pumps can be in the same order as the static pump head. This is expected to lead to an unacceptable reduction in efficiency. The robust flood defence pump gate does reduce these fluctuations over the first range of the investigated excitation frequencies (< 250 rad/s), but for several frequencies leads to a larger response at higher frequencies.

Concluding, the dynamic behaviour of the pump gate designs should be considered in further design phases, since several risks were identified. The combination of a robust gate design and limited high frequency pump excitations may lead to an acceptable design.

Contents

1 | Introduction

This chapter starts with background information on the Afsluitdijk project (1.1). Further, the topic (1.2) and research questions (1.3) of this thesis are elaborated. The research method is briefly treated in section 1.4 and the structure of this report is explained in section 1.5.

1.1   The Afsluitdijk project

The Afsluitdijk was built in 1932 and has not been changed significantly since. The 32 kilometre long dam acts as a primary flood defence and separates the Waddensea from Lake IJssel, which has become a freshwater lake. In the assessments of 2006 and 2011, the Afsluitdijk appeared not to comply with the present safety requirements, which state that the Afsluitdijk should withstand conditions with an occurrence frequency of 1/10.000 years [24]. In addition, it was shown that the current discharge capacity will likely be inadequate in the future. It was therefore decided to strengthen the Afsluitdijk and its structures and apply pumps at one of the existing sluice complexes. The tender procedure of the Afsluitdijk project is planned to start in 2016, construction works at the end of 2017 [3].

The dam itself is mainly susceptible to failure due to wave overtopping. The decision was made to increase the resistance of the Afsluitdijk to this, rather than reducing overtopping by increasing the crest height. In order to do so, a top layer of concrete blocks or asphalt is added. When possible, a grass layer will be restored on top of this for aesthetic purposes.
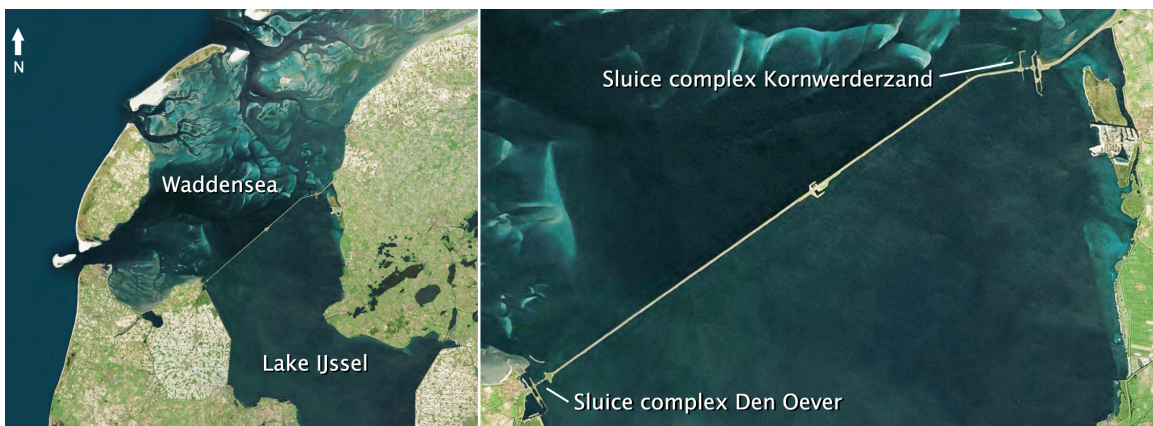
Figure 1.1: Overview Afsluitdijk [1, edited]

The Afsluitdijk contains two sluice complexes and two shipping locks. An overview of the Afsluitdijk and the location of the sluice complexes is shown in figure 1.1. The sluice complex of Den Oever is located on the far west side. The other complex, Kornwerderzand, is

located on the eastern side. Each is accompanied by a shipping lock. At all four structures, the steel gates are no longer able to withstand 1/10.000 years conditions. Furthermore, the pile foundation of sluice complex Kornwerderzand and the abutments of both shipping locks are weaknesses as well [39]. The main cause of the concrete's deterioration is alkali silica reaction (ASR).

The primary reason for the required increase in discharge capacity is the expected sea level rise. This decreases the present discharge capacity in two ways, as can be seen in figure 1.2. Firstly, the time window in which discharging by gravity is possible reduces. Due to wind set-up on the Waddensea and other water level variations, during some days discharging is not possible at all. Secondly, the average head difference is reduced. The proportional[1] discharge is therefore reduced as well. Due to the decreased discharge capacity, the number of days the sluices need to be in operation increases.
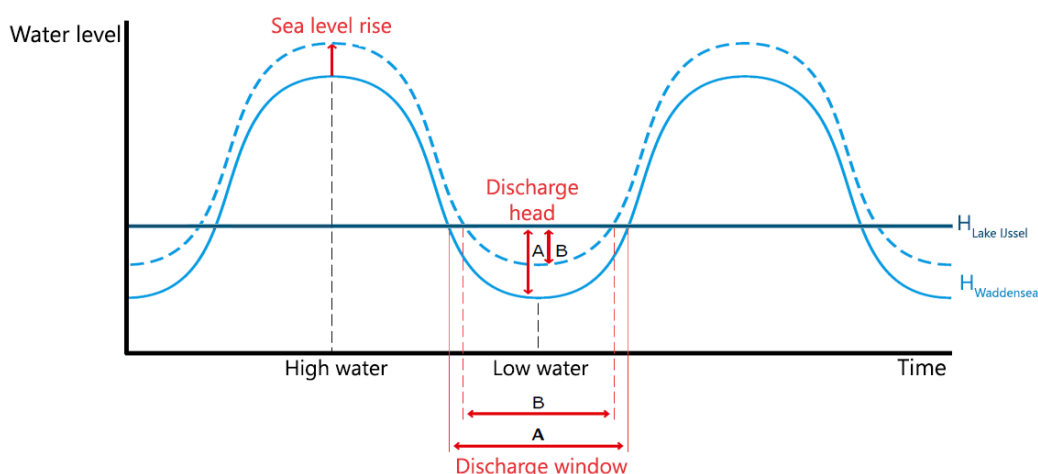
Figure 1.2: Free flow discharge window decreasing due to sea level rise [39, edited]

Although the first thought was to increase the discharge capacity by constructing a third sluice complex, the decision was finally made to use pumps. These will not be part of a new pump complex, but will be implemented into the existing sluice complex Den Oever. To do so, an innovative solution will be used: the pump gate. In this design, the pumps will be implemented into newly placed steel lifting gates. These can be lifted so that during regular free flow discharge the capacity is not reduced due to the presence of the pumps. The motto is: "discharging by gravity when possible, pumping when necessary" [40].

The reason that the pumps will be applied at Den Oever, is that this sluice discharges less effectively than the one at Kornwerderzand. Due to the lower tidal difference at Den Oever, the average positive head (H_{lake} - H_{sea} > 0) between the relatively constant (on a daily time scale) Lake IJssel water level and the Waddensea water level is lower [39]. A potentially negative effect of the pumps on the free flow discharge capacity will therefore have less impact at Den Oever than at Kornwerderzand.

---

[1]The discharge is proportional to the square root of the head difference: $Q \propto \sqrt{\Delta H}$.

1.2   Topic description

Pumps are generally situated on a heavy concrete foundation, which supports the pumps and guides the flow as is shown in figure 1.3. The pump gate concept shown in figure 1.4, implements (three) heavy pumps directly into each relatively light-weight steel gate, which is innovative and challenging both in design and construction. Designs for the pump gates at Den Oever have been made by Witteveen+Bos [40]. These 'reference designs' are used as a starting point in this thesis.

The pump gate has been designed for (quasi-)static loading caused by the water level difference and waves during design storm conditions, and pump thrust, so that they fulfil the ultimate limit state (ULS) requirements in terms of maximum stresses. The dynamic behaviour of the gate is not investigated, but accounted for by safety factors.
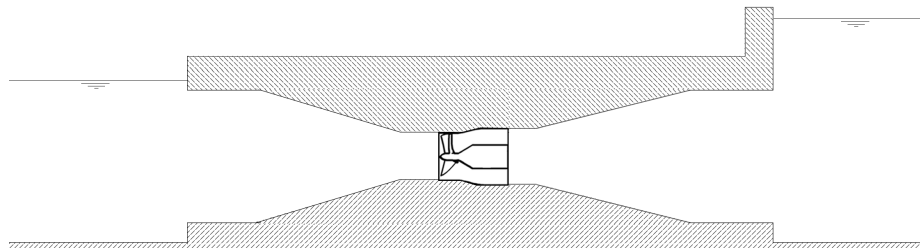
Figure 1.3: Side view of a conventional pump complex
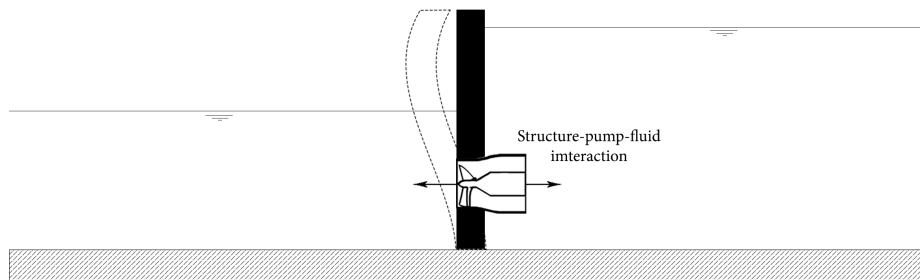
Figure 1.4: Side view of the pump gate solution

In practice, the design of gates on dynamic loading is often limited to checking whether resonance may occur. For relatively small scale gates such as those at Den Oever, direct failure to excessive vibrations is not very common. Fatigue is a more frequent problem for which standardized design requirements exist. The dynamic behaviour of the existing wave defence beam and flood gates at Den Oever has received some attention in the past [24, 38].

The relatively large weight of the three pumps compared to that of the gate, and possible forces resulting from interaction between pumps and fluid, might change the behaviour significantly in comparison to a regular flood gate of the same dimensions. Secondly, the presence of the pumps poses additional, potentially more strict, requirements on the gate. To ensure the required efficiency and lifetime of the pumps, their movement should be limited. Furthermore, pressure fluctuations in the fluid can have adverse effects on the pumps,

such as a reduced efficiency and increased wear and tear. A more thorough investigation of the dynamic behaviour of the pump gate and fluid is therefore required.

To explore this dynamic behaviour, insight in the interaction between the gate structure, pumps and fluid must be obtained. Standard expressions for the linear hydrodynamic pressures do exist for some two-dimensional cases, but do not suffice when geometry complicates or three dimensional behaviour plays a significant role. Especially due to the presence of the pumps, this is the case at Den Oever. Methods to analyse the fluid-structure interaction and vibrations must therefore be investigated first.

1.3   Research questions

From the topic description in previous section, it is clear a quick estimation of the occurring vibrations and resulting stresses in the gate is not possible. Hence, a more thorough investigation is needed that combines the fluid motion and forces with the structural vibrations. The best method to model the involved processes and solve the behaviour of structure and fluid simultaneously must therefore be found, which poses the following research question:

(I)   In what way can the fluid-structure interaction for (pump) gates be modelled for the order of magnitude of the water depth, sluice width and excitation frequencies present at Den Oever?

Insight into the dynamic behaviour of the pump gates, is especially relevant because of the innovative character of operating pumps in such a gate. This thesis therefore focuses on the behaviour of the gate in closed (downward) position, when pumps are in operation. Although in some cases relevant for regular flood gates, the behaviour of the pump gate during closure and opening will not be researched. The second research question is posed as follows:

(II)   What will be the (order of) magnitude of the vibrations in the gates and especially the pumps for the reference designs under governing conditions?

Two sub questions that should be answered with the help of the result of this main research question, are:

(II.a) What is the direct (due to pump-gate vibrations) and indirect (due to pressure fluctuations in the fluid as a result of gate vibrations) effect on the efficiency, lifetime and required maintenance of the pumps?

(II.b) What are the resulting stresses onto the existing sluice structure and in the pump gate and do these exceed the strength of any of the system elements (which comply in the static analysis)? Do the vibrations result in a significant increase in maintenance or fatigue of the steel gates?

If these research questions are answered, this shows whether additional measures are needed for the pump gate reference designs, but also says something about the technical feasibility

of the pump gate concept in general. Furthermore, insight is obtained in the dynamic behaviour and design of flood gates and the involved fluid-structure interaction.

1.4 Research methodology

The fluid and resulting hydrodynamic pressures are expected to play an important role in the dynamic behaviour of the pump gate. Estimations will be made based on analytical expressions known from literature to check whether this is indeed the case.

The interaction between gate, fluid and pumps potentially alters the behaviour of the system from what is found by these estimations. Therefore, an efficient method to model this interaction is searched for. Due to the many uncertainties in this phase of the Afsluitdijk project, a simplified analytical or numeric approach is preferred to the use of more extensive finite element or computational fluid dynamics models.

An effort is made to derive a general method that can aid in the dynamic design of the pump gate or gates under similar conditions. Application of the chosen model to obtain quantitative conclusions about the vibration magnitude of the pump gate designs is therefore done in a later stage of the report.

1.5 Report structure

An overview of this report's structure is shown in figure 1.5. Chapter 2 and 3 together form the system description of the Den Oever pump gate case. This includes background on the pump gate concept, the reference designs and input for further analysis. An indication of the desired output of further models is based on the requirements that are stated with respect to vibrations in section 3.4. The system analysis is limited to the gate structure, pumps and fluid. Theoretical background on the behaviour of these components during vibrations is given in chapter 4.

Based on this, it is decided to set-up two semi-analytical models in the frequency domain which can solve the structure-pump-fluid interaction directly. A two-dimensional beam model is set-up in chapter 5 to gain insight in the fluid response for the governing water depths and excitation frequencies. When the reader is interested in the semi-analytical method to model fluid-structure interaction for closed flood gates in sluices more generally, it is referred to this chapter, the analytical derivations of chapter 6, and the related appendices F and G.

Quantitative conclusions on dynamic behaviour of the pump gate are based on the analytical plate model in chapter 6. This model includes the effect of surface waves and fluid compressibility. In chapter 7 a numeric validation of the fluid response is made for a geometry including the pump conduits. Finally, conclusions and recommendations are made in chapter 8.
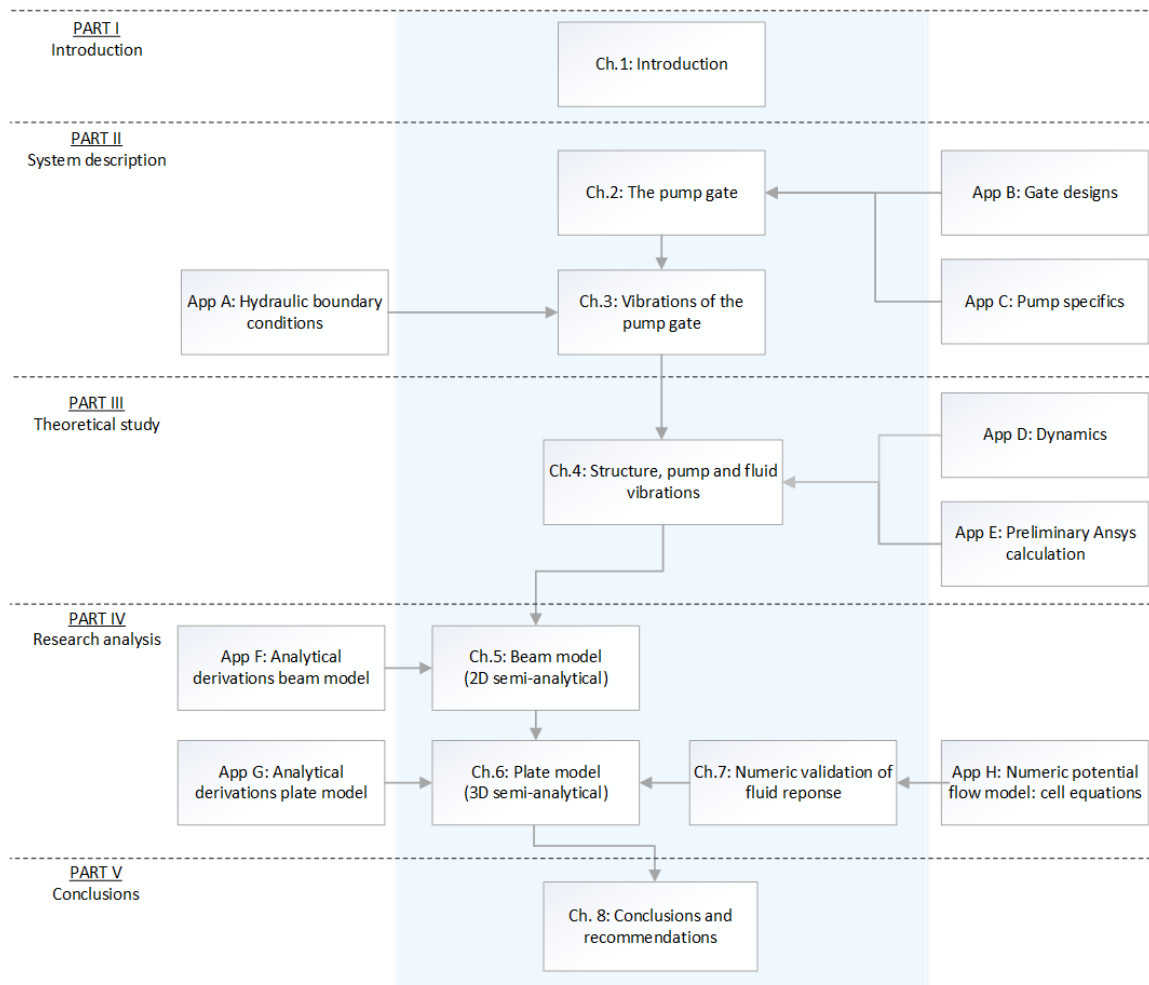
Figure 1.5: Thesis structure

2 | Pump complex Den Oever

This chapter provides a description of the present (section 2.1) and future (section 2.2) Den Oever complex. In section 2.3 and 2.4 the pump gate concept and gate reference designs by Witteveen+Bos [40] are elaborated. In appendices B and appendix C background on the gate designs and pumps is given.

In chapter 3 the focus is laid on the vibrations of these designs and the design cases for further analyses are determined. The hydraulic boundary conditions are therefore elaborated in the following chapter.

2.1   Present sluice complex

Sluice complex Den Oever has three equal parts, each consisting of five sluices. An overview of the complex is given in figure 2.1. The width of the waterway between the concrete piers is 12 metre.
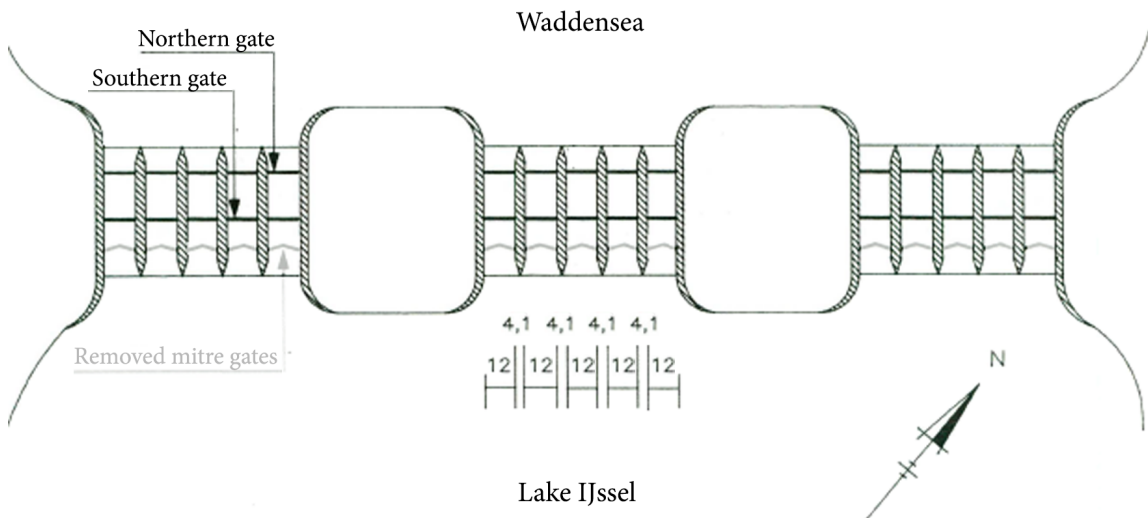
Figure 2.1: Top view sluice complex Den Oever [38, edited]

Each sluice has four concrete lifting towers that lift the two steel flood defence gates. A side view of the sluice is given in figure 2.2. To reduce the load on the currently insufficiently strong gates, holes have been implemented in the northern (left) gate. In the present situation the southern (right) gate therefore retains the water, while the nothern gate reduces the wave impact [24, 39]. The current gates have a height of 7.03 metre. It was decided to replace both steel gates.

Studies have been done into wave slamming on the northern gate and the effect of the wave impact defence beam in front of the gate [14, 24]. While it was concluded the defence beam
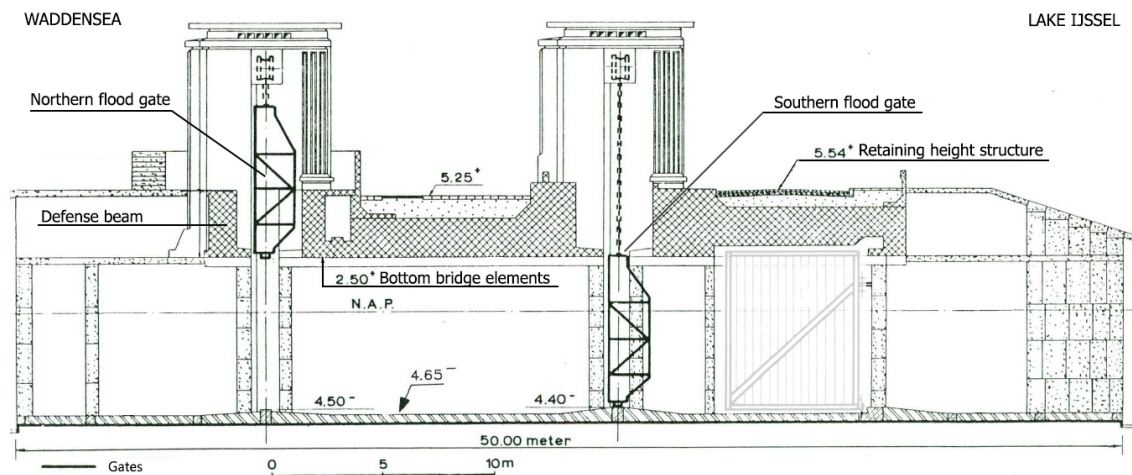
Figure 2.2: Cross section sluice Den Oever. The opened mitre gate has a lightened color in the drawing, as it has been removed. [38, edited]

does not have a significant negative effect on the gate, its own strength is insufficient to withstand wave impact of design storms.

The upper structure on the piers, except for the lifting towers and defence beam, also consists of two bridge girders providing space for the two by two vehicle lanes of highway E22 (A7) plus a smaller one for the bicycle road on the Waddensea side.

2.2 Conceptual design of the pump complex

The works at complex Den Oever consist of the replacement of the steel gates and the construction of seepage screens. To realise the increase in discharge capacity by pumps, four variants were considered. Prior to the more detailed reference design of Witteveen+Bos [40], the decision has been made to choose design alternative B, seen in figure 2.3, as most desirable. Alternative C (figure 2.4) is still kept in the solution space as a possibility.

The intention of the chosen design (alternative B) is to integrate the pumps into the newly placed southern gate, and therewith prevent large scale alterations of the eighty year old concrete sluice structure. Except for saving costs, the advantage of this alternative is that the pumps will not hamper the discharge capacity under gravity flow when in lifted position.

The more conventional method of constructing the pumps on a large and heavy concrete foundation (figure 2.5a), is thus not considered a solution any more. Also, the possibility of constructing a new foundation for a pump gate (figure 2.5b) is excluded from the solution space.

In this thesis the focus is on alternative B, in which a pump gate is implemented at the location of the present southern flood gate. At this location, two gate designs are still an option differing mainly in strength: the regular pump gate and the pump gate as primary flood defence. Both designs will be treated in section 2.4 and appendix B.
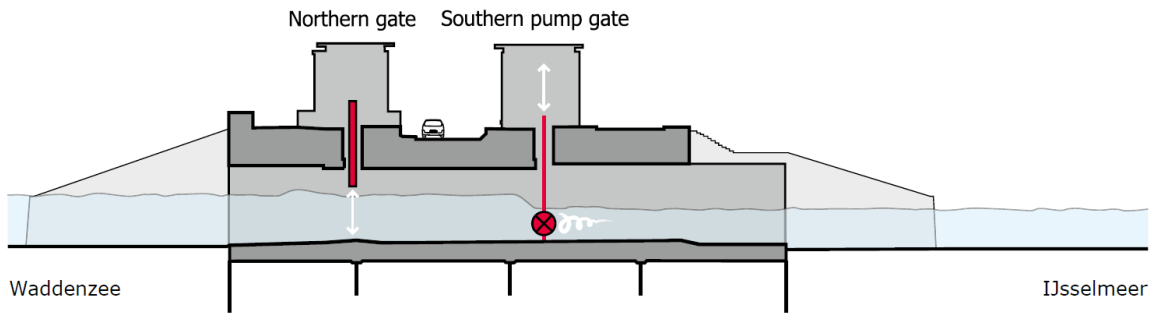
Figure 2.3: Preferred pump complex design (alternative B) [39]
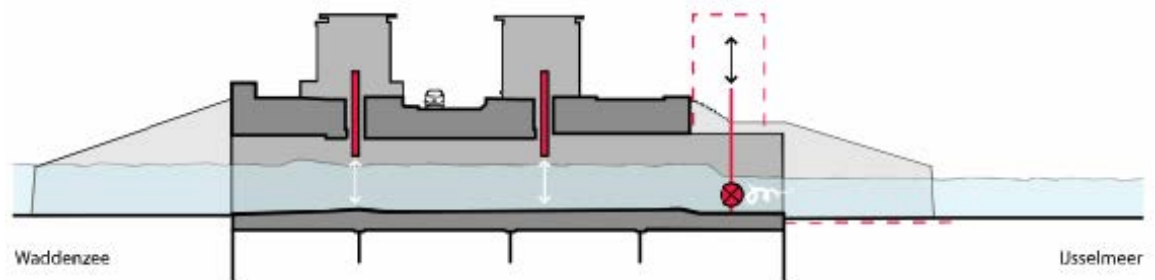
Figure 2.4: Alternate pump complex design (alternative C), still in the solution space [39]

(a) Alternative A

(b) Alternative D
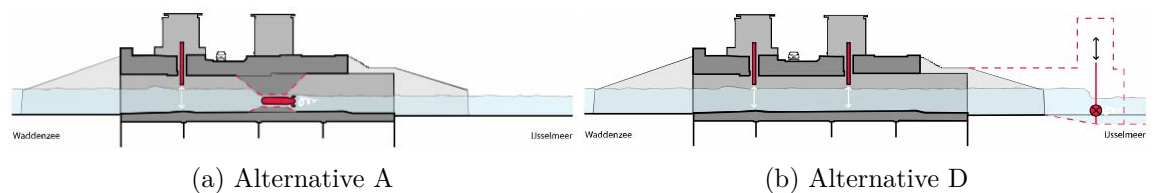
Figure 2.5: Two in the previous phase of the project considered variants with regard to the water discharge capacity, that do now fall outside of the solution space.

2.3 Pump gate concept

The pump gate is a combination of two main concepts: the movable barrier or flood gate and the water pump. The combination of these concepts, can be taking literally in a geographical sense. By applying pump gates, there is no need for a pump complex separately from the main waterway. This is shown in figure 2.6. The same is in fact done at the Afsluitdijk. Instead of constructing a new pump station integrated in the dam the existing waterway is used, in this case being sluice complex Den Oever. This solution saves space and is therefore also likely to reduce costs. Two examples of pump gates are shown in the figures below. In section 2.3.3 some existing pump gate projects are elaborated.

2.3.1 Gate and barrier types

The pump gates at Den Oever will regulate the water level at Lake IJssel under daily circumstances, both by retaining and discharging water. Whether it will also serve as a primary flood defence is not yet decided upon. This will be clarified further in section 2.4.
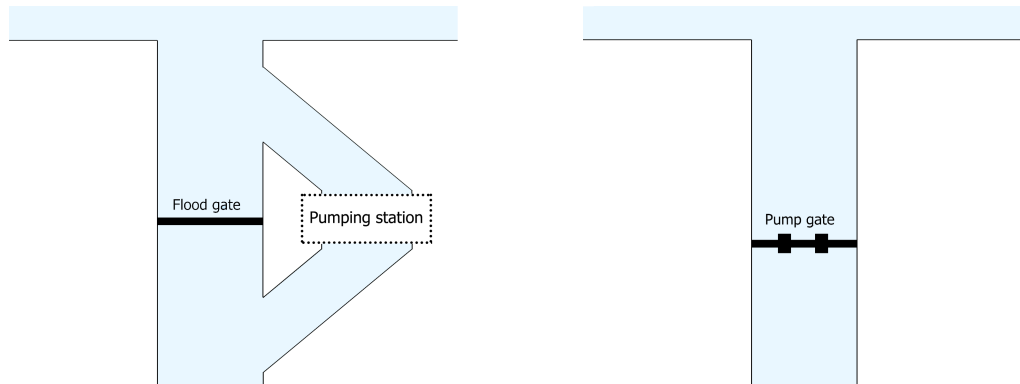
Figure 2.6: Plan view of conventional method with a pumping station separately from the main waterway (left) and of the pump gate solution (right), which combines these two functions and therewith saves space and costs.

Figure 2.7: Photos of two Hasuh pump gates applied in South-Korea. Noticing the guidance system at the sides of the gate in the photo on the left [12], these are likely to be vertical lifting gates. The photo on the right [13] shows a hinged pump gate.

Due to the existing structure at sluice complex Den Oever, a vertical lifting pump gate is evidently the best solution. For the purpose of the pump gate concept in general, several gates and barriers and their suitability to function as a pump gate are briefly inventoried. These are shown in figure 2.8. Advantages of the lifting, radial and sliding gate are the relative easy access to the pumps in opened position, as these require regular maintenance. Barrier types such as the inflatable and parachute barrier are not suitable for obvious structural reasons. Mitre and flap gates will likely have issues with stability and leakage.

2.3.2 Pump types

A pump is defined as "a mechanical device using suction or pressure to raise or move liquids...". By adding energy to the flow, a water level difference can be overcome. Two major pump categories can be distinguished: displacement and dynamic [18].

In the first category, energy is periodically added by application of force on an enclosed volume, resulting in a direct increase in pressure. Two examples are given in figure 2.9a and

(a) Lifting gate   (b) Mitre gate   (c) Sliding gate   (d) Radial gate   (e) Flap gate

(f) Sector gate   (g) Visor gate   (h) Inflatable bar-   (i) Parachute bar-   (j) Barge gate
                                      rier   rier
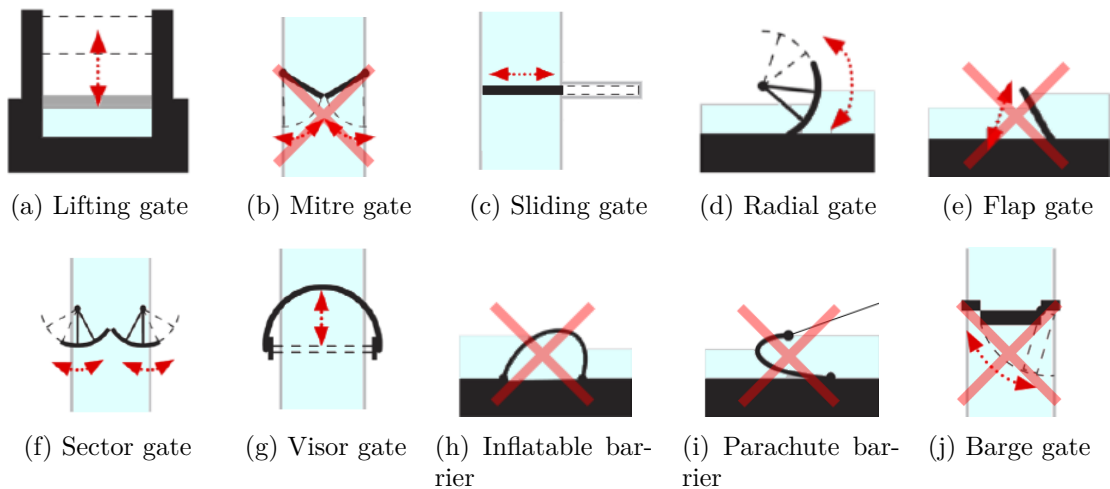
Figure 2.8: Examples of gate and barrier types [6, edited] and their suitability to function as pump gate.

2.9b. A third example of the displacement pump type is the rotary pump. The maximum discharge of a displacement pump is generally lower than the dynamic type pumps.

(a) Diaphgram pump   (b) Piston and plunger   (c) Axial flow centrifu-   (d) Radial flow cen-
                      pumps   gal flow   trifugal pump
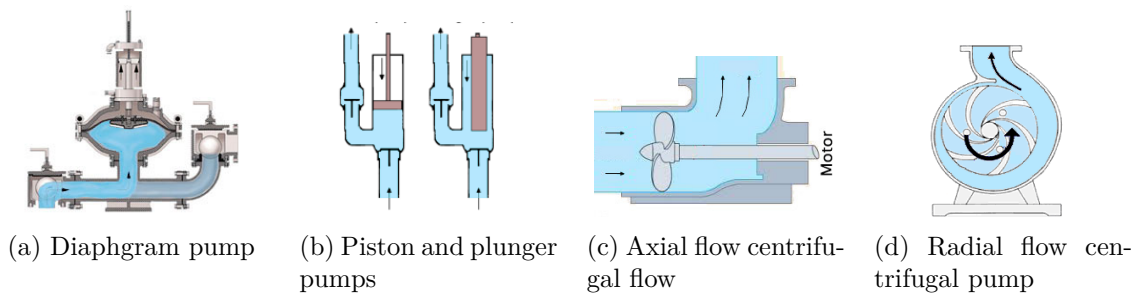
Figure 2.9: Four examples of displacement (a,b) and dynamic pumps (c,d)

Dynamic pumps continuously add energy to the fluid to increase the fluid velocity. When the fluid slows down, a higher pressure remains and thus a head difference has been overcome. Figure 2.9c and 2.9d both show examples of dynamic pumps. These are both centrifugal pumps, which is the most common dynamic pump. For a further classification of dynamic pumps, see appendix C.1.

2.3.3   Reference designs

Although the planned pump gate at Den Oever is considered innovative on its scale, some pump gate projects do exist. In the Netherlands two projects in Terneuzen and Hoek have been realised, where a single pump was implemented in a gate [24]. Little information is available on those projects however.

In Korea, the company Hasuh has designed and applied the pump gate [13] at over 50 projects in the past ten years. They have patented some of these technologies as well. Most often applied, is the horizontal shaft pump gate with axial flow pump. A pump

complex project in which bulb pumps (or horizontal axial flow pumps) are used, is shown in figure 2.10. A design with a vertical pump shaft and bent flow exists as well. Other variations mainly concern the gate opening and closure system. The vertical lifting pump gate is applied most. When vertical space is limited, horizontally or vertically hinged gates provide possible solutions.

Figure 2.10: Gangmae Pump Station with vertical lifting pump gates

In all of Hasuh's pump gate designs, the pump can be closed off by valves from both sides. It is therefore able to retain water at both positive and negative head. In figure 2.10 these valves can be seen in closed position. No second gate is applied in most of these projects.

In table 2.1 key dimensions are given of pump gates and surrounding structure for different pump diameters. A few basic relations can be deducted from these standard sizes. For a gate with two pumps, the width of the gate used is 4D. Based on the 500, 1000 and 1500 mm diameter data, the heart to heart distance used is about 1.6D. This leaves 0.7D between the sides of the gates and the outer pump diameters. The height of the pump gate is about $0.5 + 1.5D$ metre. A single 1500 mm diameter pump is approximated to discharge 4-6 m^3/s at a head of three metre [13].

Using the above relations, the gate of about 12 m at Den Oever should then indeed be able to geometrically contain three pumps with a 2 m diameter. The larger span and high number of pumps at the Den Oever gates may also result in higher loads and less resistance to it. Exact values for the thickness or flexural rigidity of the Hasuh pump gate designs are not known. In figure 2.7 the gate's thickness seems to be in the order of a fourth to a third of its span, which would be very robust compared to regular flood gates subjected to non-extreme design conditions. This indicates that the dynamic behaviour of the pump gates may have been a determining factor in these designs.

Table 2.1: Dimensions (in mm) of standard horizontal shaft pump gate design by Hasuh Industries Corporation [13]. Table is shortened for clarity, multiple sizes exist in between.
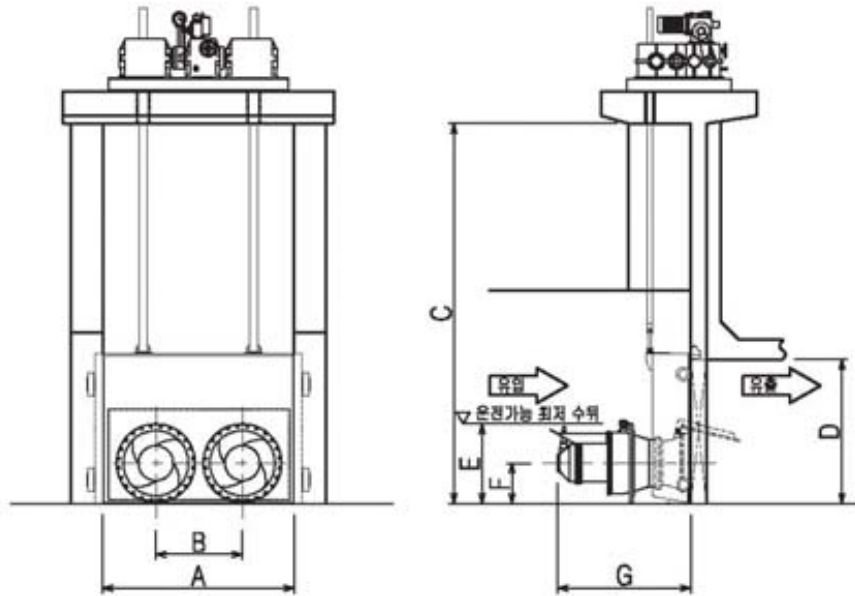
Model	A	B	C	D	E	F	G
HPG-300	1400(850)	550(-)	3000	1000	600	350	1100
HPG-500	2000(1160)	840(-)	3500	1250	800	450	1650
HPG-1000	4000(2400)	1600(-)	5000	2000	1300	740	2800
HPG-1350	5400(3280)	2120(-)	5500	2250	1650	935	3200
HPG-1500	6000(3650)	2350(-)	6000	2750	1800	1020	3500

2.4 Gate designs Den Oever

Two designs will be analysed in this thesis. These will both be considered at the location of the present southern flood gate, which is the preference alternative (see figure 2.3). The designs differ in design head and therefore in weight and rigidity, and will be denoted by:

- Primary flood defence pump gate
- Regular pump gate

By means of a reliability analysis, Witteveen+Bos [40] has concluded using a single flood gate provides sufficient reliability. For the entire pump complex, the requirement states that the failure chance must be smaller than:

$$P_{\text{failure}} < 0.1 \cdot \text{frequency norm} = 0.1 \cdot 10^{-4} = 1/100,000 \quad \text{[per year]} \quad (2.1)$$

Two requirement 'tracks' of maximum allowed water level rise at Lake IJssel were evaluated [40]:

- A rise of 0.8 metre at storm conditions with a return period of 10 years gradually decaying to no rise at a return period of 4,000 years.

- A rise of 0.8 metre at storm conditions with a return period of 10 years gradually decaying to 0.075 metre rise at 10,000 years and no allowed rise for higher return periods.

These requirements lead to a failure probability of 1/147.000 and 1/243.000 per year, both complying with the requirement. This is mainly due to the large Lake IJssel basin and a redundant central control. Whether a single or double primary flood defence will be implemented, is decided in the final project stage by the contractor. Both pump gate designs are therefore still a possibility for the preference alternative.

The reference designs by Witteveen+Bos [40] are used as the basis for the two considered designs. However, some alterations are made. To keep the solution space broad the design for the preference alternative by Witteveen+Bos [40] has been made only for the governing case (in both costs and space), which is when the pump gate serves as primary flood defence. A regular design has been made for alternative C (at the existing foundation on the Lake IJssel side), for which slightly other geometrical conditions such as a lower bottom level apply. The latter is therefore altered to comply to the considered location.

The geometry of both reference designs is shown in figure 2.11. The flood defence gate design is characterised by a smaller number of large vertical profiles, while the regular design has a higher number of smaller vertical profiles. Both gates have three main horizontal profiles. In figure 2.12 the structural design of the flood defence pump gate is shown as is used in the FEM model by Witteveen+Bos [40].
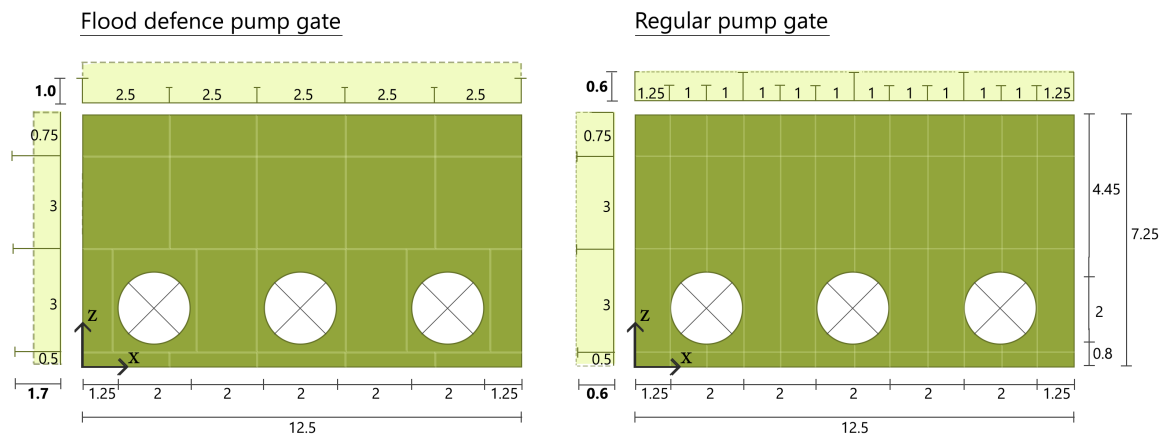
Figure 2.11: Reference pump gate designs (front view). Both designs will be considered at the location of the most desired conceptual design alternative (B).

The flexural rigidities of the reference designs have been determined in appendix B. In the analyses in further chapters, the gate is considered simply supported at its edges. The gate supports are further elaborated in section 2.4.2. The vertical edge profiles were therefore not taken into account when determining the body rigidity. For both gate designs this resulted in a higher flexural rigidity per running metre in horizontal than in the vertical direction. To simplify further analyses both gate designs are considered isotropic[2], taking

---

[2]The gate designs evidently have a three-dimensional layout with stiffening profiles at distinct locations. An equal body rigidity in horizontal and vertical direction is in this case considered isotropic, and also schematized as such in further models.

14
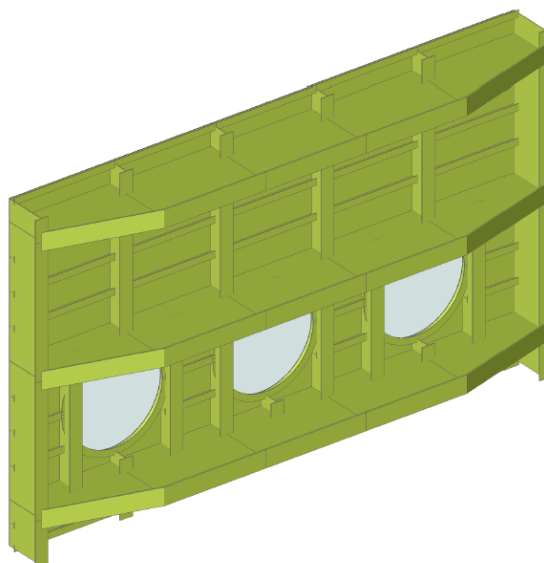
Figure 2.12: Structural design of pump gate as used in the calculation FEM model by Witteveen+Bos [40], dimensioned as primary flood defence.

the higher horizontal rigidity as representative for both directions. The vertical profiles shown in section 2.11 therefore do not correspond to the investigated rigidity of the gate designs. It must be noted that the increased vertical rigidity is favourable compared to the actual present reference designs, which must be kept in mind for the presented results. The most important parameters of both designs are given in table 2.2. The input for the analyses of both designs only differ in rigidity and weight.

Table 2.2: Structural parameters of both gate designs used as input for further analyses. In the determination of the flexural rigidity the stiffness of the edge elements is neglected, as these will be considered supported. The gate weight includes these elements.

Parameter	Flood defence pump gate	Regular pump gate
Design head [m]	6.75	2
Steel type	S355	S355
Gate thickness [m]	1.7	0.6
Bending stiffness[3] D [Nm]	$3.0 \cdot 10^9$	$2.0 \cdot 10^8$
Gate weight [kg]	30,000	18,040

To take into account fatigue for the regular pump gate design, the bending moment unity check was done for 0.7 (a number based on experience). In case of the flood defence pump gate, fatigue was assumed insignificant due to the high strength of the gate as a consequence of the 6.75 head difference. For both designs, the dynamic behaviour was not investigated further. More insight in the dynamic behaviour and demands could indicate whether the regular pump gate design is indeed sensitive to vibrations and whether, except

---

[3]The plate bending stiffness, or flexural rigidity EI per running metre, is equal in both directions since the gates will be schematized as homogeneous and isotropic. As was mentioned, this is not the case for the reference designs by Witteveen+Bos [40].

for fatigue, the stronger flood defence pump gate fulfils all other vibration related demands (see section 3.4).

In figure 2.11, the geometrical integration of the three pumps in the gate is shown as well. The maximum pump diameter was determined by Witteveen+Bos [40] to be 2 metre, based on the following design rules [27, 40]:

- Distance above bottom level: $\geq 0.5D$;
- Distance between pumps: $\geq 1D$;
- Distance pump and wall: $\geq 0.5D$.
- Water coverage: $\geq 0.5D$;

The stated distance are with respect to the pump edge (thus not center). The width required to house three pumps of 2 metre is then exactly the available sluice at Den Oever:

$$W_{\text{required}} = 2 \cdot 0.5D + 3 \cdot D + 2 \cdot D = 6 \cdot D = 6 \cdot 2 = 12 \quad [\text{m}] \tag{2.2}$$

The available length in vertical and lateral direction are elaborated in the following section.

2.4.1 Implementation of gates into present structure

By applying pump gates at the location of the southern flood gates, extensive alterations to the existing concrete structure are avoided. Locally, the northern bridge girder is adjusted to generate the 3.5 metre available length needed for the pumps in lifted position. Specialists of Nijhuis B.V. have indicated this length is enough for an axial flow pump with direct driving [40]. In figure 2.13 the proposed integration of the pump gate in the existing structure is shown.

As a first estimate, often twice the pump diameter is used for the pump length [27]. In the designs of Hasuh, see table 2.1, the pump length is even larger than that. The largest pump diameter of the Hasuh designs is 1.5 metre, for which the pump length is already 3.5 metre. The available length could therefore be seen as a minimum to house the pump impellers, motor and in- and outflow diffusers. The shorter length does result in an increase of in- and outflow losses. An alternative would be to house the motor above the pump impellers and connect it through gears. The efficiency is expected to be lower in that case.

The sill will be slightly lowered from -4.4 to -4.5 m NAP. In that case the bottom of the pumps (0.8 m above gate bottom) will at a height of -3.7 m NAP. The required distance between bottom level sluice (-4.7 m NAP) is therewith complied to. In appendix A the hydraulic boundary conditions are elaborated. The minimum Lake IJssel water level for which the pumps will be in operation is stated to be -0.60 m NAP, which results in a minimum water coverage of $(1.7 - 0.6) = 0.525 \cdot D$.
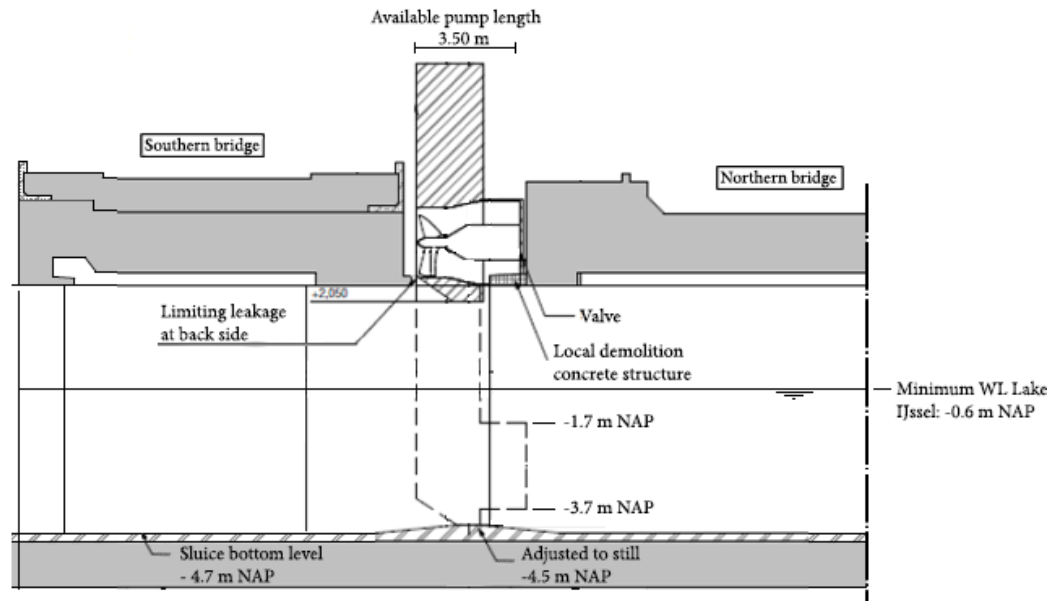
Figure 2.13: Integration of pump gate in southern part of the sluice [40, edited]. Lifting towers are not included in the drawing.

2.4.2 Gate suspension and support

What happens at the four edges of the gate, is of importance to the dynamic behaviour of the gate. The top edge of the gate is free. Besides that, the bottom of the gate is the most straightforward connection with respect to geometry. In order to minimize the resultant upward water pressure in extreme events, a bottom element is constructed as close as possible to the Waddenzee side. In figure 2.14 this detail is shown for the old flood gates. In the original design the bottom element was still in the middle of the gate, but was changed in a further design stage. A similar connection is intended in the design for the new gates as well. The connection point is not horizontally embedded, and relatively thin in comparison with the gates' width. The latter results in little capacity to transfer resulting moments onto the foundation.

The vertical connections at the sides of the pump gate will have to be roller guides due to the large weight of the pump gate, in contrast to glide connections which would be possible for the new flood gates. Currently, a guiding system with roller guides is in place as well. Since no detailed design is available, the present connection is taken as representative, given in figure 2.15. The gate layout obviously does not apply to the pump gate designs.

2.4.3 Pump specifics

At pump complex Den Oever, it is intended to apply an axial flow pump [40]. This pump type is suitable for high discharges at low head differences. More specifically, a bulb pump will be used, which is an axial flow pump with direct driving. With this pump type, the

Figure 2.14: Bottom detail of present flood gates, placement on sill. A similar bottom detail is intended for the new (pump) gates. [40, edited]
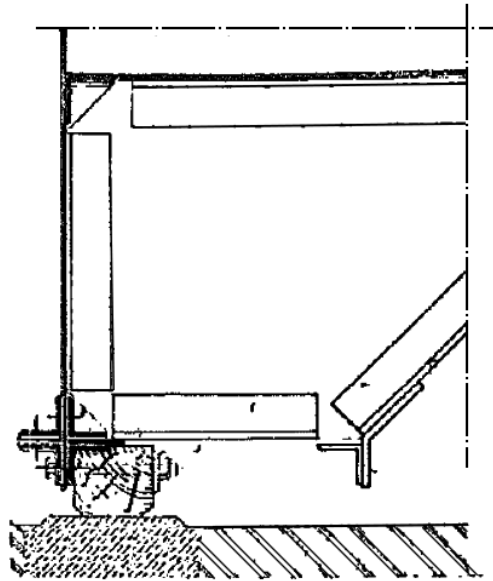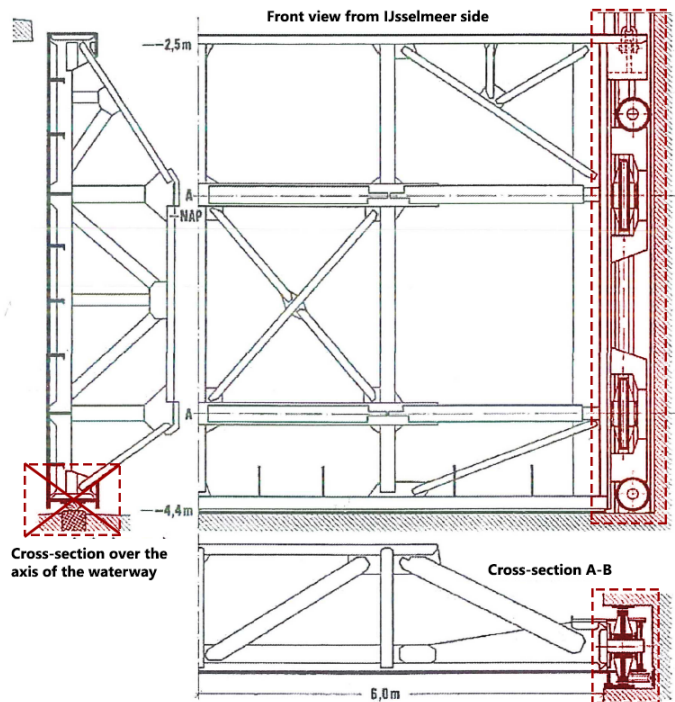

Figure 2.15: Drawing existing flood gate. Gate supports highlighted in red. Bottom detail on sill as depicted is later changed to the design given in figure 2.14. [24, edited]

flow is not bent as was shown in figure 2.9c, but the flow is guided around the rotor. In figure 2.16 examples of a bulb pump and bulb turbine are given.

Figure 2.16: Left: bulb pump IJmuiden [16]. Right: Alstom bulb turbine [28].

Exact specifics on the pumps that will be used, are not yet available. In section 2.4.1 it was seen that the maximum pump diameter between the geometric constraints is about 2 metre. The geometry of the pump gate and the implementation of the pumps is given in appendix B, figure B.2. Witteveen+Bos [40] has, in consultation with specialists of Nijhuis B.V., determined the following values for the design point of that size pump:

- Design head $H_d = 1.0$ m;
- Design discharge $Q_d = 18$ m^3/s.

In table 2.3 below the estimations for the total pump station are given. The number of pumps includes one reserve.

Table 2.3: Provisional assumptions and data pump capacity [25]

	till 2028	till 2050
Number of gates	8	13
Designed number of pumps	24	39
Pump capacity [m^3/s]	414	684

The radial velocity of the pumps is not relevant when evaluating the static behaviour of the gate designs. Therefore, an estimation of this velocity has not been made by Witteveen+Bos [40]. For a potential power plant in the Brouwersdam, guidelines have been deduced by Nijhuis Pompen BV [27] based on experiments and experience for the design values of low head (till approximately 6 m) bulb pump turbines. These are able to function both as a pump and as a turbine. These guidelines are used to make a global estimation of the pump radial frequency. The diameter, in relation to the design discharge, is estimated by:

$$D \approx 0.5 \cdot \sqrt{Q_d} \quad [\text{m}] \tag{2.3}$$

This results in $D = 0.5 \cdot \sqrt{18} \approx 2.1$ m, which is thus reasonably in accordance with the 2 metre that was used by Witteveen+Bos [40]. The rotation speed of the pump impeller is

then estimated as follow:

$$N_d \approx \frac{750}{\sqrt{Q_d}} = \frac{750}{\sqrt{18}} \approx 177 \quad \text{[rpm]} \tag{2.4}$$

This is equal to $177/60 = 2.95$ Hz ≈ 18.5 rad/s.

Based on a constant pump rotational velocity, a pump curve has been estimated [40] which gives the discharges at hydraulic heads different from the design point. This curve is shown in chapter 4 (figure 4.9) in which it is used to estimate the motion-dependent pump forces, specific values are given in appendix C.2. The actual discharge through the sluice is not only determined by this pump curve, but also by the total system curve, which consists of the static head plus the dynamic head (friction losses). This is elaborated further in appendix C. In the report by Witteveen+Bos [40], this distinction has not been made and a constant system efficiency is used.

2.5 Conclusion

The pump gate concept has large benefits compared to the more conventional method of constructing a pump complex separately from the main waterway or, in case of Den Oever, the sluice complex. Due to this innovative solution, the free flow discharge capacity is not hampered and costs can be reduced. This however also brings along some uncertainty and challenges. Instead of the pumps being on a heavy concrete foundation, they are now situated in a relatively light weight steel gate. Excessive vibrations of the pumps and gate therefore become a larger risk.

Compared to the Korean reference projects, the pump gate designs for Den Oever have a large span and height. This results in higher loads and a lower stiffness of the gate. Furthermore, although exact values of their stiffness are not known, the Korean pump gates appear to be robust with a thickness of a fourth to a third of their spans and a small heart to heart distance between the stiffening elements. The flood defence pump gate, which is dimensioned on extreme storm conditions, has a significantly higher flexural rigidity than the regular pump gate. The regular pump gate design, subjected to the same variable loading during operation, is therefore much more prone to vibrations.

Whether the pump gate will have to function as flood gate, is decided by the contractor in a later phase of the Afsluitdijk project. A dynamic analysis of the pump gate designs can support such a decision. If the regular pump gate appears not to comply with vibration requirements, and has to be designed with a larger thickness, the benefits of not using the pump gate as a second flood defence reduce.

Although the pump gate designs are elaborated in detail, the exact geometry of its vertical supports remains unknown. A detailed design of these connections is not available and therefore a similar guidance system as for the previous gates is assumed. The supports of the gate are an important parameter in its dynamic behaviour. To simplify further analyses,

both designs will be considered with an isotropic bending stiffness. This is favourable compared to the designs by Witteveen+Bos [40] and should be kept in mind.

In the following chapter (3), the causes and consequences of vibrations of the Den Oever pump gates are elaborated and hydraulic conditions are determined. This forms the input for further analyses in chapter 5 to 7.

3 | Vibrations of the pump gate

In section 3.1 a quick overview of the components influencing the dynamic behaviour of the gate is given. The analyses in the remainder of this report are limited to a few of these components. Subsequently, the hydraulic design conditions are elaborated (3.2). The possible causes of vibrations are elaborated in section 3.3. Furthermore, the consequences of these vibrations and the requirements with respect to these consequences are stated in section 3.4.

3.1 System influencing pump gate vibrations

The pump gates at Den Oever are part of a larger system. One of the reasons why the dynamic behaviour of the pump gate is complex, is due to the many components involved that influence it. A schematic representation of these components, is given in figure 3.1.
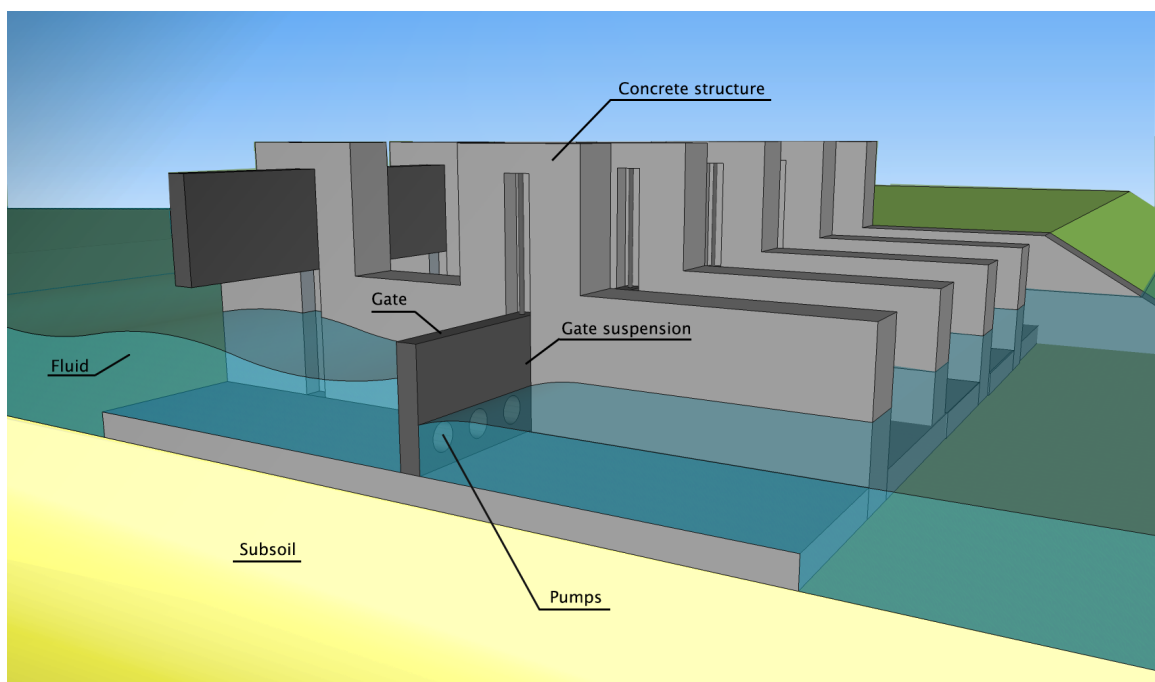
Figure 3.1: Schematic presentation components dynamic system of the pump gate. The upper structure has not been drawn for clarity.

Vibrations of the gate will have an effect on and will be affected by the gate structure, the pumps, fluid, concrete structure and subsoil. Due to the large volume of the concrete structure, the weight of the concrete structure is relatively large in comparison to that of the gate and pumps. The concrete pillars in between each water way alone have a weight of about:

$$m_{\text{pillar}} = 4.1 \cdot 10 \cdot 50 \cdot 2400 = 4920 \cdot 10^3 \text{ kg} \tag{3.1}$$

This is 55-60 times larger than the weight of the pump gate. Including the concrete towers, girders and floor slab, the difference in weight will be much larger. For this reason, the movement of the concrete structure and subsoil is neglected in the analysis of the system. This limits the analysis of the system to the following components:

- Gate structure, including its supports and suspensions;
- Pumps;
- Fluid.

Although the concrete structure is not included in the analysis, forces from the gates onto its support may involve risks. This is not explicitly investigated, but the amplification of static gate deflections is a first indication of whether these forces may be significant.

Theoretical background on the dynamic behaviour of each of the three included components is given in chapter 4.

3.2 Hydraulic design conditions

Especially relevant to the pump gate, is the behaviour during operation. The analyses in further chapters are therefore, as was mentioned before, focused on the closed pump gate with operating pumps. Since, the governing dynamic response of the designs may not simply be at the highest water levels, a possible range is determined. Subsequently, a few likely governing cases are investigated.

The absolute minimum Lake IJssel water level for which the pumps are required to operate is -0.6 m NAP. The maximum allowable water level at Lake IJssel is $+0.55 \approx +0.6$ m NAP, based on a historical event in which this water level was reached [22]. These two water levels give the possible water level range on the Lake IJssel side of the pump gate.

During extreme (1/10,000 year) storm conditions and corresponding water levels on the Waddensea, the pump gate will not be in operation. A requirement for the maximum return period at which operating must be possible, is not stated. The maximum water level at the Waddensea side is therefore based on the assumed requirement of open channel flow. As was shown in figure 2.1 the bottom of the upperstructure is located at +2.50 m NAP. Even if the pumps will indeed not operate at higher water levels and corresponding return periods, they may have a significant favourable effect on the resistance against extreme storm conditions. The water level at Lake IJssel can be lowered more effectively in anticipation and at the beginning of extreme conditions.

Although the pump is theoretically able to operate at negative heads, it is expected that in that case discharging by gravity will be preferable. The minimum Waddensea level during operation is therefore taken 0.1 metre above that of Lake IJssel. The hydraulic conditions are summarized in table 3.1.

The maximum head during operation is thus $7.2 - 4.1 = 3.1$ metre. The pumps are able to operate at this head. The regular pump gate is however dimensioned on a head of 2 metre

Table 3.1: Design water level ranges Lake IJssel and Waddensea during pump operation

Location	Min. water level	Corr. water depth	Max. water level	Corr. water depth
Lake IJssel (h_S)	-0.6 m NAP	4.1 m	+0.6 m NAP	5.3 m
Waddensea (h_N)	-0.5 m NAP	4.2 m	+2.50 m NAP	7.2 m

[40]. To ensure an unambiguous comparison between the regular and more robust flood defence pump gate design, both designs will be evaluated for a maximum pump head of 2 metre. Based on above defined water level ranges, three possibly governing load cases will be investigated:

- Minimum water depths: $h_S = 4.1$ m, $h_N = 4.2$ m
- Cavitation risk: $h_S = 4.1$ m, $h_N = 6.1$ m
- Maximum water depths: $h_S = 5.3$ m, $h_N = 7.2$ m

The minimum and maximum water levels will likely results in respectively the highest and lowest eigenfrequencies of the entire system. The cavitation water levels are based on minimum water coverage, and maximum pump head. The requirements and background with respect to cavitation are elaborated in section 3.4 and appendix C.6

The maximum Waddensea water level of +2.50 corresponds to the present 1/1 year storm conditions. A wave spectrum is determined for this water level in appendix A and is elaborated further in section 3.3.2 as one of the excitation forces.

3.3   Causes of vibrations

A distinction should be made between the 'external' forces and those which are part of the dynamic system and are responsive to the vibrations. The fluid and pumps contribute to both these categories. The presence of the fluid results in hydrodynamic damping and mass (or stiffness), which is part of the responsive system. The same applies to the pumps, which are likely to have a certain response to the motion of the gate. The responsive forces, dependent on the deflection, velocity or acceleration of the structure, influence the eigenfrequencies and modes of the entire system. The responsive forces of both the fluid and pumps are elaborated in chapter 4.

These forces are however not the cause of vibrations. In this section the possible excitation mechanisms of the pump gate are inventoried, of which the followings can be distinguished:

- The motion-independent mechanic and hydraulic pump forces;
- Waves;
- Other fluid-induced interactions;

Other loads are considered insignificant in magnitude, such as wind loading, in likelihood of occurrence, such as earthquake loading, or not governing in the design concerning vibrations, such as collision impact loads.

3.3.1   Motion-independent pump forces

Due to inevitable inaccuracies in the pump, unbalanced forces will be a result of the rotations of the pump rotor. Mechanical unbalance is the result of a deviation in mass of the different propellers. The resulting net centrifugal force has harmonic horizontal and vertical components. A bent shaft and the run-out of individual components can result in such forces as well. The forces resulting from mechanical inaccuracies have their peak at the rotation frequency of the pump [11].

Given the orientation of the axial flow pumps, the blades are rotating in the same plane as the gate. Unbalance forces therefore do not directly lead to a bending motion of the gate. Mechanical unbalance often goes accompanied with hydraulic forces in the pumps. Furthermore, the inherent turbulent behaviour of the fluid leads to certain periodic forces. Florjancic and Frei [11] state the following hydraulic forces leading to pump vibrations (and their corresponding frequencies):

- Hydraulic unbalance (peak at ω_p)
- Vane pass (peaks at $n \cdot n_{\text{blades}} \cdot \omega_p$, $n = 1, 2, 3, ...$)
- Recirculation/separation, and similar phenomena (no peak, $0\text{-}1.5 \cdot \omega_p$)
- Rotating stall (peak at $0.5\text{-}0.95 \cdot \omega_p$)
- Cavitation (broad band 0.5-10 kHz)

in which: ω_p =   pump radial velocity [rad/s]
            n_{blades} =   number of rotor blades of the pump [-]

The extremely high frequencies corresponding to the implosion of cavitation bubbles (≈ 10 kHz) can in some cases, due to disturbance of the flow, also lead to pressure fluctuations with much lower frequencies (< 10 Hz) [11].

Vane passage forces are, as is in the name, the result of the blades passing by the vanes which support the pumps. The vane passage excitation frequencies depend on the number of impeller blades: $n \cdot n_{\text{blades}} \cdot \omega_p$. Florjancic and Frei [11] state vane passage becomes insignificant for $n > 3$.

Generally, the pump manufacturer states limits for the forces that may originate from the pumps. As was stated in section 2.4.3, specifics on the pumps are yet unsure in this phase of the Afsluitdijk project. Data on pump forces is therefore not yet available, and also the pump radial frequency may vary from what was estimated. A more broad and roughly estimated force envelope is therefore defined. Results will give insight in whether certain pump radial velocities should be avoided or whether the pump gate must be adjusted to this.

Since the radial pump velocity is roughly estimated and the number of pump blades is not certain yet, these parameters are varied. In figure 2.16 it can be seen that the bulb pumps of IJmuiden have five impeller blades. The following possibilities are considered:

- Pump radial velocity: $\pm 50\% \cdot 18.5$ rad/s

- Number of blades: 4-6

Subsequently excitation frequencies are considered within 0.5-1.5 times the radial pump velocity, which corresponds to most of the listed pump forces. For the vane passage forces frequencies three multiples of $n_{blades} \cdot \omega_p$ are considered. The above leads to excitation frequencies from $(0.5 \cdot 0.5 \cdot 18.5 \approx)$ 4.6 to $(3 \cdot 6 \cdot 1.5 \cdot 18.5 =)$ 499.5 rad/s.

Witteveen+Bos [40] has, in consultation with Nijhuis B.V., assumed the total peak amplitude of the variable pump forces is no more than ten percent of the constant pump thrust, see equation (3.2). This obviously is a crude assumption and does not distinct between the motion-independent and dependent forces. Due to lack on better data, this value is used as a possible maximum for each of the estimated possible frequencies. Since energy decays for higher vane passage multiples, the energy is reduced with one third for each higher multiple n. The given ranges and assumed values then result in the excitation force-frequency 'envelope' shown in figure 3.2. The values given in this envelope do not act simultaneously, but each of these forces is evaluated as a maximum. This differs from a usual spectrum, which represents a time signal transformed to the frequency domain as a *summation* of harmonics (such the wave spectrum in section 3.3.2)
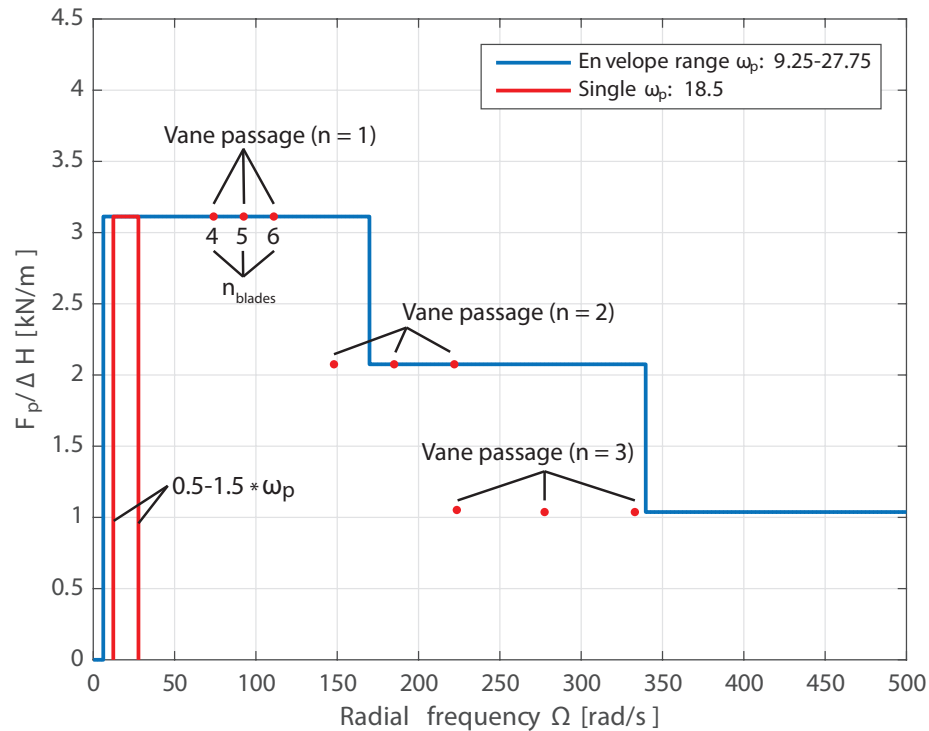

Figure 3.2: Amplitude-frequency envelope for the forces resulting from the pumps based on varied pump radial velocities and the number of pump blades (blue). In red, the peak excitation frequencies are shown given for a single pump rotation speed ($\omega_p = 18.5$ rad/s). In reality some kind of distribution would be present around each peak frequency. Since only the envelope is considered in the analyses, such a distribution was not determined.

The maximum force amplitude as a function of the pump thrust is given by:

$$\hat{F}_p = 0.1 \cdot F_{thrust} = 0.1 \cdot A_p \, \Delta p = 0.1 \cdot A_p \, \rho_f g \, H_p \tag{3.2}$$

in which:
$$\begin{aligned} A_p \quad &= \quad \text{pump propeller area } [\text{m}^2] \\ H_p \quad &= \quad \text{pump head } [\text{m}] \end{aligned}$$

Since especially for the flood defence pump gate, pump thrust is small compared to the governing extreme storm conditions, response is likely to be limited unless resonance occurs. The exact value is therefore less important than the corresponding frequency ranges, although both are used to give a first estimate of the response magnitude.

3.3.2 Waves

In appendix A.2 a wave spectrum is quantified for the location of the sluice complex. This depth-limited JONSWAP spectrum is depicted in figure 3.3. The peak frequency (and related wave length) depend on the fetch for an undeveloped sea state. Due to the short fetch at the Waddensea, the peak frequency is relatively high and corresponding energy relatively low. Locally, the waves are possibly distorted due to the change of depth and the counterflow generated by the pumps. This has not been taken into account however when determining the wave spectrum.
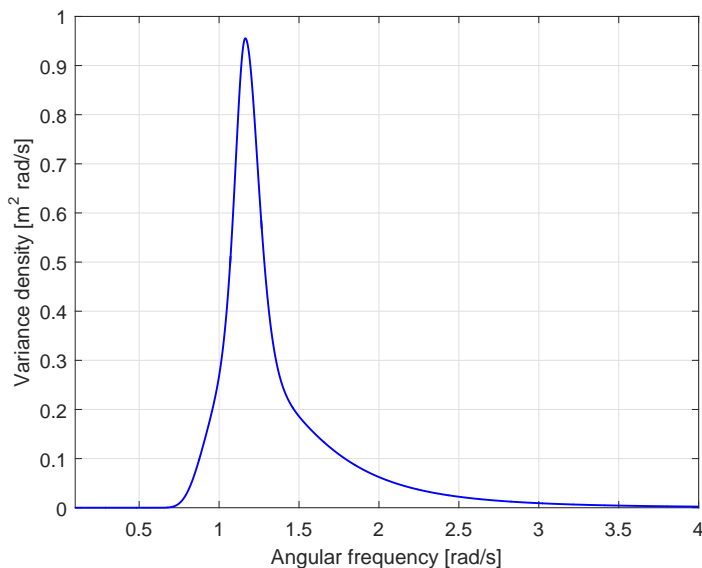

Figure 3.3: Depth-limited JONSWAP wave spectrum at the Waddensea

As can be seen, the waves correspond to much lower frequencies than the forces originating from the pumps, with minimal periods of about two seconds. Therefore, these waves potentially excite no natural frequencies of the gate system. This is the case for many regular hydraulic flood gates. Due to the pump masses and stricter requirements for the pump gate, it should be investigated whether this also applies to the pump gate designs.

The response to a wave spectrum is determined by frequency-dependent transfer functions. First, the variance density spectrum is transformed to the wave force spectrum. Subsequently, a response spectrum can be determined. This is further explained in section A.3.

3.3.3 Fluid-induced vibrations

The following fluid induced structural vibrations are mentioned in literature [9, 17, 19, 21, 26]:

- Excitation due to turbulence;
- Excitation by stable vortices;
- Excitation due to flow instability;
- Self-excitation;
- Excitation due to fluid oscillations in a basin;
- Excitation due to fluid oscillations coupled with the structure motion.

The distinction between the 'responsive' system and the motion-independent excitation force is less clear for some of these excitations. When the fluid is part of the dynamic system, the latter two categories listed above can actually be considered as the excited system itself. These are therefore included in the analyses in further chapters of this report.

In appendix D.4 each of these six phenomena is discussed briefly with respect to gates. Self-excitation occurs when the velocity of the structure is accompanied by a force in the same direction. This can be expressed by a negative damping coefficient. In such cases often the permanent flow is the component adding energy to the system, and can thus be seen as the external forcing. Most of the self-excitation mechanisms and flow instabilities are therefore relevant to gates with under- or overflow. These are therefore not considered in this thesis.

3.4 Vibration requirements and failure mechanisms

Extensive vibrations can lead to a number of unwanted effects or even failure of the structure. Possible failure due to vibrations in the existing structure or gate can be due to:

1. Exceedance of ultimate strength in the steel pump gates or its support;
2. Exceedance of ultimate strength in the concrete structure;
3. Fatigue of a structural component.

Furthermore vibrations can lead to:

4. Increased maintenance of structural components.

Effects of vibrations could further have the following negative effects on the pumps:

5. Decreased efficiency;
6. Decreased lifetime;
7. Increased maintenance.

Finally, the water tightness of the gate might be influenced by vibrations, which indirectly decreases the efficiency of the pumps. Predicting the effect of vibrations on the leakage of

the gate is however, even qualitatively, difficult. It depends on the exact geometrical design of the supports and borders. For now, it is assumed the water tightness will receive special attention in the final design if necessary and measures will be taken to such an extend that leakage can be neglected.

Below, for each of the above mentioned effects it is described briefly how it can be determined, and what the requirements are.

1) The ultimate stresses resulting from the vibrations can be described by a structural model. The ultimate allowable tensile stress in the gate is given by the steel used (S355).

2) Although, similar to steel fatigue, repetitive loads on the concrete structure might be more harmful than the same static load, the concrete structure itself is not investigated in this thesis. Instead, the amplification of static gate deflection is used as a first indication of the magnitude of the support forces.

3+4) The occurrence of fatigue and required maintenance of the structural elements due to vibrations are closely related. In appendix D.2 the phenomenon of fatigue and the approach of the Eurocode 3 is given, which uses a standard S-N curve. The cumulative fatigue damage in case of variable amplitude loading is determined by the so called Miner rule, which states that in order for an element not to fail:

$$D_d = \sum \frac{n_i}{N_i} < 1 \qquad (3.3)$$

in which: D_d = fatigue damage factor during design life [-]
n_i = number of times load S_i occurs [cycles]
N_i = fatigue endurance to load S_i [cycles]

The higher this damage factor, the greater the likelihood of damage and needed maintenance. A simplified structural model will most likely not describe occurring (peak) stresses in every gate element and might neglect effects like torsion. Factors could be used to account for this.

5) Extensive vibrations can lead to a decrease in pump efficiency, which would mean a higher energy consumption. The occurrence of cavitation has a large influence on the pumps' efficiency. An important notion in the prediction of cavitation is the net positive suction head (NPSH). Vibrations of the gate can possibly reduce the active NPSH due to resulting pressure fluctuations in the fluid. The concept of cavitation is elaborated further in section C.6.

6+7) On top of the normal wear and tear of the pump parts, extensive vibrations can significantly reduce pump lifetime. In this, damage due to cavitation (and thus the NPSH) plays a role as well. Secondly, guidelines exist stating maximum allowable vibration speeds in the non-moving parts of pumps. These will be used as a limit, above which lifetime is significantly reduced. These limits are given in appendix C.5, table C.2.

3.5   Conclusion

Together with chapter 2, the input has been provided for further analyses of the pump gate designs with respect to vibrations. The system has been limited to the gate structure, pumps and fluid. The relevant causes of vibrations independent of the system itself that will be included in further analyses are waves and pump forces. The quantification of the latter includes high uncertainties in this phase of the project. A broader envelope of potential pump radial speeds and corresponding excitation frequencies is therefore determined.

The focus of further analyses will be on the pump gate during operation, for which hydraulic design conditions have been determined. Since it is not known in advance which hydraulic boundary conditions will lead to governing eigenfrequencies, a range is inventoried.

The vibration requirements with respect to the gate come down to the demand of not exceeding stresses occurring in the static situation, since also with fatigue the maximum number of repetitive loads allowed is a function of the stress amplitude. The ratio between the force amplitude and maximum responsive spring force is given by the amplification factor, which is introduced in appendix D.1.1. Considering (quasi-)static loading the gate designs complied to the requirements.

The requirements for the pump are twofold. To limit wear and tear of the pumps, vibration velocities should be limited. On the other hand, excessive pressure fluctuations in the fluid can lead to inefficient operation and in extreme cases to cavitation damage. These pressure fluctuations can be caused by the gate, the pumps or be the result of fluid oscillations in the sluice.

A model of the pump gate should thus not solely focus on the pump-gate structure, but also quantify pressure fluctuations in the fluid. Since the fluid is part of the excited system, it is likely that this is a prerequisite to determine gate vibrations in any case. The theoretical background on the behaviour of the structure, pump and fluid during vibrations each is given in the following chapter, after which a model strategy is determined.

4 | Fluid, pump and structure dynamics

As a start of the quantification of pump gate vibrations, in this chapter a theoretical investigation of the pump gate system is made. Subjected to harmonic forcing, the pump gate will vibrate in a certain shape. In figure 4.1 the two-dimensional motion of the gate is shown for both the vertical and the horizontal direction. In reality, the motion will be three dimensional.
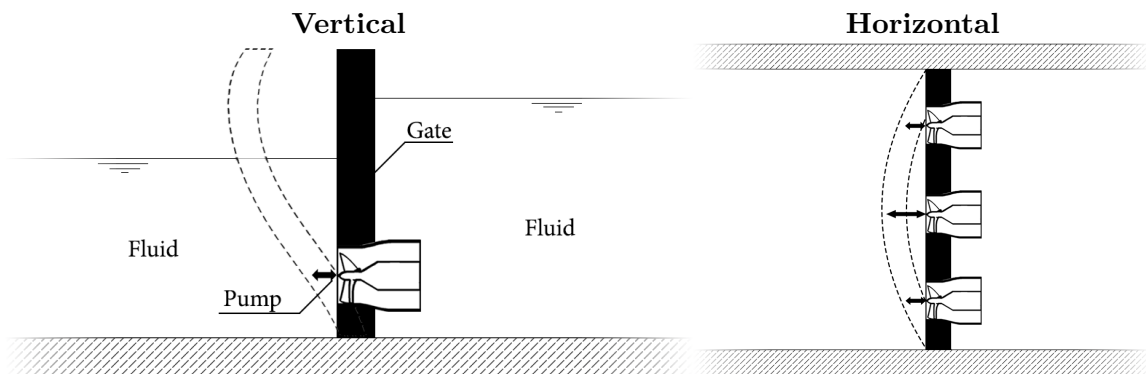

Figure 4.1: Representation of the vibrating pump gate

In figure 4.1 the three key elements of the dynamic system that will be included in future analyses, are shown. As mentioned in chapter 3 these are the gate structure, pumps and fluid. Theoretical background is given on the dynamic behaviour of each of these components in section 4.1, section 4.2 and section 4.3. Analytical estimations are given for these components. Based on these estimations and their relative magnitude, it can be decided whether a more specific model approach is necessary.

Furthermore, the interaction between the vibration (shape) of the structure and the fluid and pump pressures is not yet included in each of these separate theoretical expressions. The hydrodynamic forces are both dependent on the amplitude as well as the shape of the vibrating gate. The motion of the gate is turn determined by these forces and the hydrodynamic response. To include and solve these interactions, multiple methods exist. A model strategy is elaborated in section 4.4.

4.1 Structural dynamics

4.1.1 Basic notions

When a structure is subjected to a force, this causes deformations and internal stresses. In a static analysis, variations in time are not taken into account and the structure will be in

equilibrium:

$$\sum F = 0, \qquad \sum T = 0 \tag{4.1}$$

in which:
F = external force [N]
T = external moment [Nm]

When the forces do vary in time, the inertia of the structure might not be negligible any more. In that case the response is dynamic and vibrations can occur. A well-known theoretical example is that of the single degree of freedom mass-spring-dash pot system, which can be seen in figure 4.2. This system can be described by the following equation:

$$m\frac{d^2y}{dt^2} + c\frac{dy}{dt} + ky = F(t) \tag{4.2}$$

in which:
m = mass [kg]
c = damping [Ns/m]
k = spring stiffness [N/m]
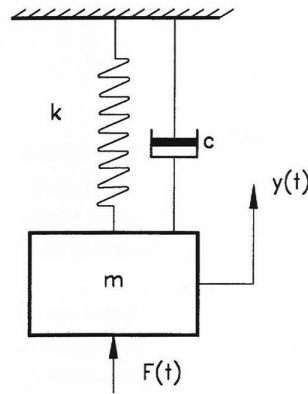y = displacement in y-direction [m]
t = time [s]

Figure 4.2: Single degree of freedom mass dash pot spring system [17]

An important notion in the field of dynamics, is resonance. This is the phenomenon that consists of a given system being driven by a force to oscillate with greater amplitude at certain frequencies. The natural frequency or eigenfrequency at which this occurs, is given in equation (4.3) for the mass-dashpot-spring system. To avoid resonance in practice, structures are designed stiff enough so that its first natural frequency is about twice the excitation frequency.

$$f_n = \frac{\omega_n}{2\pi} = \frac{1}{2\pi}\sqrt{\frac{k}{m}} \tag{4.3}$$

in which:
f_n = natural frequency or eigenfrequency [Hz = s^{-1}]
ω_n = natural radial frequency or radial eigenfrequency [rad/s]

When such a system is submerged in water, its behaviour and eigenfrequencies will change. This is elaborated in section 4.2.

Many structures can not be sufficiently described by a single degree of freedom and should thus be represented as continuous systems or systems with n-degrees of freedom. In numerical software the systems will often be represented as a discrete system (or lumped mass systems) with limited but many degrees of freedom. The equations of motion can then best be presented in matrix form:

$$\mathbf{M\ddot{y}} + \mathbf{C\dot{y}} + \mathbf{Ky} = \mathbf{f} \tag{4.4}$$

In appendix D.1.1 the behaviour of the single and multiple degree of freedom (SDOF and MDOF) system is treated further.

4.1.2 Continuous systems: the bending beam

A continuous system is in fact an infinite degree of freedom system. Hence, it has an infinite number of eigenmodes and natural frequencies. The first three eigenmodes of a simply supported bending beam are given in figure 4.3. The lowest natural frequency is linked to the first eigenmode, and so on.
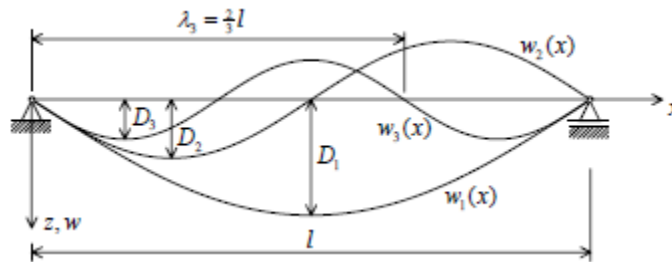

Figure 4.3: The first three eigenmodes of a simply supported bending beam [32]

In the two-dimensional space the pump gate could be described as a bending beam. Dynamic and kinematic boundary conditions apply at each side of the continuous function. Some possibilities for a bending beam and the corresponding eigenfrequencies and eigenmodes, are given in figure D.2. Using Euler-Bernouilli theory, a bending beam is described by:

$$\rho_b \frac{\partial^2 w(x,t)}{\partial t^2} + EI \frac{\partial^4 w(x,t)}{\partial x^4} = q(x,t) \tag{4.5}$$

in which:
ρ_b	=	specific weight of the beam per running metre [kg/m]
E	=	elasticity modulus [N/m^2]
I	=	moment of inertia [m^4]
q	=	distributed force [N/m]

Euler-Bernoulli beam theory can be considered as a specific case of the Timoshenko beam theory. This model takes into account shear deformation and adds a term to equation (4.5). In Euler-Bernouilli theory the beam planes remains perpendicular to the beam's axis, which is not the case for Timoshenko beam theory, as is shown in section 4.4.

Taking into account this deformation mechanism, results in lower eigenfrequencies and in the static case a larger deflection. Kirchhoff-Love plate theory neglects shear deformation
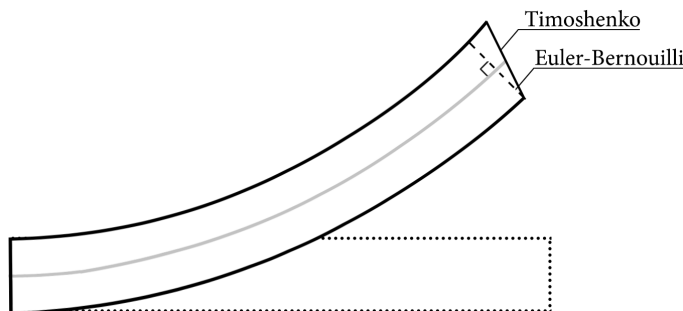
Figure 4.4: Comparison between a bent Euler-Bernouilli and Timoshenko beam

as well and is therewith the equivalent of Euler-Bernouilli beam theory. The equation of motion for plates is given in the chapter 6, where it is applied to the pump gate design.

Whether shear deformation must be taken into account depends mainly on the thickness to height and width ratios. In case of static loading, Blaauwendraad [2] states the following requirement:

$$\frac{t}{L_{x/z}} < \frac{1}{5} \tag{4.6}$$

in which: t = plate or beam thickness [m]
$L_{x/z}$ = length in x- or z-direction [m]

A quick estimation is made to check the width over length ratios for both Den Oever gate designs. As these designs are in reality non-homogeneous, an equivalent plate thickness (or beam thickness per running metre) is determined for the rigidities of both designs.

$$t_e = (12 \cdot I_{zz})^{1/3} \tag{4.7}$$

in which: t_e = equivalent plate or beam thickness [m]
I_{zz} = moment of inertia per running metre around the z-axis [m^4 m^{-1}]

Since the plate designs were considered as isotropic, the inertia is equal in both directions. For the regular and flood defence pump gate designs, this results in a thickness of 0.23 and 0.56 m respectively. This gives the following ratios:

- Regular pump gate: $r_x = \frac{t_e}{L_x} = \frac{0.23}{12.5} \approx \frac{1}{54}$ $r_z = \frac{t_e}{L_z} = \frac{0.23}{7.25} \approx \frac{1}{32}$
- Flood defence pump gate: $r_x = \frac{t_e}{L_x} = \frac{0.56}{12.5} \approx \frac{1}{22}$ $r_z = \frac{t_e}{L_z} = \frac{0.56}{7.25} \approx \frac{1}{13}$

These ratios are sufficiently small compared to the required 1/5 ratio to neglect shear deformation under static loading. Considering the dynamic behaviour of a plate or beam, higher eigenmodes result however in a reduced distance between opposite shear forces. Shear deformation therefore becomes more significant for higher modes and corresponding frequencies. Especially in case of the flood defence gate design, neglecting this deformation results in less accurate results for higher modes. Since the first few eigenmodes are generally governing in the dynamic behaviour, Euler-Bernouilli and Kirchhoff-Love theory are considered sufficient in this design phase.

An additional requirement that is often stated is that the amplitude to thickness ratio should be small. Since amplitudes are required to be in the order of millimetres to avoid pump wear and tear that this requirement is expected to be fulfilled in the final design.

It is noted that in the analysis by Molenaar [24] of the concrete defence beam, which has the same length, both theories were used. Differences in maximum deflection between both models were in that case not negligible, but less than ten percent. The respective beam consists of reinforced concrete however and has a high thickness of 1.55 m.

4.1.3 Analysis in the time or frequency domain

The dynamic behaviour of a structure can be analysed and described in the time or frequency domain. Both ways have their advantages and disadvantages. Any time signal can be represented by a summation of harmonics, and vice versa. This is done with the help of a so called Fourier transform.

In the frequency domain the forcing is described with a (discrete) spectrum of amplitudes versus frequencies. Analysis of the structure results in a response amplitude operator (RAO), which describes the response of the structure to a certain force (shape) for each excitation frequency. The multiplication of the forcing amplitude at each frequency with the RAO value at that frequency yields the response spectrum. In a time-history analysis the motion of the structure is evaluated step-by-step, generally using a form of numerical integration.

Analysis in the frequency domain is mathematically favourable. Furthermore, frequency dependency can be included, which is a difficulty in the time domain. Non-linearity however, can only be included in the time domain. A more advanced method when it is necessary to include both frequency dependency and non-linearity, is the hybrid frequency time domain (HFTD) analysis. This method iterates between the frequency and time domain.

The analysis of the pump gate will be made in the frequency domain, mainly due to the frequency dependency of the hydrodynamic response and the mathematical advantage. It will thus not be able to include non-linearity in the analysis. Linearising of the system equations generally relies on the prerequisite of small amplitude vibrations. As structural failure will generally occur for larger amplitudes, this is expected to be the case in the final design.

4.1.4 Two dimensional plate behaviour

In appendix E a quick estimation is made of the modal shapes of a plate with similar dimensions as the pump gate. Given the arbitrary gate thickness and pump weights, no quantitative conclusions can be drawn from such a schematization. However, figure 4.5 does give insight in the possible shapes and two dimensional behaviour of the gate.

(a) First modal shape   (b) Second modal shape   (c) Third modal shape

(d) Fourth modal shape   (e) Fifth modal shape   (f) Sixth modal shape
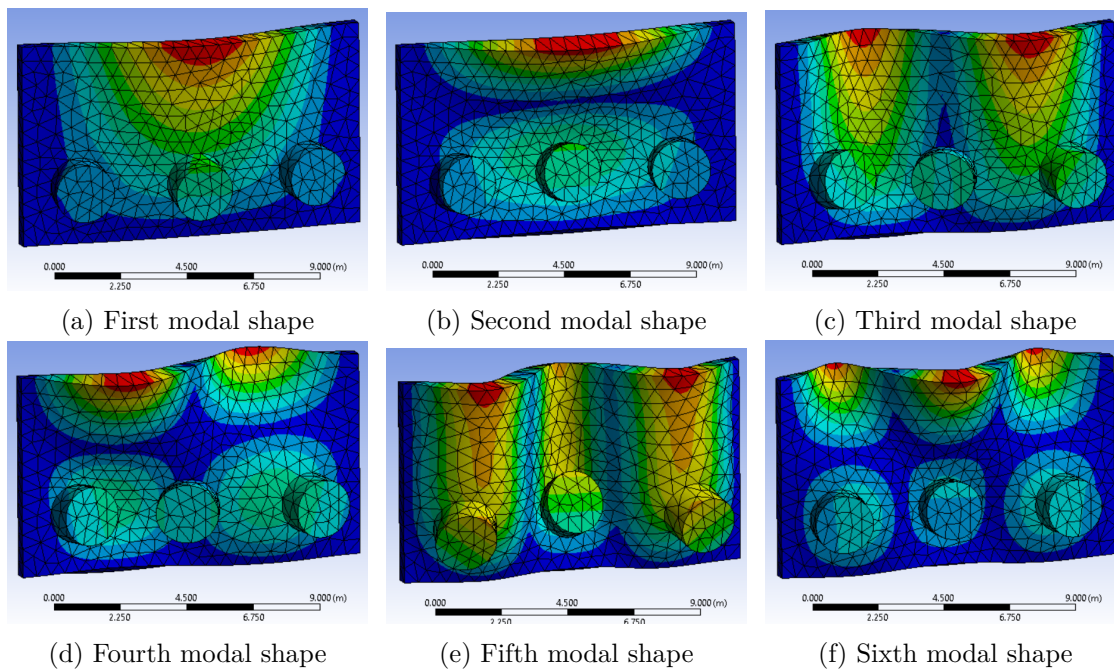
Figure 4.5: Modal shapes of a (dry) plate with length and width equal to the Den Oever gates, but arbitrary thickness and added pump weights. Fixed supports on left and right side, simple support at bottom.

In figure 4.5 both horizontal and vertical modes are relevant. Furthermore, it can be seen that even the approximate horizontal modes are significantly influenced by the bottom boundary condition. Neglecting this boundary condition, and schematizing the gate as a horizontal beam, is therefore likely inadequate.

4.2 Fluid dynamics

4.2.1 Hydrodynamic pressures

The motion of a structure in water results in a certain fluid pressure response, i.e. hydrodynamic pressures. Dividing these pressures into contributions linearly proportional to the structures motion (y, y' and y") results in the hydrodynamic coefficients. By making use of these coefficients, the analysis of the structural motion can remain similar to that of a 'dry' structure.

The linear forces are called the hydrodynamic stiffness force, damping force and mass inertia force [17], often appearing in literature as 'added mass, damping and stiffness'. The equation of motion for the same single degree mass-spring-dashpot system as in section 4.1.1 (but now submerged) is shown in equation (4.8) below [21].

$$(m + m_w)\frac{d^2y}{dt^2} + (c + c_w)\frac{dy}{dt} + (k + k_w)y = F_{w1}(t) + F_{w2}(y, \frac{dy}{dt}, etc.) \qquad (4.8)$$

in which: m_w =   hydrodynamic mass or added water mass [kg]
              c_w =   hydrodynamic damping [Ns/m]
              k_w =   hydrodynamic spring stiffness [N/m]

F_{w1} represents the force by the water not dependent on the systems motion and F_{w2} represents the non-linear forces. The latter can be neglected in most practical situations as long as amplitudes are small.

The added coefficients (m_w, c_w, k_w) can alter the dynamic behaviour considerably. In some cases, especially for thin structures like gates, the added water mass can be a multiple of the structures own mass. The added water mass lowers the natural frequencies, in case of the single degree of freedom mass-spring system (and no added stiffness) by:

$$\frac{f_{dry}}{f_{wet}} = \sqrt{\frac{m + m_w}{m}} \tag{4.9}$$

For systems with multiple degrees of freedom, equation (4.8) should again be presented in matrix form. The added mass matrix $\mathbf{M_w}$ can also contain non-diagonal terms, representing coupling forces. For example in case of an L-shaped gate, a vertical motion will push the water upwards, but also sidewards against the vertical part. This example is shown in figure 4.6.
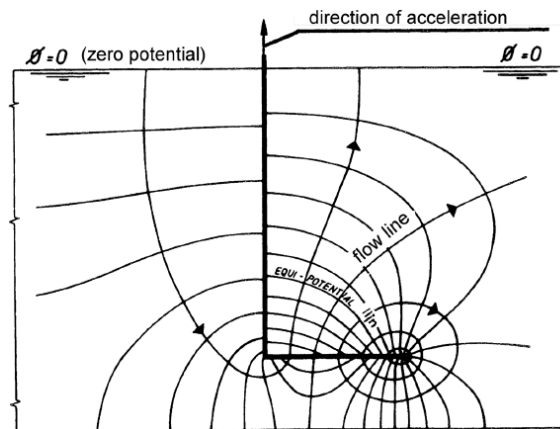

Figure 4.6: Periodic potential flow in case of a vibrating L-shaped gate. The motion in the vertical degree of freedom results in pressures (added mass) in both directions, the motions are thus coupled [21].

A structure in water has either a net hydrodynamic stiffness or hydrodynamic mass. This can be seen when the motion of the structure is described harmonically:

Displacement $y = A_y \sin(\omega t)$ (4.10)

Acceleration $\ddot{y} = -\omega^2 A_y \sin(\omega t)$ (4.11)

in which: A_y =   amplitude in x-direction [m]
              ω =   radial vibration frequency [rad/s]

The hydrodynamic stiffness describes the force that is proportional to the structure's motion: $k_w = F_{w,k-part}/y$, and the hydrodynamic mass the force that is proportional to the acceleration: $m_w = F_{w,m-part}/\ddot{y}$. As can be seen from equation (4.10) and (4.11), the acceleration is in anti-phase with the structure's displacement. The resultant hydrodynamic force will either be opposite to the structure's motion, when the hydrodynamic stiffness is governing, or in the same direction, when the hydrodynamic mass is governing.

Hydrodynamic stiffness is especially relevant for water-piercing structures (or vessels) with a degree of freedom in the vertical direction as in that case the upward water pressure increases with submergence. For gates with under or overflow so called sudden stiffness exists as well [21]. These three types of stiffness are shortly discussed in appendix D.3, but not considered relevant to the bending pump gate in closed position. The hydrodynamic mass is expected to have the highest contribution, which would thus decrease the eigenfrequencies of the gate compared to the dry situation.

As the dynamic behaviour of the pump gate is investigated during pump operation, a permanent flow field will be present around the pump gate. The vibrating pump gate alters this flow field. The non-viscous Navier-Stokes equation, split into permanent flow and a dynamic component, is given for the x-direction [21]:

$$\frac{\partial(p+p')}{\partial x} = -\rho\frac{\partial(u+u')}{\partial t} - \rho(u+u')\frac{\partial(u+u')}{\partial x} - \rho(v+v')\frac{\partial(u+u')}{\partial x} - \rho(w+w')\frac{\partial(u+u')}{\partial x}$$
$$(4.12)$$

Only considering the extra pressure field p' that is generated by the vibration, the following terms remain [21]:

$$\frac{\partial p'}{\partial x} = -\rho\frac{\partial u'}{\partial t} - \rho\left(u'\frac{\partial u}{\partial x} + u\frac{\partial u'}{\partial x}\right) - \rho\left(v'\frac{\partial u}{\partial y} + v\frac{\partial u'}{\partial y}\right) - \rho\left(w'\frac{\partial u}{\partial z} + w\frac{\partial u'}{\partial z}\right) + .. \quad (4.13)$$

Terms with u'^2 were neglected as vibration velocities are relatively small to the permanent flow velocities. From equation (4.13) it can be seen in which ways the water responds to vibrations. The fact that there are terms with $\frac{\delta u'}{\delta t}$ indicates that there is an added water mass. As can be seen, this term is not dependent on the initial flow field. The hydrodynamic damping, represented by terms with u', does have terms proportional to the permanent flow however. In appendix D.3 general examples of hydrodynamic damping are given.

Determination of the hydrodynamic coefficients taking into account the permanent flow, is very complex. In practice, despite the dependence these coefficients are often determined assuming still standing water [21].

4.2.2   Potential flow

In fluid dynamics, potential flow theory can be used to describe the fluid flow. This is a simplified approach that does not include effects caused by viscosity and boundary layers. Nevertheless, it can describe many physical phenomena and is used in e.g. wave theory.

The fluid domain is described by a potential function, such that:

$$\frac{\partial \mathbf{\Phi}}{\partial \mathbf{s}} = -\mathbf{v} \tag{4.14}$$

In which $\mathbf{s}$ is a streamline element. The velocity vector can be separated into each direction (x,y,z). For incompressible flow, the following equation holds:

$$\frac{\partial^2 \Phi}{\partial x^2} + \frac{\partial^2 \Phi}{\partial y^2} + \frac{\partial^2 \Phi}{\partial z^2} = 0 \qquad \text{or} \qquad \nabla^2 \Phi = 0 \tag{4.15}$$

In case compressibility of the fluid plays a role, which is investigate further for the Den Oever case in section 4.2.3 and chapter 5, the fluid equation is extended by an additional term:

$$\frac{\partial^2 \Phi}{\partial x^2} + \frac{\partial^2 \Phi}{\partial y^2} + \frac{\partial^2 \Phi}{\partial z^2} = \frac{1}{c_p^2} \frac{\partial^2 \Phi}{\partial t^2} \tag{4.16}$$

with:

$$c_p = \sqrt{\frac{K}{\rho_f}} \tag{4.17}$$

in which: c_p = celerity of pressure waves in water (or the speed of sound) [m/s]
K = bulk modulus of water [N/m^2]

Relevant in the dynamic analysis of hydraulic structures, are the fluid pressures as a result of the structure's motion. According to the *linearised* Bernoulli equation, requiring small flow velocities ($\mathbf{v} \ll 1$), the pressures in the fluid for unsteady flow are equal to:

$$p_f = -\rho_f \frac{\partial \Phi}{\partial t} - \rho_f g z \tag{4.18}$$

In which only the first term represents pressures generated by the oscillatory flow:

$$\tilde{p}_f = -\rho_f \frac{\partial \Phi}{\partial t} \tag{4.19}$$

With the potential flow equations, the fluid response to a moving gate can be evaluated through the interface condition which states that the velocity of the fluid at the gate's surface is equal to that of the gate:

$$\left.\frac{\partial \Phi(x, z, t)}{\partial y}\right|_{y=0} = \frac{\partial w}{\partial t}(x, z, t) \tag{4.20}$$

in which: w = structural deflection in y-direction [m]

Among others, the method by Kolkman [20] to determine the hydrodynamic mass for varying geometries is based on the above described equations. In chapter 5 and 6 these equations are used and further elaborated in the analytical models.

4.2.3   Hydrodynamic pressures for a rigid vertical gate (Westergaard)

Approximations and analytical solutions of the hydrodynamic pressures have been derived for several standard two-dimensional situations with still standing water. As the sluice walls confine the flow, the vertical representation of the pump gate at Den Oever is to a large extent similar to an infinitely long vertical wall or gate.

Westergaard has developed a widely used analytical derivation for such a situation, namely the hydrodynamic pressures for a vertical dam during earthquakes. The following simplifications were used to come to this derivation [37]:

- Pressure at water level is zero; no vertical movement or waves at the water surface;
- Infinitely long rigid dam;
- Reservoir extends to the infinity.

The pressures as a result of the horizontally accelerating wall are then described by:

$$p_f(z) = \frac{8\,\rho_f g\,k_h h}{\pi^2} \sum_{n=1,3,5,..}^{\infty} \frac{1}{n^2 C_n} \sin\left(\frac{n\pi z}{2h}\right) \tag{4.21}$$

with:

$$C_n = \sqrt{1 - \frac{16\rho_f h^2}{n^2 K T_e^2}} \tag{4.22}$$

in which:
h	$=$	water depth [m]
k_h	$=$	horizontal seismic coefficient [-]
K	$=$	bulk modulus of water [Pa]
p_f	$=$	hydrodynamic pressure [N·m^{-1}]
T_e	$=$	excitation period [s]
z	$=$	vertical coordinate along the water depth [m]
ρ_f	$=$	density of water [kg/m^3]

As can be seen from K in this expression, the compressibility of the water is taken into account. The hydrodynamic pressures are in that case dependent on the excitation period T_e, which is the vibration period of the structure. Westergaard has developed a simplified relation, based on incompressible flow as well. Since surface waves are neglected, incompressible flow will lead to frequency independence. In this case the hydrodynamic pressures are completely in phase with the structure's acceleration and the hydrodynamic pressures can be considered as hydrodynamic mass. The simplified expression for the pressure over the depth is as follows:

$$p(z) = \frac{7}{8}\rho_f g k_h \sqrt{zh} \tag{4.23}$$

The seismic horizontal coefficient is defined as the horizontal ground acceleration divided by the gravitational acceleration: $k_h = a_h/g$. This parameter is useful for earthquake design, when the ground acceleration is known in advance as a design parameter. The hydrodynamic pressures resulting from a unit acceleration, thus the hydrodynamic mass,

are more insightful in this case:

$$m_w(z) = \frac{7}{8}\rho_f\sqrt{zh} \tag{4.24}$$

Versluis [37] has investigated the validity of these expressions for large lock gates, which generally have a smaller water depth and a finite reservoir. Among others, the following conclusions were drawn:

- For a typical earthquake frequency spectrum and large lock water depths (≈ 30 m), the amplitude of the hydrodynamic pressure is almost independent of the excitation frequency. The assumption of incompressible water is valid.
- Including the bending stiffness of the gate or wall can have a significant influence on the amplitude of the hydrodynamic pressures.
- Surface waves and effects like sloshing have little to no influence on the total pressure distribution. Therefore the assumption that the pressure at the water surface is equal to zero is also valid for navigation locks and recommended for practical design.

Since conclusions were drawn for earthquake frequencies, the latter statement is not necessarily valid for lower frequencies. When waves are the excitation mechanism, evidently the frequency range is in the region where surface waves are of significant importance. Also at the frequencies of the pump forces, surface waves might still play a role. This should be investigated for the given geometry. Sloshing effects over the length of the sluice are unlikely to occur, as in the semi-infinite environment the surface waves are not (significantly) reflected. Possibly, at certain horizontal modes and frequencies, a standing wave could occur over the width of the sluice, which would be a three-dimensional effect.

A quick check is made to see whether the fluid can be considered incompressible for governing frequencies and water depths at the pump gate as well. A comparison between compressible and incompressible fluid response is shown in figure 4.7. When the excitation frequency becomes close to the a resonance frequency of the fluid, hydrodynamic pressures increase greatly and the error of assuming compressible flow becomes extremely large. The fundamental resonance period of water is given by [37]:

$$T_1 = \frac{4h}{c_p} \tag{4.25}$$

The pressure wave celerity (or the speed of sound) is approximately 1500 m/s for water. In table 3.1 the design water levels were shown. The maximum water level of 7.2 metre will lead to the lowest fundamental eigenfrequency of:

$$f_1 = \frac{1}{T_1} = \frac{c_p}{4h} = \frac{1500}{4 \cdot 7.2} \approx 52 \quad \text{[Hz]} \tag{4.26}$$

As can be seen in figure 4.7 results are reasonable for excitation frequencies lower than about a third of the fundamental resonance frequency of water. Wave excitation frequencies are
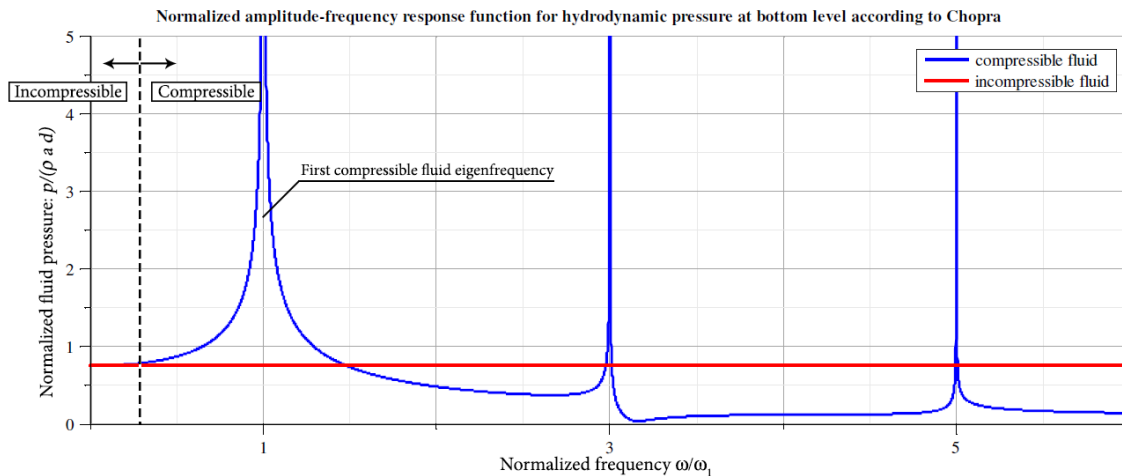
Figure 4.7: Comparison between relations for hydrodynamic pressures with compressible and non compressible fluid [37]

well within this limit. In section 3.3.1 most of the pump excitations were estimated have a frequency of 0.75 to 6.6 Hz, for which the response can be considered incompressible as well. However, vane passage involves higher excitation frequencies up to 80 Hz and can therefore certainly excite the system's compressible resonance frequencies.
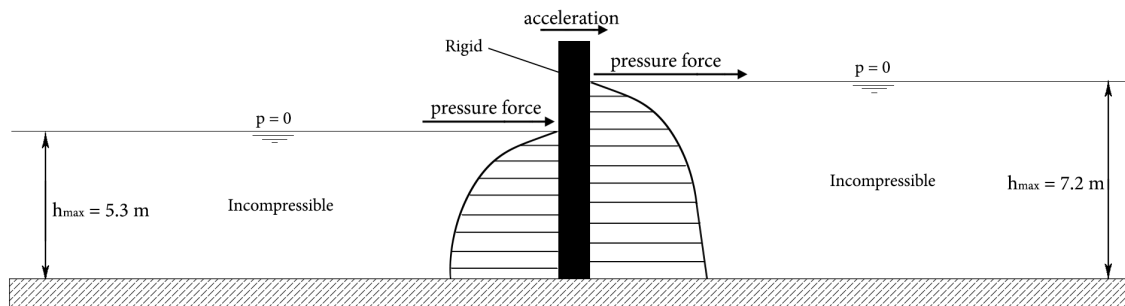

Figure 4.8: Pressure waves

Based on the simplified Westergaard parabola, a rough estimation of the hydrodynamic mass is made for the pump gate. The motion of the pump gate is for the time being thus considered rigid and without pumps. The hydrodynamic inertia force acts for both sides in the same direction. The hydrodynamic mass is therefore maximum (in this approximation) for maximum water levels, being 5.3 and 7.2 metre as shown table 3.1. This would result in an added water mass of:

$$m_{w,oneside} = L_x \int_{z=0}^{z=H} mw(z) = L_x \int_{z=0}^{z=H} \frac{7}{8} \rho_f \sqrt{zh} = L_x \frac{7}{12} \rho_w \sqrt{h} \left[z^{3/2} \right]_0^{z=H}$$

$$m_{w,total} = 12 \cdot \frac{7}{12} \cdot 1010 \cdot (5.3^2 + 7.2^2) = 565 \cdot 10^3 \quad [kg]$$

(4.27)

In which L_x is the width of the sluice, and ρ_f the mass density of the fluid. As the pumps only discharge from Lake IJssel to the Waddensea, the water is expected to be relatively fresh. The density used throughout this report is therefore 1010 kg/m^3. The hydrodynamic mass found is much more than the weight of the gates including pumps ($\approx 80 \cdot 10^3$ kg).

Given this estimated magnitude, the hydrodynamic mass will have a large effect on the behaviour of the pump gate, likely reducing its natural frequencies. The finite bending stiffness of the pump gate is expected to change the distribution and magnitude of the hydrodynamic mass however. In addition, this flexibility leads to horizontal modes, at which the assumed two-dimensionality of the gate is no longer valid.

Furthermore, the presence of the pumps is expected to significantly change the hydrodynamic mass in comparison to that of a closed vertical wall. At most of the gate's surface, the fluid is forced by the vibrating gate. The pumps have a different effect on and response to the fluid however. This pump-fluid interaction is treated in section 4.3.

4.3 Pump vibrations

In section 3.3.1 the motion-independent pump forces were elaborated. In this section the forces generated by the motion of the gate and thus pumps are treated. The way in which the entire pump will move due to the excitation forces, is dependent on the gate and fluid, and will be part of the models in further chapters.

In the static situation the pump generates a certain discharge at a given hydraulic head. The relation between the discharge and hydraulic head is given by the pump curve. When the pumps vibrate with a certain velocity $\dot{w}$, the instantaneous velocity between the pump and fluid flow changes by that velocity. Subsequently, the change in instantaneous discharge ΔQ will lead to a change in generated hydraulic pump head ΔH_p, and thus a force response. From figure 4.9, in which the pump curve estimated by Witteveen+Bos [40] is shown, it can be seen that the curve is shaped such that a decrease in discharge will result in an increase in pump head (or force).

A vibration velocity in flow direction means a decrease in instantaneous pump discharge, which leads to a decrease in hydraulic pump head. Since the pump forces the fluid in flow direction, a decrease in this permanent force is directed against the flow direction. Summarizing, a vibration velocity in flow direction will lead to a force in the opposite direction and vice versa. This is thus a stabilizing force induced by the velocity of the pump and can be considered a positive damping force.

The pressure change inflicted by a change in pump thrust is given by:

$$\Delta p_p = \rho_f g \Delta H_p \tag{4.28}$$

in which: H_p = static pump head [m]
            F_p = total pump thrust [N]

The local gradient $\Delta H_p / \Delta Q_p$ is named d_{HQ}. In further models the gate is considered continuous and a deflection is field is therefore determined over the surface where the pumps are present as well. The average velocity at this surface could be taken as representative
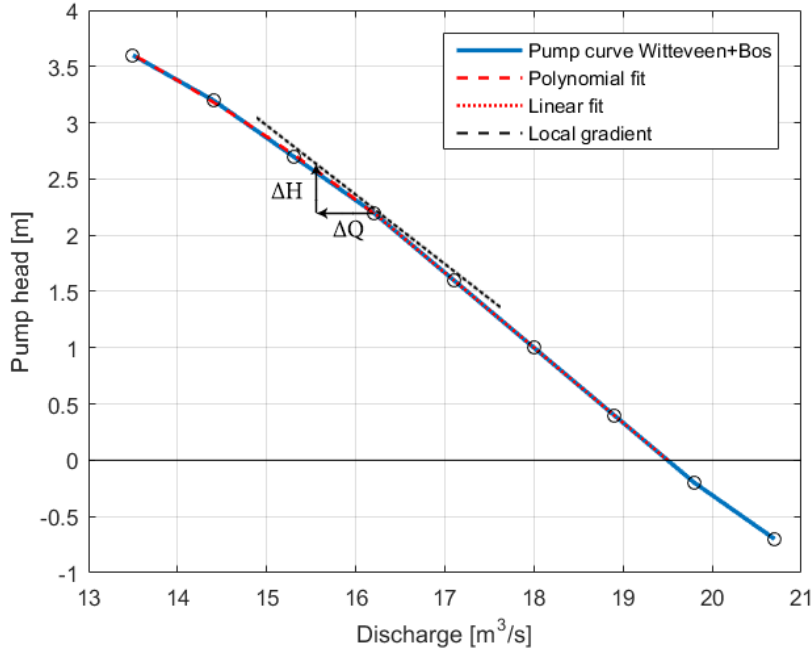
Figure 4.9: Pump curve for Den Oever with the local gradient shown at H = 2.2 m. To be able to describe the pump curve gradient continuously, the pump curve is approximated by a polynomial above this point and linearly beneath.

for the pumps, in which case the change in instantaneous discharge is given by:

$$\Delta Q_p = A_p \frac{\partial \bar{w}}{\partial t} \tag{4.29}$$

in which: A_p =   pump propeller area $[\text{m}^2]$

When substituted in equation (4.28), the corresponding pressure force is obtained:

$$\Delta p_p = \rho_f \, g \, d_{HQ} \, \Delta Q_p = \rho_f \, g \, d_{HQ} \, A_p \frac{\partial \bar{w}}{\partial t} \tag{4.30}$$

The distributed pump damping coefficient is then given by:

$$c_{pump} = \rho_f \, g \, d_{HQ} \, A_p \quad [\text{Ns/m} \cdot \text{m}^{-2}] \tag{4.31}$$

To be able to apply this damping in a frequency domain analysis, it must be linear. From $H_p = 0$ to 2.2 m, the estimated pump curve is linear. For the non-linear part, the pump curve must be approximated as its local gradient, which is valid as long as ΔQ and thus vibration amplitudes, are small. To be able to describe the damping terms continuously at each pump work point, a second order polynomial fit is used for $H > 2.2$ m. The local gradient is then given by:

$$d_{HQ} = 1.5 \quad [\text{s/m}^2] \qquad\qquad \text{for:} \qquad 0 < H_p \leq 2.2 \text{ m} \tag{4.32}$$

$$d_{HQ} = 0.4313 \, H_p + 0.6605 \quad [\text{s/m}^2] \qquad \text{for:} \qquad 2.2 < H_p < 3.1 \text{ m} \tag{4.33}$$

It must be noted that a few simplifications are made in the previous derivation. In first instance, the pump curve estimated by Witteveen+Bos has been highly simplified. Furthermore, in the above it has been assumed the pump head directly adjusts to the change in instantaneous discharge and the pump radial velocity remains constant. The rotor and pump system have their own inertia, which can change the magnitude and phase of the response. Based on consultation with an pump expert of Deltares, it is expected that the damping due to change in instantaneous discharge is the main contribution to the pump response however. One of the reasons for this, is the stabilizing effect of the pump's electro motor. An increase in radial velocity of the pump, will lead to a reduced force applied by the electro motor.

4.4 Conclusion and model strategy

In this chapter, theoretical background on the dynamic behaviour of each of the three components (structure, fluid and pumps) was treated. The following conclusions can be made based on this theoretical investigation:

- The structure, fluid and pumps are expected to influence each other significantly and must therefore be modelled as one interacting system. The fluid couples the modes of the structure and causes an interdependence so that the contribution of each component can not be determined separately from the others.

- Euler-Bernouilli beam theory and Kirchhoff-Love plate theory are expected to describe the first few eigenmodes of the gate with reasonable accuracy. For higher vibration frequencies results become less accurate.

- Quantitative conclusions on the response of the gate must be based on a three-dimensional model schematization due to the presence of the pumps and the expected vibration modes of the gate.

- Excitation frequencies related to surface waves and the radial velocity of the pump result in a response for which the fluid body can be considered as incompressible. Vane passage frequencies do however result in a response for which the compressibility of the fluid must be taken into account.

- For the linearised flow equations the hydrodynamic damping is influenced by the permanent flow field, the hydrodynamic mass is not.

- The most significant contributor of the motion-dependent pump response is a damping force onto the gate, which is a reaction to a change in instantaneous discharge. Inertia of the rotor system and delay in the reaction of the pump may change this behaviour, but it is expected that this remains the largest component of the force.

An overview of the components that will be considered in further analyses and the interaction between these components is shown in figure 4.10. As stated above, the hydrodynamic

mass can be influenced by the permanent flow field. The simplification of still standing water is made nevertheless, as taking into account this permanent flow complicates the analysis greatly. The flow field generated by the gate and pump vibrations is thus considered superimposable.
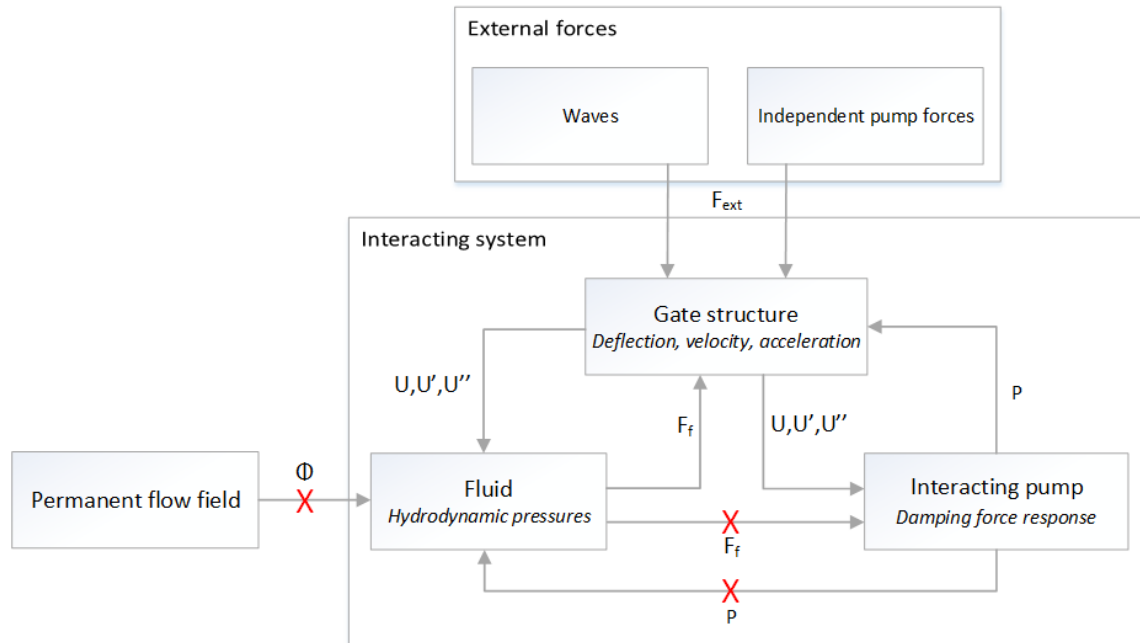

Figure 4.10: Components of the dynamic system influencing each other. The effect of the permanent flow field on the hydrodynamic pressure field will not be included in further analysis.

Since the pump gate is a continuous structure which may vibrate in many possible shapes, and as it was concluded the interaction between structure, fluid and pumps will be significant, solving its motion by applying constant hydrodynamic coefficients is not possible. The choice was made to model the linearised system in the frequency domain (section 4.1.3), in which multiple methods exist to solve this interaction. Firstly, a structural and fluid model could be set-up separately. Subsequently, iterating between these models could solve the final combined structure-fluid deflection and pressure vibration shapes.

A method directly solving the combined behaviour is more efficient computationally and deemed theoretically more insightful. This direct solving is possible through a so called semi-analytical coupled modal analysis. In this method the motion of the structure and fluid are both described as an (semi-)infinite summation of their eigenmodes and corresponding modal coefficient. The influence between the structure (with pumps) and the fluid is given by interface conditions, through which the eigenmodes can be interrelated. For above mentioned reasons, this analytical method is preferred over numerically iteration. Nevertheless, an analytical method has some drawbacks as well, such as the need for a simplified geometry. This method is further elaborated in chapters 5 and 6.

Also indicated in figure 4.10 is the exclusion of secondary effects between pumps and fluid. The force onto the gate generated by movement of the pumps respective to the fluid, is

taken into account. The simultaneous pressure change in the fluid, and through this fluid on the surface of the gate, is neglected however. Vice versa, the pump response to pressure changes at the inlet of the pumps due to the movement of the gate is not considered.

In Versluis [37] the hydrodynamic pressures were investigated for locks. In the respective study the hydrodynamic pressures were not significantly affected by the second gate (of the closed lock chamber) for $L > 4 \cdot h$. For larger lengths, the lock chamber could thus be considered infinite. For the maximum water level north of the pump gate (7.2 m), this is about equal to the sluice length at that side. The model domain is therefore limited to a single infinitely long sluice, excluding any interaction between adjacent sluices. Whether this assumption remains valid with the effect of surface wave and the pumps included, should be checked. An overview of the model domain in the vertical space is given in figure 4.11.
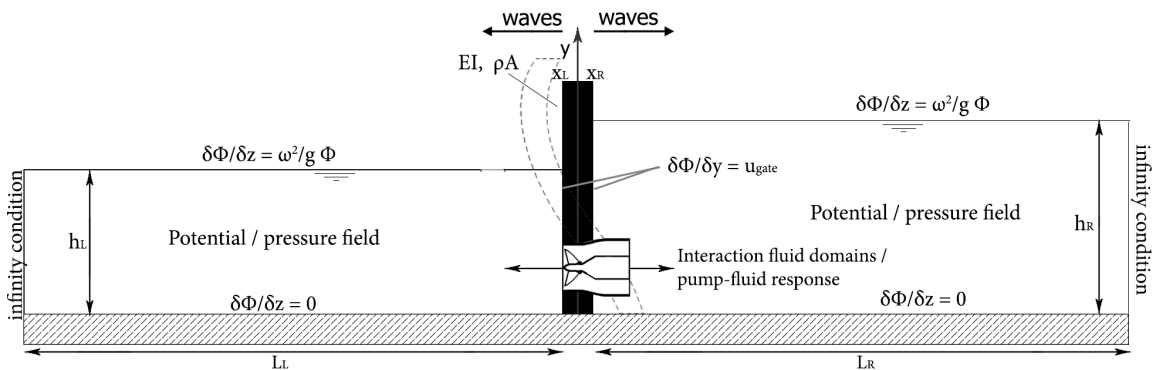
Figure 4.11: Vertical model space representing the three dynamic domains that influence each other: the gate, fluid and pumps. The sluice is considered infinitely long. Boundary conditions for the fluid domain when described by potential flow have been included.

The coming three chapters together form the research analysis in this report. This includes two models based on the mentioned semi-analytical method:

- Beam model (chapter 5)
- Plate model (chapter 6)

As mentioned, using an analytical method requires several geometrical simplifications, such as neglecting the pump conduit length. In chapter 7 a numeric validation of the fluid response is therefore made for one frequency case, comparing the results to the plate model.

The two-dimensional beam model especially serves to investigate the effect of the surface waves and compressibility and compare the results with the expressions known from literature. Final conclusions about the response of the pump gate are based on the plate model.

5 | Beam model

In this chapter, a semi-analytical vertical beam model is used to investigate gate vibrations and the involved processes. In section 5.1 and 5.2 this model and the corresponding equations are elaborated, which are generally applicable to (pump) gates in a confined waterway. Subsequently analytical derivations, based on a modal expansion (5.3) of the structure and fluid, are made to deduce a system of equations describing the beam vibrations. An extensive elaboration of these derivations can be found in appendix F.

In section 5.4 the hydrodynamic mass and damping are investigated for the compressible and incompressible fluid, the latter including the effect of surface waves. The structure is considered rigid for this purpose. Results are compared to what is known from existing literature, which was elaborated in chapter 4. Based on the findings, validity ranges for the several fluid schematizations are deduced.

In section 5.5 the beam model is applied to the pump gate designs of Den Oever, including the fluid-pump-structure interaction. This gives a first estimate of the eigenfrequencies and magnitude of vibrations. More accurate quantifications must however be based on the plate model in chapter 6.

5.1   Model description

An analytical method is used to solve the interaction between the fluid and structure. The gate is simplified as a thin beam, which is surrounded by water at both sides to a certain height. In this analytical approach the vibrations of the structure and fluid are described in terms of eigenmodes, which amplitudes are given by modal coefficients and result from the applied force. The behaviour of the fluid is described by potential flow theory. Using the interface condition, the fluid response can be described in terms of structural modal coefficients. This derivation is explained further in section 5.3.

This method has been applied by Tsouvalas and Metrikine [33, 34] to describe the vibro-acoustic behaviour during offshore pile driving. In Tsouvalas et al. [35] it has specifically been applied to a thin bending beam. Mentioned studies focus on high frequency vibrations for which the compressibility modes, but not the surface waves, are of significant importance.

The beam model in this report will be extended to represent the dynamic behaviour of the fluid-beam system over a wide frequency range. As was estimated in chapter 4, for the governing water depths the compressible behaviour of the fluid is expected to play a minor role at wave and pump rotation periods. Mechanisms in the pumps such as vane passage corresponds to higher excitation frequencies and therefore could be in this 'compressibility

Figure 5.1: Model schematization of beam-pump-fluid system in the vertical direction (side view)

range'. The fluid response for this model is determined based on two approaches: the incompressible fluid with surface waves and the compressible fluid without. This is elaborated further in section 5.2.

The model schematization is given in figure 5.1. To represent the pump gates at Den Oever, a certain sill height Δz is included in the model. The sluice bottom level is therefore located at $z = \Delta z$, while the bottom of the gate is at $z = 0$. Since the pump gate has a relatively small contact surface with the sill (see figure 2.14), it is considered to have no rotational resistance. The resultant downward force of the gate is further expected to be sufficiently large to consider the gate supported in translational (y-)direction at the bottom boundary.

The pumps are schematized to be rigidly attached to the gate. The flexural rigidity is assumed not to be affected by the presence of the pumps, as most stiffening elements are not interrupted (see appendix B).

The rigidity provided by supports at both edges of the gate is included by vertically distributed springs. These can not represent the dynamic behaviour of the gate accurately as the response in horizontal direction is of course frequency-dependent as well. This therefore is a crude schematization for the pump gate. This model is used to obtain a first estimate of the relevant processes. More accurate results will be obtained in the three-dimensional model in chapter 6.

A few other simplifications are made in this model:

- Detailed geometry of the pump gate structure, such as the stiffening profiles and pump conduits length, are not included. Secondly, the indirect effect of the induced fluid velocities and pressures on the pumps are not included in the model. In chapter 7 it

is investigated whether this is a reasonable assumption, based on the length of the pump conduits.

- The sluice is schematized as infinitely long (in y-direction, see figure 5.1). This assumption is investigated in section 5.4.2 and in the numeric validation of chapter 7. It is considered valid for most of the investigated frequency range.

- As was discussed in section 4.4 second order effects in the pumps and between the fluid domains at both sides of the gate are neglected. The primary force generated by a change in instantaneous discharge was described in section 4.3.

- Material damping is neglected.

The use of potential flow theory further inherits some fundamental assumptions. It neglects viscous effects and energy dissipation due to friction. The relative significance of this effect depends on the magnitude of other damping terms, which might be low at certain frequencies. Due to the large dimensions of the sluice (in contrast to e.g. detailed pump or pipe flow) the viscous effects are expected to have a limited influence on the global behaviour.

5.2 Governing equations and analytical derivation

The governing equations are directly written in the frequency domain by substitution of the assumed solutions: $w(z,t) = W(z) \cdot e^{i\Omega t}$ and $\Phi(y,z,t) = \tilde{\Phi}(y,z) \cdot e^{i\Omega t}$. As was shown in section 4.1.2, the motion of a thin beam can be described by:

$$EI_z \cdot \frac{d^4 W(z)}{dz^4} - \rho_b \Omega^2 \cdot W(z) = \sum \tilde{q}(\Omega, z) \tag{5.1}$$

Specified to the system schematization given in previous section, this equation can be expanded to:

$$EI_z \cdot \frac{d^4 W(z)}{dz^4} - \rho_b \Omega^2 \cdot W(z) = [H(z-z_1) - H(z-z_2)] \cdot \left(\rho_p \cdot \Omega^2 - c_{pump} \cdot i\Omega \right) \cdot W(z)$$
$$- k \cdot W(z) - q_{f_N}(z) - q_{f_S}(z) - F_{ext}(\Omega, z) \tag{5.2}$$

in which:

EI_z	=	flexural rigidity (in z-direction) [Nm^2]	
W	=	deflection of the structure [m]	
ρ_b	=	beam's weight [kg/m]	
Ω^2	=	frequency of the external forcing [rad/s]	
ρ_p	=	pump's weight per running metre [kg/m]	
$H(z - z_i)$	=	heaviside step function[4]	
k	=	distributed spring stiffness [N/m^2]	
F_{ext}	=	external forcing [N]	
$q_{f_{N/S}}$	=	hydrodynamic forcing (North/South) [N/m]	
c_{pump}	=	distributed pump damping [Ns/m^2]	

The analytical derivations are made as if both fluid mediums are present at the 'positive-y' or northern side of the beam. The fluid of both domains then extents to $+\infty$ and the equations are equal. In equation (5.2) both hydrodynamic contributions are therefore accompanied by a minus sign.

Although it is more conventional to include the inertia force due to the weight of the pumps and the spring force on the left-hand side of previous equation, those are considered as separate forces in the used analytical method. They are therefore not included in the homogeneous equation either.

The boundary conditions of the beam are fairly straightforward. The simply supported bottom results in zero displacement and momentum. The free end of the beam leads to zero momentum and shear force. The boundary conditions are as follows:

$$W(0) = \left.\frac{d^2W}{dz^2}\right|_{z=0} = \left.\frac{d^2W}{dz^2}\right|_{z=L_z} = \left.\frac{d^3W}{dz^3}\right|_{z=L_z} = 0 \tag{5.3}$$

As mentioned, the fluid response is based on two models: a compressible and incompressible response. It is known that for low frequencies the effect of surface effect can be significant, while the fluid acts as incompressible. Towards higher excitation frequencies, the effect of surface waves becomes less while the compressibility of the fluid will start to have a larger effect. At certain transition frequencies, the fluid can possibly be considered both incompressible as without surface waves, which would be the most simple case. This will be investigated further in section 5.4. The division results in different equations of motion and surface boundary condition for both systems as is shown in figure 5.2.

The equations of motion for both the compressible as incompressible fluid were treated in section 4.2.2. The bottom impedance condition and interface condition are equal for both components and given below. The condition at $y = \infty$ states that the solution $\Phi(y = \infty)$ must be finite and no energy may be propagating from infinity.

Closed gate surface: $$\left.\frac{\partial\tilde{\Phi}}{\partial y}\right|_{y=0} = i\Omega W \tag{5.4}$$

---

[4]The heaviside step function $H(z - z_i)$ is simply zero for all z smaller than z_i and equals one above. The statement $H(z - z_1) - H(z - z_2)$ therefore equals one for $z_1 \le z < z_2$, in this case denoting the presence of the pumps between these coordinates.
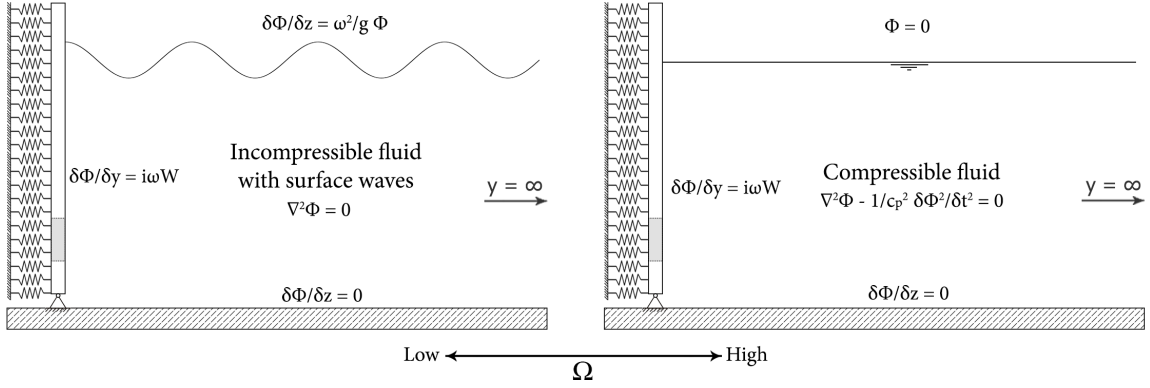
Figure 5.2: The incompressible fluid including surface waves and the compressible fluid response can be superimposed.

Sluice floor:
$$\frac{\partial \tilde{\Phi}}{\partial z}\bigg|_{z=\Delta z} = 0 \tag{5.5}$$

When surface waves are not taken into account, a pressure release boundary condition can be used for the compressible modes.

$$p\big|_{z=h} = -\rho_f \frac{\partial \Phi_c}{\partial t} = 0 \tag{5.6}$$

Substituting the assumed solution $\Phi_c(y, z, t) = \tilde{\Phi}_c(y, z) \cdot e^{-i\Omega t}$, results in the following frequency domain equations:

Equation of motion (compressible):
$$\frac{\partial^2 \tilde{\Phi}_c(z, y, t)}{\partial z^2} + \frac{\partial^2 \tilde{\Phi}_c(z, y, t)}{\partial y^2} + \frac{\Omega^2}{c_p^2} \tilde{\Phi}_c = 0 \tag{5.7}$$

Surface condition (compressible):
$$-\rho_f \cdot \Omega i \cdot \tilde{\Phi}\big|_{z=H} = 0 \quad \leftrightarrow \quad \tilde{\Phi}\big|_{z=H} = 0 \tag{5.8}$$

When free surface waves will be taken into account, there will be a surface elevation above still water level. This elevation is named η and is superimposed on the mean water level H. The following linearised conditions then apply at y = H:

$$\frac{\partial \tilde{\eta}}{\partial t} = v_y = \frac{\partial \tilde{\Phi}}{\partial y} \tag{5.9}$$

$$\frac{\partial \tilde{\Phi}}{\partial t} + g\tilde{\eta} = 0 \tag{5.10}$$

Combining these equations results in the free surface condition:

$$\frac{\partial^2 \Phi}{\partial t^2} + g\frac{\partial \Phi}{\partial y} = 0 \tag{5.11}$$

Substitution of the steady state solution into this equation results in the following conditions:

Equation of motion (incompr, surface waves):
$$\frac{\partial^2 \tilde{\Phi}_{in}}{\partial y^2} + \frac{\partial^2 \tilde{\Phi}_{in}}{\partial z^2} = 0 \tag{5.12}$$

Surface condition (incompr., surface waves): $\qquad \dfrac{\partial \tilde{\Phi}_{in}}{\partial z}\bigg|_{z=h} = \dfrac{\Omega^2}{g} \cdot \tilde{\Phi}_{in}(z = H)$ (5.13)

When both incompressibility and surface waves are included, the surface condition for the incompressible wave schematization should be combined with the compressible equation of motion. Derivations are similar for all three schematizations, which is elaborated in next section.

5.3 Modal expansion

As was stated in section 5.1, with the so called coupled modal analysis method used, both the motion of the structure and the response of the fluid are expanded into eigenmodes. These modes must comply to the boundary conditions. The modal coefficients of the fluid modes are subsequently described in terms of the modal coefficients of the structure. This finally leads to a system of analytical equations including the external forcing, which can be solved for the structural modal coefficients. Summarizing, the following steps are taken in the derivation:

- Expressing the displacement of the structure in terms of an infinite summation of modal shapes and coefficients found for the homogeneous structural equation of motion;
- Expressing the fluid response in terms of (its own) modal shapes and coefficients;
- Using the interface condition (eq. 5.4) to express this fluid response in terms of the structural coefficients;
- Substitution of the found expressions into the forced equation, obtaining an analytical system of equations with the modal coefficients as the only unknowns;
- Solving the system of equations for each (modal) external force amplitude and frequency.

5.3.1 Structural and fluid modes

In appendix F.2 the eigenmodes of the 'simply-free' unforced beam are derived. The pumps weights and springs are not included in determination of these modes. Instead, these forces are implemented as 'external' forces in the forced equation. The bending beam modes are given by:

$$W_m(z) = A_m \cdot \left[sinh(\beta_m z) + \frac{\sinh(\beta_m L_z)}{\sin(\beta_m L_z)} \cdot sin(\beta_m z) \right], \qquad \beta_m = \frac{(m + \frac{1}{4}) \cdot \pi}{L_z} \qquad (5.14)$$

The eigenfrequencies of the determined theoretical beam modes, directly follow from the definition of β_m:

$$\beta_m^2 = \left[\frac{(m+\frac{1}{4})\cdot\pi}{L_z}\right]^2 = \omega_m\sqrt{\frac{\rho_b}{EI_z}} \quad\leftrightarrow\quad \omega_m = \left[(m+\frac{1}{4})\cdot\pi\right]^2\cdot\sqrt{\frac{\rho_b}{EI_z\cdot L_z^4}} \tag{5.15}$$

In the analysis the rigid body mode must be included as well, which corresponds to an eigenfrequency of zero (as no springs are included yet). These and the first few bending modes are shown in figure 5.3. In figure 5.13 an example is shown of how these these individual beam modes will form the final solution.
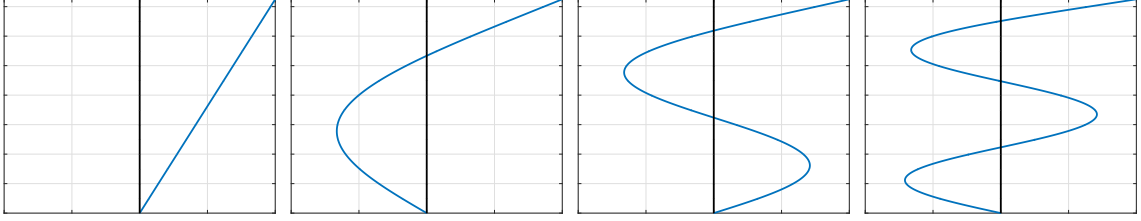
Figure 5.3: The rigid body and first few bending beam modes. The deflection of the beam is a summation of these - theoretically infinite number of - eigenmodes.

In appendix F.3 the fluid's incompressible wave modes and compressible modes are derived. Since both fluid schematizations, incompressible with surface waves and compressible, are investigated separately in section 5.4, the fluid equations are derived separately below as well. The full solution, which is similar, is stated after.

The total fluid response is described as a summation of the multiplied modes in z- and y-direction. In case of the incompressible fluid with surface waves, the solution is as follows:

$$\tilde{\Phi}_{in} = \sum_{p=1}^{\infty} B_p Z_p(z)Y_p(y) = \sum_{p=1}^{\infty} B_p\cdot\cos(k_{z,p}\cdot(z-\Delta z))\cdot e^{-ik_{y,p}y} \tag{5.16}$$

With Δz the sill height and $k_{y,p}$ given by:

$$\Omega^2 = gk_y\cdot\tanh(k_y h) \tag{5.17}$$

The boundary condition at infinity requires (see note[5]):

$$\text{Re}(k_{y,p}) \geq 0 \tag{5.18}$$

$$\text{Im}(k_{y,p}) \leq 0 \tag{5.19}$$

And $k_{z,p} = k_{y,p}i$. In appendix F.3 the system is split into a real and imaginary part as it is known that one propagative wave mode ($k_{y,p}$ = real) and an infinite number of evanescent

---

[5]Obeying these requirements, for real values of $k_{y,p}$ the solution is propagating in positive-y direction: $Y(y) = e^{-i(+k_{y,real})\,y} = e^{-ik_{y,real}\,y}$. Imaginary values lead to a decaying solution in positive-y direction and thus obey the requirement of finite energy at infinity: $Y(y) = e^{-i(-k_{y,imag}i)y} = e^{-k_{y,imag}\,y}$.

modes (see figure 5.4) will exist. To maintain a clear similarity with the compressible fluid modes, the equations above are written as is.
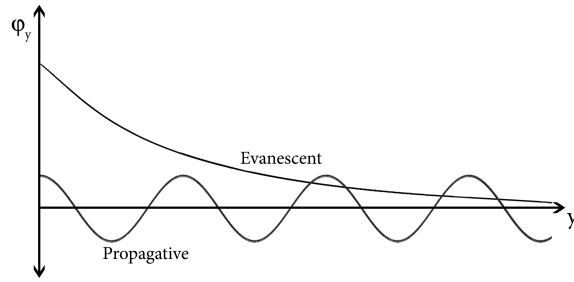
Figure 5.4: Propagative versus evanescent potential in y-direction

As can be seen in figure 5.5 and 5.6, the propagative mode in y-direction corresponds to a cosine hyperbolic shape in z-direction. This is well known from linear wave theory. In the particular figures, all shapes are normalized to have a value of 1 at the free surface. Comparing figure 5.5 to 5.6, showing the modes at radial frequencies of 1 and 5 rad/s respectively, it can be seen clearly that the relation between the value at the free surface and the rest of the shape is strongly frequency-dependent. As the fluid modes depend on h, the modes are different for both sides of the gate.
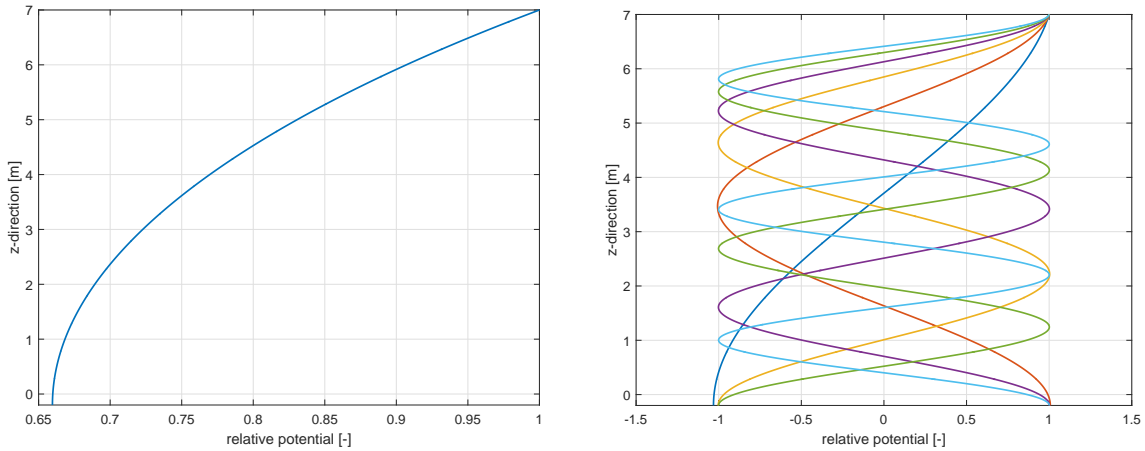
Figure 5.5: Propagative (left) and first few evanescent (right) modes of the fluid at $\Omega = 1$ rad/s and $h = 7.2$

The potential of the compressible system is given by:

$$\tilde{\Phi}_c = \sum_{t=1}^{\infty} C_t Z_t(z) Y_t(y) = \sum_{t=1}^{\infty} C_t \cdot \cos(k_{z,t} z) \cdot e^{-ik_{y,t} y} \tag{5.20}$$

With

$$k_{z,t} = \frac{(2t-1) \cdot \pi}{2h} \qquad \text{for: } t = 1, 2, .., \infty \tag{5.21}$$

$$k_{y,t} = \pm \sqrt{k_f^2 - k_{z,t}^2} \tag{5.22}$$

$$k_f = \frac{\Omega}{c_p} \tag{5.23}$$
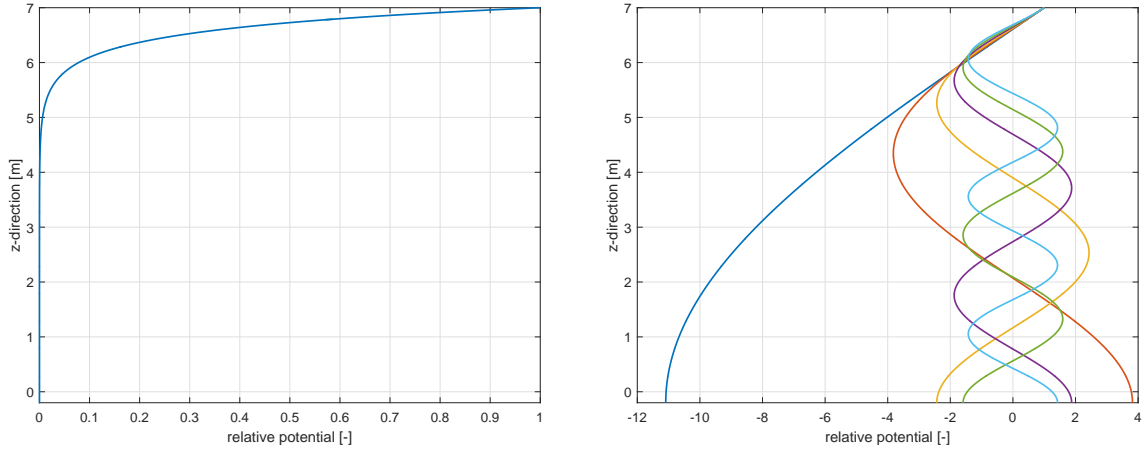
Figure 5.6: Propagative (left) and first few evanescent (right) modes of the fluid at $\Omega = 5$ rad/s and $h = 7.2$

The boundary condition at infinity, which states finite and no negatively propagating energy, then requires:

$$\text{Re}(k_{y,t}) \geq 0 \tag{5.24}$$

$$\text{Im}(k_{y,t}) \leq 0 \tag{5.25}$$

In this case the real values of $k_{y,m}$ again represent propagative modes while imaginary values result in evanescent modes. In contrast to the incompressible case when only one propagative mode was present, with the incompressible no or multiple propagative modes may exist depending on the excitation frequency (at a given water depth). Similar to the incompressible case, an infinite number of evanescent modes will exist. This will be further elaborated in section 5.4. Whether propagative or evanescent, all modes are simply cosine functions for the compressible case with zero surface pressure.

From the compressible and incompressible solutions above, it can be seen that for high frequencies surface waves and for low frequencies the effect compressibility indeed become insignificant. In figure 5.6 it is shown that the average pressure of the propagative wave mode diminishes for higher frequencies and that the surface pressure goes to zero in comparison to the pressures over the total water column. In turn, for low frequencies k_f^2 becomes very small and thus $k_{y,p}$ becomes the compressible solution ($\sqrt{-k_{z,p}^2}$).

The fluid response including both compressibility and the effect of surface waves, combines previous solutions and is as follows:

$$\tilde{\Phi}_p(x,y,z) = \sum_{p=1}^{\infty} B_r \cos(k_{z,p} \cdot (z - \Delta z)) \cdot e^{-ik_{y,p}y} \tag{5.26}$$

With the following constants:

$$\Omega^2 = -gk_{z,p} \cdot \tan(k_{z,p}h) \tag{5.27}$$

$$k_{y,p} = \pm\sqrt{k_f^2 - k_{z,p}^2} \tag{5.28}$$

The same conditions for the positive and negative $k_{y,p}$ apply as stated for the separate systems.

5.3.2 Forced system of equations

Using the interface condition (5.4), the modal coefficients (B_p) of the fluid can be written in terms of those of the beam. For this derivation, the orthogonality of the fluid modes is used. The fluid pressure is written for the incompressible summation of modes, which series is denoted by p, but is identical for the compressible case.

$$p_f(y = 0, z) = i\Omega^2 \rho_f \sum_{m=1}^{\infty} A_m \sum_{p=1}^{\infty} \frac{Q_{mp}}{k_{y,p}\Delta_p} Z_p(z) \tag{5.29}$$

in which:

$$Q_{pm} = \int_0^H Z_p(z)W_m(z)dz \tag{5.30}$$

From equation (5.29) it can be seen that the evanescent fluid modes, which correspond to an imaginary value of $k_{y,p}$ (or $k_{y,p}$), result in a real value for the fluid pressure. In that case the fluid pressure can be considered as an added mass (or stiffness). The propagative modes result in an added damping, which is expected as they carry energy away from the structure. This is further elaborated in section 5.4.

The forced equation is now written with the structural modes and expression for the fluid pressures included. It is further used that each of the modal shapes complies to the homogeneous beam equation. In appendix F.4 and F.5 this is further elaborated. Finally, the forced equation is multiplied by another beam mode. Due to the orthogonality of the beam modes, the forced equation simplifies to the following system of linear equations:

$$\sum_{m=1}^{\infty} \left[\left(\rho_b \cdot (\omega_m^2 - \Omega^2) + k^*\right) \cdot \delta_{mn} \cdot \Gamma_n + Z_{N,mn} + Z_{S,mn} - I_{mn} + P_{mn} \right] \cdot A_n = F_n \tag{5.31}$$

Fluid impedance (north/south):
$$Z_{N,mn} \text{ or } Z_{S,mn} = i\Omega^2\rho_f \sum_{p=1}^{\infty} \frac{Q_{mp}Q_{pn}}{k_p\Delta_p} \tag{5.32}$$

Pump intertia:
$$I_{mn} = \rho_p \cdot \Omega^2 \cdot \int_{z_1}^{z_2} W_m(z) \cdot W_n(z)\, dz \tag{5.33}$$

Pump damping:
$$P_n = c_{pump} \cdot i\Omega \cdot \int_{z_1}^{z_2} W_m(z) \cdot W_n(z)\, dz \tag{5.34}$$

Modal force:
$$F_n = \int_0^{L_z} F_{ext}(z,\Omega) \cdot W_n(z)\, dz \tag{5.35}$$

The integral Q was defined in equation (5.30). These, and the values for k_p and Δ_p are of course different for the northern and southern fluid body.

The term between brackets on left-hand size of equation (5.31) results in a coupled $m \times m$ matrix. The modal coefficient for each modal shape n (or m) results from dividing the modal force by this matrix: $A(\Omega) = F/M(\Omega)$. The beam inertia terms and spring stiffness results in diagonal matrices, as can be seen from the δ_{mn} term in (5.31). The pump intertia, damping and fluid involve coupling terms. An example of this system of equations this matrix, only including the fluid and beam inertia terms, is shown below:

$$
\begin{bmatrix} \rho_b \cdot (\omega_1^2 - \Omega^2) & 0 & 0 \\ 0 & \ddots & 0 \\ 0 & 0 & \rho_b \cdot (\omega_m^2 - \Omega^2) \end{bmatrix} \begin{bmatrix} A_1 \\ \vdots \\ A_m \end{bmatrix} +
$$
$$
i\Omega^2 \rho_f \sum_{p=1}^{\infty} \left(\begin{bmatrix} \frac{Q_{1,p}Q_{1,p}}{k_p\Delta_p} & \cdots & \frac{Q_{1,p}Q_{n,p}}{k_p\Delta_p} \\ \vdots & \ddots & \vdots \\ \frac{Q_{m,p}Q_{1,p}}{k_p\Delta_p} & \cdots & \frac{Q_{m,p}Q_{n,p}}{k_p\Delta_p} \end{bmatrix} \right) \begin{bmatrix} A_1 \\ \vdots \\ A_m \end{bmatrix} = \begin{bmatrix} F_1 \\ \vdots \\ F_m \end{bmatrix} \tag{5.36}
$$

In the fluid impedance matrix , the non-diagonal terms represent the fluid pressure exceeded on the specific mode as a result of the motion of all other structural eigenmodes. The fluid pressure induced by each mode, is in turn a summation of all excited fluid modes.

Due to the pump and fluid damping, the matrix M and thus also the modal coefficients are complex. The complex response amplitude is given by:

$$
\tilde{W}(z, \Omega) = \sum_{m=1}^{\infty} A_m \cdot W_m(z, \Omega) \tag{5.37}
$$

The absolute amplitude is subsequently given by $\hat{W}(z, \Omega) = \sqrt{\mathrm{Re}(\tilde{W}) + \mathrm{Im}(\tilde{W})}$.

To evaluate the found solution, the two infinite series should be truncated. In this m and n represent the structural series of eigenmodes and p the fluid modes. This truncation introduces an error. In case of the structural modes this decision can be based on the frequency range of the external force compared to the eigenfrequencies of the system. The amount of evanescent fluid modes to include, is less straightforward. In Tsouvalas et al. [35] this is investigated and it was concluded that the average displacement error is larger than 10% when 20 or less evanescent modes are considered and becomes less than 1% when more than 80 evanescent modes are included. For the number of fluid modes, 80 is therefore chosen initially.

As can be seen from equation (5.36), the size of the system of equations that should be solved, depends only on the amount of structural modes included. In first instance, 20 structural modes are deemed sufficient. The energy that each mode contains is expected to decay relatively quickly for higher modes (depending on the excitation frequency). This is checked for the obtained results.

5.4 Hydrodynamic pressures for a rigid horizontally vibrating gate

The system of equations deduced in section 5.3 can be used immediately to solve the entire structure-pump-fluid system. However, in this section the behaviour of the fluid only is investigated. Results are obtained for the two fluid schematizations elaborated in previous sections and compared over a wide range of frequencies and water depths.

A well known expression to determine the hydrodynamic mass for rigid vertical walls is that of Westergaard, which was elaborated in section 4.2.3. The numeric method to give a quick estimation of the hydrodynamic mass given by Kolkman [20] is based on a zero pressure surface and an incompressible fluid. In this section, an analytical solution is derived for the case in which these assumptions apply. The validity of these estimations is investigated and discussed. The gate is therefore considered rigid and without pumps and the fluid response is determined for a unit amplitude.

The sill height Δz is set to zero for this purpose. Furthermore, the fluid is considered at a single side of the beam. The only two parameters that determine the two-dimensional fluid response in that case, are the frequency and water depth. Since only one structural (unit) mode is considered, equation (5.29) and (5.30) reduce to:

$$p_f(y = 0, z) = i\Omega^2 \rho_f \sum_{p=1}^{\infty} \frac{Q_{mp}}{k_{y,p}\Delta_p} Z_p(z) \tag{5.38}$$

in which:

$$Q_{pm} = \int_0^H Z_p(z)dz \tag{5.39}$$

In figure 5.7 and F.3, the hydrodynamic mass and damping are compared for both fluid model schematizations over a wide frequency range (0-1200 rad). These are defined as:

$$m_w(z = 0) = \frac{\text{Re}\left(p_f\left(y = 0, z = 0\right)\right)}{-\Omega^2} \tag{5.40}$$

$$c_w(z = 0) = \frac{\text{Im}\left(p_f\left(y = 0, z = 0\right)\right)}{\Omega i} \tag{5.41}$$

The results are given for the maximum water level at Den Oever of 7.2 metre and $c_p = 1500$ m/s. Three distinct regions can indeed be distinguished:

a. Significant influence of surface waves; $\omega < 8$ [rad/s]
b. Transition region with approximately zero surface
    pressure and incompressible fluid; $8 < \omega < 100$ [rad/s]
c. Significant influence of fluid compressibility. $100 < \omega$ [rad/s]

The pattern of region (b) and (c) is similar to that given in figure 4.7, in which the compressible fluid was compared to the non-compressible case both without surface waves. In

(a) Significant surface waves

(b) Transition region

(c) Significant compressibility
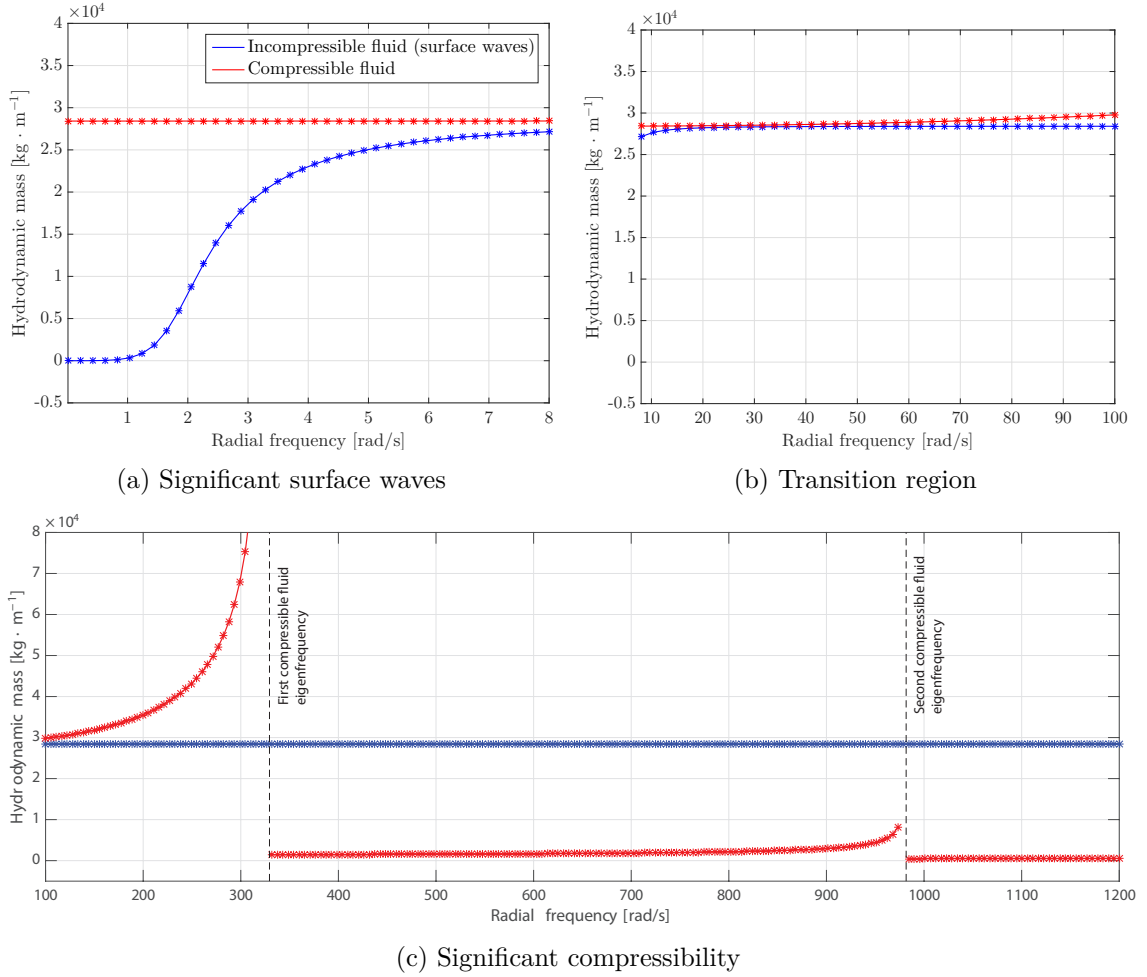
Figure 5.7: The depth-integrated hydrodynamic mass compared for the compressible and incompressible system of equations for a water level of $h = 7.2$ m. Three regions can be distinguished (a,b,c). Note: the frequency axes of the subplots are not equal, as well as the hydrodynamic mass axis of subfigure (c).

this case, the pressures are divided into hydrodynamic mass and damping. From equation (5.38), it can be seen the fluid pressure at the beam's surface becomes infinite for $k_y = 0$. For the compressible fluid this is the case when:

$$k_{y,t} = \sqrt{k_f^2 - k_{z,t}^2} = 0 \tag{5.42}$$

This is the case when $k_{z,t} = k_f$. Substituting the solutions for $k_{z,t}$ and k_f, this can be expressed explicitly in terms of the frequency:

$$\omega_t = \frac{(2 \cdot t - 1) \cdot \pi}{2h} \cdot c_p \tag{5.43}$$

With $t = 1$ and $\Omega = 2\pi/T$, the same expression is obtained for the fundamental compressible eigenperiod of the system as was given in equation (4.25). At each of the frequencies given by equation (5.43), the pressures corresponding to mode t are infinite and change from hydrodynamic mass to damping as k_y goes from an imaginary to a real value. This is shown for the first two eigenfrequencies in figure 5.7 and F.3.

The hydrodynamic damping due to surface waves diminishes to zero for high frequencies as the propagative wave loses its energy and the surface pressure tends to zero. This was demonstrated in section 5.3.1. It must be noted that the hydrodynamic mass going to zero for low frequencies in figure 5.7 is a result of the undistorted beam motion. The integral over the depth of all fluid modes does become zero for (extremely) low frequencies, as each mode becomes negatively symmetric at $h/2$.
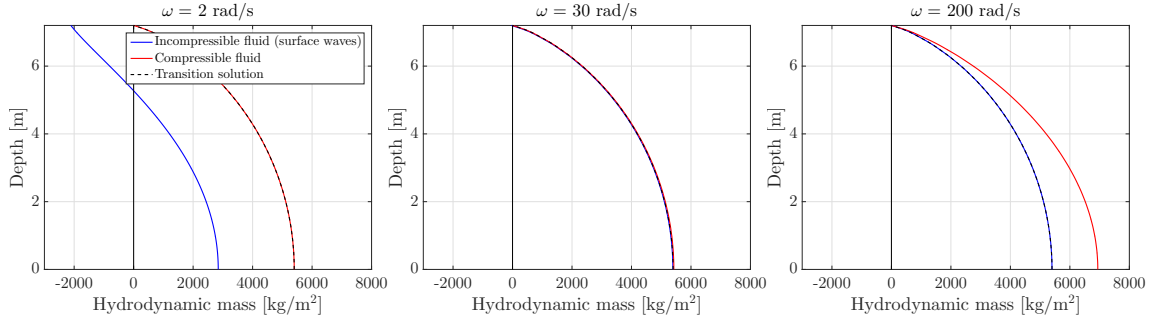
Figure 5.8: Hydrodynamic mass over the depth for three different frequencies, according to the three model schematizations ($h = 7.2$ m)

5.4.1 Analytical solution for the transition region

Modelling the fluid response as incompressible and without surface waves, greatly simplifies the analysis. From equation (5.38) and equation (5.39) an analytical solution can be derived for the hydrodynamic mass in the transition region. As was mentioned before, this becomes frequency independent for zero surface pressure and incompressible fluid.

The integral Q can easily be determined for a structural unit deflection:

$$Q_p = \int_0^h 1 \cdot Z_p(z)dz = \int_0^h cos(k_z z)dz = \left[\frac{1}{k_z}sin(k_z z) \right]_0^h = \frac{1}{k_z}sin(k_z h) \tag{5.44}$$

The $sin(k_z h)$ term simply equals $+1$ for each odd value of p and -1 for each even value, which could be expressed as $-1^{(t-1)}$. The integration constant Δ_p equals $18/5$ for each p. Furthermore in case of incompressibility $k_y = -k_z i$. As in this case only real values of k_z exist, all modes lead to hydrodynamic mass. From above, the analytical expression for the hydrodynamic pressures at the gate's surface over the water depth can be written as:

$$p_f(z) = -\Omega^2 \rho_f \sum_{p=1}^{\infty} -1^{(t-1)} \frac{5}{18 k_{z,p}^2} cos(k_{z,p}z) \qquad \text{with: } k_z = \frac{(2 \cdot p - 1) \cdot \pi}{2h} \tag{5.45}$$

In case one is only interested in the total hydrodynamic mass, the shape must be integrated one more time and the expression simply becomes:

$$m_{w,total} = \rho_f \sum_{p=1}^{\infty} \frac{5}{18 k_{z,p}^3} \tag{5.46}$$

The derived shape differs from the simplified Westergaard shape, discussed in chapter 4, as can be seen in figure 5.9. The damping in the transition region is approximately zero, since the energy of the propagating surface wave has strongly decayed and the first propagative compressible mode is not yet present.
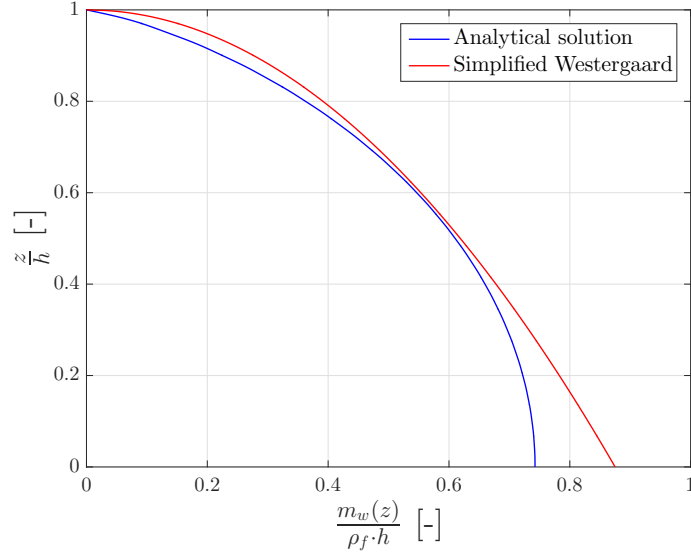
Figure 5.9: Comparison between dimensionless simplified Westergaard shape for incompressible flow and the derived analytical solution for the transition region

It is generally interesting for which combination of frequencies and water depths this approximation is valid and when surface waves or compressibility must be taken into account. The error made when considering the fluid without both is therefore investigated, i.e. the validity of the transition region. For this purpose, the total hydrodynamic mass is considered. Given other uncertainties in the dynamic analysis of such gate systems, a maximum deviation of 5% is deemed acceptable. It is of course possible to determine validity regions for other allowed deviations as well. The error function δ is defined as follows:

$$\delta = \frac{m_{w,total,actual} - m_{w,total,transition}}{m_{w,total,actual}} \tag{5.47}$$

Numerically limit values are evaluated, for which an analytical fit has been made to find expressions that can be generally used. This resulted in the following:

$$6.47 \cdot \sqrt{\frac{g}{h}} < \omega < 0.313 \cdot \frac{c_p \cdot \pi}{2h} \tag{5.48}$$

The lower limit is due to the deviation that results from not including surface waves, while the upper is due to the neglect of compressibility. An overview of the results is shown in figure 5.10.

As can be seen, for the water depths at Den Oever the transition region schematization is valid from approximately 10 to 105 rad/s. With wave excitations below this range (approximately 0.5 to 3.5 rad/s) and possible pump excitations from in and above this
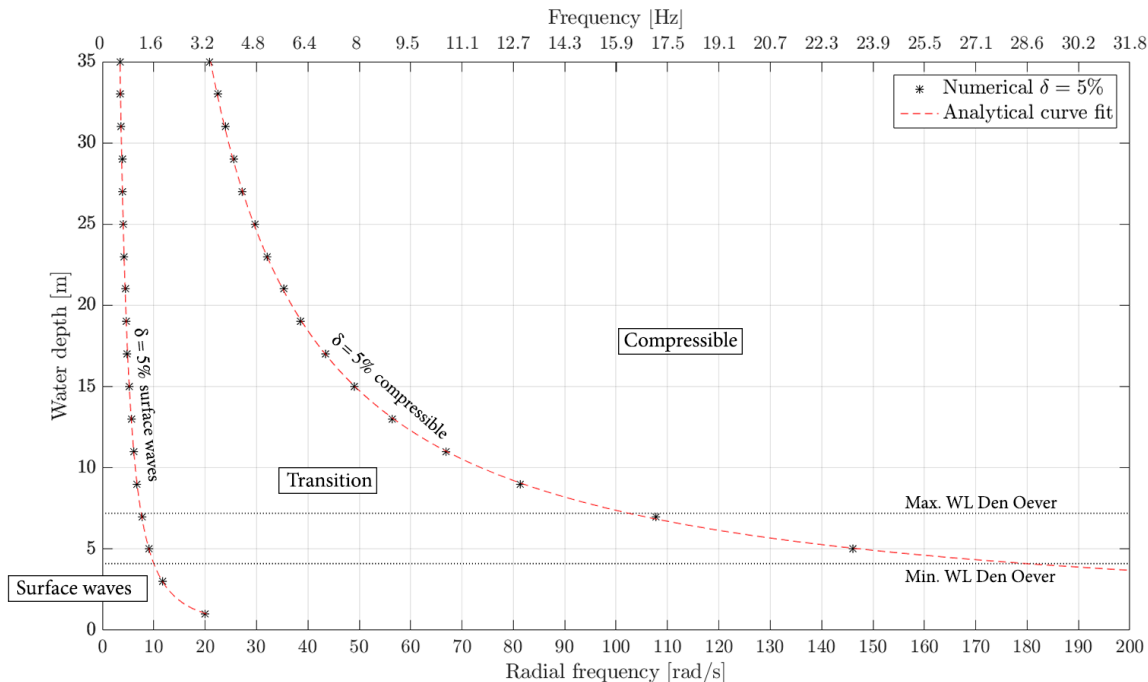
Figure 5.10: Frequency and water depth regions for which surface waves and compressibility play a role for the two-dimensional fluid system. The line on the left indicates a 5% deviation of the total hydrodynamic mass when not including surface waves, while the line on the right indicates 5% deviation when not including the compressibility of the water. The dotted lines indicate the minimum and maximum water level at Den Oever.

region (4.5 to 500 rad/s), both surface waves and compressibility must be included in the analysis.

The validity regions can be used to obtain a quick indication of which methods or expressions from literature may be used in case of a two-dimensional schematization with a closed bottom boundary and free surface. The numeric scheme presented by Kolkman [20] is only valid for the transition region, as it neglects both compressibility and surface waves.

5.4.2 Influence of limited sluice length

In the used analytical method, the sluice was extended to infinity. In reality the sluice length will of course be limited, which may affect the hydrodynamic mass. In case of Den Oever, the length at the Waddensea side is approximately 28 metres, about four times the maximum water depth. As was mentioned in section 4.2, Versluis [37] investigated the hydrodynamic pressures for closed lock reservoirs and concluded that a limited lock length did not have a significant effect for $L > 4 \cdot h$.

Based on the simple equations describing the hydrodynamic mass for the transition region, an estimation is made of the effect of a limited sluice length. In that case k_y is given by:

$$k_{y,p} = -\frac{(2 \cdot p - 1) \cdot \pi}{2h} \cdot i \tag{5.49}$$

And a corresponding solution for the potential in y-direction of:

$$Y_p(y) = e^{-k_{y,p} \cdot y} \tag{5.50}$$

The first mode will result in the lowest value of $-k_{y,p}$ and thus the slowest decay of the potential. In case of $L = 4 \cdot h$ the solution at the end of sluice has decayed to the following value:

$$Y_p(y) = e^{-\frac{\pi}{2h} \cdot 4h} = e^{-2\pi} = 0.0019 \tag{5.51}$$

In other words: the fluid potential at a distance of four times the water depth has reduced to 0.19% compared to that at the gate's surface. At $L = 2h$ the potential has decayed to approximately 5%. When the sluice no longer confines the fluid (at its end), pressures disperse and therefore likely decay faster. Based on above estimation the influence of the limited sluice length can be neglected for the transition region for sluice length above approximately two to four times the water depth.

For frequencies increasing towards the first fluid eigenfrequency, $k_{y,p}$ grows towards zero. At that point the fluid pressures become infinite (according to the theoretical model) and there is no decay of the potential. A further increase of excitation frequency results in positive values of $k_{y,p}$ and thus propagative modes. The limited sluice length can therefore have an effect on the hydrodynamic pressures in when compressibility becomes significant. As a start an infinite half space could be modelled at the end of the sluice to estimate this effect. This is however not investigated further in this thesis.

For the lower wave frequency range the evanescent values of $k_{z,p}$ and thus $k_{y,p}$ increase to $p \cdot \pi / h$ (see figure F.2) and thus the potential decreases faster in y-direction. The propagative mode does not decay and can therefore be affected by the geometry change at the end of the sluice. Especially the reflection of waves could change the behaviour of the generated pressures significantly.

5.5 Analysis of the Den Oever pump gate

In section 5.3.2 the forced system of equations was derived. Although the vertical beam representation of the pump gate is too simplified for final results, some estimations are made in this chapter. The analysis is limited to the regular pump gate design.

5.5.1 Parameters

In table 5.1 the parameters that describe the gate are shown. The isotropic bending stiffness of the gate per running metre was elaborated in section 2.4 and is multiplied by the gate's width or height to obtain the total flexural rigidity shown in table 5.1. The weight of the gate is considered distributed equally over its height.

Table 5.1: Mass and flexural rigidity of both gate designs

Variable	L_x [m]	L_z [m]	Δz [m]	ρ_{b_y} [kg/m]	EI$_{xx}$ [Nm^2]	EI$_{zz}$ [Nm^2]
Regular pump gate	12.5	7.25	0.2	2505	$2.51 \cdot 10^9$	$1.46 \cdot 10^9$

The pumps are simplified as square with the following dimensions and (vertically) distributed weight:

- Square pumps: $1.8 \cdot 1.8$ m^2;
- Distributed pump weight ρ_p: $3 \cdot 20,000/1.8 = 33,333$ kg/m.

Flexural rigidities and weight of the gate are given for the total width of the gate. The fluid response should therefore be given for the total width of the sluice, which is 12 metre.

The distributed translation spring stiffness is based on integrated static deflection caused in horizontal direction by a distributed load. For this purpose the gate is considered simply supported at its edges. In that case the deflection is found by solving the static beam equation, which results in:

$$w_{static}(x) = \frac{q\,x^5}{120EI_{zz}} - \frac{q\,x^4 L_x}{48EI_{zz}} + \frac{q\,x^2 L_x^3}{48EI_{zz}} \tag{5.52}$$

The average deflection caused by a distributed load is then:

$$\bar{w} = \frac{\int_0^{L_x} w_{static}(x)\,dx}{L_x} = \frac{qL_x^4}{120\,EI_{zz}} \tag{5.53}$$

The equivalent stiffness to a force summed over the width $(q\,L_x)$ per metre height will then be given by:

$$k^* L_z = \frac{120\,EI_{zz}}{L_x^3} \qquad \leftrightarrow \qquad k^* = 1.24 \cdot 10^7 \quad [\text{N/m} \cdot \text{m}^{-1}] \tag{5.54}$$

It must be noted that this is a crude assumption, while eigenfrequencies are affected significantly by this stiffness. As mentioned, more accurate results will be obtained for the plate model in chapter 6.

Due to the presence of the pumps, the gate interface condition does not apply over the full width of the gate at the height of the pumps. Between z_1 and z_2, the gate motion effective for the fluid is therefore reduced by the relative pump surface: $3 \cdot 1.8/12 \cdot 100 = 45\%$. This is applied by determining the integral Q defined in equation (5.30) with this reduced motion.

5.5.2   Eigenfrequencies of the dry (vertical) pump gate

The eigenfrequencies of the vertical beam without any pumps and springs were determined in section 5.3, as these are used in the modal analysis method. In table 5.2 the first eight eigenfrequencies are shown for the regular pump gate. These eigenfrequencies will no longer

be valid for the total fluid-pump-structure system, but have been determined obtain insight in the relative influence of the fluid.

The pump masses lower the eigenfrequencies of the gate significantly compared to those of a regular gate. This effect is expected to be higher in the horizontal direction.

Table 5.2: The first six structural radial eigenfrequencies for the regular pump gate design, with and without springs and pumps

Regular gate	ω_1	ω_2	ω_3	ω_4	ω_5	ω_6
Beam only (mathematical) [rad/s]	0	294	952	1985	3395	5181
Beam and springs [rad/s]	70	302	954	1987	3396	5181
Beam, pump weight and springs [rad/s]	55	165	615	1127	2197	3194

The first few eigenmodes of the structural system are shown in figure 5.12. For the fourth eigenshape the separate beam only modes that together form this shape are shown in figure 5.13.
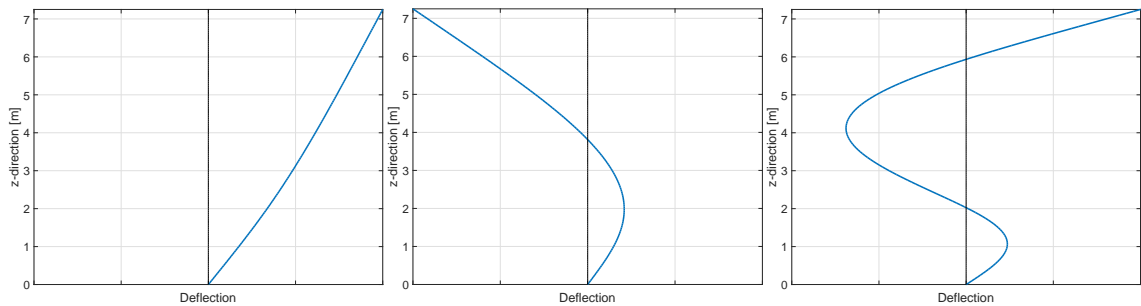
Figure 5.12: First three eigenmode of the dry pump gate including pumps
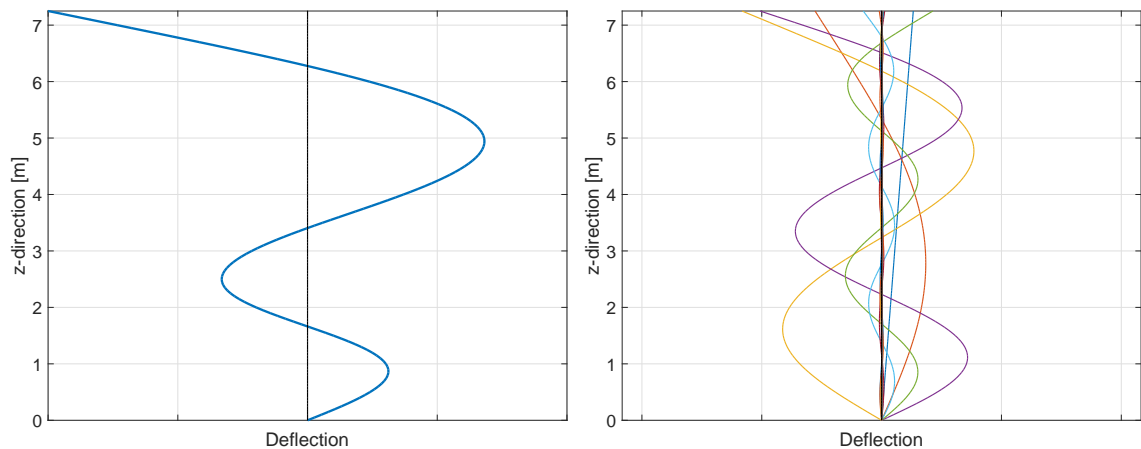
Figure 5.13: The fourth eigenmode of the dry pump gate (left). On the right it is shown how the beam only modes together form this shape.

Without the presence of the fluid, the eigenfrequencies of the system typically lie above the wave frequency range which is in the order of a few rad/s. The first eigenfrequency is still slightly above those of excitations close to the possible range of pump radial velocities as well. Vane passage could already be harmful for these frequencies. The full system is analysed in the following section.

5.5.3 Response to pump forces

Due to the high uncertainties, instead of a pump excitation spectrum an envelope was determined. The maximum force estimated from the pumps is for this purpose ascribed to a single frequency, and subsequently evaluated for each possible frequency. In contrast to the wave spectrum these are thus not force-frequency combinations that happen simultaneously. The response could therefore be determined immediately for each possible pump excitation frequency and corresponding maximum force amplitude. Nevertheless a response function is determined for the pump force as well, as this gives a clear insight in the sensitivity of the structure. In the two-dimensional model, all pump excitation forces being in phase is evidently the governing case.

The response spectra, which are thus the result of a distributed pump load of 1 N/m^2, are given in appendix F.6 (fig.F.4) for the maximum possible water levels. The eigenfrequencies can be clearly distinguished in this response, the first four are shown in table 5.3.

Table 5.3: Eigenfrequencies (in rad/s) found for the 'wet gate' for different water levels compared to those of the dry gate[6]

Case	h_L [m]	h_R [m]	ω_1	ω_2	ω_3	ω_4
Dry gate	0	0	55	165	615	1127
Wet gate	4.1	4.2	41	151	452	566
Wet gate	5.3	7.2	20	101	330	751

The estimated radial velocity of the pumps (18.5 rad/s) is close to the first eigenfrequency of the system (20 rad/s)[7] at maximum water levels. The response spectrum is multiplied by the pump force envelope of figure 3.2 to obtain the quantified response. This results in a envelope for the deflection, which is shown in figure 5.14. Maximum deflection of the gate is in the order of mm's, which is very small compared to its width and height.

When the deflection is multiplied by $\Omega/\sqrt{2}$ velocity rms values are obtained. Furthermore, from the quantified structural deflection, the pressures in the fluid can be determined by equation (5.30). Both results are shown in figure 5.15. It can be seen that for some pump configurations, the ISO velocity hazard limit (see appendix C.5) is reached. It must be noted that these limits are denoted for individual components, and that the simultaneous vibration of the entire pump might have a higher resilience to these vibrations.

The pressure fluctuations at the pump inlet caused by the motion of the gate, are significant as well. A head amplitude of several decimetres, and thus fluctuations of double this value, can have a detrimental effect on the efficiency and may increase the chance of cavitation.

In chapter 6 it will be investigated whether the three dimensional effects of the fluid will increase the pressure fluctuations and what eigenfrequencies are obtained with the more accurate plate model.

---

[6]These eigenfrequencies, based on the two-dimensional model, are a rough indication. Results of the plate model in the following chapter are significantly higher.

[7]The more accurate plate model in the following chapter results in a higher first eigenfrequency.
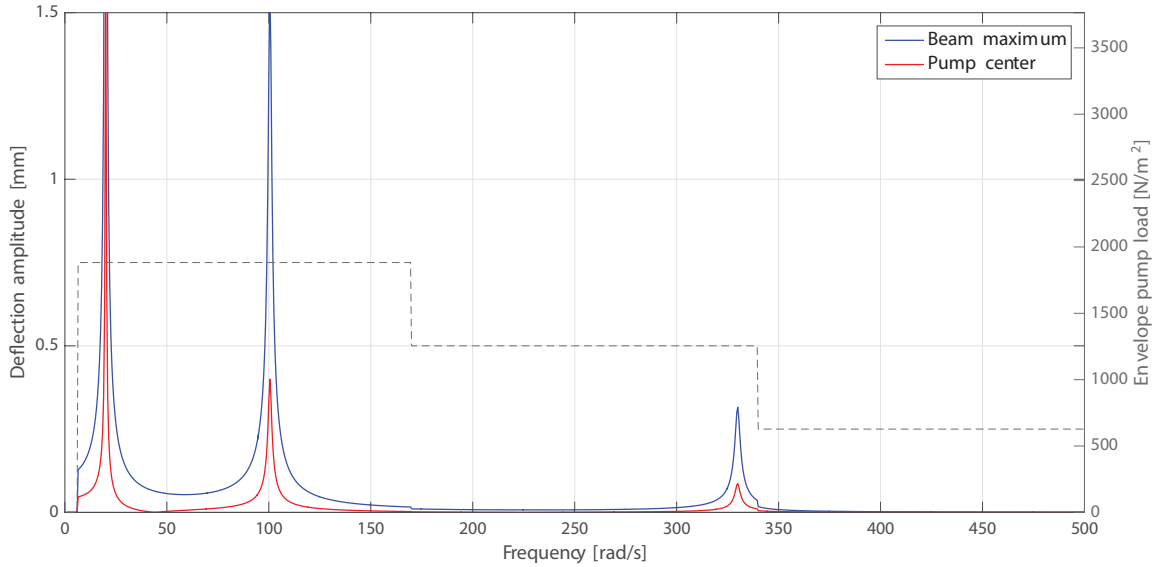
Figure 5.14: Envelope of deflection amplitude at the pump center and for the total beam under a pump force excitation at maximum water levels ($h_S = 5.3$ m, $h_N = 7.2$). The applied pump load per frequency is shown in grey.
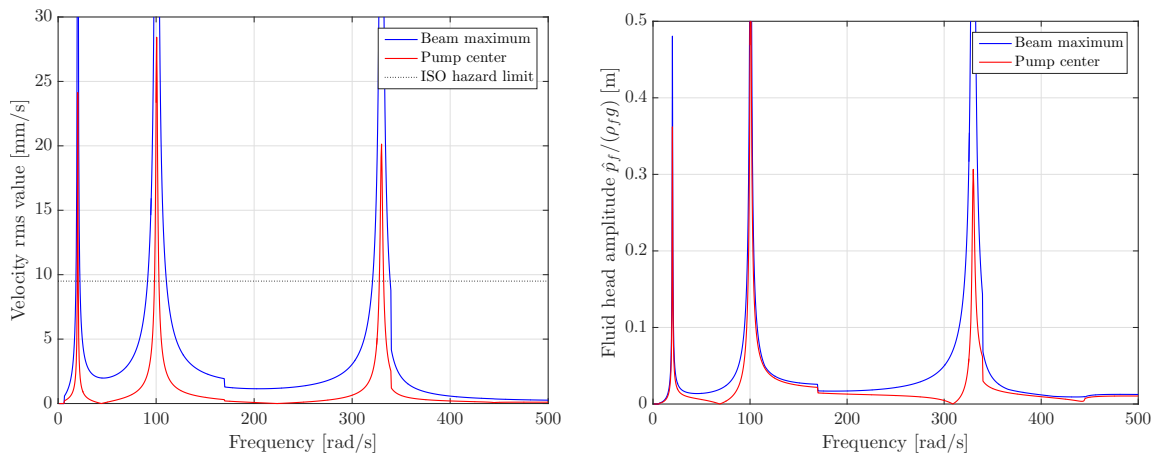
Figure 5.15: Envelope of fluid head amplitude (left) and the velocity rms value (right) at the pump center and the maximum of the total beam under a pump force excitation at maximum water levels ($h_S = 5.3$ m, $h_N = 7.2$).

5.5.4 Response to waves

The response to the wave spectrum is determined differently from above, namely by response amplitude operators. However, the eigenfrequencies (> 20 rad/s) of the regular pump gate are significantly above the typical wave frequencies (<3.5 rad/s).

Secondly. the wave force integrated over the depth diminishes for higher frequencies. This was shown for the responsive propagative wave in figure 5.5 and 5.6, but of course also applies to incoming propagative waves.

The excitation due to waves will therefore be approximately quasi-static. Since corresponding vibration velocities ($\propto \Omega$) and fluid pressures ($\propto \Omega^2$) are relatively low as well, the static

reference design of the pump gate suffices for wave loads. The response to waves is therefore not further researched, and the system is analysed further in chapter 6 for pump forces only.

5.6   Coupling effect of the fluid

In section 4.2 the coupling effect of the fluid was introduced. In case of a discrete system, the motion of one degree of freedom results in pressures effecting (all) other possible motions. In the coupled modal analysis, this coupling of the fluid results in a non-diagonal fluid impedance matrix, of which an example was given in equation (5.36).

In case this coupling could be neglected, the analysis would simplify greatly. For a regular gate (without the pump inertia and damping) the modal coefficient of each mode is then directly given by the derived analytical expressions, without the necessity of solving a coupled system of equations. To estimate the effect of 'decoupling' the influence of the fluid, thus neglecting a part of the generated pressures, the response to a pump excitation force is evaluated based on this simplification. For this purpose, the damping and inertia of the pumps are neglected.
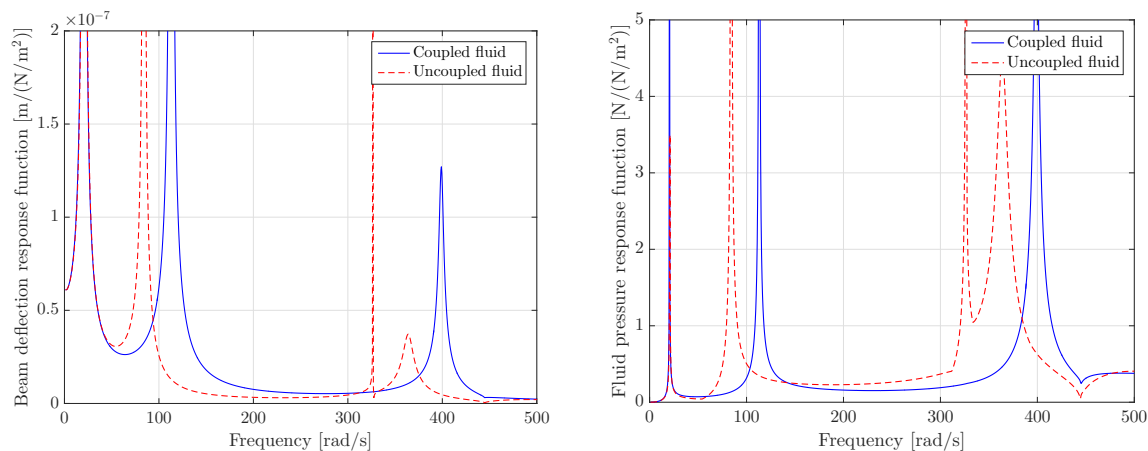
Figure 5.16: Maximum response for the beam schematization without pumps in terms of the beam deflection (left) and fluid pressure (right) to a unit distributed pump load, determined with a coupled and uncoupled fluid impedance

As can be seen in figure 5.16 the response near the first eigenfrequency of the system differs relatively little for the coupled and uncoupled fluid system. For the remainder of the frequency range, the difference is significant.

This could be ascribed to the fact that the beam despite the effect of the fluid, has its first eigenmode close to that of the 'beam only' mode. The magnitude of one of the beam modes is therefore much larger than all other. This is not explicitly quantified for the beam, but is shown in figure 6.4 for the plate model results in the following chapter.

This behaviour can be explained by the increasing importance of the mass inertia (of the plate, pumps and fluid) compared to the flexural rigidity of the gate. Whether the first

or even more eigenfrequencies and shapes of a fluid-gate system (without pumps) can be determined accurately by the uncoupled fluid, is therefore dependent on the ratio between the rigidity of the plate, the mass of the plate and the hydrodynamic mass of fluid. In this behaviour the size of the plate, the plate boundary conditions and the water depth play a role as well. This behaviour will be investigated further.

Based on above, it is recommended to include the coupling motion of the fluid, especially when higher frequency excitations such as those of the pumps in the Den Oever case, play a role.

5.7 Conclusions

A semi-analytical beam model was set-up and used to evaluate the fluid response for a rigid gate and the fully interacting Den Oever pump gate system. It can be concluded that this method is able to efficiently and quickly determine the dynamic response of such a system, taking into account the linear interaction between the structure, fluid and pumps. A plate model based on same method is expected to describe the structural and fluid response more accurately, and is set-up in next chapter.

The validity of different fluid schematizations was tested, based on including or neglecting surface waves and compressibility effects. In the most simple case, where both of these effects are small, the hydrodynamic pressures over the depth can be described by a simple analytical expression equation (5.45). Validity limits for this schematization were determined and shown in figure 5.10.

The semi-analytical method takes into account the coupled fluid impedance. Neglecting this coupled effect would simplify the analysis of the gate. The effect of this decoupling was therefore researched. For the Den Oever regular pump gate design results deviated significantly for frequencies higher than the first eigenfrequency. In general, whether decoupling is allowed depends on the examined frequency range, structural and hydrodynamic mass, and flexural rigidity.

In section 5.5 the beam model was applied to the regular pump gate design at Den Oever. It was concluded that wave excitation plays a subordinate role in the design of the gate as eigenfrequencies of the gate-pump-fluid system lie significantly above the wave frequency range. Pump excitation frequencies can certainly excite some of the eigenfrequencies. This potentially leads to unacceptable vibration velocities of the pumps and fluid pressure fluctuations at its inlet. This is therefore researched further based on the more accurate plate model in next chapter.

6 | Plate model

In this chapter the beam model of the previous chapter is extended to a plate model, based on the same semi-analytical method. The beam model was mainly used to get insight in the fundamental behaviour and compare it to the theoretical expressions. For the plate model, focus will be on the quantification of pump gate vibrations.

In section 6.1 and 6.2 the model and governing equations are described. The forced system of equations is derived in appendix G, which is based on a modal expansion. The result, together with the plate and fluid modes, is elaborated in section 6.3. In section 6.4 to 6.6 the response of the Den Oever gate designs is investigated.

6.1 Model description

In figure 6.1 the plate model domain is shown. Similar to the beam model of chapter 5 the sluice is simplified to extent to infinity.
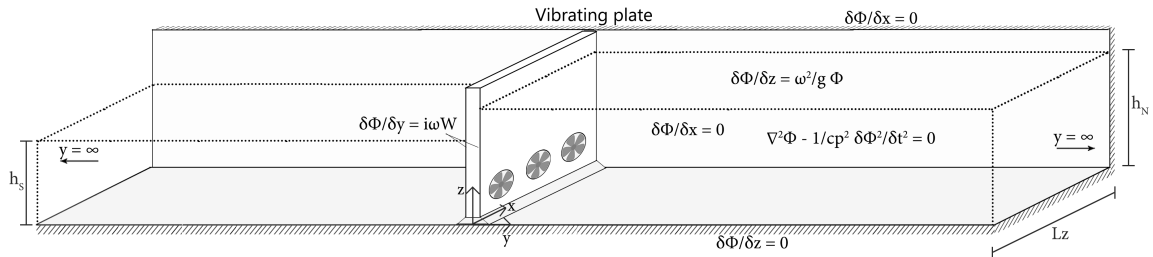
Figure 6.1: Three dimensional overview of the plate model space

The semi-analytical method [33–35] used to determine the plate-pump-fluid vibrations is the same as used for the beam model and is described in chapter 5. The analytical derivations are therefore for a large part similar to - and continued from - those of chapter 5 and appendix F. Based on the conclusions of section 5.4, both the compressibility of the fluid and the effect of surface waves will be included in the model. The associated equations of motion and boundary conditions are given in section 6.2.

The vertical direction is unchanged from the beam model of chapter 5. As is shown in figure 6.1, the fluid is simplified as constraint by the sluice in y-direction to infinity. As was mentioned in chapter 2, the heart to heart distance between the supports of the pump gate is slightly larger (0.5 m) than the width of the sluice. Similar to the offset in z-direction representing the sill, in x-direction at each side an offset of Δx (reduction in sluice width compared to that of the gate) is introduced on each side of the gate. The exact geometry of the gate's vertical edges is unknown in this stage. It has been assumed they behave as

simply supported. The two-dimensional schematization of the gate, representing it as a plate, is shown in figure 6.2.
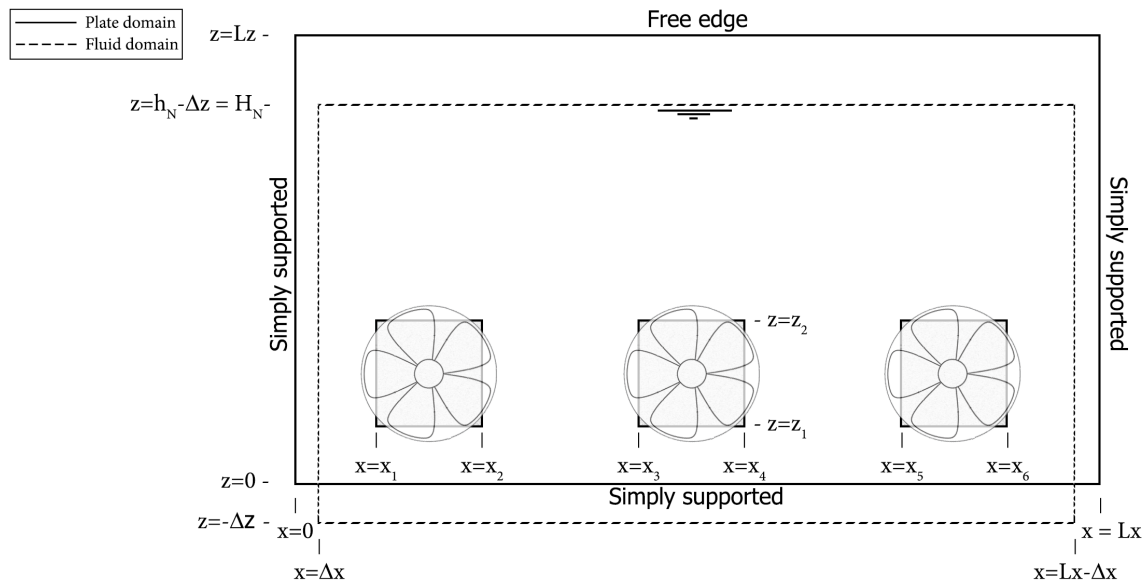
Figure 6.2: Geometrical overview (front) of the plate schematization

The flexural rigidity at the location of the pumps is assumed not to be reduced by the pumps' presence. In appendix B it can be seen that in the design of the flood defence gate, the number of stiffening elements is increased at the height of the pumps. In case of the regular design, most elements are still continuous. Furthermore, the pumps can provide strength as well. The girder elements at the boundaries of the gate are not included in the calculation of the plate's bending stiffness, since the gate is considered rigidly supported in translational direction. The connection between gate and pumps is assumed rigid.

The focus of the analysis is in first instance on the regular pump gate design, as this design is most likely governing. Secondly, this design is approximately isotropic which simplifies the analysis, see equation (6.1). Subsequently, the robuster flood defence gate is investigated to see whether weaknesses can be solved by this design. The input for these designs is further clarified in section 6.4.

6.2 Governing equations

In the three dimensional model, the gate is described two-dimensionally by Kirchhoff-Love plate theory. This, similarly to Euler-Bernouilli to beams, applies to thin plates and small amplitude vibrations. Since the plate is simplified as homogeneous and isotropic, the equation of motion in the time domain becomes ($w = w(x, z, t)$):

$$\rho_s \frac{\partial^2 w}{\partial t^2} + D \cdot \left[\frac{\partial^4 w}{\partial x^4} + 2 \cdot \frac{\partial^4 w}{\partial x^2 \partial y^2} + \frac{\partial^4 w}{\partial z^4} \right] = \sum f(x, z, t) \qquad (6.1)$$

With:

$$D = \frac{t^3 E}{12 \cdot (1 - \nu^2)} \tag{6.2}$$

in which: $\quad D \quad = \quad$ plate bending stiffness $[\text{Nm}^2]$

$\qquad\qquad t \quad = \quad$ plate's thickness $[\text{m}]$

The term $t^3/12$ can be considered as the flexural rigidity of the gate per running metre. It is thus not necessary to determine an equivalent plate thickness. In the frequency-domain (assuming $w(x, z, t) = W(x, z) \cdot e^{i\Omega t}$) this becomes:

$$-\rho_s \Omega^2 \cdot W(x, z) + D \cdot \left[\frac{\partial^4 W(x, z)}{\partial x^4} + 2 \cdot \frac{\partial^4 W(x, z)}{\partial x^2 \partial y^2} + \frac{\partial^4 W(x, z)}{\partial z^4} \right] = \sum \tilde{f}(x, z, \Omega) \tag{6.3}$$

The forces on the right-hand side are mostly equal to those discussed for the beam model, equation (5.2). No springs are present however, and the pump inertia force is now present at three (two-dimensional) locations:

$$\sum \tilde{f}(x, z, \Omega) = \tilde{H}(x, z) \cdot \left[-i\Omega \cdot c_{pump} + \rho_p \cdot \Omega^2 \right] \cdot W(x, z) - F_{f_N}(x, z) - F_{f_S}(x, z) - F_{ext}(\Omega, x, z) \tag{6.4}$$

In which $\tilde{H}(x, z)$ represents the somewhat lengthy combination of step functions denoting the presence of the pump weight:

$$\tilde{H}(x, z) = [H(z - z_1) - H(z - z_2)] \cdot [H(x - x_1) - H(x - x_2)] \cdot \\ [H(x - x_3) - H(x - x_4)] \cdot [H(x - x_5) - H(x - x_6)] \tag{6.5}$$

The three simply supported edges and the free top of the gate result in the following boundary conditions:

$$W(0, z) = \left. \frac{\partial^2 W(x, z)}{\partial x^2} \right|_{x=0} = W(L_x, z) = \left. \frac{\partial^2 W(x, z)}{\partial x^2} \right|_{x=L_x} = 0 \tag{6.6}$$

$$W(x, 0) = \left. \frac{\partial^2 W(x, z)}{\partial z^2} \right|_{z=0} = \left. \frac{\partial^2 W(x, z)}{\partial z^2} \right|_{z=L_z} = \left. \frac{\partial^3 W(x, z)}{\partial z^3} \right|_{z=L_z} = 0 \tag{6.7}$$

In the three dimensional domain the compressible fluid is described by the following equation of motion:

$$\frac{\partial^2 \tilde{\Phi}(x, y, z, t)}{\partial x^2} + \frac{\partial^2 \tilde{\Phi}(x, y, z, t)}{\partial y^2} + \frac{\partial^2 \tilde{\Phi}(x, y, z, t)}{\partial z^2} + \frac{\Omega^2}{c_p^2} \tilde{\Phi} = 0 \tag{6.8}$$

The boundary conditions for the z-direction are equal to the incompressible wave equations used in chapter 5. The closed boundaries for the x-direction are straightforward.

$$\left. \frac{\partial \tilde{\Phi}}{\partial x} \right|_{x=\Delta x} = 0 \qquad\qquad \left. \frac{\partial \tilde{\Phi}}{\partial x} \right|_{x=L_x - \Delta x} = 0 \tag{6.9}$$

$$\left. \frac{\partial \tilde{\Phi}}{\partial z} \right|_{z=-\Delta z} = 0 \qquad\qquad \left. \frac{\partial \tilde{\Phi}}{\partial z} \right|_{z=H} = \frac{\Omega^2}{g} \cdot \tilde{\Phi}(z = H) \tag{6.10}$$

The interface conditions remains as follows:

$$\left.\frac{\partial \tilde{\Phi}}{\partial y}\right|_{y=0} = i\Omega W \tag{6.11}$$

And also the condition at $y = \infty$, which states energy only propagates in positive direction and is finite, remains equal to that of the beam model.

6.3 Modal expansion

6.3.1 Structural modes and fluid modes

The plate modes will be two dimensional, and are therefore described as the product of modes in two directions: $W_{km}(x, z) = W_{x,k}(x) \cdot W_{z,m}(z)$. In this notation, it is anticipated that the solution will be an infinite summation of the multiplication of k modes in x-direction and m modes in z-direction. Equation 6.3 can not be separated into equations for the x- and z-direction directly, as was done with the two-dimensional fluid in chapter 5. A solution for the x-direction, which complies to the boundary conditions at both gate edges, is therefore assumed:

$$W_{x,k}(x) = sin(\beta_k x), \qquad \beta_k = \frac{k\pi}{L_x}, \text{ with: } k = 1, 2, .., \infty \tag{6.12}$$

When this solution is substituted in (6.3), and subsequently divided by $sin(\beta_k x)$, this results in:

$$-\rho_s \omega_{km}^2 \cdot W_{z,m}(z) + D \cdot \beta_k^4 \cdot W_{z,m}(z) - 2D \cdot \beta_k^2 \cdot \frac{\partial^2 W_{z,m}(z)}{\partial z^2} + D \cdot \frac{\partial^4 W_{z,m}(z)}{\partial z^4} = 0 \leftrightarrow$$
$$D \cdot \frac{\partial^4 W_{z,m}(z)}{\partial z^4} - 2D \cdot \beta_k^2 \cdot \frac{\partial^2 W_{z,m}(z)}{\partial z^2} + \left[D \cdot \beta_k^4 - \rho_s \omega_{km}^2 \right] \cdot W_{z,m}(z) = 0 \tag{6.13}$$

For each mode k in x-direction, a homogeneous fourth order differential equation is thus obtained. An infinite number of modes m can be found for each differential equation. These modes will be numerically evaluated with Matlab's *bvp4c* function. In appendix G.1 this is elaborated further. For each m and k, the eigenfrequency ω_{km} is an unknown that is found along with the two-dimensional eigenshape. The first four eigenmodes and corresponding eigenfrequencies are shown in figure 6.3. The total plate deflection is again a summation of these modes:

$$W(x, z) = \sum_{m=1}^{\infty} \sum_{k=1}^{\infty} A_{km} W_{km}(x, z) \tag{6.14}$$

The fluid response includes both compressibility and the effect of surface waves, and is expressed as follows:

$$\tilde{\Phi}_{pr}(x, y, z) = \sum_{p=1}^{\infty} \sum_{r=1}^{\infty} B_{pr} \cos(k_{x,p} \cdot (x - \Delta x)) \cdot \cos(k_{z,r} \cdot (z - \Delta z)) \cdot e^{-ik_{y,pr}y} \tag{6.15}$$
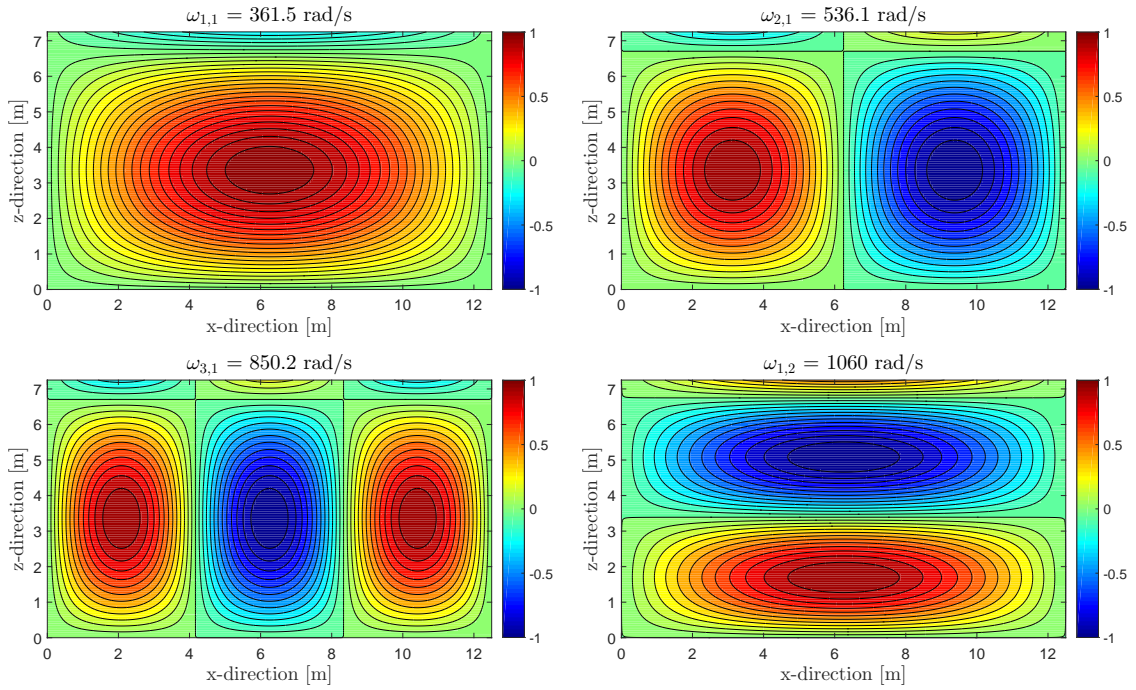
Figure 6.3: The first four numerically evaluated eigenmodes of the plate (without pump weights) for the regular pump gate design. The deflection of each mode is normalised to a unit maximum.

With the following constants:

$$k_{x,p} = \frac{r\pi}{Lx - 2\Delta x} \tag{6.16}$$

$$\Omega^2 = -g k_{z,r} \cdot \tan(k_{z,r}h) \tag{6.17}$$

$$k_{y,pr} = \pm\sqrt{k_f^2 - k_{x,p}^2 - k_{z,r}^2} \tag{6.18}$$

And the following requirement:

$$\text{Re}(k_{y,pr}) \geq 0 \tag{6.19}$$

$$\text{Im}(k_{y,pr}) \leq 0 \tag{6.20}$$

The derivations of these solutions can be found in appendix G.2.

6.3.2   Forced system of equations

In appendix G.3 the boundary condition is used to express the modal coefficient of the fluid (B_{pr}) in terms of those of the beam (A_{km}). At the gates' interface (y = 0), the pressures are then described by:

$$p_f(x, y = 0, z) = i\Omega^2 \rho \sum_{m=1}^{\infty} \sum_{k=1}^{\infty} A_{km} \sum_{p=1}^{\infty} \sum_{r=1}^{\infty} \frac{Q_{km,pr}}{k_{y,pr}\Delta_{pr}} \Phi_{pr}(x, z) \tag{6.21}$$

With:

$$Q_{km,pr} = \iint\limits_{S_W} W_{km}(x,z) \cdot \Phi_{pr}(x,z) \, dx \, dz \qquad (6.22)$$

In which S_W is the gate's wet surface. In appendix G.4, using orthogonality of the plate modes and the fact that they comply to the homogeneous equation, a system of equations is derived for which the modal coefficients can be solved. This system can be expressed as follows:

$$\sum_{k=1}^{\infty} \sum_{m=1}^{\infty} \left[\rho_s \cdot (\omega_{km}^2 - \Omega^2) \cdot \delta_{kl}\delta_{mn} \cdot \Gamma_{ln} + Z_{N,km,ln} + Z_{S,km,ln} - I_{km,ln} + P_{km,ln} \right] \cdot A_{ln} = F_{ln}$$

$$(6.23)$$

Fluid impedance (N/S): $\quad Z_{N,km,ln}$ or $Z_{S,km,ln} = i\Omega^2 \rho_f \sum_{p=1}^{\infty} \dfrac{Q_{km,pr} Q_{ln,pr}}{k_{y,pr} \Delta_{pr}}$

Inertia pumps: $\quad I_{km,ln} = \rho_p \cdot \Omega^2 \cdot \iint\limits_{S} \tilde{H}(x,z) \cdot W_{km}(x,z) \cdot W_{ln}(x,z) \, dx \, dz$

Pump damping: $\quad P_{ln} = c_{pump} \cdot i\Omega \iint\limits_{S} \tilde{H}(x,z) \cdot W_{km}(x,z) \cdot W_{ln}(x,z) \, dx \, dz$

Modal force: $\quad F_{ln} = \iint\limits_{S} F_{ext}(z,\Omega) \cdot W_{ln}(x,z) \, dx \, dz$

The term between brackets on left-hand size of equation (6.23) results in a coupled $(k \cdot m) \times (k \cdot m)$ matrix. The modal coefficient for each two-dimensional shape ln (or km) results from dividing the modal force by this matrix: $A = F/M$.

6.4 Pump gate parameters

The plate bending stiffness was defined in equation (6.2), in which $t^3/12$ represent the moment of inertia per running metre. In section 2.4 and appendix B the flexural rigidity of the gate designs were elaborated. The moment of inertia around the z-axis has been taken as representative for both directions. The investigated designs therewith differ from the reference designs by Witteveen+Bos [40]. The weight has been assumed equally distributed over the gate's surface. It is expected that small deviations in the distribution of this mass have little effect on the total behaviour. Especially since the gate's mass is relatively low to the hydrodynamic and pump mass. The stiffness and weight parameters of both gate designs are repeated in table 6.1.

Table 6.1: Weight and bending stiffness of both gate designs

Parameter	Flood defence pump gate	Regular pump gate
Bending stiffness D [Nm]	$3.0 \cdot 10^9$	$2.0 \cdot 10^8$
Distributed gate weight [kg/m^2]	331	199

The geometrical parameters are equal for both gate designs and given in table 6.2. The definition of these parameters was shown in the plate overview of figure 6.2.

Table 6.2: Geometrical parameters of the gate

Variable	L_x	L_x'	L_z	$-\Delta z$	x_1	x_2	x_3	x_4	x_5	x_6	z_1	z_2
Value [m]	12.5	12.0	7.25	-0.2	1.35	3.15	5.35	7.15	9.35	11.15	0.70	2.50

The eigenfrequencies of the system are elaborated for the regular pump gate design. The response to pump forces is elaborated in most detail for the governing regular design as well. Subsequently, in section 6.6.4 the response of the flood defence gate is treated. After quantification of the response, a reflection of the assumptions and uncertainties this analysis is made in section 6.7.

6.5 Eigenfrequencies of the system

Based on the response to the pump forces in next section, the eigenfrequencies are inventoried. The modal expansion is truncated to 10 structural shapes in each direction, resulting in a total of 100 plate shapes, and 40 fluid modes in each direction, resulting in 1600 fluid potential shapes at the gate's surface.

In table 6.3 the eigenfrequencies are shown for the three design water level combinations stated in section 3.2. As can be seen the first eigenfrequency of the plate at maximum water levels is three times higher than that estimated with the beam model. As was expected the beam model is thus not sufficient to model the behaviour of the gate correctly.

This can firstly be explained by the fact that in the three dimensional the fluid pressures distribute over the width of the sluice. Since the edges of the gate are supported, the fluid is forced less at these locations. This is not included in the beam schematization. Secondly, the estimated stiffness of the edge supports included in the beam model was in-precise and is not valid in a dynamic analysis.

Table 6.3: Eigenfrequencies beneath 500 rad/s of the system for minimum and maximum water levels

Case	h_L [m]	h_R [m]	ω_1	ω_2	ω_3	ω_4	ω_5	ω_6	ω_7	ω_8
Minimum WL's	4.1	4.2	109.5	168.5	174.5	373.5	429.5	>500	>500	>500
Cavitation risk	4.1	6.1	88	146	165.5	319.5	344	405	484.5	>500
Maximum WL's	5.3	7.2	74	128.5	157.5	277.5	317.5	363.5	408.5	493.5

Compared to the beam model, more eigenfrequencies are found in the same range (<500 rad/s). This is a logical consequence of the two-dimensional plate schematization. It is almost impossible to avoid eigenfrequencies above the value of the first eigenfrequency, due to the range of possible water levels. As can be seen in table 6.3, a change in water levels has a large effect on the eigenfrequencies.
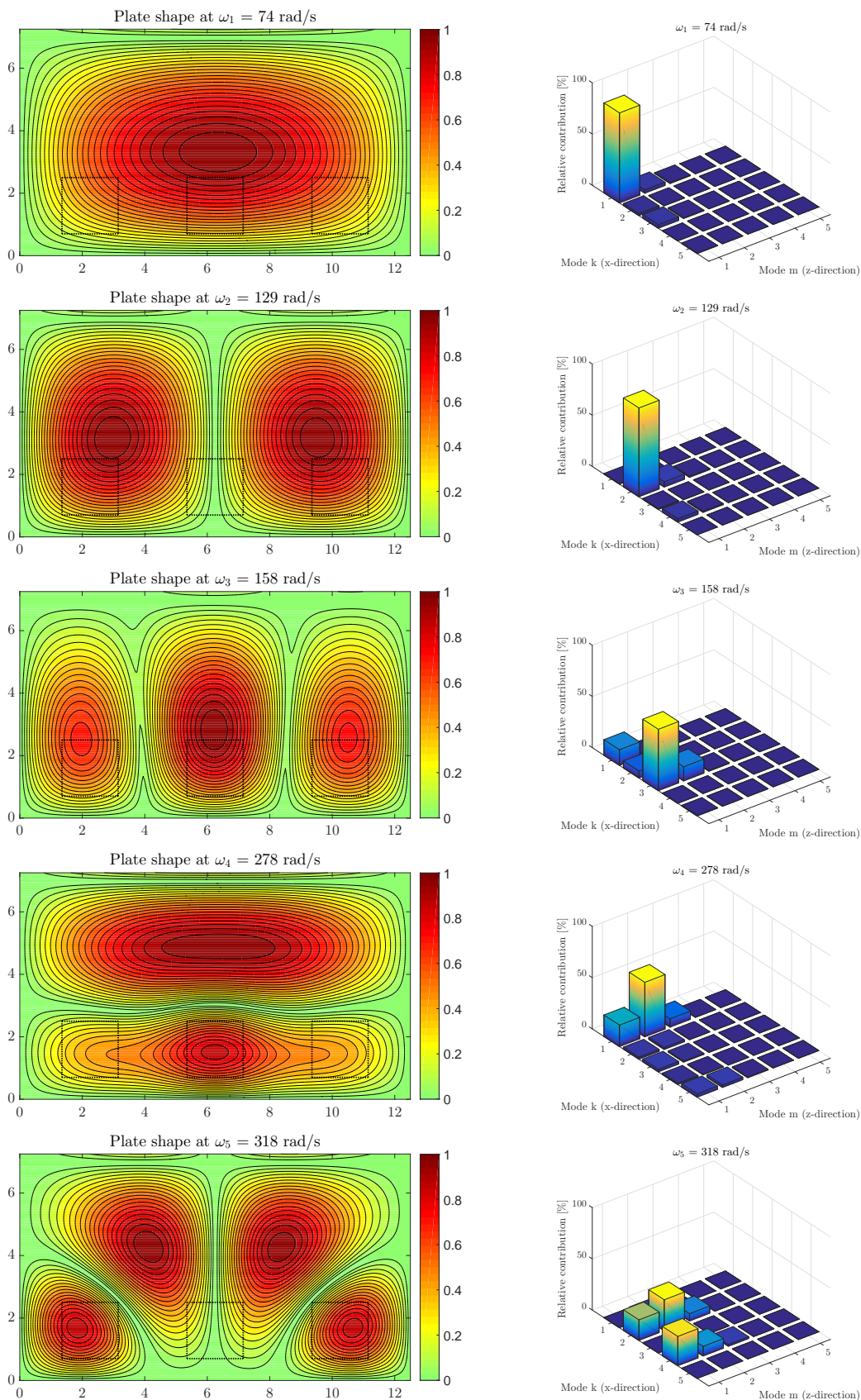
Figure 6.4: The shapes of the plate at the first five (approximate) eigenfrequencies of the structure-fluid system (left) and the contributions of the first 25 'plain' plate shapes (right). In total 100 plate only eigenmodes are used in the analysis.
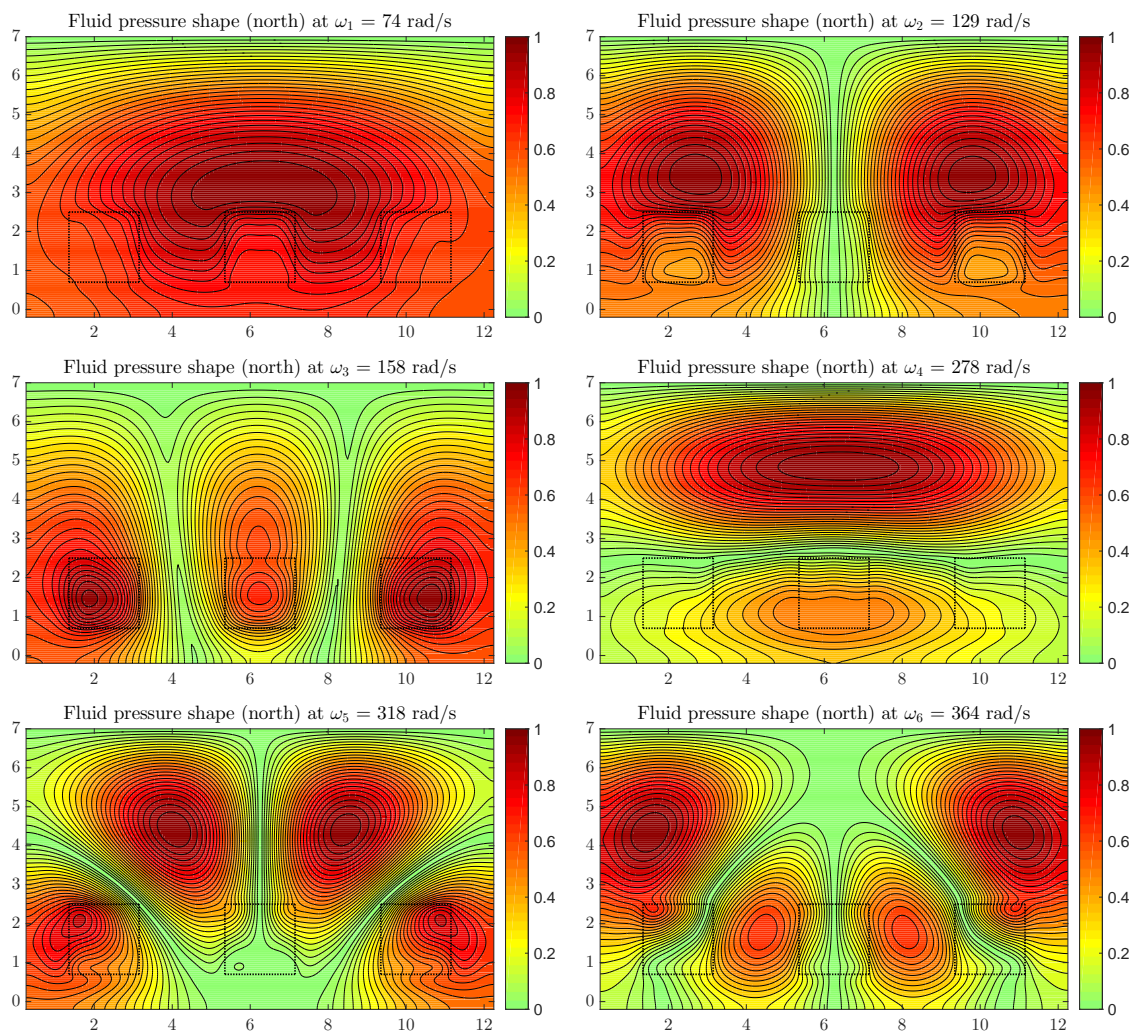
Figure 6.5: The shapes of the fluid pressures at the (northern) gate's surface at the first six (approximate) eigenfrequencies of the structure-fluid system ($h_S = 5.3$ m, $h_N = 7.2$ m). The locations of the pumps, where the interface condition is not applied, are shown in black.

The minimum first system eigenfrequency of 74 rad/s lies sufficiently above the excitations around the pump's radial velocity ($\approx 5 - 40$ rad/s).

When the exact pump specifics are known, excitations will likely only occur at several distinct peak frequencies. However, due the varying water levels, designing the gate such that its resonance frequencies lie in between these excitation frequencies is not viable. Instead, the gate should designed such that effects of these vibrations limited. As energy decays towards higher frequencies, both for the response and pump forcing, a stiffer gate design will be favourable. Secondly, pump forces are highest at high pump heads. Eigenfrequencies at water levels with maximum head difference are therefore most relevant.

The vibration shapes of the plate, normalised to a unit maximum, at the first five peak frequencies are shown in figure 6.4. The relative contribution of each of the homogeneous plate shapes (dry and without pumps) to these eigenshapes, is shown for each of these shapes. For the first two modes, there is still one homogeneous plate mode that governs.

In that case, a rough estimation of the the corresponding eigenfrequency can still be made by only considering one plate mode and determining the fluid response to this mode. The fact that the plate shape changes due to the fluid and pumps is then neglected. This is however not generally recommended as this behaviour depends on the exact case specifics.

The fluid pressure shapes corresponding to the eigenfrequencies are given in figure 6.5. Since eigenshapes of the plate and fluid are only dependent on the system, which is symmetric over its width, these shapes are symmetric or antisymmetric as well.

6.6 Response to pump forces

The response to pump forces was investigated for the vertical schematization in section 5.5.3. In this section, the response is evaluated more based on the more accurate plate model. The pump forces can have phase differences. In case of the plate, except for all forces being in phase, the middle or edge pump can be out of phase with those of the other two pumps. Since the system is symmetric, the response will be symmetric in case of the pump forces are as well. The likelihood of the pump forces actually acting in phase or out of phase, depends whether a so-called lock-in effect may occur. Through a dependency, the vibration of the gate and pumps in of out of phase could then cause the pump forces to act in a similar way.
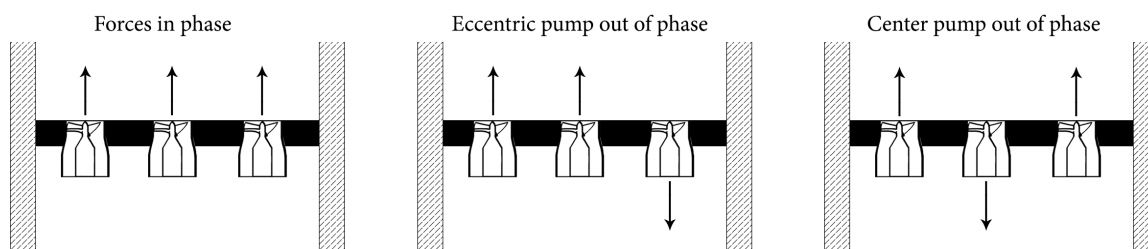
Figure 6.6: The three possibly governing pump force combinations.

Similar to the beam model three response types are investigated, stated below. The latter two will aid in the answer to research question (I.a) of this thesis, the first research question (I.b).

1. Plate's deflection and amplification factor. This is especially relevant to the requirements of the gate itself, which involve fatigue and the forces on the surrounding concrete structure.

2. Pump's vibration velocity, which is relevant to the maintenance and lifetime of the pumps.

3. Pressure fluctuations in the fluid at the pump's inlet, which influences especially the efficiency of the pumps. Excessive head differences may also induce cavitation at low water levels, and therewith lead to the increased damage and required maintenance as well.

Each of these responses may be governing at different water levels and pump force phases. This is reasoned for each of these responses.

In the following subsections the response of the regular pump gate is evaluated. In section 6.6.4 the results for the flood defence gate are summarized and compared.

6.6.1 Plate deflection and stress amplification

With the beam model, it was demonstrated that deflections of the plate are very small. As can be seen in figure 6.7, this is the case with the plate model as well. This is explained by the fact that the estimated pump forces are small compared to the static loads the gate is designed for. With the three pumps in phase, the ratio between the resultant force and the pump force amplitude at maximum water levels is about:

$$r_{\mathrm{F}_{stat}/\mathrm{F}_{dyn}} = \frac{L_x\, L_z\, \rho_f g\, \Delta H_d}{0.1 \cdot 3 \cdot A_p\, \rho_f g\, H_{pump}} = \frac{1724}{17.74} \approx 97 \tag{6.24}$$

In which H_d is the gate's design head of 2 metre and H_{pump} is the pump head, which is 1.9 metre at maximum water levels. Instead of determining the exact stresses in the gate and supports, the amplification of the (maximum) deflection at the first mode is taken as representative. For this mode, the deflection shape is still relatively close to the first plain shape mode (see figure 6.4) and possibly the static deflection shape.
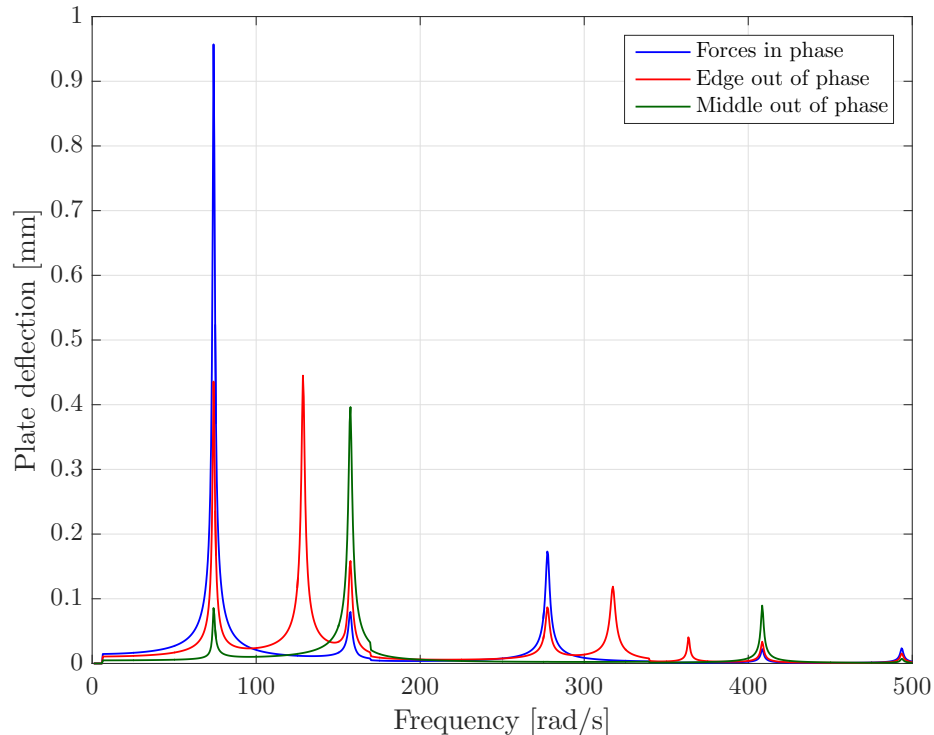
Figure 6.7: Maximum gate deflection at maximum water levels ($h_N = 7.2$ m, $h_S = 5.3$ m) for the regular pump gate design for three pump phase possiblities, quantified for the pump force envelope.

When the quantified deflection of figure 6.7 is expressed in terms of amplification of the static deflection caused by the three pumps in phase, a maximum amplification factor of approximately 65 is obtained at the first eigenfrequency.[8]

The regular gate was dimensioned to a bending moment unity check of 0.7. Stresses are therefore likely just within strength limits. Given the many uncertainties and the fact that the favourable isotropic bending stiffness is used in the analysed design (compared to the Witteveen+Bos [40] regular gate design) direct failure can be considered a risk, which is definitely concerning.

Since the existing concrete foundation is designed to withstand the 6.75 metre design head of the flood (pump) gate, the existing structure will likely suffice for these loads. As was elaborated in section 3.4, repetitive loads might however be more harmful than static loads. The stresses in the concrete structure are not further investigated in this thesis.

Due to the high frequencies involved and the frequent operation of the pumps, fatigue in the steel gate may be an issue as well. In section D.2 the concept of fatigue and the Eurocode requirements are elaborated. The pumps will operate around 100 days a year [40]. If the pumps would vibrate one hour per operating day at the systems first eigenfrequency, in 35 years this would lead to:

$$35 \cdot 100 \cdot 3600 \cdot \frac{62}{2 \cdot \pi} \approx 1.24 \cdot 10^8 \quad \text{[cycles]} \tag{6.25}$$

This is above the fatigue cut-off limit at which the maximum allowed stress amplitude is given by:

$$\Delta\sigma_l = \left(\frac{5}{100}\right)^{1/5} \left(\frac{2}{5}\right)^{1/3} \Delta\sigma_c \tag{6.26}$$

In the estimations by Witteveen+Bos [40] a detail category ($\Delta\sigma_c$) of 80 was used, which results in a maximum allowed repetitive stress of 32.4 N/mm². For the[40] designs a maximum stress of 167 N/mm² was found caused for the two metre design head (excluding safety factors). Using again the rough estimation that the static design head leads to the same deflection over force ratio as the pump head which is present at the three distinct locations, a maximum allowed amplification factor can be estimated. This results in:

$$r_{\text{ampl}} = r_{\text{F}_{stat}/\text{F}_{dyn}} \frac{\sigma_l}{\sigma_d} = 97 \cdot \frac{32.4}{167} \approx 19 \tag{6.27}$$

In that case the gate would not suffice, as an amplification factor of about 65 was found. This is of course a crude estimation, but indicates that even though the gate was designed with a unity check of 0.7 to account for fatigue, it is still a risk. Fatigue increases the chance on required maintenance to the gate as well.

---

[8]The frequency range in which the first eigenfrequencies are located has little hydrodynamic damping as was demonstrated in section 5.4. Other damping phenomena such as material damping and friction less that are not included in the present model, will likely lower this amplification factor. This is further elaborated in section 6.7.

6.6.2 Pump vibration velocity

As was discussed in section 3.4, certain limits are stated for non-rotating parts of the pumps. A root-mean-square (rms) value of 9.5 mm/s is stated as limited operation, above which there is hazard of damage. This value if taken as an indicative limit, but it is noted that axial flow pumps are relatively robust and that the simultaneous vibration of the entire pump is likely to be less damaging than individual components. The results for at maximum water levels are given in figure 6.8.

As can be seen, at several frequencies and pump force cases the limit is exceeded considerably. For the regular pump gate design a reduced efficiency or damage due to high pump vibration velocities are therefore risks.
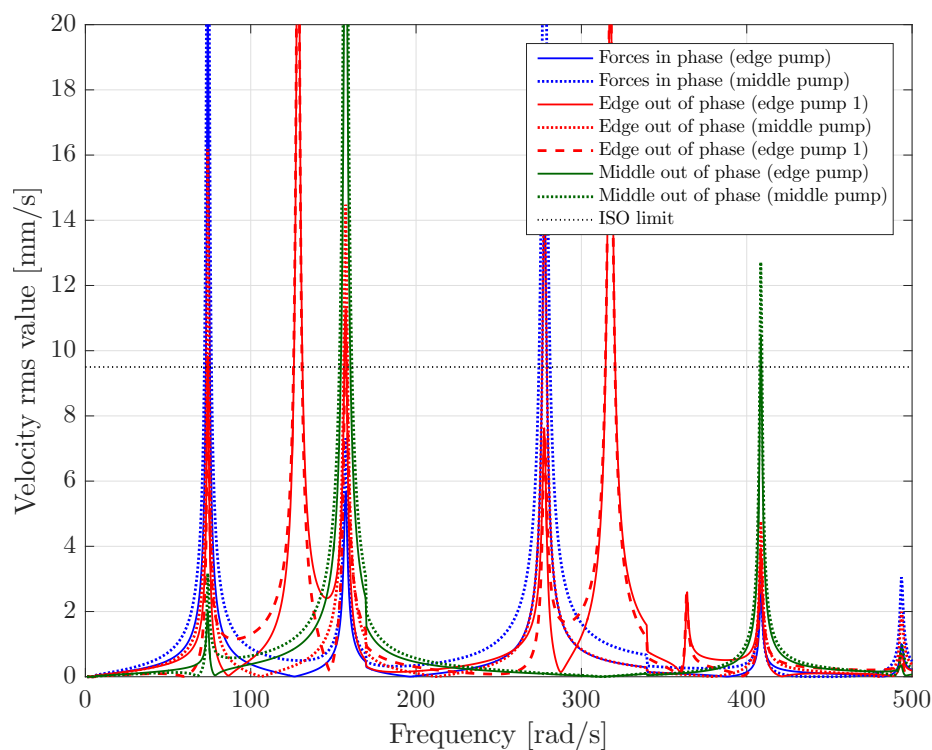
Figure 6.8: Pump vibration velocity (rms) at maximum water levels ($h_N = 7.2$ m, $h_S = 5.3$ m) for the regular pump gate design for three pump phase possibilities, quantified for the pump force envelope.

6.6.3 Fluid pressure fluctuations

Pressure fluctuations can have an adverse impact in two ways. Firstly these can have a direct effect on the efficiency of the pumps. Secondly, the fluctuations can induce cavitation. This phenomenon leads to a reduced efficiency, impeller blade damage, and dynamic fluctuations in the fluid. The latter can after initiation of cavitation, thus also aggravate vibrations. The concept of cavitation is elaborated in appendix C.6.

A clear limit for maximum pressure fluctuations at the pump's inlet is not available. The design rule requiring a minimum water coverage of half the pump's diameter is based on the

prevention of cavitation. Since cavitation will occur at low water coverage, the minimum water level at the Lake IJssel side is considered, which is -0.60 m NAP and corresponds to a water depth of 4.1 metre. In section 2.4.1 it was shown that the water coverage is 1.10 metre in that case. This in reference to the $0.5 \cdot 2 = 1$ metre required minimum coverage. Feedback from the pumps onto the fluid is not taken into account in this model. The pressures corresponding to this feedback generally apply to robustly founded pumps and are therefore assumed to be included in the required water coverage. Amplitudes of the pressure head fluctuations higher than approximately 0.1 m at the minimum Lake IJssel water level are therefore considered problematic.

In chapter 7 the effect of the pump conduit on the pressures at the gate's surface is investigated. In that chapter it is concluded that the fluid pressures are relatively unchanged from the present schematization when taking into account the pump conduit length. It must however also be taken into account that the pump inlet is at a certain distance from the gate's surface as potentials decay when moving away from the gate's surface. This was elaborated in section 5.4.2.

The potential corresponding to each fluid mode at a distance y from the gate's surface is given by:

$$\tilde{\Phi}_{pr}(x, y, z) = \tilde{\Phi}_{pr}(y = 0, x, z) \cdot e^{-ik_{y,pr}y} \tag{6.28}$$

Modes corresponding to higher (real) values of $k_{y,pr}$ decay quicker. The shape of the fluid pressures at a distance from the gate's surface will thus also change. The fact that the geometry of the conduit affects the fluid pressure is neglected based on the mentioned conclusions of chapter 7.

For above reasons, the generated pressures at the pump locations are both considered at the gate's surface and at a distance of 1.75 metre, which is half the total conduit length. The exact center of pumps with respect to the gate's plate is however not certain. This is especially relevant when considering the suction (southern) side of the pumps, as pressures at this location should comply to the requirements for cavitation.

In figure 6.9 the results are shown. As can be seen, head amplitudes at the suction (southern) side of the gate can be considerably higher than the mentioned 0.1 metre. Even at a distance of 1.75 metre most peaks correspond to amplitudes of 0.2 to 0.3 metre, with a single peak higher than 0.5 metre.

The pressure forces at both sides act in the same direction, which means the relative head amplitude generated over the pump is the summation of the amplitudes at both sides. In figure G.3 the pressure fluctuations are given for maximum water levels. This gives about the same response at slightly shifted eigenfrequencies. Considering the pump's inlet at 1.75 metre from the gate's surface (at both sides), maximum head amplitudes up to 1 metre are found. This corresponds to head fluctuations (double the amplitude) over the pump in the same order as the pump head, which can definitely be considered unacceptable.

It must be noted that at such great fluid responses, the linearised equations on which the analysis is based become invalid. Non-linear effects should thus be taken into account. As
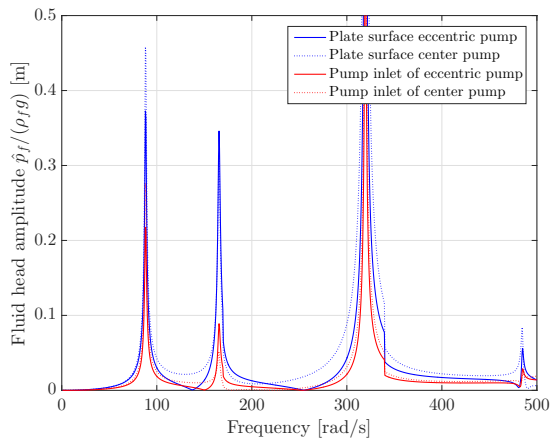
(a) Southern side of the gate, pump force in phase
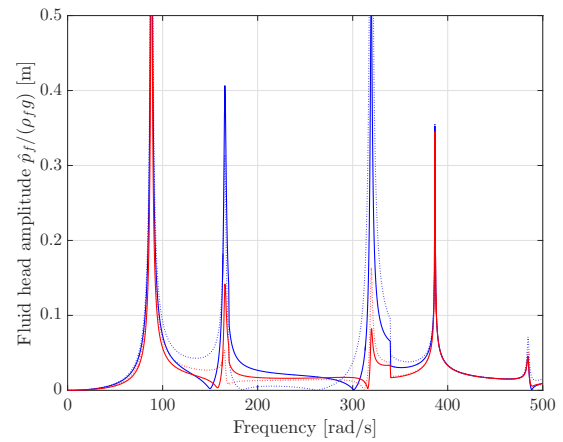
(b) Northern side of the gate, pump force in phase
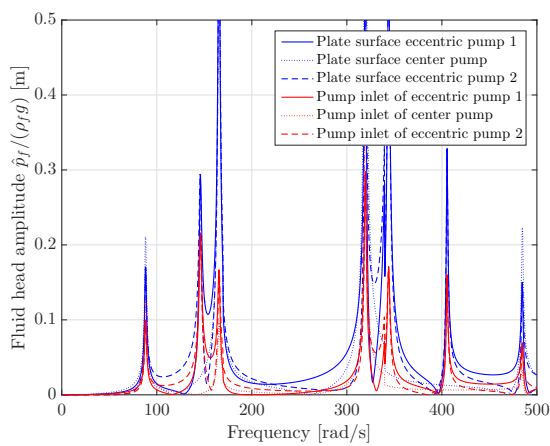
(c) Southern side of the gate, eccentric pump force out of phase
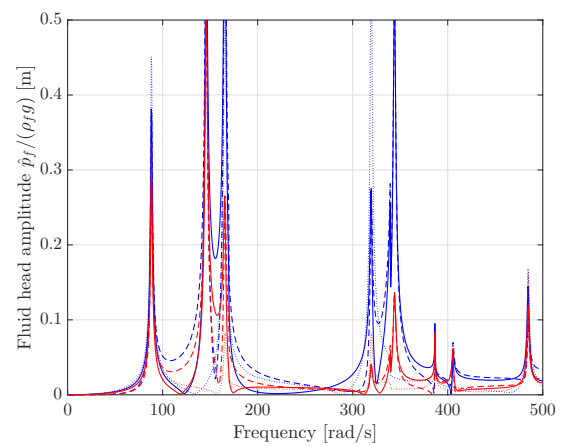
(d) Northern side of the gate, eccentric pump force out of phase
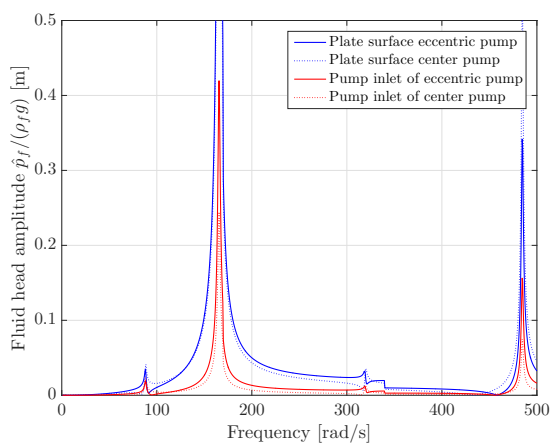
(e) Southern side of the gate, center pump force out of phase
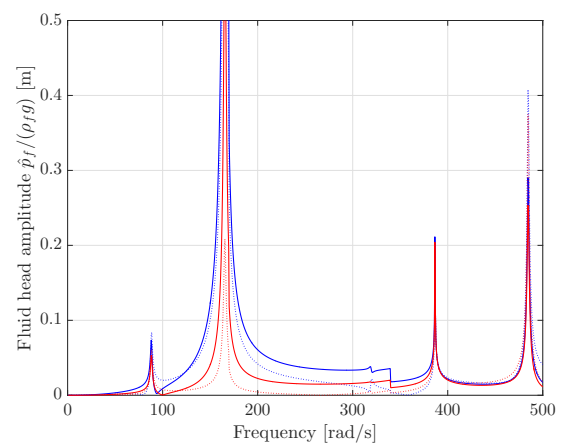
(f) Northern side of the gate, center pump force out of phase

Figure 6.9: Pump fluid head amplitude at water levels $h_S = 4.1$ m and $h_N = 6.1$ m for the regular pump gate design for three pump phase combinations at both sides of the gate, quantified for the pump force envelope.

these pressure fluctuations are considered unacceptable, it is expected amplitudes will be limited in a final design. In that case the model becomes reasonably valid again.

6.6.4 Flood defence pump gate

An inquiry is done into the response of the much more robust flood defence pump gate. As elaborated in section 6.4 for this purpose the rigidity in both directions is increased with a factor of approximately 15. The gate's weight increases to 30,000 kg.

The deflection for this design is shown in figure G.4. As expected, deflection amplitudes become even more insignificant. With the increased strength, stresses reduces significantly as well and therefore fatigue is most likely not an issue for this design. In the same range ($1 < \Omega < 500$ rad/s) less eigenfrequencies are now found. At maximum water levels the first eigenfrequency is 284.5 rad/s.

Although the deflection response is considerably lower, the vibration velocity, shown in figure 6.10, still exceeds the limit at the system's first eigenfrequency. Considering assumptions discussed in next section, the likelihood of unacceptable vibrations is deemed small for this design however.
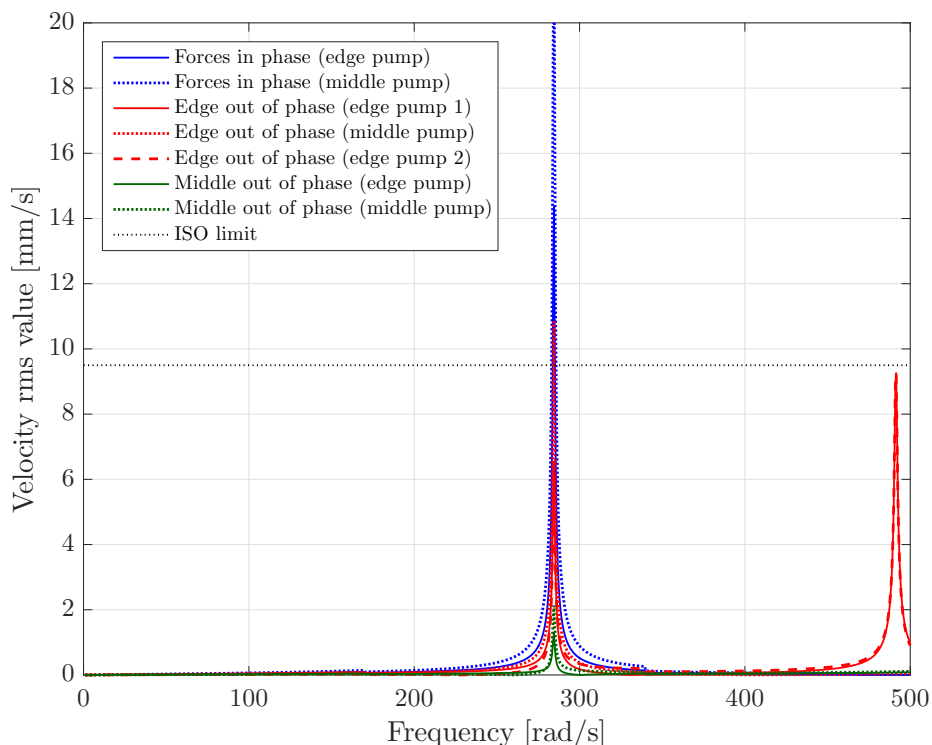
Figure 6.10: Pump vibration velocity (rms) at maximum water levels ($h_N = 7.2$ m, $h_S = 5.3$ m) for the flood defence pump gate for the three pump phase possibilities, quantified for the pump force envelope.

In figure G.5 the fluid head fluctuations are shown for the cavitation risk water levels $h_S = 4.1$ and $h_N = 7.2$ metre. The increased stiffness of the gate has lead to almost no amplifications beneath radial frequencies of 250 rad/s. However, above this frequency

responses are found that can be considerably larger than for the regular gate design. When regarding the pressures for the maximum water levels (figure G.6), pressure fluctuations over the pump in the same order as the pump head are still possible.

This is likely caused by the larger overlap of structural and compressible fluid eigenfrequencies. Since the fluid eigenfrequencies are dependent on the existing sluice structure, it is quite difficult to prevent these pressure fluctuations. Secondly, the first eigenfrequencies which generally contain most energy are now present higher frequencies. The pressure fluctuations ($\propto \Omega^2$) corresponding to the same deflection amplitude are larger for high frequencies.

This is thus a general concern for pump gate design. A robust gate design and low energy corresponding to higher excitations are required to limit the pressure fluctuations.

6.7 Conclusions and reflection

A dynamic analysis of the regular pump gate design with surrounding fluid was made. A few assumptions should be kept in mind when considering the quantifications and conclusions of previous section.

The maximum pump force amplitude was assumed to be ten percent of the pump thrust by Witteveen+Bos [39] based on experience. In the absence of more detailed pump specifics or data in this phase of the project, this value was used in the analyses. Response envelopes were determined based on the determined pump force envelope. This assumes the possibility of the total pump force being present at a single frequency. On one hand, this may lead to an overestimation of the response, since in reality energy is spread over multiple frequencies. One the other hand, the relatively large vibration motion of the pumps compared to a conventional set-up may lead to an increase of the forces compared to what is based on experience.

In addition, friction and viscous effects of the fluid and material damping of the gate will potentially limit the peaks somewhat compared to what was found with the current model.

Considering the gate schematization, especially the supports involve uncertainties. If the edge supports can be designed such that they have significant rotational stiffness, this is favourable to the response. The lateral movement was however assumed completely supported over the height while in reality the guiding system provides support only at several locations of the guiding system. The vertical stiffening elements at the edges were not included in the determination of the plate's rigidity. If designed robust like with the flood defence pump gate, the approximation of zero lateral movement is valid.

Keeping above considerations in mind, the results of the analysis in this chapter still give a reasonable indication of the risks involved with the pump gate. For the regular pump gate design, direct failure of the steel gates due to exceedance of ultimate stresses is a risk, but less likely than failure due to steel fatigue. Even though a safety factor in the design was

used to account for dynamic effects, when the response of the gate is amplified this appears to be a risk.

Also vibration velocities can exceed limits at distinct frequencies. Whether this will indeed be an issue should be decided by the pump manufacturer based on the forces and frequencies from originating from the specific pumps and its sensitivity to vibration velocities. The responses can simply be linearly scaled with the force amplitude.

For both the regular and the much stronger flood defence pump gate designs, pressure fluctuations in the fluid are a serious concern. With the almost minimal water coverage at the suction side of the pumps, cavitation may be induced by this fluctuations. In addition, operation is hampered with possible pressure fluctuations in the order of half the pump head, which may reduce efficiency.

Considering above, the regular gate design did not suffice on many of the considered requirements. The flood defence gate reduces most of these risks to acceptable levels, but pressure fluctuations in the fluid as a result of high frequency excitations may still be a problem. Since the pumps will act as part of the primary flood defence, and will become a vital part of the water regulation of Lake IJssel, further insight in these risks is required.

7 | Numerical fluid validation

In the previous chapter the response of the pump gate was determined based on an analytical plate model. This included the presence of the fluid and the first order response of the pumps to vibrations. The effect of the pumps on the fluid was accounted for by not applying the interface condition (forcing the fluid) at the respective part of the gate's surface. An additional reduction of the pressures due to the possible flow through the pumps was not accounted for.

To validate this assumption, a quick indication of the effect of the presence of the pumps is obtained by numerically evaluating the fluid pressures for a single case. The transition region, defined in section 5.4, allows for the most simple fluid schematization where both surface pressures and compressibility have an insignificant effect.

In first instance, the results of the numeric model are validated based on the undistorted vertical gate without pumps. In section 5.4.1 an analytical solution was derived for this schematization. Subsequently, the geometrical presence of the pumps is included, both as plain openings and with a certain conduit length. Results depend mainly on the geometry of the gate and pumps and are therefore expected to give a valid indication of the pump's effect for frequencies outside of the transition zone as well.

7.1 Model description

7.1.1 General

Kolkman [20] presents a numerical calculation method, based on potential flow theory, in order to estimate the hydrodynamic mass for varying geometries. It is referred to as a spread-sheet type calculation, as a square mesh grid is used. In previous chapter is was demonstrated that when the fluid is considered incompressible and without surface waves, the hydrodynamic mass becomes frequency independent. The mentioned numeric method is based on these assumptions. The obtained hydrodynamic mass is therefore only a function of the geometry and gate vibration *shape*.

The gate is given a certain vibration shape $W(x, z)$ which corresponds to a velocity of $i\Omega W(x, z)$. The potential field is then determined with the procedure laid out in next sections. For the given geometry and vibration shape this results in an unique ratio $\Phi/(i\Omega W)$ for the potentials in the entire domain. Only those at the gate's surface are relevant to the gate and thus:

$$\Phi(x, z) = r_m(x, z) \cdot i\Omega W(x, z) \tag{7.1}$$

In which $r_m(x,z)$ is the ratio between the given gate's velocity shape and the resulting potentials at the gate's surface. The pressures at the gate's surface are then described by:

$$\hat{p}_f(x,z) = -\rho_f \cdot i\Omega \cdot \tilde{\Phi}(x,z) = r_m(x,z) \cdot \rho_f \cdot \Omega^2 \cdot W(x,z) \tag{7.2}$$

Since the structure's acceleration in the frequency domain is expressed by $a_s = \Omega^2 \cdot W(x,z)$, it can be seen this pressure force acts as an hydrodynamic mass:

$$m_w(x,z) = \frac{p_f(x,z)}{a_s(x,z)} = \rho_f \cdot r_m(x,z) \tag{7.3}$$

The governing equations and method are further explained based on the most simple schematization, given in figure 7.1. This schematization is used to validate the numeric model and subsequently extended to implement the pumps as openings and conduits. In case an interaction is possible between the fluid domains at each side of the gate. The model domain is limited to the sluice length, which is allowed based on the estimations made in section 5.4.2.

Since only the fluid is considered, the width of modal domain is the 12 metre width of the sluice (and not that of the somewhat larger gate). For simplicity, the sill is not considered in this schematization and the bottom level of gate is considered at bottom sluice level (-4.7 m NAP). Water depth are still varied between 4.1 and 7.2 metre.
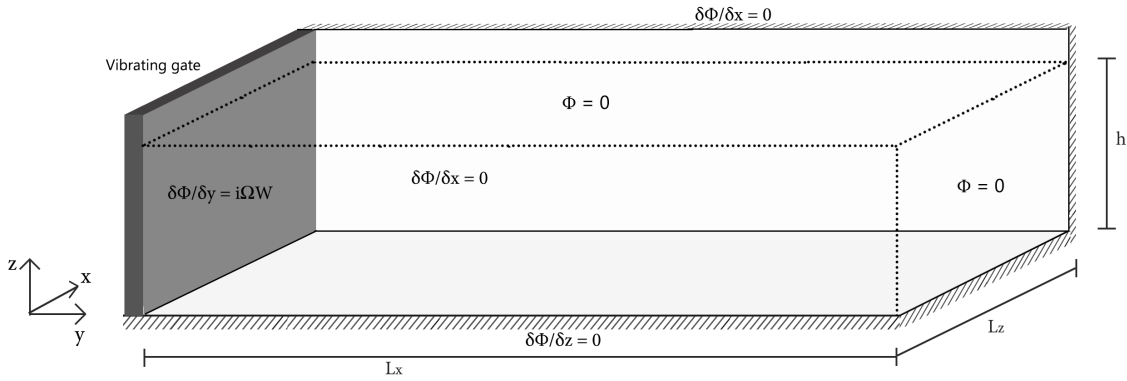
Figure 7.1: Numeric model domain including boundary conditions for the symmetric case without pumps

As was elaborated before, the fluid can be described as incompressible in the transition region, and thus the equation of motion becomes:

$$\frac{\partial^2 \Phi}{\partial x^2} + \frac{\partial^2 \Phi}{\partial y^2} + \frac{\partial^2 \Phi}{\partial z^2} = 0 \tag{7.4}$$

Furthermore the surface pressure is approximately zero, thus a $\tilde{\Phi} = 0$ boundary condition applies. Instead of the infinity conditions, a $\tilde{\Phi} = 0$ condition is used as well. In section 5.4.2 it was demonstrated that for the transition region generated potentials and pressures have

decayed to zero at that point. Other boundary conditions were elaborated for the plate model in section 6.2.

7.1.2 Numerical grid and cell equations

The three dimensional domain is divided into cells with equal height, width and length (ΔL). The entire domain then contains $N_x \cdot N_y \cdot N_z$ cells, with: $N_i = L_i/\Delta L_i$. In figure 7.2, this grid is shown with a division into 27 regions is shown, denoted as y_1-1 to y_1-9, y_{body}-1 to y_{body}-9 and y_{end}-1 to y_{end}-9. Each of these regions has a different type of cell equation. In comparison to the scheme used in Kolkman [20], the amount of different cell equations increases largely when extended to the three dimensional domain.
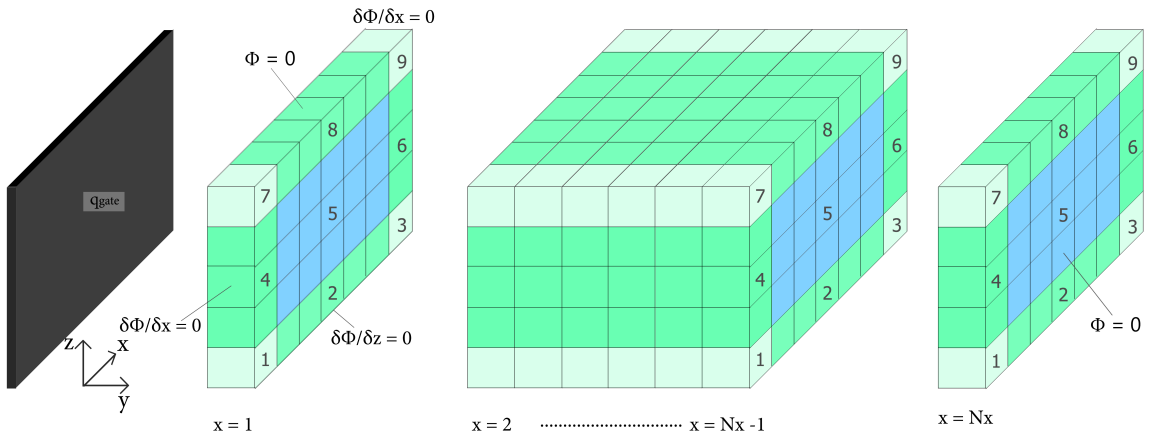
Figure 7.2: Calculation grid of symmetric gate with regions of different cell equations (27 total). Region 5 of the middle part contains the body cells, obeying equation (7.5), all other cells have changed equations directly influenced by the boundary conditions.

The equations for all cells are based on the continuity, which states sum of all discharges must be zero (for the incompressible fluid). In appendix H it is shown that for the regular cells (region y_{body}-5), this leads to:

$$\Phi_{x,y,z} = (\Phi_{x-1,y,z} + \Phi_{x+1,y,z} + \Phi_{x,y-1,z} + \Phi_{x,y+1,z} + \Phi_{x,y,z-1} + \Phi_{x,y,z+1})/6; \qquad (7.5)$$

Region x_{body}-5 contains by far the largest part of all cells. When adjacent to a boundary, the cell equation changes. For example, x_1-5 has the following cell equation:

$$\Phi_{x,y,z} = (q_{x,z}/\Delta L + \Phi_{x,y+1,z} + \Phi_{x-1,y,z} + \Phi_{x+1,y,z-1} + \Phi_{x,y,z-1} + \Phi_{x,y,z+1})/5 \qquad (7.6)$$

In which $q_{x,z}$ is the discharge generated by the movement of the gate ($\dot{W} \cdot \Delta L^2$). When the pump conduits are introduced, this leads to an increase in regions with altered cell equations. For this and the other model geometries, the cell equations are elaborated in appendix H.

7.1.3   Iterative procedure

In the numeric method the gate is given a unit velocity, which will result in potentials throughout the numeric domain. From point ($x = 1$, $y = 1$, $z = 1$) to ($x = N_x$, $y = N_y$, $z = N_z$) the cell equations are executed. After each iteration, the hydrodynamic pressures are determined. To do so, the calculated potentials at the contact coordinates to the gate ($x = 1$) must be adjusted to represent the potential at the gate surface, which is at the cell boundary (instead of its center). This correction is as follows:

$$\phi_{gate}(x, z) = \Phi(y = 1, x, z) + \frac{1}{2}q_{gate}(x, z) \tag{7.7}$$

In equation (7.2) it was shown how the fluid pressures relate to the potential. The hydrodynamic mass of the entire gate is then calculated by:

$$m_w = \sum_{x=1,z=1}^{x=N_x,z=N_z} \rho_f\, \phi_{gate}(x, z)\, \Delta L^2/\dot{W} \tag{7.8}$$

In which $\dot{W}$ is absolute as it is the unit velocity given to the gate. Kolkman [20] introduces the following accuracy criterion:

$$acc = \frac{\frac{m_{w_n} - m_{w_{n-1}}}{m_{w_n}}}{n} \tag{7.9}$$

When the added mass is set out as a function of the iteration number, it can be seen that this accuracy is the ratio between the local slope and global slope. This is depicted in figure 7.3. The stop criterion stated in the figure is the inverse of accuracy criterion.
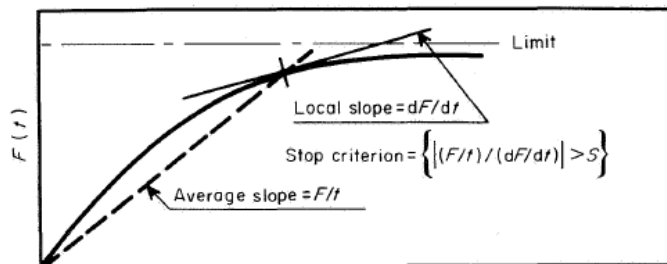
Figure 7.3: The stop criterion for acc[20]

When the accuracy is less than a certain value, the calculation stops. Kolkman [20] obtains valid result with a required accuracy of $acc_r = 0.025$. Due the low computational resources this numeric method requires, an accuracy of $acc_r = 0.005$ is used throughout the analyses in this chapter.

7.2   Gate without pumps

In further sections, a more complex geometry of the pump gate will be researched. First, the numeric method is validated based on the analytical solution for a rigid horizontally vibration gate, which was derived in section 5.4.1. In that case the fluid response is two-dimensional. In figure 7.4 the results are shown for two
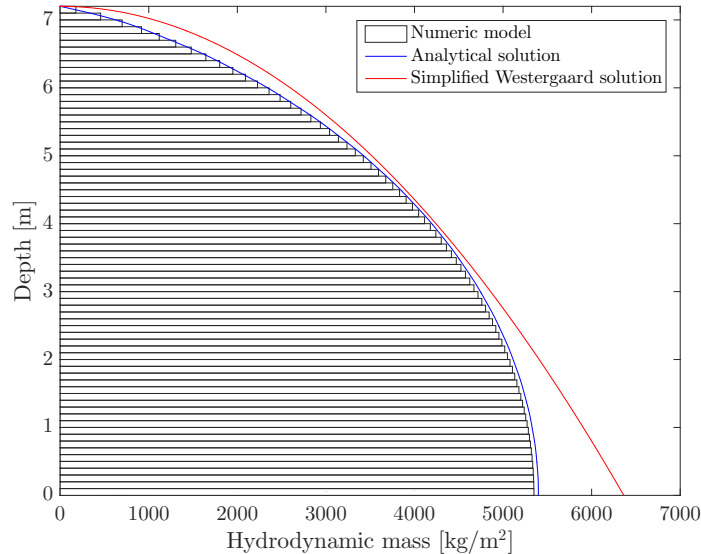
Figure 7.4: Water pressures resulting from the numeric model compared to the exact analytical solution and the simplified Westergaard solution for dl= 0.1 metre

The total hydrodynamic mass found with the numeric method for the gate at 12 metre sluice width and h = 7.2 metre is $337 \cdot 10^3$ kg. This is considered sufficiently accurate compared to the result of the analytical solution: $341 \cdot 10^3$ kg. The simplified Westergaard parabola overestimates the hydrodynamic mass.

To validate the analytical estimation that the sluice length is indeed sufficiently long not to be affected by the boundary condition at its end, the numeric model is evaluated for a series of sluice lengths. From figure 7.5 it can be seen that this is indeed the case for the 28 metre long sluice.

7.3   Effect of pumps for several schematizations

Two estimate the effect of the present pumps on the hydrodynamic mass, three schematizations are compared to the closed gate case:

1. Closed gate with zero displacement/velocity at the location of the pumps;
2. Gate with openings and zero thickness
3. Gate with pump conduits of a certain length.

The first of these is in fact the schematization used in previous analytical models, where the interface condition was not applied at the pump locations. In case of the latter two
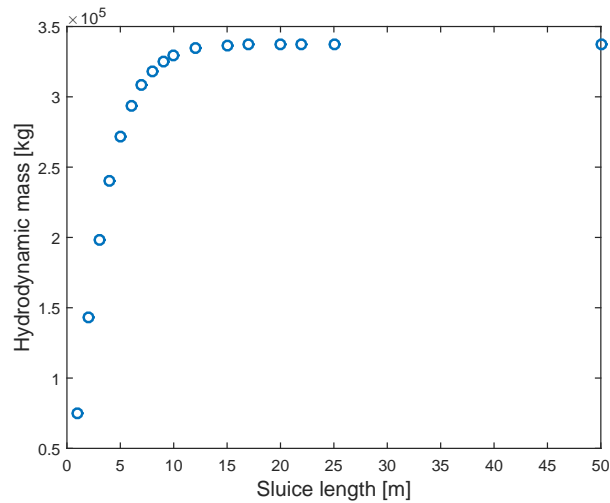
Figure 7.5: The hydrodynamic mass as a function of the sluice lengths for a water depth of 7.2 m

schematizations the fluid at both sides of the gate may interact. The full fluid domain must therefore be included in the model. An overview of the domain for the gate with pump conduits is given in figure 7.6.
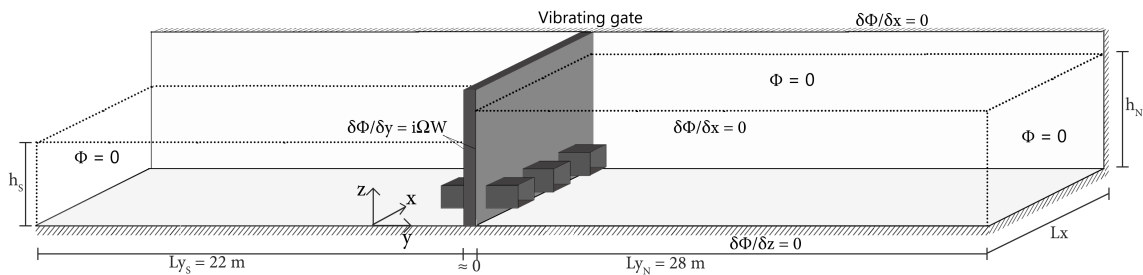
Figure 7.6: Numeric model domain including boundary conditions for the symmetric case without pumps

In all schematizations the gate, which in fact has a plate thickness of 10 to 15 mm, is considered infinitely thin. In case of plain gate openings the fluid domains are thus in direct contact. The pumps are in accordance with the analytical models schematizated as square $(1.8 \times 1.8 \text{ m}^2)$.

In figure 7.7 an overview of the hydrodynamic mass is shown for the schematization of the gate with pump openings. The result is given for the anti-symmetric case, thus with equal water levels (7.2 m) at both sides of the gate.

The hydrodynamic mass at this water level for one side of the gate is $130 \cdot 10^3$ kg. This is a reduction of about 62% compared to the mass that was found for the closed gate. For lower water levels, the relative reduction is even larger. This reduction is partially caused by the possible flow through the openings and partially due to the fact the reduced gate surface that forces the fluid. For the closed gate with adjusted displacement at the pump
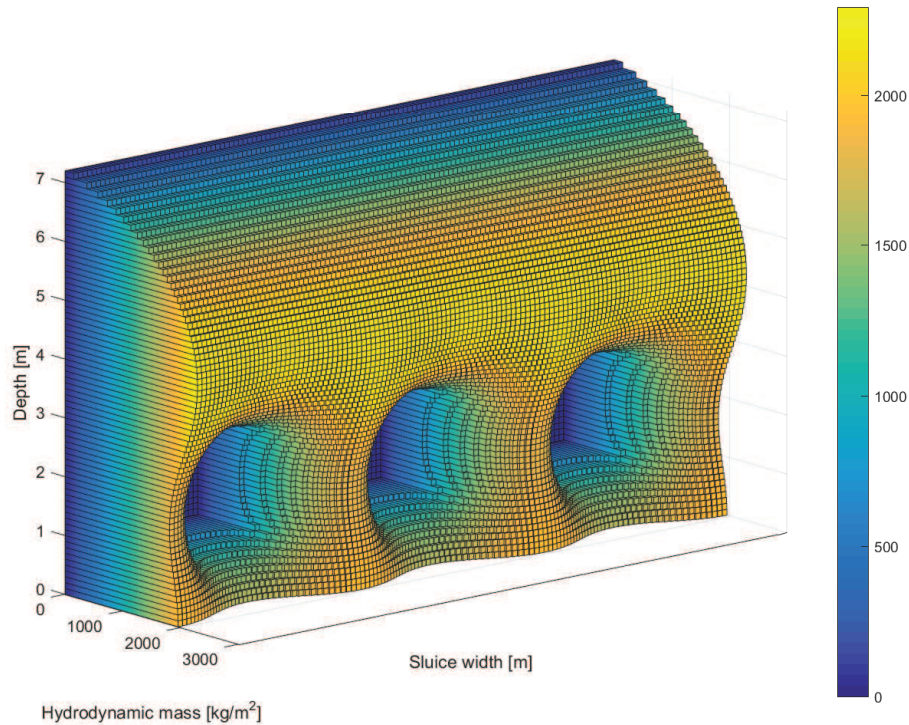
Figure 7.7: Overview of the hydrodynamic mass for the gate with openings as a result of a undistorted translating motion

location a total hydrodynamic mass of $249 \cdot 10^3$ kg is found, which is still significant above that of the gate with openings.

Due these large difference in hydrodynamic mass, the pumps are modelled more accurately as conduits. The maximum available length for the pumps is approximately 3.5 metre (see chapter 2). An equal conduit length of 1.75 metre at both sides is therefore assumed. In appendix H.4 the equations to determine the potential field for this schematization are elaborated.

The hydrodynamic mass over the depth is given for each of the three pump gate schematizations and the closed gate in figure 7.8. As can be seen, the length of the conduits leads to pressures that are almost equal to the adjusted closed gate schematizations. The effect of the possible flow to the conduits is thus low in that case. The response of the pumps is expected to decrease differences even more. The pump conduits have, especially compared to the sluice, a small hydraulic radius. Even when response of the pumps would be neglected, friction effects would therefore lead to a resistance of additional flow through the pump conduits. This further decreases differences between the conduit and adjusted gate schematization.

In table 7.1, a comparison between of the total hydrodynamic mass at both sides of the gate between the adjusted closed gate and pump conduit schematization is made for different water levels at each side of the gate. The maximum head and maximum water level cases are considered. Although the values at separate sides of the gate differ, the difference in total hydrodynamic mass for the gate is in the order of merely a few percent. The relatively

(a) At the edge of the gate

(b) At the middle of the eccentric pumps

(c) At the edge of the center pump

(d) At the middle of the middle pump
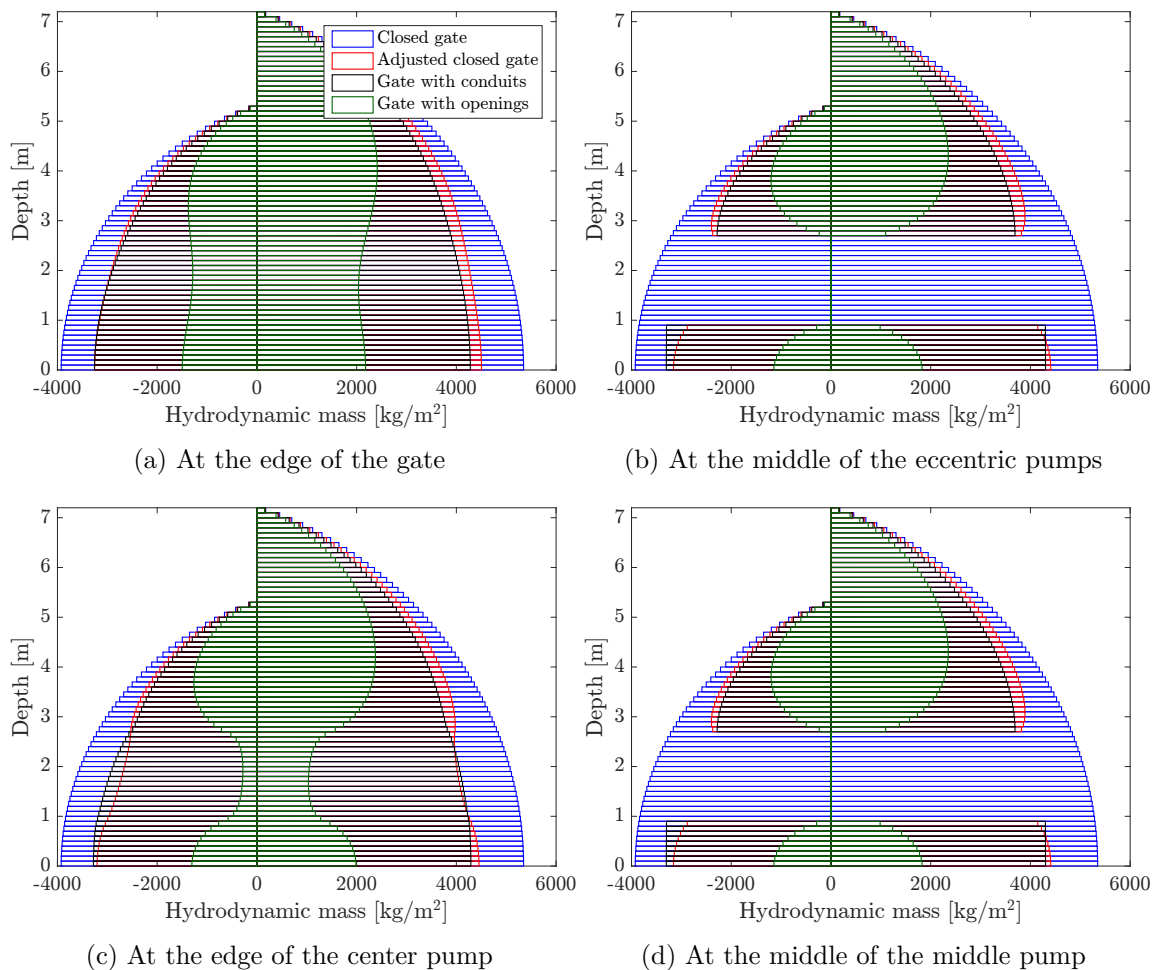
Figure 7.8: Comparison hydrodynamic mass as a result of the gate's undistorted translating motion for four schematizations

small local differences that occur over the height are not expected to influence the behaviour of the gate to a large extent.

Table 7.1: Comparison hydrodynamic mass between the geometry with conduits and the 'adjusted' closed gate

Water level case	$h_S[m]$	$h_N[m]$	Geometry with conduits			Adjusted closed gate		
			$m_{w_S}[kg]$	$m_{w_N}[kg]$	$m_{w_\text{total}}[kg]$	$m_{w_S}[kg]$	$m_{w_N}[kg]$	$m_{w_\text{total}}[kg]$
Max. head	4.1	7.2	$71.8 \cdot 10^3$	$241 \cdot 10^3$	$312 \cdot 10^3$	$67.0 \cdot 10^3$	$249 \cdot 10^3$	$316 \cdot 10^3$
Max. water levels	5.3	7.2	$122 \cdot 10^3$	$237 \cdot 10^3$	$359 \cdot 10^3$	$122 \cdot 10^3$	$249 \cdot 10^3$	$371 \cdot 10^3$

For different shapes the hydrodynamic mass and thus also differences between the schematizations will change. This is however not expected to significantly change results.

7.4 Conclusions

It can be concluded that when the pumps' conduit length of 3.5 metre is taken into account, the adjusted gate surface schematization used in the analytical models in previous chapters is reasonable. Although the method used in this chapter is only valid in the 'transition region' without compressibility and surface waves, the results depend especially on the geometry and are therefore expected to be representative for a wider frequency range as well. Eccentric placement of the pumps might reduce the hydrodynamic mass. When this is the case in a more detailed design phase, this should be investigated further.

8 | Conclusions and recommendations

In this thesis a method is developed to model the fluid-structure interaction at sluice gates. Subsequently, this method was applied to the pump gate designs at Den Oever. The conclusions are divided into those that generally apply to fluid-structure interaction at sluice gates and the way in which this can be modelled and those specifically to the Den Oever pump gate case.

8.1 Conclusions fluid-structure interaction

Semi-analytical coupled modal analysis
The semi-analytical method used in this thesis is very suitable to determine the dynamic behaviour of the gate's in confined waterway. It can efficiently model and solve linear fluid-structure interaction. It is applicable to complex plate geometries, as long as the eigenmodes and -frequencies of the gate can be numerically evaluated. In existing software based on finite element models, this is often possible for the dry structure together with the static analysis. The semi-analytical model can then determine the dynamic behaviour of system taking into account the structure-fluid interaction and its effect on the gate's vibrations.

The behaviour of the pump gate designs was investigated both with a two-dimensional beam model and a three-dimensional plate model. Although the effect of the gate's vertical edges was incorporated by springs in the beam model, results differed significantly from what was found with the more accurate plate model. Given this result, the plate model is generally recommended when investigating these type of sluice gates.

The system of equations for the plate model has been derived such that it is applicable to a wide range of geometries. This includes a sill, different widths of the gate and sluice structure and the ability to include additional mass at certain locations. A relatively simple software package based on this method can be useful in preliminary dynamic hydraulic gate design.

Whether a dynamic analysis is required for regular hydraulic gates depends on excitation frequencies and the size of the gate and sluice structure. For the pump gate designs it was found that even with the significantly added pump weight, regular wave frequency range was significantly below the first fluid-structure eigenfrequency. The dynamic behaviour of closed bending gates therefore only becomes relevant for higher excitation frequencies, such as those corresponding to pumps, earthquakes or breaking wave impact, or for much larger dimensions. Additionally, when the gate's edges do not provide full support in translating motion, eigenfrequencies can be lower.

The applicability of the derived semi-analytical model further depends on the sluice length. The required length to be able to model the fluid as confined (till infinity) depends on the frequency and water depth. For the transition region in which surface waves and compressibility play a minor role (see next conclusion) a minimum length of 3 to 4 times the water depth is required.

Surface waves and compressibility

In the semi-analytical models both the effect of surface waves and compressibility was included. Three regions for the fluid have been determined:

- Significant surface waves;
- Transition region (approximately no effect of either surface waves or compressibility);
- Significant compressibility.

Numeric schemes such as that of Kolkman [20] exist to quickly determine the hydrodynamic mass for different geometries and water levels. This method neglects both surface waves and compressibility and is therefore only valid in the transition region. This region is characterised by a frequency-independent hydrodynamic mass and no hydrodynamic damping. Validity limits for modelling the fluid as such were determined in this thesis based on a 5% deviation:

$$6.5\sqrt{\frac{g}{h}} < \omega < 0.31 \cdot \frac{c_p \cdot \pi}{2h} \tag{8.1}$$

For this region an analytical expression was obtained of the hydrodynamic mass for a two dimensional horizontally vibrating vertical gate.

8.2 Conclusions pump gate Den Oever

Two reference gate designs for the pump gates at Den Oever were investigated: the 'regular pump gate' and 'flood defence pump gate'. The latter will function as a primary flood gate and is therefore dimensioned on a much higher design head. Both designs were considered with an increased rigidity in vertical direction compared to the reference designs by Witteveen+Bos [40], so that they could be analysed as isotropic plates. This should be kept in mind when considering the results, which might be less favourable for the reference designs.

Wave excitation

Eigenfrequencies of the gate-fluid system (>20 rad/s) are well above frequencies corresponding to typical regular waves (0.5-3.5 rad/s) at the Waddensea. Amplification of wave loads will therefore not occur and the quasi-static approach suffices. In addition, due to the excitation frequencies corresponding vibration velocities and fluid pressures are low as well.

Deflection and stresses
The deflection caused by pump forces, even at resonance frequencies, is insignificant for both gate designs. Due to the amplification of the static stresses, for the regular gate design fatigue and potentially even direct failure can be a risk. Even though the gate was designed with a unity check of 0.7 to account for dynamic loads. Whether this will indeed be a problem depends on the final specified pump forces and frequencies (see recommendations). If so, a stronger gate design such as the flood defence gate can effectively reduce stresses.

Vibration velocities
ISO states limits for the non-rotating parts of pumps. For the regular pump gate design this limit is exceeded at several excitation frequencies, which can lead to a reduced efficiency or even damage of the pumps. This therefore appears to be a risk of the regular pump gate design.

It must however be noted that axial flow pumps are known to be relatively robust. Secondly, the simultaneous motion of the entire pump might be less damaging than the vibration of individual components.

The more robust flood defence pump gate reduces vibration velocities significantly. Close to a single system eigenfrequency, peak values still exceeded the limit slightly. Considering above, the risk to excessive vibrations for this design is expected to be sufficiently small.

Pressure fluctuations in the fluid
Excessive pressure fluctuations at the pump's inlet may reduce the efficiency of the pumps. Secondly, since the water coverage is limited for the pumps at Den Oever, cavitation can be a risk. The magnitude of the pressure fluctuations depends on the distance of the pump inlet to the gate. Results were obtained for a pump length of 3.5 metre, with its center at the gate's plate.

For the regular pump gate design pressure head amplitudes up to 0.5 metre were found. In reference to the 1.1 metre water coverage at the minimum Lake IJssel water level during operation, this poses a risk. Considering both sides of the pumps, head fluctuations (twice the summed amplitude) over the pump can be in the same order as the pump head. This is considerable and may significantly influence the pumps' efficiency.

The robust flood defence pump gate design reduces the fluid pressure response over first part of the investigated frequency (< 250 rad/s). For the higher frequencies, significant larger fluid responses are found however. This is likely due to the closer overlap of the structural and fluid eigenfrequencies in this case. High pump excitation frequencies can therefore still be harmful.

As was mentioned, it is important to note that the investigated designs were isotropic, and have a higher vertical rigidity than the designs made by Witteveen+Bos [40]. Results may thus be worse for the reference designs.

A more detailed design of the gate and pumps certainly must pay attention to the fluid fluctuations. These are caused by the movement of the gate, which forces the fluid over a large surface. This in contrast to a conventional pump complex layout, where the pump is founded on a relatively rigid concrete foundation. The Korean pump gate designs, appearing extremely robust with a large thickness and relatively small span, are likely designed as such to limit these fluctuations.

8.3   Recommendations

As was stated in the conclusions, given the identified risks, a general recommendation is to investigate the dynamic behaviour of the pump gate further.

Pump manufacturer data
The analyses in this thesis have been made for a rough estimation of the maximum pump force. When in a later phase of the Afsluitdijk project, a pump manufacturer is involved in the project, more accurate data on the to be used pumps should be obtained. Not only the forces, but also specifics on the sensitivity to pressure fluctuations and vibration velocities should be obtained. Based on this data, a more pump specific response could be determined and recommendations could be made on which eigenfrequencies should be avoided.

Gate supports
At the time of this thesis, a detailed design of the gate's guiding and support system was not available. Since it was demonstrated that these boundaries can have a significant influence on the gate's behaviour, this should be investigated further in a final design. The analysis can be adjusted relatively easy to alternative boundary conditions by numerically evaluating a new set of plate shapes and corresponding natural frequencies.

Gate: detailed geometry
In the analyses the gate was considered as a plain plate. Certainly for the more robust design which has a thickness of 1.7 metre, the local geometry may influence the fluid pressure distribution. A first indication of this effect could be based on the same numeric method used in this thesis to investigate the effect of the pump conduit length.

Permanent flow
Due to the complexity of the fluid-structure interaction, the analysis of the pump has been done for still standing water. In reality, high flow velocities are present in the sluice due to the pumps' discharge. It was demonstrated that for the linearised equations, this has an effect on the hydrodynamic damping. An increase in damping has favourable effects on the gate's vibrations. Whether this should be investigated in more detail therefore depends on the significance of the dynamic behaviour in the final design.

Pump support

In the present model, the pump was considered to be rigidly attached to the gate. Furthermore, the rigidity of the gate was assumed not to be affected by the presence of the pumps. It should be investigated in a further design phase whether this is indeed the case, or whether the pumps should be modelled with 'spring supports'.

Linearised equations

Since the analysis was done in the frequency domain, the governing equations were linearised. The validity of this linearisation is based on the assumption of small amplitudes. This is generally the case in final design as high amplitudes will lead to structural failure. In the fluid high pressure amplitudes were found. The exact value of these fluctuations have therefore become inaccurate. Nevertheless, reduction of these pressure amplitudes by alternative designs can be based on the linearised model used in this thesis.

Cavitation

Since high pressure amplitudes were found, the risk of cavitation is present. Based on an analysis of the pressures in the permanent situation and more accurate data on the required net present suction head ($NPSH_r$) a requirement for the dynamic pressure fluctuations at the pump's inlet can be obtained. In this thesis the pressure head fluctuations were compared to the present water coverage.

Safety factors

Since the analyses of the reference designs in this thesis functions as an indication of the risks and is not set-up to come up with a final design, no safety factors were used. Furthermore, the uncertainty of the pump forces lead to an envelope of possibilities that were evaluated. In final design attention should be paid to safety factors or uncertainty should be incorporated in a probabilistic design.

Wave impact

It was concluded that resonance will not occur for wave loads and corresponding vibration velocities are low for regular waves. It is interesting to investigate whether impulse forces corresponding to breaking wave impacts may lead to responses that can affect the pumps.

Finite element or scale model

When based on the outcome of the analyses in this thesis and more specific pump data, vibrations of the pump gate remain a point of concern, modelling the gate and fluid with an advanced finite element or scale model would be recommended. This could include a more detailed geometry of e.g. the gate profile and pump inlet.

When more advanced models (and more accurate pump data) still indicate risks, a real size test gate is a possibility as well.

Bibliography

[1] Bing Maps. Flash Earth, 2015. URL `www.flashearth.com`.

[2] J. Blaauwendraad. Plate analysis, theory and application, November 2006.

[3] M. Brendel. Afsluitdijk krijgt een nieuw jasje. *Technisch Weekblad*, TW21, May 2015.

[4] C. E. Brennen. *Hydrodynamics of pumps*. Oxford University Press, 1994.

[5] *NEN-EN 1993-1-9*. CEN, January 2006. Eurocode 3: Design of steel structures - Part 1-9: Fatigue.

[6] P. de Vries. The bolivar roads surge barrier. Master's thesis, Delft University of Technology, January 2014. A conceptual design for the environmental section.

[7] J. Den Hartog. *Mechanical vibrations*. Dover Publications, Inc., New York, USA, 1956.

[8] Det Norske Veritas. *Environmental conditions and environmental loads*, 2010.

[9] C. D. Erdbrink. *Modelling flow-induced vibrations of gates in hydraulic structures*. PhD thesis, Universiteit van Amsterdam, 2014.

[10] European association of pump manufacturers. *Pump vibration standards guidelines*, first edition edition, July 2013.

[11] S. Florjancic and A. Frei. Dynamic loading on pumps - causes for vibrations. In *Proceedings of the tenth international pump users symposium*, pages 171–184, 1994.

[12] gobizkorea.com. Gate Pump ®, 2015. URL `http://www.gobizkorea.com/blog/ProductView.do?blogId=hasuh&id=919833`.

[13] Hasuh Industries Corporation. *Pump gate* ®, April 2015. URL `http://www.hasuh.co.kr/eng`.

[14] G. Hofste. Steven outlet sluices - wave impact under a beam. Master's thesis, Delft University of Technology, August 2012.

[15] L. Holthuijsen. *Waves in Oceanic and Coastal Waters*. Cambridge University Press, 2007.

[16] R. Jacob. De nieuwe pomp voor het gemaal ijmuiden worden door middel van een zwaar transport wagen van een ponton naar het gemaal getransporteerd ten behoeve van de uitbruiding van het gemaal ijmuiden id273929, 2004. URL `beeldbank.rws.nl`.

[17] T. H. G. Jongeling and C. Erdbrink. Dynamica van beweegbare waterkeringen. Technical report, Deltares, 2010.

[18] I. J. Karassik, J. P. Messina, P. Cooper, and C. C. Heald, editors. *Pump handbook*, volume Third edition. McGRAW-HILL, 2001.

[19] P. A. Kolkman. *Flow-induced gate vibrations.* PhD thesis, Technische Hogeschool Delft, 1976.

[20] P. A. Kolkman. A simple scheme for calculating added mass of hydraulic gates. Technical Report 439, Delft Hydraulics, December 1990.

[21] P. A. Kolkman and T. H. G. Jongeling. *Dynamic behaviour of hydraulic structures.* Delft Hydraulics, 2007.

[22] T. Manen. Adaptive pumping station at the afsluitdijk. Master's thesis, Delft University of Technology, March 2014.

[23] A. V. Metrikine. Lecture slides Structural Dynamics CIE 4140. Delft University of Technology, 2015 March. Lecture slide number 14.

[24] W. Molenaar. Golfklappen op de spuisluis den oever. Technical report, Delft University of Technology, 2013.

[25] W. Molenaar. Pompen ingebouwd in de hefdeuren van de spuisluis bij den oever. Intern onderzoeksvoorstel TU Delft, December 2014.

[26] E. Naudascher. *Hydrodynamic forces.* A.A. Balkema, Rotterdam, 1991.

[27] Nijhuis Pompen BV. *Afmetingen, Prestatie en Kosten Propeller Pomp-Turbines*, 2009. Director R & D J. Arnold.

[28] power-technology.com. Alstom to supply equipment for world's second largest bulb-type turbine hydroelectric plant in brazil, December 2013. URL `www.power-technology.com`.

[29] B. Schiavello and F. C. Visser. Pump cavitation - various npshr criteria, npsha margins, and impeller life expectancy. In *Proceedings of the twenty-fifth international pump users symposium*, pages 113–144, 2009.

[30] J. Schijve. *Fatigue of structures and materials.* Springer, 2001.

[31] D. Schönfeld. Fatigue of steel lock gates. Master's thesis, Delft University of Technology, 2013.

[32] J. Spijkers, A. Vrouwenvelder, and E. Klaver. Lecture notes structural dynamics ct4140. Delft University of Technology, 2005 January. Part 1 - Structural Vibrations.

[33] A. Tsouvalas and A. Metrikine. A semi-analytical model for the prediction of underwater noise from offshore pile driving. 332:3232–3257, January 2013.

[34] A. Tsouvalas and A. Metrikine. A three-dimensional vibroacoustic model for the prediction of underwater noise from offshore pile driving. 333:2283–2311, November 2013.

[35] A. Tsouvalas, K. van Dalen, and A. Metrikine. The signicance of the evanescent spectrum in structure-waveguide interaction problems. Journal of the Acoustic Society of America, January 2015.

[36] M. van Reijen, 2015/2016. Personal communications.

[37] M. Versluis. Hydrodynamic pressures on large lock structures. Master's thesis, Delft University of Technology, April 2010.

[38] Waterloopkundig Laboratorium. Spuisluizen afsluitdijk den oever - dynamisch gedrag hefschuiven bij golfbelastingen. Technical report, Rijkswaterstaat, Directie Zuiderzeewerken, July 1990.

[39] Witteveen+Bos. Startdocument planuitwerking afsluitdijk. Technical report, Rijkswaterstaat Midden-Nederland, 2013.

[40] Witteveen+Bos. Systeemontwerp spuisluizen dov. Technical report, Rijkswaterstaat Midden-Nederland, December 2014.

Nomenclature

Roman

Symbol	Description	Unit
A	surface area	m^2
A_m	structural modal coefficient for mode m	m
A_p	pump's surface area	m^2
B_p	fluid modal coefficient for mode p	
c	damping	Ns/m
c_{crit}	critical damping	Ns/m
c_p	velocity of sound in water	m/s
c_{pump}	distributed pump damping	$N/ms \cdot m^2$
C_t	fluid modal coefficient for mode t	
c_w	hydrodynamic damping	Ns/m
D	pump diameter	m
D	plate bending stiffness	Nm^2
D_d	fatigue damage factor	Nm^2
E	elasticity modulus	N/m^2
F	external force	N
F_n	modal force for mode n	N
f_n	natural frequency or eigenfrequency	$Hz = s^{-1}$
F_{thrust}	pump thrust	N
g	gravitation constant	m/s^2
h	water depth	m
$H_{\text{lake/sea}}$	water level head	m +NAP
H_d	pump design head difference	m
H_{m0}	significant wave height	m
H_{pump}	pump head	m
$H(x - x_1)$	heaviside step function	-
$H_{F,\eta}$	amplitude-force transfer function	
i	imaginary unit	-
I_{mn}	pump inertia force for structural mode m and n	N
I_{xx}	moment of inertia around the x-axis	m^4
k	spring stiffness	N/m
K	bulk modulus of water	N/m^2
k_f	fluid compressibility number	m^{-1}
k_h	horizontal seismic coefficient	-
k_w	hydrodynamic stiffness	N/m
$k_{x,t}$	wave number in x-direction for mode t	m^{-1}
L_x	length in x-direction	m
m	mass	kg

Roman (continued)

Symbol	Description	Unit
m_w	hydrodynamic mass	kg
n_{blades}	number of pump blades	-
N_d	rotation velocity pump	rpm
n_i	number of times load S_i occurs	cycles
N_i	fatigue endurance to load S_i	cycles
p	fluid pressure	N/m^2
p_f	fluid pressure	N/m^2
P_{failure}	failure probability	year^{-1}
P_n	pump damping force for structural mode n	N
p_v	vapour pressure	N/m^2
q	distributed force	N/m^2
q	discharge	m^3/s
q_f	distributed hydrodynamic force	N/m^2
q_p	distributed pump force	N/m^2
Q_d	pump design discharge	m^3/s
Q_{mp}	integral of structural mode m and fluid mode p	-
t	time	s
t	plate thickness	m
S_F	force spectrum	N^2/(rad/s)
S_{JON}	JONSWAP wave spectrum	m^2/(rad/s)
S_{TMA}	TMA depth-limited wave spectrum	m^2/(rad/s)
T	external moment	Nm
T_e	excitation period	Nm
u	fluid velocity in x-direction	m/s
U_{10}	wind velocity at 10 metre height	m/s
v	fluid velocity in y-direction	m/s
w	fluid velocity in z-direction	m/s
w	structural deflection in y-direction	m
W	width	m
W	structural deflection frequency-domain amplitude	m
x	coordinate in x-direction	m
X	fluid potential solution in x-direction	m^2/s
y	coordinate in y-direction	m
Y	fluid potential solution in y-direction	m^2/s
z	coordinate in z-direction	m
Z	fluid potential solution in z-direction	m^2/s
Z_{mn}	fluid impedance for structural mode m and n	N

Greek

Symbol	Description	Unit
β_m	beam or plate solving variable	
γ	relative damping	-
ΔH	head difference	m
δ_{HQ}	local pump curve gradient	m/(m^3/s)
δ_{mn}	dirac delta function for m and n	-
Δx	offset sluice width compared to gate structure	m
Δz	offset sluice bottom (sill height)	m
η	pump efficiency	-
η	surface elevation	m
λ	wave length	m
ρ_b	distributed beam weight	kg/m
ρ_f	fluid density	kg/m^3
ρ_p	distributed plate weight	kg/m^2
σ	cavitation number	-
ω	radial velocity or frequency	rad/s
ω_n	natural radial frequency or radial eigenfrequency	rad/s
ω_p	pump radial velocity	rad/s
Ω	excitation frequency	rad/s
Φ	fluid potential	

Notations

Symbol	Description
$\mathbf{X}$	matrix
$\mathbf{x}$	vector
$\hat{x}$	amplitude
$\tilde{x}$	frequency-domain amplitude

Abbreviations

Symbol	Description
amp	amplitude
cog	center of gravity
CFD	computational fluid dynamics
FEM	finite element method
FSI	fluid-structure interaction
MDOF	multiple degree of freedom
NPSH	net positive suction head
NPSH$_a$	NPSH available
NPSH$_r$	NPSH required
rms	root mean square
SDOF	single degree of freedom

List of Figures

List of Tables

A | Hydraulic boundary conditions

The operating conditions of the pumps are of importance, as these partially determine the load cases on the gate. In a dynamic analysis the governing conditions are not as straightforward as in a static safety analysis. The response of the structure does not only depend on the force amplitude, but also its frequency. Therefore not only the highest water levels, discharges and waves are of importance, but a range of these combined conditions should be determined and checked.

A.1 Water levels

In section 3.2 the water levels during pump operation were determined. The maximum considered water level at the Waddensea of +2.50 m NAP corresponds to the present 1/1 year storm conditions. For design conditions in 2050, sea level rise must be included. Witteveen+Bos [40] has used water levels corresponding several return periods in their analyses, as shown in table A.1.

Table A.1: Maximum Waddensea and corresponding Lake IJssel water levels for different exceedance frequencies in 2050 [40]

Exceedance frequency [years]	1/1	1/10	1/100	1/1,000	1/10,000	1/100,000
Maximum Waddensea [m +NAP]	2.78	3.52	4.19	4.76	5.28	5.76
Corresponding Lake IJssel [m +NAP]	-0.60	-0.69	-0.83	-1.09	-1.29	-1.49

A maximum water level of +2.50 m NAP is maintained for the pump gates at Den Oever during operation, also as 2050 design conditions, since this is the bottom level of the sluice's upperstructure.

A.2 Wave spectrum

As was mentioned, the maximum water level during pump operation (+2.50 m NAP) corresponds to the current once per year storm conditions. Hofste [14] has researched peak wave pressures on the defence beam present at the northern side of the sluice for this water level. To do so, the required wind set-up, and corresponding wind velocities, were determined that lead to this water level. The highest wind velocity was then obtained when this water level is reached at low tide (highest wind set-up). This wind velocity therefore corresponds to a storm with a lower return period.

In figure A.1 the incoming wave directions are shown, as has been used to determine the hydraulic boundary conditions for the Den Oever lock. The 42° waves do not reach the

sluice gates, and thus only the 340° waves are significant to the pump complex. For this wave direction, the fetch is about 20 km, as can be seen in figure A.2. This assumes waves from the North Sea do not deflect onto the Waddensea.
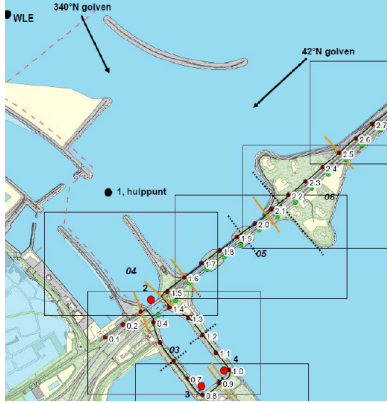

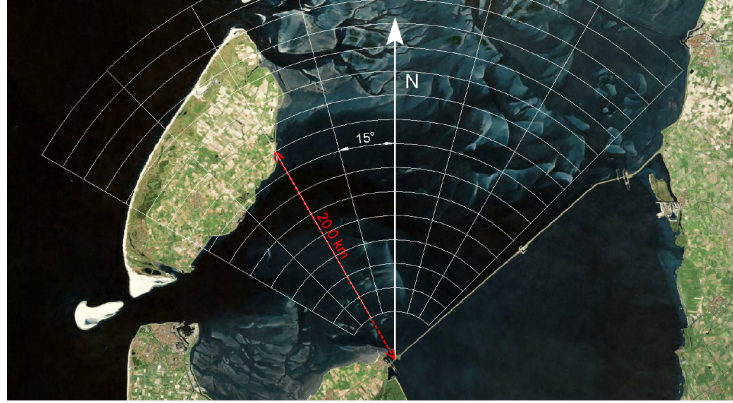Figure A.1: Local layout of the sluice area with the directions of the incoming waves [14]

Figure A.2: Fetch corresponding to the governing wave direction [14]

In the mentioned thesis [14], a JONSWAP spectrum was assumed. This spectrum applies to young sea states in deep water. The water depth in the Waddensea is however limited. The JONSWAP spectrum is an enhancement of the Pierson-Moskowitz spectrum. The latter applies to fully developed sea states. A depth function is used to adjust the JON-SWAP spectrum to the limited depth, according to Det Norske Veritas [8]. The JONSWAP spectrum can be described by the following equation:

$$S_{\text{JON}}(\omega) = \frac{\alpha g^2}{\omega^5} \exp\left[-\frac{5}{4}\left(\frac{\omega_p}{\omega}\right)^4\right] \gamma^r \tag{A.1}$$

with:

$$r = \exp\left[-\frac{(\omega - \omega_p)^2}{2\sigma^2\omega_p^2}\right] \tag{A.2}$$

The four constants α, ω_p, γ and σ were determined based on collected wave data (of the North Sea) and are dependent on the fetch F and wind velocity U_{10}.

$$
\begin{aligned}
\alpha &= 0.076 \cdot \left(\frac{U_{10}^2}{Fg}\right)^{0.22} \\
\omega_p &= 22 \cdot \left(\frac{g^2}{U_{10}F}\right)^{1/3} \\
\gamma &= 3.3 \\
\sigma &= \begin{cases} 0.07 & \omega \leq \omega_p \\ 0.09 & \omega > \omega_p \end{cases}
\end{aligned}
\tag{A.3}
$$

The depth function is described as follows [8]:

$$\phi(\omega) = \frac{\cosh^2(kh)}{\sinh^2(kh) + \dfrac{\omega^2 h}{g}} \tag{A.4}$$

And thus the final wave spectrum by:

$$S_{\text{TMA}}(\omega) = \phi(\omega) \cdot S_{\text{JON}}(\omega) \tag{A.5}$$

Based on Hofste [14], a wind velocity of $U_{10} = 32.4$ m/s and a fetch of $F = 20$ km are used. The depth of 5 metre used in the respective thesis seems an underestimation of the Waddensea water depth, instead d = 10 m is used. It is neglected that this influences the set-up calculation on which the wind speed is based. The resultant spectrum is shown in figure A.3.
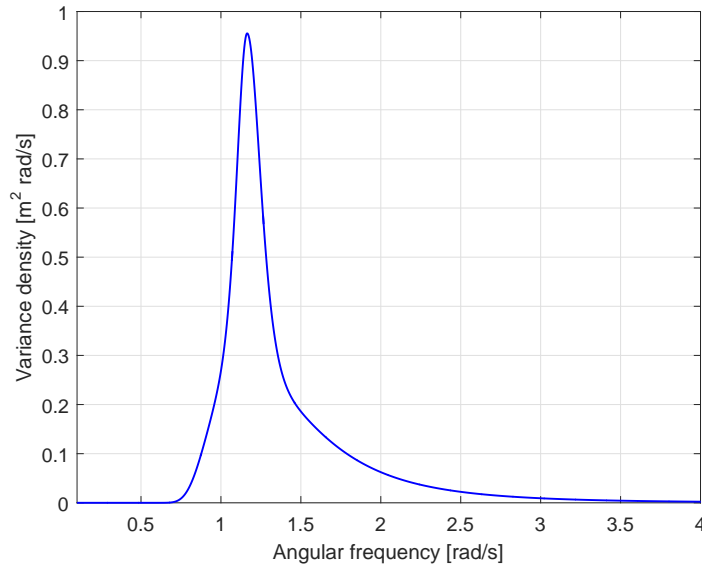
Figure A.3: Fetch corresponding to the governing wave direction [14]

The significant wave height corresponding to this spectrum is 2.47 m, given by:

$$H_{m0} \approx 4 \cdot \sqrt{m_0} \qquad \qquad \text{with: } m_0 = \int_{-\infty}^{+\infty} S(\omega)\, d\omega \tag{A.6}$$

This is based on a Rayleigh distribution of individual wave heights and a certain characteristic storm duration, see Holthuijsen [15].

Close to the discharge sluice, effects like wave shoaling might play a role. The difference between the Waddensea and sluice water depth is however relatively small. Secondly, the discharge channel close to the sluice has larger water depths as well. The Waddensea spectrum is therefore used directly at the location of the pump gate.

A.3 Wave force

To transform the wave spectrum to a force on the sluice gate, a transfer function should be determined. It is not certain to what extent waves (and resulting pressures in the water column) can reach the pump gate at the maximum water level of +2.50 m, as waves will break on the upperstructure such as the defence beam. The effect of this defence beam has been researched, for which it was concluded that it might result in even higher wave pressures on the northern flood gate [24]. Only the wave pressures beneath still water are taken into account and are assumed unaffected by the structure.

By linear wave theory, the wave pressures given by a wave amplitude η are defined over the depth. The amplitude force function is defined as the force amplitude divided by the amplitude of the deflection. This is thus:

$$H_{F,\eta}(\omega) = \frac{\hat{p}_w(z)}{\hat{\eta}} = \rho_f g \cdot \frac{\cosh(kz)}{\cosh(kh)} \tag{A.7}$$

With z = 0 at the bottom level, similar to the derivations used in the models of chapter 5 and 6. The frequency dependence is implicit in the wave number, given by the dispersion equation. It is thus assumed the wave length is adjusted to the water depth in the sluice.

$$\omega^2 = kg \cdot \tanh(kh) \tag{A.8}$$

A requirement to use the transfer function on the wave spectrum, is that the pressure amplitude varies linearly with the wave amplitude. From above equations it can be seen that for $0 \geq z \leq h$ this is the case (although only for the pressures beneath mean water level). The shape of the wave pressures over the depth differs with the frequency and must be taken into account when determining the response of the gate on the force. The force spectrum is found as follows:

$$S_F(z,\omega) = H_{F,\eta}(z,\omega)^2 \cdot S_{\text{TMA}}(\omega) \tag{A.9}$$

B | Gate designs: input to the dynamic analysis

In this appendix the two reference gate designs for Den Oever made by Witteveen+Bos [40] are discussed. Furthermore the flexural rigidity and weight, both input for the analyses in this thesis, are determined. Subsequently, both designs are altered to 'fit' in the same global alternative and to have an isotropic bending stiffness.

B.1 Standardized gate designs

As discussed in 2.4, two gate designs are considered: the flood defence pump gate and the regular pump gate. These designs will these gates will be considered at the same location: that of the current southern flood gate. Since the designs by Witteveen+Bos have been made for different pump complex alternative, i.e. gates at the present southern gate and at the existing foundation on the Waddensea side, global dimensions differ slightly.

To consider both gate designs at the location of the present southern flood gate, dimensions of the second gate design are adjusted to the general gate layout. An overview of this layout is given in figure B.1. This geometry is based on the design of the flood defence pump gate, which was made for the considered location and is elaborated in most detail by Witteveen+Bos [40].

The location of the pumps in the standard design is based on design rules, which were elaborated in section 2.4, and on what is stated in the report of Witteveen+Bos [40]. This conflicts however with what is used in the 'Scia' calculation model of figure 2.12, in which the center of the pumps is equally spaced over the width of the gate and the distance between the pumps is the same as between wall and pumps.

The detailed design was in first instance made for a width of 12 m and a height of 7.5 metre. Later insight showed however the gate is 12.2 wide and should be 7.25 metre high. The heart-to-heart span of the supporting wheels is 12.5 metre [40]. These altered dimensions result in some changes that affected the total weight.

The layout of the stiffening elements for each gate, is taken from the designs by Witteveen+Bos [40] as much as possible. Due to the changes in the location of the pumps, the layout of the stiffening elements is altered slightly as well.

The dynamic behaviour of the gate is determined by its flexural rigidity and its distributed weight, as was shown in section 4.1.2. The weight of each gate is therefore inventoried and the moment of inertia I of both gates in each direction is determined in the following sections. The modulus of elasticity E of construction steel is 210,000 N/mm^2.
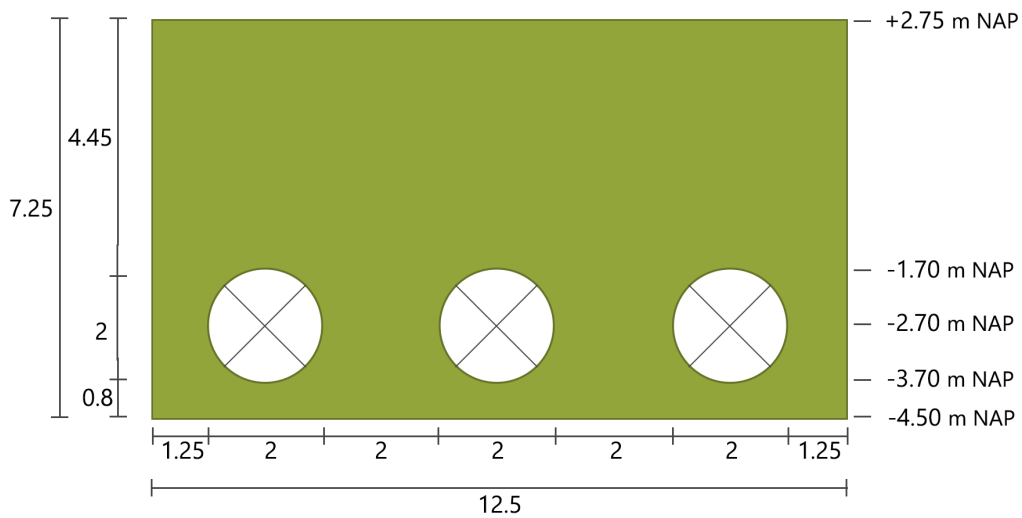
Figure B.1: Schematic front view of the standard pump gate layout, used for both designs, with dimensions in metres. Pump location differs from what is used in the calculation model by Witteveen+Bos [40]. In appendix B the layout has been further elaborated.

B.2 Flood defence pump gate

The 'standard' design of the flood flood defence gate is based on the detailed design made by Witteveen+Bos [40]. Due to the different location of the pumps in the gate than in that design, the location stiffening elements are slightly shifted. The lowest main horizontal element is at 0.5 above bottom gate instead of 1 metre. The heart-to-heart distance is kept the same. The vertical elements are shifted along with the pumps at the respective height. An overview is given in figure B.2.
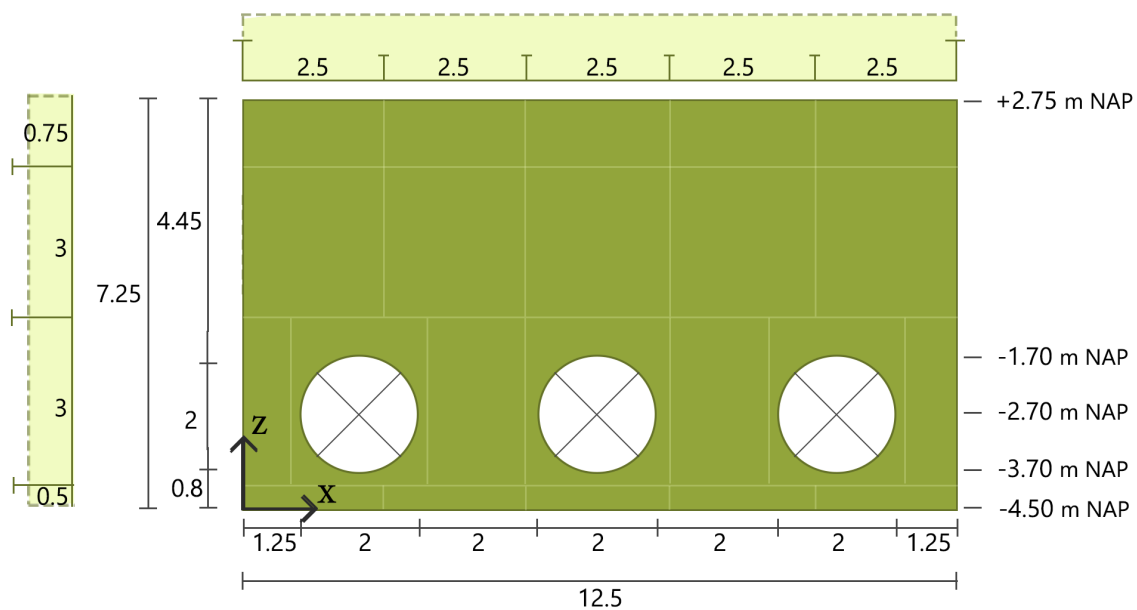
Figure B.2: Schematic front view of the standard pump gate layout with dimensions (in metres)

The three large stiffening elements, together with the front plate, are assumed to provide the stiffness in horizontal direction. The smaller elements only direct local pressures to the vertical stiffening and large horizontal stiffening elements. The large elements have a moment of inertia of $1.22 \cdot 10^{10}$ mm^4 and the smaller elements of $5.55 \cdot 10^6$ mm^4, which is more than 2000 times smaller. At the edges of the gate the main girders gradually decrease in size in order to optimize material use. This local decrease in stiffness is not taken into account.

In vertical direction the largest elements are the two at each side. When the gate is considered supported over that height, these would not provide additional stiffness to the body however. In the body four vertical elements provide stiffness, locally at the gate this is increased to six elements. This deviation could be included in a 3D model of the gate, but in the calculation of the moment of inertia this is not included.

An overview of the elements used, is given in figure B.3. The front plate thickness in this design is 15 mm. This dimensions are used to determine the moment of inertia in the following subsection.
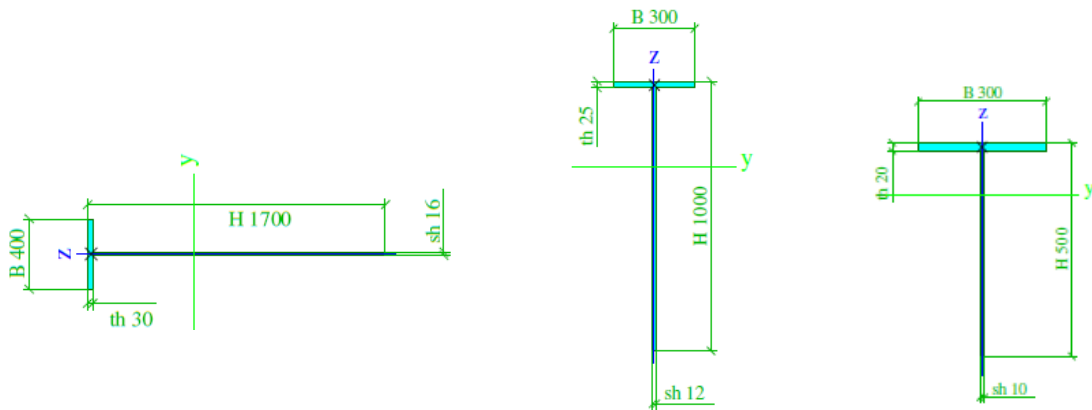
(a) Main horizontal element.
A= 38720 mm^2;
$I_{xx} = 1.2194 * 10^{10}$ mm^4;
$cog_x = 1098$ mm.

(b) Vertical elements at edges.
A= 19200 mm^2;
$I_{zz} = 2.0698 * 10^9$ mm^4;
$cog_z = 683$ mm.

(c) Vertical elements body.
A= 10800 mm^2;
$I_{zz} = 2.5903 * 10^8$ mm^4;
$cog_z = 379$ mm.

Figure B.3: Stiffness elements of flood defence pump gate [40]

The flood defence gate has a weight of 30,000 kg, which includes 10 percent of estimated finishing material.

B.2.1   Moment of inertia

The moment of inertia and center of gravity of each separate element is given by Witteveen+Bos [40, page 261] and shown in figure B.3. This simplifies the determination of the moment of inertia of the total gate. Each contribution can be added by applying steiner.

In horizontal direction (thus for a vertical cross-section) the I_{xx} of the plate is $\frac{1}{12} \cdot 7250 \cdot 15^3 = 2039063$ mm^4. The center of gravity of the total gate, measured from the outer side of the plate, becomes:

$$cog_x = \frac{3 \cdot (1098 + 15) \cdot 38720 + 7250 \cdot 15 \cdot 0.5 \cdot 15}{3 \cdot 38720 + 7250 \cdot 15} = 578.5 \text{ mm} \tag{B.1}$$

And the total moment of inertia in horizontal direction:

$$
\begin{aligned}
I_{xx,total} &= I_{xx,el} + I_{xx,el,steiner} + I_{xx,plate} + I_{xx,plate,steiner} \\
&= 3 \cdot 1.2194 \cdot 10^{10} + 3 \cdot (1098 + 15 - 578.5)^2 \cdot 38720 \\
&\quad + 2039063 + (578.5 - 0.5 \cdot 15)^2 \cdot 15 \cdot 7250 \\
&= 1.0523 \cdot 10^{11} \text{ mm}^4
\end{aligned}
\tag{B.2}
$$

The same can be done for the vertical direction. Like mentioned, the elements at the edges will not be taken into account in this calculation and thus only the four body elements provide stiffness. The center of gravity then lies at:

$$cog_z = \frac{4 \cdot (379 + 15) \cdot 10800 + 12500 \cdot 15 \cdot 0.5 \cdot 15}{4 \cdot 10800 + 12500 \cdot 15} = 79.87 \text{ mm} \tag{B.3}$$

And the total moment of inertia in vertical direction:

$$
\begin{aligned}
I_{zz,total} &= I_{zz,el} + I_{zz,el,steiner} + I_{zz,plate} + I_{zz,plate,steiner} \\
&= 4 \cdot 2.5903 \cdot 10^8 + 4 \cdot (379 + 15 - 79.87)^2 \cdot 10800 \\
&\quad + 3515625 + (79.87 - 0.5 \cdot 15)^2 \cdot 15 \cdot 12500 \\
&= 6.2845 \cdot 10^9 \text{ mm}^4
\end{aligned}
\tag{B.4}
$$

When the edge elements would be included the following results would be obtained: $cog_z = 168.1$ mm and $I_{zz} = 22.7 \cdot 10^9$ mm^4.

The following flexural rigidities are thus found:

- $EI_{zz} = 22.1 \cdot 10^9 \quad$ [Nm^2]
- $EI_{xx} = 1.32 \cdot 10^9 \quad$ [Nm^2]

The plate bending stiffness is equal to the flexural rigidity per running metre. For the horizontal direction this would result in:

$$D_{zz} = \frac{EI_{zz}}{L_z} = \frac{22.1 \cdot 10^9}{7.25} \approx 3.0 \cdot 10^9 \quad \text{[Nm]} \tag{B.5}$$

Since the plates are analysed as isotropic in the beam and plate models of chapter 5 and 6, this bending stiffness is taken as representative for both directions. However, in reality the stiffness of the body in vertical direction is almost 17 times smaller than in horizontal direction. With the beam edges included this would be about 5 times.

B.3   Regular pump gate

The less detailed design of the pump gate of Witteveen+Bos [40] is with respect to layout in horizontal direction quite similar to the flood defence gate. Also in that case, the lowest horizontal element is at 1 metre above the bottom. Again, this is changed to 0.5 metre. The heart-to-heart distance between these elements of 2.5 is changed to 3 metre for this reason and due to the slightly larger height of the gate. This might result in greater loading of especially the middle horizontal element. Its dimensions are not changed however as the gate is statically checked on $u_c = 0.7$. The dynamic behaviour will be investigated further. Plating at the top and bottom of the gate is not taken into account.

In vertical direction 13 elements provide stiffness, of which 2 main edge elements, 3 main body elements and 8 smaller body elements. In the original design a heart-to-heart distance of 1 metre was used for all elements. Due to the enlarged width, this distance increases to 1.25 at the edges. The two edge elements are again assumed to provide no additional support.
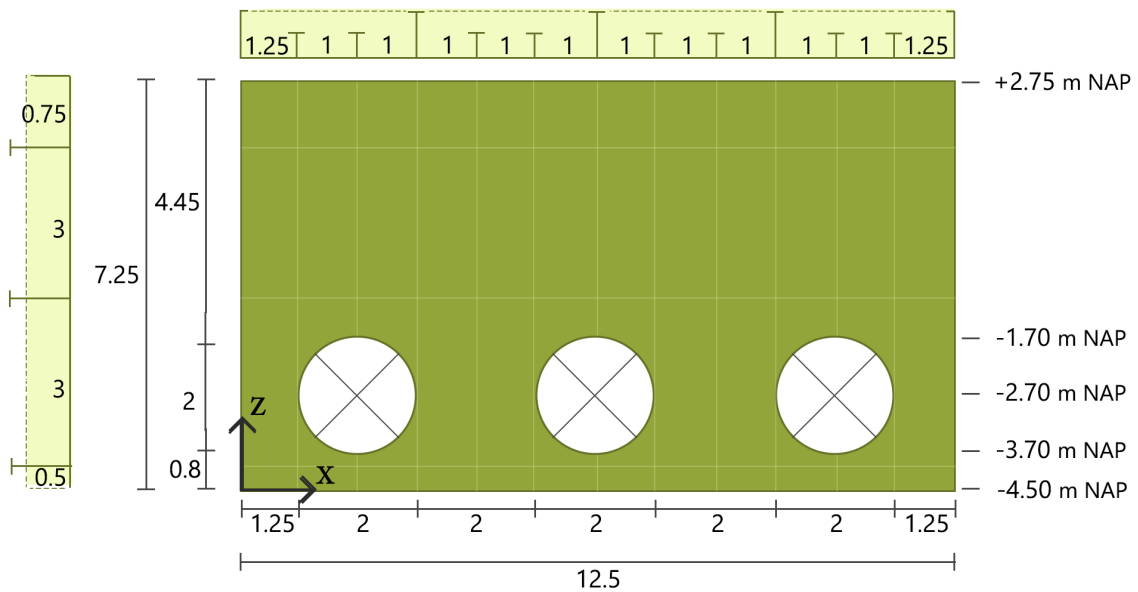
Figure B.4: Schematic front view of the standard pump gate layout with dimensions (in metres)

The gates plate thickness is in this design is 10 mm. The elements are shown in figure B.5. The indicated height is in this case including the flange thickness and front plate thickness. The latter is thus deducted when determining the area, moment of inertia and center of gravity of the separate elements, indicated below the figures. The vertical edge elements are the same as in figure B.5b, but with a shaft thickness of 15 mm and half the flange width (extended to one side).

The weight of the regular gate is estimated to be 16400 kg. When similar to the flood gate 10 percent is added for finishing, a total weight of 18040 kg is obtained.

(a) Main horizontal element.
A= 15975 mm^2;
I$_{xx}$ = 5.7210 $* 10^8$
mm^4;
cog$_x$ = 421 mm.

(b) Main vertical
body elements.
A= 14280 mm^2;
I$_{zz}$ = 4.9064 $* 10^8$
mm^4;
cog$_z$ = 437 mm.

(c) Secondary vertical
elements.
A= 3480 mm^2;
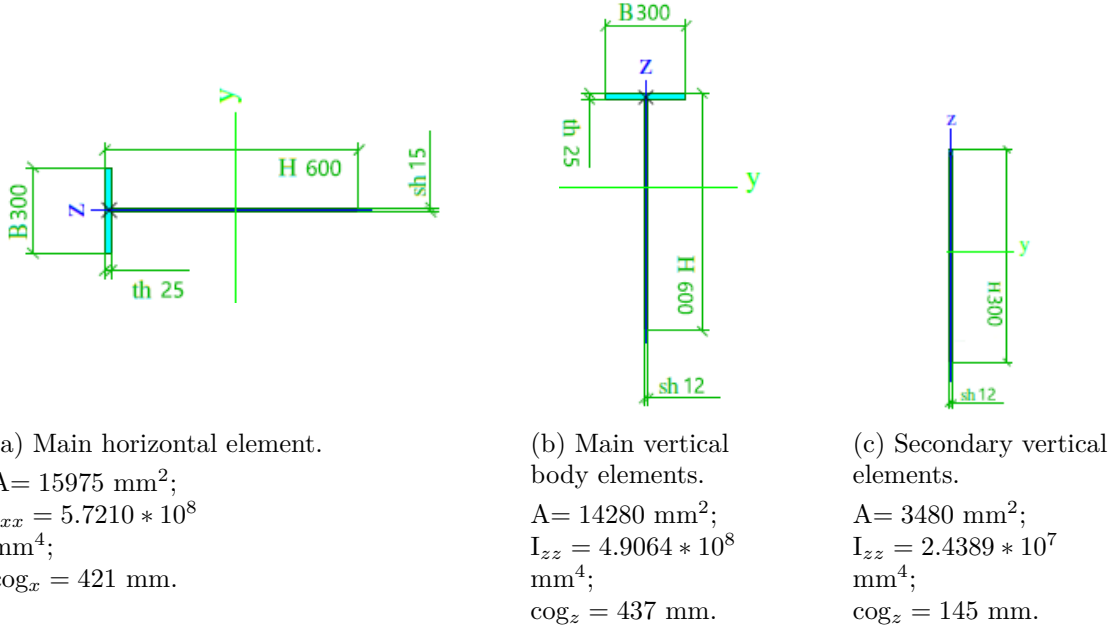I$_{zz}$ = 2.4389 $* 10^7$
mm^4;
cog$_z$ = 145 mm.

Figure B.5: Stiffness elements of flood defence pump gate [40]

B.3.1 Moment of inertia

The moment of inertia and center of gravity of each separate element is given in figure B.5. In horizontal direction (thus for a vertical cross-section) the I$_{xx}$ of the plate is $\frac{1}{12} \cdot 7250 \cdot 10^3 = 604167$ mm^4. The center of gravity of the total gate, measured from the outer side of the plate, becomes:

$$cog_x = \frac{3 \cdot (421 + 10) \cdot 15975 + 7250 \cdot 10 \cdot 0.5 \cdot 10}{3 \cdot 15975 + 7250 \cdot 10} = 174.5 \text{ mm} \tag{B.6}$$

And the total moment of inertia in horizontal direction:

$$\begin{aligned}
I_{xx,total} &= I_{xx,el} + I_{xx,el,steiner} + I_{xx,plate} + I_{xx,plate,steiner} \\
&= 3 \cdot 5.7210 \cdot 10^8 + 3 \cdot (421 + 10 - 174.5)^2 \cdot 15975 \\
&+ 604167 + (174.5 - 0.5 \cdot 10)^2 \cdot 10 \cdot 7250 \\
&= 6.954 \cdot 10^9 \text{ mm}^4
\end{aligned} \tag{B.7}$$

The same can be done for the vertical direction. Like mentioned, the elements at the edges will not be taken into account in this calculation and thus only the 11 body elements provide stiffness.

$$cog_z = \frac{3 \cdot (437 + 10) \cdot 14280 + 8 \cdot (145 + 10) \cdot 3480 + 12500 \cdot 10 \cdot 0.5 \cdot 10}{3 \cdot 14280 + 8 \cdot 3480 + 12500 \cdot 10} = 122.7 \text{ mm} \tag{B.8}$$

And the total moment of inertia in vertical direction:

$$
\begin{aligned}
I_{zz,total} &= I_{zz,el} + I_{zz,el,steiner} + I_{zz,plate} + I_{zz,plate,steiner} \\
&= 3 \cdot 4.9064 \cdot 10^8 + 8 \cdot 2.4389 \cdot 10^7 + \cdot(437 + 10 - 122.7)^2 \cdot 14280 \\
&\quad + \cdot(145 + 10 - 122.7)^2 \cdot 3480 + 1041667 + (122.7 - 0.5 \cdot 10)^2 \cdot 10 \cdot 12500 \\
&= 7.1280 \cdot 10^9 \ \text{mm}^4
\end{aligned}
\tag{B.9}
$$

When the edge elements would be included the following results would be obtained: $\text{cog}_z = 151.9$ mm and $\text{I}_{zz} = 10.058 \cdot 10^9 \ \text{mm}^4$.

In this case the stiffness of the body in vertical direction is slightly larger than that in horizontal direction. The horizontal-vertical stiffness ratio is 0.98, and 0.69 when the edge elements are included.

The following flexural rigidities are thus found:

- $EI_{zz} = 1.46 \cdot 10^9 \quad [\text{N/m}^2]$
- $EI_{xx} = 1.50 \cdot 10^9 \quad [\text{N/m}^2]$

For the horizontal direction this would result in a bending plate stiffness:

$$
D_{zz} = \frac{EI_{zz}}{L_z} = \frac{1.46 \cdot 10^9}{7.25} \approx 2.0 \cdot 10^9 \quad [\text{Nm}]
\tag{B.10}
$$

Since the plates are analysed as isotropic in the beam and plate models of chapter 5 and 6, this bending stiffness is again taken as representative for both directions.

C | Pump specifics

In this appendix additional background on pumps in general and on the expected pumps at Den Oever is treated. This includes background on pump classification (C.1), pump curve characteristics (C.2) and efficiency (C.3). Furthermore the pump curve of the pumps at Den Oever estimated by Witteveen+Bos [40] is stated in section C.4. As part of the pump requirements, vibrations limits are given in section C.5 and the concept of cavitation is elaborated in section C.6.

C.1 Classification

In section 2.3.2, an introduction was given on dynamic and displacement type pumps. The axial flow pump that is expected to be used at Den Oever, is a dynamic pump. A further classification of this category is given in figure C.1. As can be seen, centrifugal pumps are further classified into axial, radial and peripheral pumps. Each of those pump types can be single or multi stage. In case of the latter, multiple impellers and volutes are placed in series.
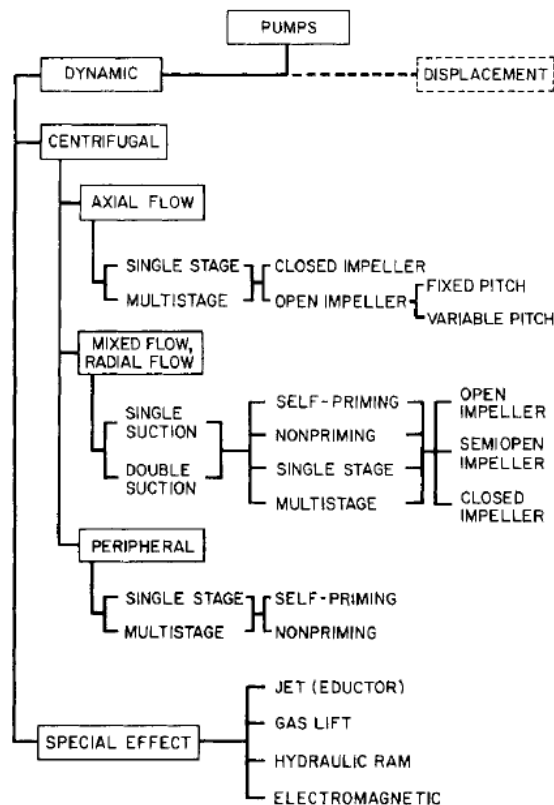
Figure C.1: Classification dynamic pumps [18]

In case of variable pitch, the blades are able to rotate around their own axis and can therefore reach a high efficiency over a larger power range.

C.2   Pump characteristic

Pumps add energy to the flow, and by doing so can overcome a head difference. In theory, the power of a pump or turbine at a certain head an discharge is given by:

$$P = \eta \, \rho g \, Q \, H_{pump} \tag{C.1}$$

in which:

P	=	power [W]
η	=	pump efficiency [-]
ρ	=	density fluid [kg/m^3]
g	=	gravitational acceleration [m/s^2]
Q	=	discharge [m^3/s]
H_{pump} (or ΔH)	=	hydraulic head difference over pump [m]

Each pump has a specific discharge-head (Q-H) relation called the pump curve or pump characteristic. The actual flow rate depends not only on the pump characteristic, but on the system characteristic as well. The pump will overcome a certain static head, which in in the case of Den Oever is the water level difference between both sides of the sluice. In addition to this, friction losses should be overcome that depend on the flow velocity. In figure C.2 an example of these curves is given. The intersection of the system and pump curve shows the discharge and head and which the pump will operate. This is called the duty point.
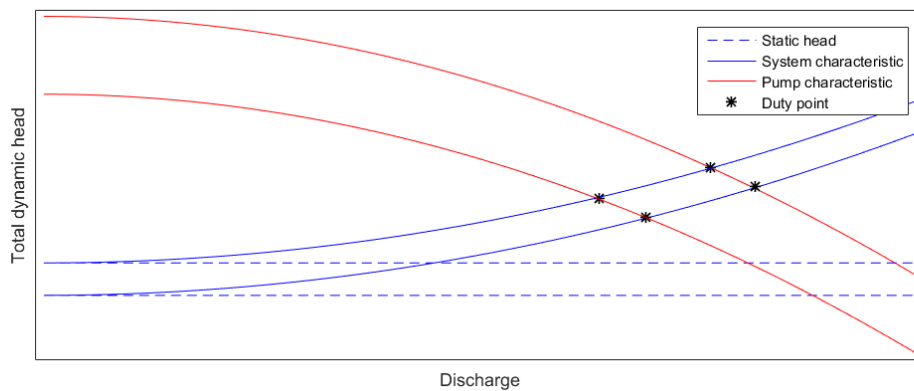
Figure C.2: Characteristic curves pump flow

In figure C.2 it is illustrated that an increase in static head will decrease the discharge through the pumps. If the pump has more than one rotation speed (ω) at which it can operate, each rotation speed has its own characteristic curve. In this way the discharge rate can be varied for a constant outside water level difference. An increase in rotation speed will results in a higher discharge as well as pump head, the latter as a result of increased

friction. The characteristics of the pumps are generally given by the manufacturer. An estimated pump curve for Den Oever is given in section C.4.

C.3   Efficiency

The efficiency during operation, for a given geometry and pump, is f($Q,\Delta H$). The energy loss consists of mechanical loss, hydraulic loss and volumetric loss [18], in terms of efficiency:

$$\eta = \eta_m \cdot \eta_H \cdot \eta_V \tag{C.2}$$

These efficiency components can be defined as:

$$\text{(Mechanical efficiency) } \eta_m = \frac{P_I}{P} = \frac{P - P_f}{P} \tag{C.3}$$

$$\text{(Hydraulic efficiency) } \eta_H = \frac{\Delta H}{\Delta H_I} = \frac{\Delta H_I - \Delta H_L}{\Delta H_I} \tag{C.4}$$

$$\text{(Volumetric efficiency) } \eta_V = \frac{Q}{Q + Q_L} \tag{C.5}$$

In this ΔH_I is the 'ideal head', which is the hydraulic head without any hydraulic losses. The pump power calculated with this ideal head is the ideal power, thus defined as $P_I = \rho g \cdot Q \cdot \Delta H_I$. P_f is the power loss due to external drag of e.g. bearings, seal and fluid.

ΔH_L is the hydraulic head loss. If pump efficiency is calculated, only the hydraulic losses in the flow passage of the pump must be taken into account. The efficiency of the total system is however lower due to inflow losses and friction of the in- and outflow at the full sluice construction.

Finally, Q_L is the leakage of water past the impeller back to the inlet. This fluid volume has received energy from the pump, but 'in vain' as it leaks back.

The efficiency of the pump depends on the combination of total head and discharge head it operates at. At the best efficiency point (BEP) this efficiency is the highest [29]. The BEP is not equal to the point of maximum power. The pump specifics should be chosen in such a way that the pump can operate most of the time at or around this point. The duty point shown in figure C.2 will have different (mechanical) efficiencies.

C.4   Den Oever pump characteristic

By some indicative data and scaling laws, a pump curve is estimated in the report of [40]. The following efficiencies are estimated:

- $\eta_{mechanical} = \eta_{motor} \cdot \eta_{cables}$
    - $\eta_{\text{motor}} = 0.98$
    - $\eta_{cables} = 0.95$

137

- $\eta_{pump} = 0.85$
- $\eta_{flow} = 0.6$

These efficiencies are assumed constant and do thus not change at different head and discharges. The validity of the pump curve is therefore less certain at points far from the known design head and discharge. The values in the design point are as follows:

- $H_d = 1.0$ m
- $Q_d = 18$ m^3/s

With 23 active pumps, total discharge of the pumping station at the design point is 414 m^3/s. The estimated curve is given in table C.1, based on a constant pump rotation speed. A graph of this curve was shown in section 2.4.3.

Table C.1: Estimated pump curve, values given for the total of 23 pumps [40]

H$_{pump}$ [m]	Reduction factor [-]	Discharge [m^3/s]	Power [kW]
3.6	0.75	311	23,095
3.2	0.80	331	21,897
2.7	0.85	352	19,631
2.2	0.90	373	16,936
1.6	0.95	393	13,001
1	1.00	414	8,554
0.4	1.05	435	3,593
-0.2	1.10	455	-1,882
-0.7	1.15	476	-6,886
-0.779	1.17	484	-7,796

C.5 Vibration limits

The pumps impose requirements on the system. As pumps are normally seen as the vibration inducers, situated on a heavy foundation, not much is known on the requirements of external vibrations. In the ISO standards some guidelines are given for the vibration velocity limits of non-rotating parts, see table C.2. These values could be taken as representative for the resulting overall vibration in the pumps due to the total dynamic system.

As these are designed for velocity measurements in situ, the root mean square (rms) value is used. In case of harmonic sine motion, the amplitude can be divided by $\sqrt{2}$ in order get the rms value. In table C.1 it can be seen that the power of the pumps at the design point is 8554 kW for 23 pumps, or $8854/23 \approx 385$ kW per pump. The pumps at Den Oever are thus of the > 200 kW category.

Category 1 is applicable to pumps in hazardous situations, like chemical pumps. The pumps at Den Oever are assumed to be of category 2 as no such direct risks are of importance. The flood reliability is treated separately from this, as a redundant pump is available and risks of failure are included in the specific study.

Table C.2: ISO standard velocity limits for non-vibrating pump parts [10]

| Zone | Description | Vibration velocity limit mm/s rms value | | | |
| | | Category 1 | | Category 2 | |
		≤ 200 kW	> 200 kW	≤ 200 kW	> 200 kW
A	Newly commissioned machines in POR	2.5	3.5	3.2	4.2
B	Unrestricted long term operation in AOR	4.0	5.0	5.1	6.1
C	Limited operation	6.6	7.6	8.5	9.5
D	Hazard damage	> 6.6	> 7.6	> 8.5	> 9.5

C.6 Cavitation

Cavitation is the forming of vapour bubbles in a liquid as a consequence of pressure reduction. In more popular terms: the boiling of water due to low pressure instead of high temperature. It is an important phenomenon in pump and turbine design. Most damage is induced when the vapour bubbles implode. These implosions result in high impacts on the runner blades or walls they are near. An example of typical cavitation damage is given in figure C.3.
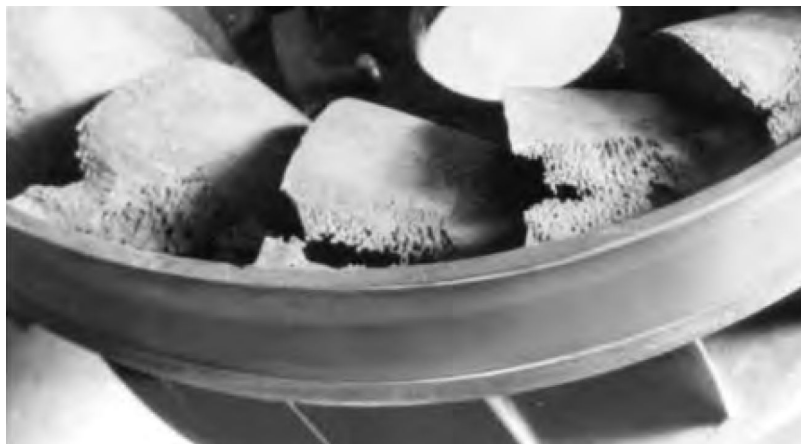
Figure C.3: Cavitation damage on Francis propeller [29]

Brennen [4] states the following three adverse effects of cavitation:

 (i) Damage on material surfaces
 (ii) Degraded performance (or efficiency)
(iii) Instabilities due to dynamic flow fluctuations

The performance drops significantly from a certain level of inlet pressure (see figure C.4). This phenomenon is called cavitation breakdown. As there are many circumstances in which it proves to be impossible to completely eliminate cavitation, efforts are done to optimize pump performance and damage resistance in the presence of cavitation.

The third effect is a consequence of the fact that cavitation affects not only the steady state fluid flow, but also the dynamic response of the flow. This leads to instabilities in the flow that do not occur in the absence of cavitation. Oscillating flow rates and pressures can threaten the structural integrity of the pump or its inlet or discharge ducts [4]. Cavitation can thus be an inducer of structural vibrations.

The basic notions to describe and quantify cavitation are elaborated below, mainly based on Schiavello and Visser [29]. The three most common parameters involved in the prediction of cavitations are:

- Cavitation number, σ
- Net positive suction head, NPSH
- Thoma cavitation number, σ_{th}

The cavitation number is defined as:

$$\sigma = \frac{p_1 - p_v}{\frac{1}{2}\rho v_R^2} \tag{C.6}$$

in which: p_1 = upstream static pressure [Pa]
$\quad\quad\quad\quad\ p_v$ = vapour pressure [Pa]

The reference velocity v_R is commonly taken as the circumferential impeller eye velocity (i.e. inlet-vane tip speed): $v_R = v_e = \Omega R_{1T}$. In this R_{1T} is the inlet-vance tip radius.

The NPSH is defined as the the total pressure of the fluid at the center line of the impeller above the vapour pressure of the fluid, see equation (C.7). This can thus be seen as the margin against vaporization of the fluid as it enters the pump.

$$NPSH = \frac{p_{tot,in} - p_v}{\rho g} \tag{C.7}$$

The total head at inlet is thus defined as:

$$p_{tot,in} = p_{static,in} + \frac{1}{2}\rho v_{in}^2 \tag{C.8}$$

in which: $p_{static,in}$ = static pressure at pump inlet [Pa]

The Thoma number is defined as:

$$\sigma_{th} = \frac{NPSH}{H_{pump}} \tag{C.9}$$

in which: H_{pump} = total pump head [m]

Since cavitation generally occurs at the inlet to the pump, the total pump head is not especially relevant to the phenomenon. The Thoma cavitation parameter is therefore not a particularly useful one [4, 29].

The first appearance of cavitation is called cavitation inception. When the suction pressure (or NPSH) is further reduced, the region of cavitation enlarges, starting to cause noise,

damage, performance change, head breakdown, loss of priming, and vapour lock [29]. Different stages are shown in figure C.4. Before head breakdown, the point in which the pump head reduces drastically, there is a point of maximum cavitation damage. Due to the cushioning effect of the surrounding bubbles, the cavitation damage decreases beyond this point. Other points often defined are the 2, 3 or 5 percent head drop.
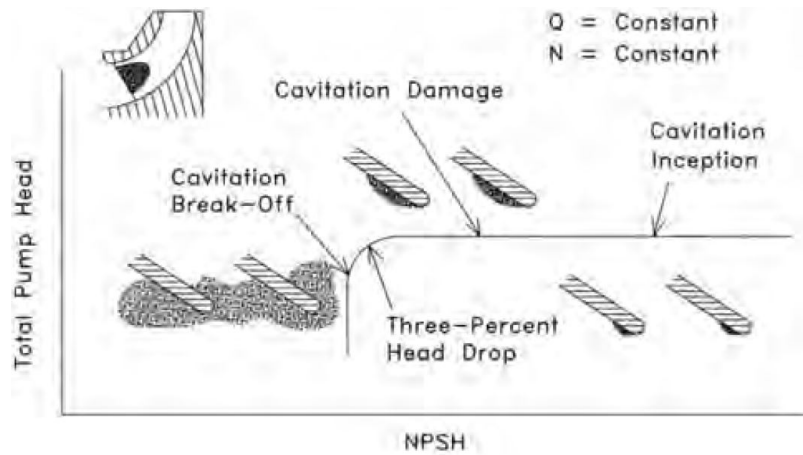
Figure C.4: Different stages in cavitation forming [29]

Florjancic and Frei [11] show that until the point of head breakdown, excitation due to cavitation is very low. The frequency of the cavitation implosions before that point is very high (> 10 kHz) and random, distributed all around the impeller. Although it was shown that the local stresses can become very high and damage the impeller, the overall forces are not very large.

Near head breakdown the cavitation becomes worse, the volume of cavitation bubbles disturbs the normal flow pattern in such a way, that pressure pulsation at lower frequencies occur. Large vapour cavities can alter the rotation symmetry and therefore produce forces (see hydraulic unbalance in the next section). The vibrations are thus caused by the large cavities and disturbed flow, and not the implosions.

D | Dynamics: theoretical background

This appendix complements chapter 4 and elaborates the theoretical background and literature on some notions of structural and hydrodynamics.

In section D.1 the amplification factor is given for the one degree of free system and several boundary conditions of the bending beam are treated. The phenomenon of fatigue is briefly discussed and Eurocode design requirements are elaborated in section D.2.

In section D.3 example and theory are discussed of the linear hydrodynamic coefficients: mass, damping and stiffness. Known fluid structure interactions that apply to flood gate are discussed in section D.4.

D.1 Structural dynamics

D.1.1 Single degree of freedom systems

In section 4.1.1 the one degree of freedom mass-dashpot-spring system was introduced. The response of this and other dynamics systems is highly depended on the eigenfrequency in relation the frequency of the forcing. When the force is harmonic as shown in equation (D.1), the response is described by equation (D.2):

$$F = F_{amp} \cdot sin(\omega t) \tag{D.1}$$

$$y = y_{amp} \cdot sin(\omega t - \Phi) \tag{D.2}$$

in which: Φ = phase shift between load and response [rad]

The amplification factor A, defined as the maximum spring force divided by the amplitude of the force F_{amp} is a function of the relative damping γ [17] and excitation frequency:

$$A = \frac{k \cdot y_{amp}}{F_{amp}} = f(\frac{1}{2\gamma}, \omega) \tag{D.3}$$

The relative damping is defined as:

$$\gamma = \frac{c}{c_{crit}} = \frac{c}{2\sqrt{km}} = \frac{c}{2m\omega_n} \tag{D.4}$$

in which: c_{crit} = critical damping coefficient [Ns/m]

In figure D.1 the relation of the amplitude factor and phase shift with the 'relative excitation frequency' f/f_n is shown. Some important relations become clear from this graph. When f/f_n is about equal to one, the response is maximal and the phase shift is $\pi/2$ or 90 degrees.

This phenomenon is called resonance. The force continuously adds energy to the system at this point. For $\gamma = 0$ none is dissipated and the excitation response will grow to infinity.

For excitation frequencies that are much higher than the natural frequency ($f/f_n > 2.5$) the excitation becomes very small. As expected, high relative damping reduces the response of the system.
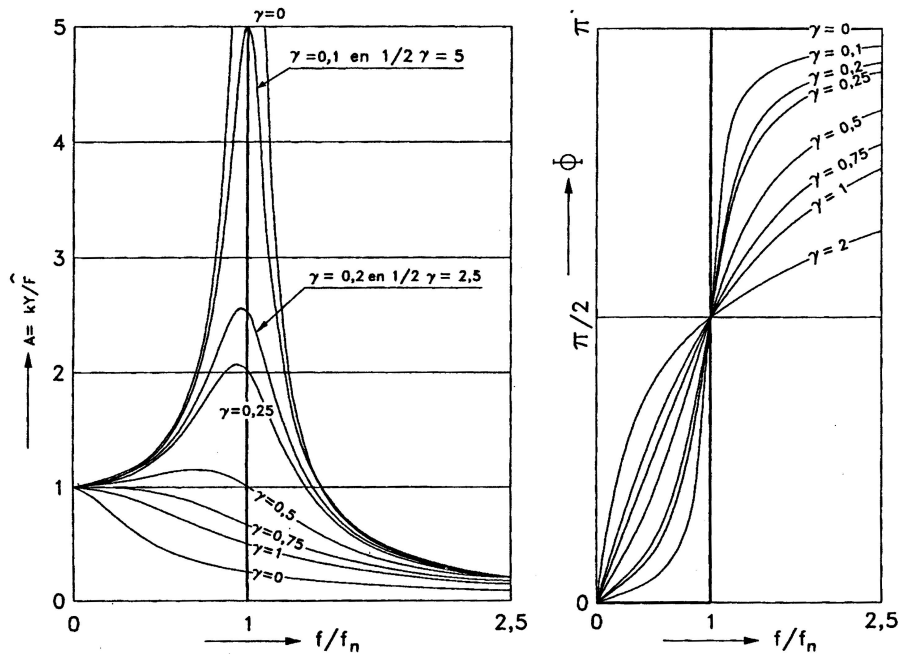
Figure D.1: Amplification factor as a function of f/f_n and relative damping γ for a single degree mass spring damper system [21]

D.1.2 Modal shapes and boundary conditions of a bending beam

In section 4.1.2 the bending beam was introduced, which can be described continuously by an equation of motion. Dynamic and kinematic boundary conditions apply at each side of the continuous function. Some possibilities for the bending beam are given in figure D.2.
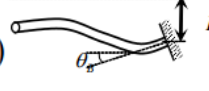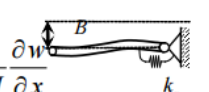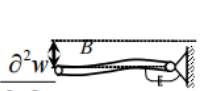
Figure D.2: Possible boundary conditions for a bending beam [23]

The eigenmodes and natural frequency of bending beams vary for different kinematic boundary conditions. This is shown in figure D.3. It can be seen that the supports have a great influence on the eigenmodes and natural frequencies of the beam. For example, there is more than a factor two between the first natural frequency of a simply supported beam and a clamped beam. The natural frequency of a beam with rotational stiffness can be imagined to behave somewhere in between.
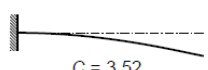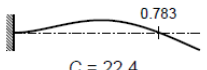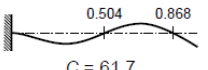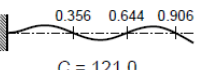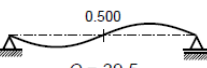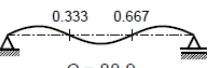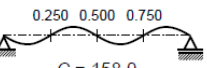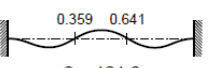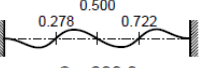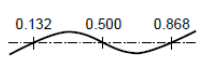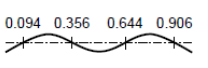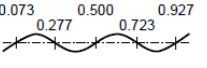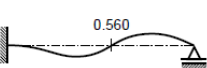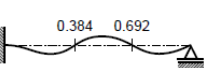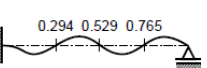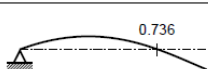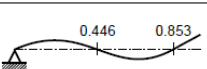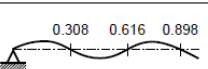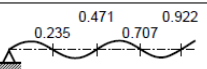
		$n = 1$	$n = 2$	$n = 3$	$n = 4$
clamped	free	$C = 3.52$	0.783 $C = 22.4$	0.504 0.868 $C = 61.7$	0.356 0.644 0.906 $C = 121.0$
simply supported	simply supported	$C = 9.87$	0.500 $C = 39.5$	0.333 0.667 $C = 88.9$	0.250 0.500 0.750 $C = 158.0$
clamped	clamped	$C = 22.4$	0.500 $C = 61.7$	0.359 0.641 $C = 121.0$	0.278 0.500 0.722 $C = 200.0$
free	free	0.224 0.776 $C = 22.4$	0.132 0.500 0.868 $C = 61.7$	0.094 0.356 0.644 0.906 $C = 121.0$	0.073 0.277 0.500 0.723 0.927 $C = 200.0$
clamped	simply supported	$C = 15.4$	0.560 $C = 50.0$	0.384 0.692 $C = 104.0$	0.294 0.529 0.765 $C = 178.0$
simply supported	free	0.736 $C = 15.4$	0.446 0.853 $C = 50.0$	0.308 0.616 0.898 $C = 104.0$	0.235 0.471 0.707 0.922 $C = 178.0$

Figure D.3: Natural frequencies and eigenmodes of bending beams for different kinematic boundary conditions $\omega_n = C_n\sqrt{EI/\rho Al^4}$ [32]

The way in which the supports are modelled is thus of great influence on the result. At the same time, the supports are most difficult to describe accurately.

D.2 Fatigue

Fatigue is the weakening of a material by a repeatedly applied load. The stress values as a result of this load can be much less than the 'normal' ultimate strength of the material.

A fatigue crack nucleus can be initiated on microscopically small scale. This is then followed by crack growth and ultimately failure of the material due to fatigue. The stages of fatigue life are shown in figure D.4.

Cyclic slip → Crack nucleation → Micro crack growth → Macro crack growth → Final failure

Initiation period   Crack growth period
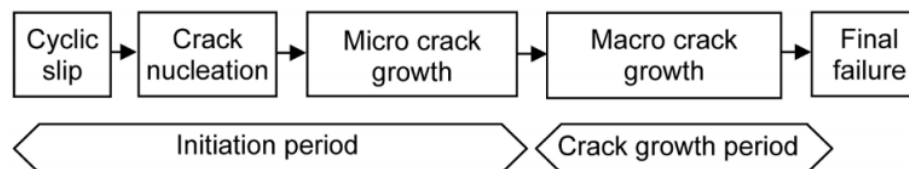
Figure D.4: Stages of fatigue life [30]

As a result of the pumps, the gates will be prone to a relatively high amount of load cycles. The gate and its connections to the structure and pumps might thus be sensitive to fatigue. The thesis work of Schönfeld [31] contains multiple examples of fatigue occurring at lock gates. One can imagine that the pump gate which are loaded with a much higher frequency, are prone to fatigue as well.

Fatigue is a complex phenomenon and predicting the exact occurrence of fatigue cracks is therefore difficult as well. Peak stresses in detailed connections are of importance and thus a finite element method (FEM) is generally needed. This thesis however does not aim to predict the location of fatigue cracks, which is more important in a later more detailed design stage, but rather the degree to which it is prone to fatigue. This in turn is closely linked to the required gate maintenance.

The Eurocode 3 describes the fatigue strength of steel in a simplified way, which is suitable for the mentioned application. The fatigue lifetime of steel material is described by a S-N curve. The 'S-part' stands for the occurring stresses, and the 'N-part' for the number of cycles the material can withstand at that stress. N is thus a strength parameter. The S-N curve for steel from the European standards is given in figure D.5.

Figure D.5: S-N curve for constant amplitude direct stress range [5]

The lines in figure D.5 represent detail categories. As can been seen, detail category 160 has the highest fatigue strength. This class contains rolled and extruded plates, rolled sections or seamless hollow sections. Witteveen+Bos [40] has used detail category 80 for the pump

gate designs. This value represents the characteristic fatigue stress at $N = 2 \cdot 10^6$ load cycles, also called the reference value $\Delta\sigma_c$.
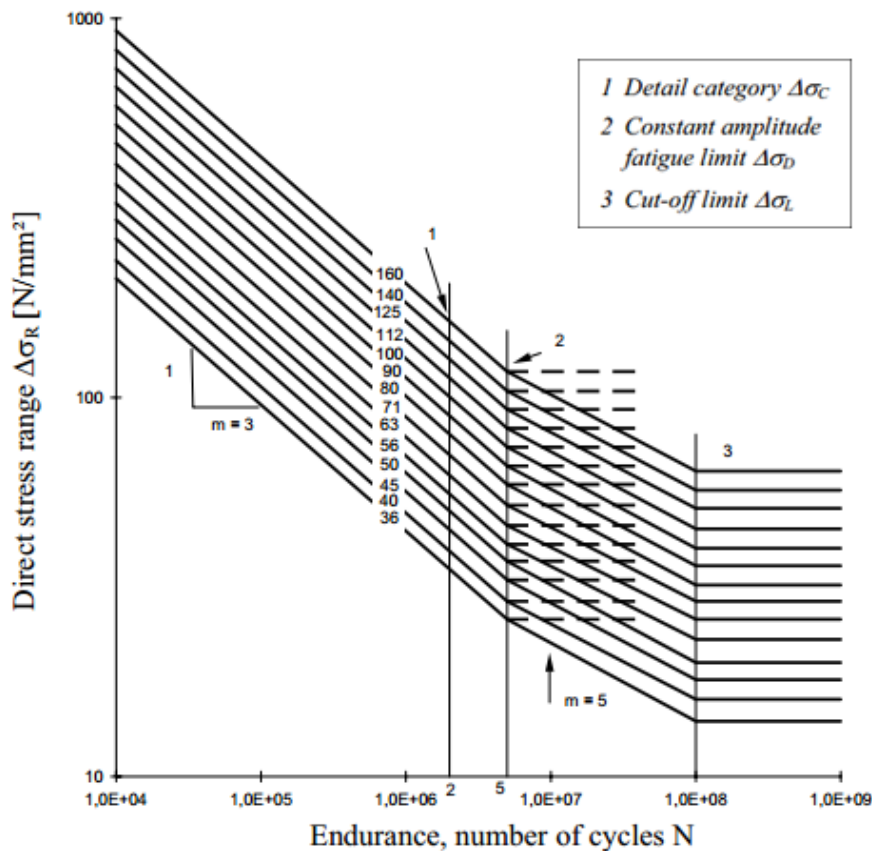
In figure D.5 two cases are represented. The first case is that of a constant amplitude loading. In that case the S-N curve becomes horizontal (dotted line) at $N = 5 \cdot 10^6$, representing unlimited strength at lower stress ranges. The second more common case is that of varying amplitude loading for which lower stress ranges are taken into account as they contribute to the damage initiated by higher stress ranges. A prerequisite is therefore that these higher stresses occur. The contribution of the lower stress ranges is relatively small, represented by m = 5 slope instead of the m = 3 slope. The S-N curve in the case of variable amplitude loading can be described by [5]:

$$\Delta\sigma_r^m * N = \Delta\sigma_c^m \cdot 2 \cdot 10^6 \qquad \text{with m = 3} \qquad \text{for} \qquad N \leq 5 \cdot 10^6 \qquad \text{(D.5a)}$$
$$\Delta\sigma_r^m * N = \Delta\sigma_d^m \cdot 5 \cdot 10^6 \qquad \text{with m = 5} \qquad \text{for} \qquad 5 \cdot 10^6 \geq N \leq 5 \cdot 10^8 \qquad \text{(D.5b)}$$

with:

$$\Delta\sigma_d = \left(\frac{2}{5}\right)^{1/3} \cdot \Delta\sigma_c \qquad \text{(D.6)}$$

and a cut-off limit at $N = 10^8$ has a value of:

$$\Delta\sigma_l = \left(\frac{5}{100}\right)^{1/5} \cdot \Delta\sigma_d \qquad \text{(D.7)}$$

in which: $\quad \Delta\sigma_c \quad = \quad$ reference value at $2 \cdot 10^6$ cycles [N/mm^2]
$\qquad\qquad \Delta\sigma_d \quad = \quad$ constant amplitude fatigue limit [N/mm^2]
$\qquad\qquad \Delta\sigma_l \quad = \quad$ cut off limit [N/mm^2]

The shear stress S-N curve has a similar, but does not have a reduced slope for $N > 2 \cdot 10^6$. It does not distinguish between variable loading or constant amplitude loading either.

To sum the effects of the variable amplitude loads, the so called Miner rule or linear cumulative damage hypothesis can be used, which states that in order for an element not to fail:

$$D_d = \sum \frac{n_i}{N_i} < 1 \qquad \text{(D.8)}$$

in which: $\quad D_d \quad = \quad$ damage factor during design life [-]
$\qquad\qquad n_i \quad = \quad$ number of times load S_i occurs [cycles]
$\qquad\qquad N_i \quad = \quad$ endurance [cycles]

In this way the damage by each load amplitude is thus linearly added.

D.3   Hydrodynamic coefficients

In section 4.2 the following three linear hydrodynamic coefficients were introduced as a way to describe the effect of the fluid on the structure:

- Hydrodynamic (or added) mass m_w
- Hydrodynamic damping c_w
- Hydrodynamic stiffness k_w

The hydrodynamic mass for gates is discussed by means of the Westergaard equations in section 4.2.3. Based on Kolkman [19] some examples of hydrodynamic damping and stiffness for gates are elaborated.

D.3.1 Added damping

There are multiple types of hydrodynamic damping, e.g. due to wave radiation or a reduce in drag force. According to Kolkman [19] the damping due to the radiation of waves for the case of a horizontally vibrating deep gate with water on both sides and penetrating the water surface, can be characterised as:

$$c_{w,radiaton} = \frac{4\rho g^2}{\omega^3} \tag{D.9}$$

It can be seen that for high vibration frequencies the added damping due to wave radiation decreases quickly.

The dominant factor in added damping is often the flow. In case of a certain flow drag the linear added damping for vibrations in flow direction can be deduced relatively easy when the expression for the drag force is known. Based on Kolkman and Jongeling [21] the following example is given.

If the flow drag force is described by:

$$F_D = C_D \cdot \frac{1}{2}\rho V^2 A \tag{D.10}$$

A vibration velocity then changes the relative velocity between the flow and the structure by $dV = \dot{y}$. Using this the change in force due to $\dot{y}$ can be calculated:

$$\frac{dF}{dV} = \frac{C_D \cdot \frac{1}{2}\rho V^2 A}{dV} = C_D \cdot \rho V A \Rightarrow dF = C_D \cdot \rho V A \cdot dV = C_D \cdot \rho V A \cdot \dot{y} \tag{D.11}$$

And thus:

$$c_{w,flow} = C_D \cdot \rho V A = \frac{2F_{D,static}}{V} \tag{D.12}$$

The latter part of equation (D.12) could be seen as a general expression in case other coefficients are used as long as $F \propto V^2$.

D.3.2 Added stiffness

Kolkman and Jongeling [21] mentions three types of added stiffness: due to immersion, due to quasi stationary flow forces and the sudden stiffness. The stiffness due to immersion is

straight-forward. An increase in submersion results in an increase in the upward pressure force ($F_{upward} = \rho g A(y - y_0)$), therefore:

$$k_{w,imm} = \rho g A \tag{D.13}$$

in which: A =   water surface piercing cross-sectional area [m^2]

When the structure piercing the water is not uniform and A = f(y) then the term is non-linear and 'moved' to the right-hand side of equation (4.8) or linearised by averaging. Stiffness due to flow occurs for example with a wind vane. A deviation of its position results in a restoring force.

The sudden stiffness is something that only occurs at gates with under or overflow and is a result of the inertia of the discharge. When discharge passes the gate trough a gap, which increases due to the gates movement, the discharge can not respond instantaneous. The same discharge will thus flow through a larger gap. When the force onto the gate is again proportional to V^2, and the movement of the gate is small relative to the gap, the sudden stiffness can be described by:

$$k_{w,sudden} \approx 2F_{static}/\delta \tag{D.14}$$

In which δ is the gap height in static position. The sudden stiffness is positive when the gate is positioned downstream of a tube or culvert, upstream the sudden stiffness is negative. In that case the gate could even be closed by the suction. The sudden stiffness is frequency dependent. The phenomenon occurs at high frequency vibration, as in that case the discharge tends to remain constant.

D.4   Fluid induced vibrations

Based on Erdbrink [9], Jongeling and Erdbrink [17], Kolkman [19], Kolkman and Jongeling [21], Naudascher [26] the following fluid induced structural vibrations, which were already mentioned in chapter 3, can be distinguished:

  (i) Excitation due to turbulence;
 (ii) Excitation by stable vortices
(iii) Excitation due to flow instability;
(iv) Self-excitation;
 (v) Excitation due to fluid oscillations in a basin;
(vi) Excitation due to fluid oscillations coupled with the structure motion.

In some sources items (ii) and (iii) or (v) and (vi) are mentioned as a single type. Here it is chosen to treat them separately in order to not overlook possible excitation mechanisms, as this is often the reason a design dynamically does not suffice. Each phenomenon is briefly discussed, especially in the relation to gates. For a more extensive elaboration the above mentioned literature is recommended.

D.4.1 Excitation due to turbulence (i)

Flow in practical civil engineering applications is always turbulent. Turbulence is generated mainly due to the viscous friction between the water and any present obstacle, including walls and the bottom.

Generally the turbulence intensity in the flow ($r = \sqrt{\overline{v'^2}}/\bar{v}$) is lower than 10 percent. However due to irregularities like obstacles or for example deceleration of the flow, this can increase. The turbulence intensity of the stream leaving pumps will be much higher.

Normally the turbulence is spread over a large bandwidth with most energy in low frequency till about 5 Hz [17]. Due to this, in case of gates the excitation due to turbulence is usually of little significance [21].

It should be kept in mind that the pumps, except for an increase in turbulence intensity, also might have an effect on the frequency spread or peak frequency of turbulence.

D.4.2 Excitation by stable vortices (ii)

The excitation due to stable vortices happens when the point of separation is fixed. Whether this is the case depends mainly on the upstream structure shape. A sharp edge leads to a fixed point of separation.

Stable vortices are less harmful than unstable ones (item (iii)) and a fixed point of separation is thus recommendable. Stable vortices, just like turbulence, often do not lead to significant vibrations as the excitation frequency is well below the natural frequency of the structural elements.

The excitation frequency of vortices can be described by the dimensionless Strouhal number. The value of this constant is depended on the geometry and determined for a large number of situations. The Strouhal number is defined as follows:

$$St = \frac{f_v L}{U_0} = \text{f(geometry)} \tag{D.15}$$

in which: $\quad f_v \quad = \quad$ vortice excitation frequency [1/s]
$\qquad\qquad\quad L \quad = \quad$ characteristic length [m]
$\qquad\qquad\quad U_0 \quad = \quad$ upstream flow velocity [m/s]

In reality also with vortex shedding, instead of a single value, a frequency band is often present. In that case f_v represents the peak value [9].

As can be seen from equation (D.15), an increasing flow velocity leads to a higher excitation frequency. It should be checked whether $f_{v,max}$ corresponding to the maximum flow velocity $U_{0,max}$ is at least two times smaller than the lowest natural frequency f_n. As said before, this is generally the case.

D.4.3 Excitation due to flow instability (iii)

Due to the specific shape of the structure sometimes flow instabilities can occur. Problems often arise due to an unstable point of separation. A well-known example is the occurrence of von Kármán vortices around a cylindrical object.

With flow underneath a gate an alternating point of separation can cause force fluctuations. A well defined point of separation due to design of the bottom of a gate can prevent this.

Besides the point of separation, also the point of reattachment can be of significance to the dynamic loading of gates, either when its fixed in space or not. When fixed, the region between separation and reattachment forms a closed volume of rotating flow with the shear layer feeding energy into this region on the downward side. In this area pressure fluctuations can develop [9]. When unfixed, a similar force fluctuation exist as with an unfixed separation point.

An important phenomenon that should be taken into account is the 'lock-in effect'. When the excitation is near the natural frequency of the gate, due to its motion the excitation frequency can adjust itself to get closer to the gates' natural frequency: a form of active interaction.

D.4.4 Self-excitation (iv)

Self-excitation of structures is quite infamous due to the large consequences this can have. Self-excitation occurs when a small initial disturbance of the structure leads to a force increasing this motion. In equation (4.8) this would be represented by a negative damping term. Self-excitation of a structure should always be prevented. Erdbrink [9] mentions three possible theories of self-excitation in case of gates:

- Galloping
- Fluctuating leakage gap
- Fluctuating discharge coefficient

Galloping occurs due to the change in the lift force coefficient as a function of the angle between relative velocity of the approach flow and the body. The condition for dynamic instability is derived by Den Hartog [7]:

$$\frac{\delta C_L}{\delta \alpha} + C_D < 0 \tag{D.16}$$

in which:
$\begin{aligned} C_L &= \quad \text{lift force coefficient [-]} \\ C_D &= \quad \text{drag force coefficient [-]} \\ \alpha &= \quad \text{angle between relative velocity of the approach flow and the body} \\ & \qquad \text{[rad]} \end{aligned}$

The fluctuating leakage gap is also known as the 'bath plug vibration'. When the gate (or bath plug) moves in the direction of the gap, the discharge decreases. The inertia force

is proportional to the discharge decrease, which is coupled to the velocity by which the gates moves in the gaps direction. Therefore a suction force is generated in the direction of the gates movement. This is thus negative damping. For a extensive elaboration of this phenomenon and of all the forces involved, reference is made to Kolkman and Jongeling [21]. Erdbrink [9] adds that in case of vertical-lift gates in free surface flows (instead of a culvert or pipe) the in-line inertia is caused by a fluid volume in a fictitious streamwise tube of length $D + (C_{Lu} + C_{Ld})a$, in which C_i are length coefficients.

Lastly, the fluctuating discharge coefficient is another way of how the movement of the gate cuts of the discharge. Due to the motion of the gate the point of flow separation differs, varying the discharge coefficient and thus causing similar pressure fluctuations as with the previous described theory. This would be more likely in case of a rounded gate bottom.

D.4.5   Fluid oscillations in a basin (v)

In same cases fluid resonance can occur in the adjacent basin. The resonating system could be a standing wave, but also e.g. communicating vessels. In this case the oscillations are not originating from the structure, but can cause loads on the structure that in turn cause it to vibrate. In figure D.6 the first and second eigenmodes of a standing wave in a confined basin are shown.
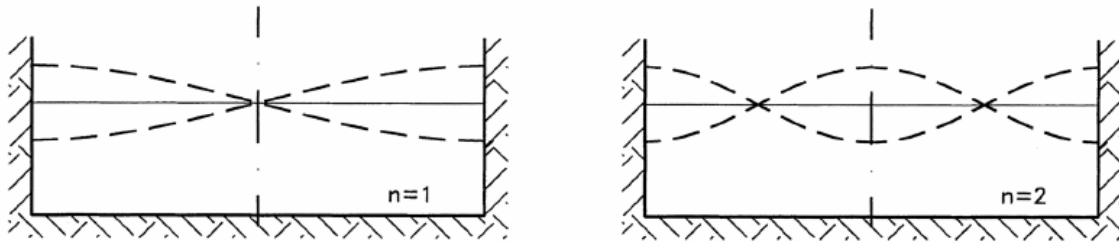

Figure D.6: First two eigenmodes of a standing wave in a confined basin [21]

The wave lengths of these harmonics simply results from the geometry:

$$\lambda = 2L/n \qquad\qquad \text{with: } n = 1, 2, ... \qquad\qquad \text{(D.17)}$$

in which: L   =   basin length [m]
            λ =   wave length [m]

The period of the oscillations depends on the wave length and celerity: $T = \lambda/c$. The wave celerity (when not in shallow water) depends in turn on the wave period and wave length:

$$c = \frac{gT}{2\pi}\, tanh\frac{2\pi d}{\lambda} \qquad\qquad\qquad \text{(D.18)}$$

in which: d   =   water depth [m]

Rewriting these equations, results in the following eigenperiod corresponding to each harmonic (n):

$$T_n = \sqrt{\frac{\dfrac{4\pi L/n}{g}}{tanh \dfrac{2\pi d}{2L/n}}} \qquad \text{with: } n = 1, 2, ... \qquad (D.19)$$

These frequencies should be checked on the forcing of the pumps and vibration frequencies of the gate. A certain lock-in effect is thinkable, where the motion and forces from the pumps somewhat adjusts to the motion of fluid oscillation.

D.4.6 Fluid oscillations coupled with structure motion (vi)

Another possibility as described in previous section is when the structure causes fluid oscillation that would otherwise not occur.

An interesting example is that of the Maeslant Barrier described in Jongeling and Erdbrink [17]. The two sector gates of the preliminary design, would be sensitive to self-excitation. This self-excitation would result in a standing wave between both banks. The self-excitation of the two sector gates would than be out-of-phase in the same frequency of the standing wave. Both motions influence and amplify each other. This was reason enough to modify the design of the Measlant Barrier.

Page intentionally left blank

E | Preliminary Ansys calculation of eigenmodes

In order to gain some insight in the possible vibration shapes of the pump gate, a plate with certain added cylindrical weights is modelled in Ansys Workbench. This plate is given the same width and height as the pump gate at Den Oever[9].

In Ansys the geometry of the plate was set up. An arbitrary, but small, thickness is given to this plate. The stiffness of the gate is thus not realistic. The same applies to size of the cylindrical elements, of which the weight is not a realistic representative for that of the pump. This kept in mind, some useful insight can still be obtained from the modal shapes of this 'model'.
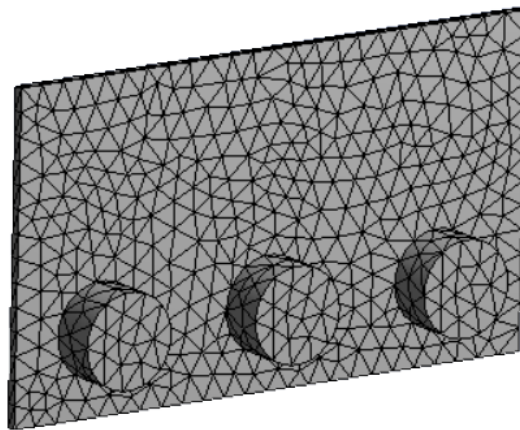

Figure E.1: Geometry of plate with tubes and automatically generated mesh of preliminary Ansys calculation

In figure E.2 and E.3 the first six modal shapes of a plate with same length and width as the original gate at Den Oever are given. The plate has been given an arbitrary thickness and cylindrical bodies with a certain weight to represent the pumps. The vertical boundaries of the gate (i.e. on the sides) are modelled as clamped. The top of the gate is free, the bottom is modelled both free and simply supported. A standard generated triangular mesh is used, automatically generated by Ansys. This can be seen in figure E.1. Using a finite element method, Ansys can perform a modal analysis based on the given geometry. The result are a number of eigenfrequencies and corresponding eigenmodes. The first are, due to the arbitrary weights and thickness, meaningless in this calculation

Although the exact behaviour is not very realistic, since the weights are arbitrary and contributions of the fluid and other are not included, the shapes gives some indication to which extent the behaviour could be one or three-dimensional. The bottom boundary

---

[9]In this calculation W = 12 m and H = 6.9 m was used. Later information showed the pump gates at Den Oever will have a span of 12.5 metre between the supporting wheels and a height of 7.25 metre. Due to the qualitative nature of this calculation, an adaptation to these dimensions was not deemed necessary.
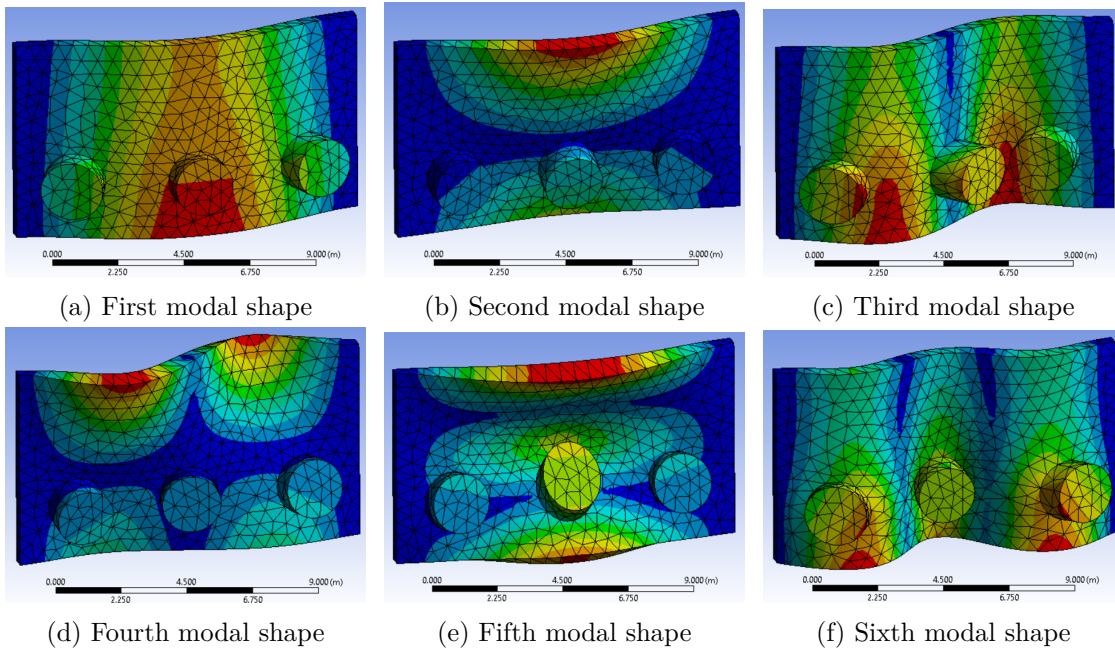
(a) First modal shape

(b) Second modal shape

(c) Third modal shape

(d) Fourth modal shape

(e) Fifth modal shape

(f) Sixth modal shape

Figure E.2: Modal shapes of a (dry) plate with length and width equal to the Den Oever gates, but arbitrary thickness and added pump weights. Fixed supports on left and right side. Free at the bottom.

(a) First modal shape

(b) Second modal shape

(c) Third modal shape

(d) Fourth modal shape

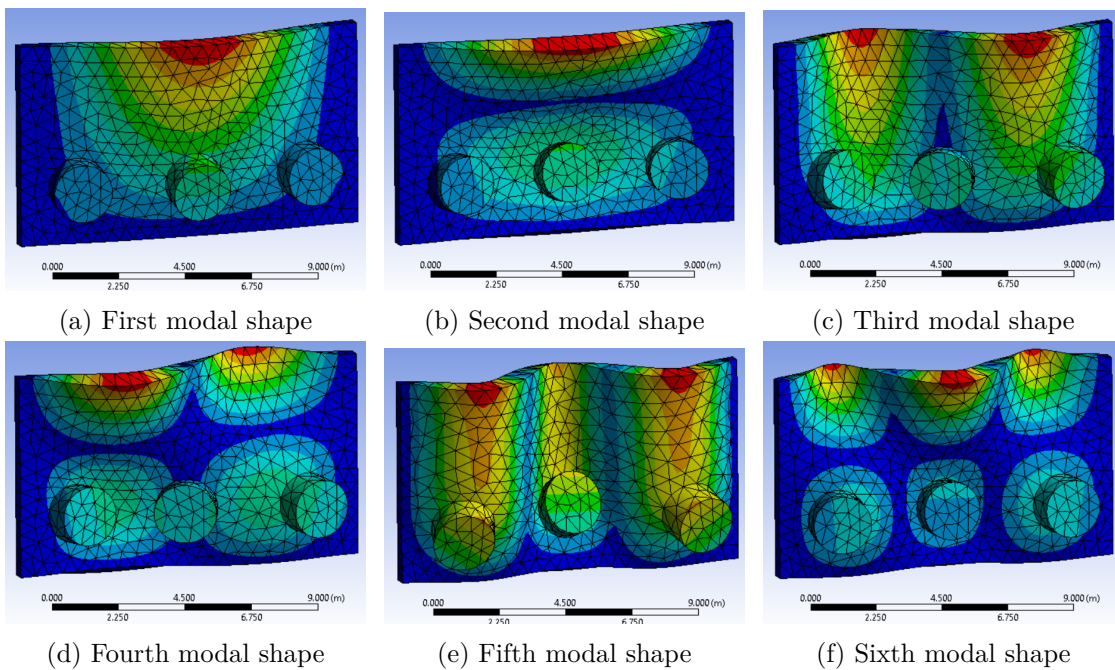(e) Fifth modal shape

(f) Sixth modal shape

Figure E.3: Modal shapes of a (dry) plate with length and width equal to the Den Oever gates, but arbitrary thickness and added pump weights. Fixed supports on left and right side, simple support at bottom.

conditions has a large influence in this, as can be seen when comparing figure E.2 to E.3. In case of the simply supported bottom, which is deemed more realistic due to the large pump gate weight and small contact surface, the behaviour can not be considered one dimensional any more.

The modal shapes in figure E.2a, E.2b and E.2f are very similar to the first three modal shapes of a beam. Due to the eccentric location of the pumps still some two dimensional effects can be seen at those shapes. This would be greater in reality due to eccentric forces. However, these modal shapes would be quite well represented by a one-dimensional model, potentially compensating for two-dimensional effects.

The lowest eigenfrequencies (corresponding to the first modal shapes) are often governing in design as generally the structure is made stiff enough so that its lowest eigenfrequency is above the excitation frequency. In case of the pump gate however, it is not known whether this will be possible. Secondly, it is not sure which of the shapes will have the lowest eigenfrequency in advance. In case of the flood defence pump gate, the stiffness in vertical direction is significantly different from that in horizontal direction, as can been seen in appendix B.

As the gate will be resting on the sluice floor slab, at least via some connection points, modelling this as a free edge is not realistic either. When the bottom edge is modelled as simply supported, the behaviour of the gate becomes much more two dimensional. As is done in chapter 5, this can be partially included in a one dimensional model by equivalent mass and stiffness.

F | Analytical derivations and additional results beam model

In this appendix from section F.1 to F.5 the of equations is derived to solve the motion of the beam. In section F.6 additional results are given.

F.1 General

With the so called coupled modal analysis method used, both the motion structure and the response of the fluid are described in terms of eigenmodes. The modal coefficients of the fluid modes are subsequently described in terms of the modal coefficients of the structure. This finally leads to a system of analytical equations including the external forcing, which can be solved for the structural modal coefficients. The following steps are taken in this derivation:

- Expressing the displacement of the structure in terms of an infinite summation of modal shapes and coefficients found for the homogeneous structural equation of motion;
- Expressing the fluid response in terms of (its own) modal shapes and coefficients;
- Using the interface condition (eq. 5.4) to express this fluid response in terms of the structural coefficients;
- Substitution of the found expressions into the forced equation, obtaining an analytical system of equations with the modal coefficients as the only unknowns;
- Solving the system of equations for each (modal) external force amplitude and frequency.

The derivations are made for a closed gate. The interface condition does not apply at the location of the pumps, which is characterised by a different response. This can be implemented easily by adjusted the determination of Q_{mp} (see equation (F.68)) in the final forced equation.

No interaction is included between the two sides of the gate. Based on the results in chapter 7 this is a reasonable approximation due to the effect of the pump conduits. The derivations are made as if both fluid domains are the same side of the gate. It is not explicitly stated that two fluid domains are present. To implement this the final fluid force should be determined twice, but with another water level, and thus modes, etcetera.

The governing equations and boundary conditions were elaborated in section 5.2. The most relevant equations are repeated in the present derivation.

F.2 Structural modes

In the frequency-domain the homogeneous equation for thin beam is as follows:

$$EI_z \frac{d^4 W(z)}{dz^4} - \rho_b \omega^2 W(z) = 0 \qquad \leftrightarrow \qquad \frac{d^4 W(z)}{dz^4} - \beta^4 W(z) = 0 \qquad \text{(F.1)}$$

With $\beta^4 = \dfrac{\rho_b \omega^2}{EI_z}$, and ω a certain natural frequency of the system. The general solution to equation (F.1) is as follows:

$$W(z) = A \cdot sinh(\beta z) + B \cdot cosh(\beta z) + C \cdot sin(\beta z) + D \cdot cos(\beta z) \qquad \text{(F.2)}$$

In which A to D are yet unknown constants, β is the fifth unknown. Substitution of this general solution into the four boundary conditions yield the following system of equations:

$$\begin{bmatrix} 0 & 1 & 0 & 1 \\ 0 & 1 & 0 & -1 \\ \sinh(\beta L_z) & 0 & -\sin(\beta L_z) & 0 \\ cosh(\beta L_z) & 0 & -cos(\beta L_z) & 0 \end{bmatrix} \begin{bmatrix} A \\ B \\ C \\ D \end{bmatrix} = \begin{bmatrix} 0 \\ 0 \\ 0 \\ 0 \end{bmatrix} \qquad \text{(F.3)}$$

The first two conditions lead immediately to $A = B = 0$. The third statement can be written as $C = \frac{\sin(\beta L_z)}{\sinh(\beta L_z)} \cdot D$. Substitution in the last equation, then yield the following condition:

$$D \cdot \left[\frac{\sin(\beta L_z)}{\tanh(\beta L_z)} - cos(\beta L_z) \right] = 0 \qquad \text{(F.4)}$$

A non-trivial solution requires the statement between brackets to be zero. From this equation β can thus be solved. For higher values of βL_z, the term $\tanh(\beta L_z)$ quickly grows to ≈ 1. In that case the equation reduces to $\sin(\beta L_z) = \cos(\beta L_z)$. Numeric evaluation of the equation shows that this approximation is valid for all found solutions of β. With the $\tanh(\beta L_z)$ term taken into account, β_1 would be $\approx 1.2499 \cdot \pi/L_z$ instead of $1.25 \cdot \pi/L_z$. For higher β's, the difference becomes even less.

$$\beta_m = \frac{(m + \frac{1}{4}) \cdot \pi}{L_z} \qquad \qquad \text{for } m = 1, 2, .., \infty \qquad \text{(F.5)}$$

Substitution of the found constants in the general equation, leads to the following solution:

$$W_m(z) = A_m \cdot \left[sinh(\beta_m z) + \frac{\sinh(\beta_m L_z)}{\sin(\beta_m L_z)} \cdot sin(\beta_m z) \right] \qquad \text{(F.6)}$$

In which A_m is the yet unknown modal coefficient of each structural mode m. The first eigenmodes and corresponding eigenfrequencies are evaluated and shown in section **??**.

The final solution for the beam's deflection is a summation of these eigenmodes:

$$W(z, \Omega) = \sum_{m=1}^{\infty} A_m \cdot W_m(z, \Omega) \qquad \text{(F.7)}$$
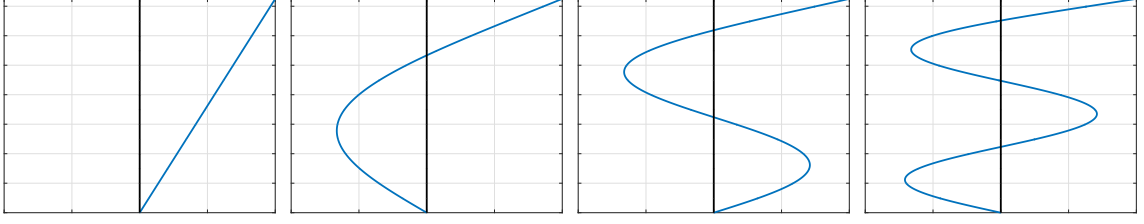
Figure F.1: The rigid body and first few bending beam modes. The deflection of the beam is a summation of these - theoretically infinite number of - eigenmodes.

F.3   Fluid modes

As was elaborated in section 5.2, to model schematizations are used to determine the fluid response: an incompressible fluid including surface waves and a compressible fluid without. Consequently, the corresponding equations of motion and surface conditions differ, as is given in figure 5.2. The fluid modes of both systems are therefore determined separately in this section. Subsequently, the general applicable solution is given, which is a combination of the two separate solution.

F.3.1   Incompressible surface wave modes

The equation of motion describing the incompressible fluid is homogeneous, when it is only 'forced' by its interface condition (which is the gate):

$$\frac{\partial^2 \Phi(z,y,t)}{\partial z^2} + \frac{\partial^2 \Phi(z,y,t)}{\partial y^2} = 0 \tag{F.8}$$

The assumed solution $\Phi(z,y,t) = \tilde{\Phi}(y,z) \cdot e^{i\Omega t}$ is again substituted. Subsequently, separation of variables is used to solve this partial differential equation. It is assumed the solution can be written as $\tilde{\Phi}(z,y) = Z(z) \cdot Y(y)$, which is then substituted in above equation:

$$Y(y)\frac{d^2 Z(z)}{dz^2} + Z(z)\frac{\partial^2 Y(y)}{\partial y^2} = 0 \leftrightarrow \frac{1}{Z(z)}\frac{d^2 Z(z)}{dz^2} + \frac{1}{Y(y)}\frac{d^2 Y(y)}{dy^2} = 0 \tag{F.9}$$

Equation (F.9) can be split into the following two equations:

$$\frac{d^2 Z(z)}{dz^2} + k_z^2 Z(z) = 0 \tag{F.10}$$

$$\frac{d^2 Y(y)}{dy^2} + k_y^2 Y(y) = 0 \tag{F.11}$$

In which case $k_y^2 + k_z^2 = 0$ should be obeyed. The general solution of equation (F.10) for the z-direction is:

$$Z(z) = \tilde{A} \cdot e^{+ik_z z} + \tilde{B} \cdot e^{-ik_z z} = A \cdot \cos(k_z z) + B \cdot \sin(k_z z) \tag{F.12}$$

The assumed solution $\tilde{\Phi}(z, y) = Z(z) \cdot Y(y)$ is substituted into the boundary conditions as well. Since the z-axis was taken equal to the bottom of the gate, which is located on the sill, the bottom of the sluice is not at z = 0. Instead, the bottom is located at Δz. This leads to the following conditions for the z-direction:

$$\left.\frac{dZ(z)}{dz}\right|_{z=\Delta z} = 0 \tag{F.13}$$

$$-\Omega^2 Z(z)\Big|_{z=h+\Delta z} + g\left.\frac{dZ(z)}{dz}\right|_{z=h+\Delta z} = 0 \tag{F.14}$$

In which h is the water depth. The z-coordinate of the still water level is given $z = h + \Delta z = H$. In case of Den Oever, Δz is negative. Substitution of the general solution into these boundary conditions yields again a system of equations, for which the constants can be solved. The first boundary conditions results in $B = A \tan(k \cdot \Delta z)$. Applying this to the second boundary condition gives:

$$A \cdot \left[-\omega^2 \left(\cos(k_z z) + \tan(k\Delta z)\sin(k_z z)\right) + gk\left(-sin(k_z z) + tan(k_z \Delta z)cos(k_z z)\right)\right]\Big|_{z=h+\Delta z} = 0 \tag{F.15}$$

Finding a non-trivial solution requires $A \neq 0$ and thus the expression between the brackets must be zero. After dividing by $\cos(k_z z)$ and substitution of $z = h + \Delta z$, the following equation is obtained:

$$\Omega^2 = -gk_z \cdot \frac{\tan(k_z h + \Delta z k) - \tan(k_z \Delta z)}{1 + \tan(k_z \Delta z)\tan(k_z h + \Delta z)} \tag{F.16}$$

From the following trigonometric relation:

$$\tan(a + b) = \frac{\tan(a) + \tan(b)}{1 - \tan(a)\tan(b)} \qquad \leftrightarrow \qquad \tan(a) = \frac{\tan(a - b) - \tan(b)}{1 + \tan(b)\tan(a - b)} \tag{F.17}$$

It can be seen that equation (F.16) is equal to:

$$\Omega^2 = -gk_z \cdot \tan(k_z h) \tag{F.18}$$

Which is the well known dispersion equation. An infinite series of values for k_z will fulfil this condition, of which one positive imaginary and infinitely positive real values. This series is named $k_{z,p}$.

Using the dispersion relation, the solution for Z(z) can be simplified. Substitution leads in first instance to:

$$Z(z) = A\left[\cos(k_z z) + tan(k_z \Delta z)\sin(k_z z)\right] =$$
$$A\left[\cos(k_z z) - tan(\Delta z k_z)\sin(k_z z)\right] \tag{F.19}$$

Using the following trigonometric rule, the found modes in z-direction can be further simplified:

$$\cos(a - b) = \cos(a)\cos(b) + \sin(a)\sin(b) \quad \leftrightarrow \quad \frac{\cos(a - b)}{\cos(b)} = \cos(a) + \tan(a)\sin(b) \tag{F.20}$$

Since $\cos(\Delta z \cdot k_z)$ is a constant for a given shape, and the amplitude of the shape A is still undetermined, it can be seen the determined function in z-direction is not different from:

$$Z(z) = A \cdot \cos(k_z \cdot (z - \Delta z)) = A \cdot \cos(k_z \cdot (z - \Delta z)) \tag{F.21}$$

In the y-direction the general solution is written in terms of exponentials:

$$Y_p(y) = A_p \cdot e^{-ik_{y,p}y} + B_p \cdot e^{+ik_{y,p}y} \tag{F.22}$$

The boundary condition states no incoming wave and finite energy at y $= \infty$. Therefore only the decaying exponential part should be present and $B_p = 0$. The following solution for the y-direction remains:

$$Y_p(y) = A_p \cdot e^{-ik_{y,p}y} \tag{F.23}$$

The infinity boundary condition then requires:

$$Re(k_{y,p}) \geq 0 \tag{F.24a}$$

$$Im(k_{y,p}) \leq 0 \qquad \text{so that: } Y(y) = A_p \cdot e^{-i(-k_p i) \cdot y} = A_p \cdot e^{-k_p \cdot y} \tag{F.24b}$$

From the definition of the separation variables the following holds: $k_{y,p} = \pm k_{z,p} i$. The infinite real values of $k_{z,p}$ given by the dispersion equation thus correspond to imaginary values for $k_{y,p}$, which should be negative conform equation (F.24a), resulting in evanescent (decaying) modes in y-direction. The real positive values of $k_{z,p}$ are therefore named $k_{eva,p}$, leading to $k_{y,p} = -k_{eva,p}i$. Each $k_{eva,p}$ solution of the dispersion equation can be found in the range $(p - 1.5) \cdot \pi/h < k_{eva} < (p - 1) \cdot \pi/h$ (with $p = 2, 3, ..\infty$), as can be seen in figure F.2.
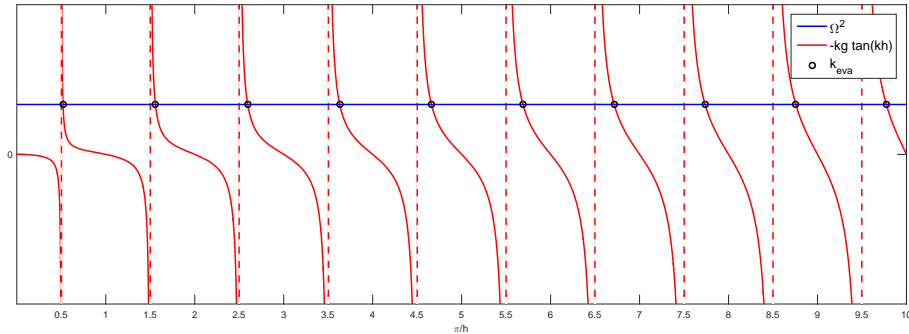

Figure F.2: Regions in which the positive values for $k_{eva,p}$ can be found

The single imaginary value of the dispersion equation leads to a propagative modes in y-direction and is therefore named $k_{z,p} = k_{prop}i$. The corresponding value for $k_{y,p}$ must be positive according to equation (F.24a) and is simply $+k_{prop}$. The imaginary $k_{z,p}$ value leads to a cosine hyperbolic shape when substituted into found expression for Z(z).

The solution for Φ is now reconstructed with the found solutions. The remaining unknowns from both directions can be combined to one modal coefficient (B_p):

$$\Phi_p = B_p\, Z_p(z)\, Y_p(y) = \begin{cases} B_p \cdot \cosh(k_{prop} \cdot (z - 0.2)) \cdot e^{-ik_{prop}y} & \text{for: } p = 1 \\ B_p \cdot \cos(k_{eva,p} \cdot (z - 0.2)) \cdot e^{-k_{eva,p}y} & \text{for: } p = 2,3,..,\infty \end{cases} \tag{F.25}$$

The potential of the incompressible fluid system is the infinite sum of these modes:

$$\Phi_{in} = \sum_{p=1}^{\infty} B_p Z_p(z) Y_p(y) \tag{F.26}$$

F.3.2 Compressible fluid modes

The full (time domain) equation of motion for the compressible fluid is as follows:

$$\frac{\partial^2 \Phi(z,y,t)}{\partial z^2} + \frac{\partial^2 \Phi(z,y,t)}{\partial y^2} = \frac{1}{c_p^2}\frac{\partial^2 \Phi}{\partial t^2} \tag{F.27}$$

Instead of the free surface boundary condition used for the incompressible fluid solution, a pressure release boundary condition can be used for the compressible modes. The bottom impedance boundary condition remains the same.

Closed gate surface:
$$p\big|_{z=h} = -\rho_f \frac{\partial \Phi}{\partial t} = 0 \tag{F.28}$$

Sluice floor:
$$\frac{\partial \Phi}{\partial z}\bigg|_{z=-\Delta z} = 0 \tag{F.29}$$

Substituting the assumed solution $\Phi(y,z,t) = \tilde{\Phi}(y,z) \cdot e^{-i\Omega t}$, results in the following frequency domain equations:

$$\frac{\partial^2 \tilde{\Phi}(z,y,t)}{\partial z^2} + \frac{\partial^2 \tilde{\Phi}(z,y,t)}{\partial y^2} + \frac{\Omega^2}{c_p^2}\tilde{\Phi} = 0 \tag{F.30}$$

$$-\rho_f \cdot \Omega i \cdot \tilde{\Phi}\big|_{z=H} = 0 \quad \leftrightarrow \quad \tilde{\Phi}\big|_{z=h} = 0 \tag{F.31}$$

$$\frac{\partial \tilde{\Phi}}{\partial z}\bigg|_{z=-\Delta z} = 0 \tag{F.32}$$

Similar to how the incompressible solution was found, separation of variables is used to solve the partial differential equations. The assumed solution, $\tilde{\Phi}(z,y) = Z(z) \cdot Y(y)$, is substituted in equation (F.30):

$$Y(y)\frac{d^2 Z(z)}{dz^2} + Z(z)\frac{d^2 Y(y)}{dy^2} + \frac{\Omega^2}{c_p^2} \cdot Z(z) \cdot Y(y) = 0 \leftrightarrow \frac{1}{Z(z)}\frac{d^2 Z(z)}{dz^2} = -\frac{1}{Y(y)}\frac{d^2 Y(y)}{dy^2} - k_f^2 \tag{F.33}$$

In which $k_f^2 = \frac{\Omega^2}{c_p^2}$. To achieve similarity with the deduced equations of the incompressible fluid, the equations are split into the same system:

$$\frac{d^2 Z(z)}{dz^2} + k_z^2 Z(z) = 0 \tag{F.34}$$

$$\frac{d^2 Y(y)}{dy^2} + k_y^2 Y(y) = 0 \tag{F.35}$$

In this case with $k_y^2 = k_f^2 - k_z^2$. The general solution for the z-direction is then again:

$$Z(z) = A \cdot \cos(k_z z) + B \cdot \sin(k_z z) \tag{F.36}$$

The bottom impedance boundary condition results in $B = 0$. The surface conditions subsequently demands:

$$Z(0) = A \cdot \cos(k_z h) = 0; \tag{F.37}$$

To find a non-trivial solution, it is required that $A \neq 0$ and thus $\cos(k_z h) = 0$. This results in a series of solutions for k_z, which will be denoted by $k_{z,t}$:

$$k_{z,t} = \frac{(2t - 1) \cdot \pi}{2h} \qquad\qquad \text{for: } t = 1, 2, .., \infty \tag{F.38}$$

With $k_{y,t}^2 = k_f^2 - k_{z,t}^2$ (and $k_{y,t} = \pm\sqrt{k_f^2 - k_{z,t}^2}$), the general solution for the y-direction can be written in terms of exponentials:

$$Y_t(y) = C_t \cdot e^{-ik_{y,t}y} + D_t \cdot e^{+ik_{y,t}y} \tag{F.39}$$

The boundary condition at infinity, which states finite and no negatively propagating energy, then requires $D_m = 0$ together with:

$$\text{Re}(k_{y,t}) \geq 0 \tag{F.40}$$

$$\text{Im}(k_{y,t}) \leq 0 \tag{F.41}$$

The full potential (of the compressible equations) is the infinite sum of these modes:

$$\Phi_c = \sum_{t=1}^{\infty} C_t Z_t(z) Y_t(y) = \sum_{t=1}^{\infty} C_t \cdot \cos(k_{z,t}z) \cdot e^{-ik_{y,t}y} \tag{F.42}$$

In this case the real values of $k_{y,t}$ again represent propagative modes, while the imaginary values result in evanescent modes. In contrast to the incompressible case when only one propagative mode was present, with the incompressible no or multiple propagative modes may exist depending on the excitation frequency (at a given water depth). Similar to the incompressible case, an infinite number of evanescent modes will exist.

Since $k_{y,t}$ is equal to $\pm\sqrt{k_f^2 - k_{z,t}^2}$, modes for which $k_{z,m}^2 > k_f^2$ result in an imaginary root and thus an evanescent mode. When $k_{z,1}^2$ corresponding to the first mode is (already) larger than k_f^2, no propagative modes will exist. As mentioned this depends on the excitation

frequency and the water depth can be seen from:

$$k_{z,1}^2 > k_f^2 \qquad \leftrightarrow \qquad \left[\frac{(2-1) \cdot \pi}{2h}\right]^2 > \frac{\Omega^2}{c_p^2} \qquad \leftrightarrow \qquad \Omega < \frac{\pi}{2h} \cdot c_p \qquad \text{(F.43)}$$

Substitution of $T = 2\pi/\Omega$ results in:

$$T < \frac{4h}{c_p} \qquad \text{(F.44)}$$

This is the same expression as was given in equation (4.25) for the fundamental eigenperiod of the compressible fluid.

F.3.3 Total fluid response

The fluid response including both compressibility and the effect of surface waves, combines previous solutions and is as follows:

$$\tilde{\Phi}_p(x,y,z) = \sum_{p=1}^{\infty} B_r \cos(k_{z,p} \cdot (z - \Delta z)) \cdot e^{-ik_{y,p}y} \qquad \text{(F.45)}$$

With the following constants:

$$\Omega^2 = -gk_{z,p} \cdot \tan(k_{z,p}h) \qquad \text{(F.46)}$$

$$k_{y,p} = \pm\sqrt{k_f^2 - k_{z,p}^2} \qquad \text{(F.47)}$$

The same conditions for the positive and negative $k_{y,p}$ apply as stated for the separate systems.=

F.4 Fluid response in terms of structural coefficients

The interface condition is now used to link the two systems and express the fluid response in terms of the structural modal coefficients. The interface condition was as follows:

$$\left.\frac{\partial \phi}{\partial y}\right|_{y=0} = \frac{\partial w}{\partial t} \qquad \text{(F.48)}$$

Substitution of the found expressions for both the structure and fluid, yields:

$$-ik_p \sum_{p=1}^{\infty} B_p Z_p(z) \cdot e^{-ik_p0} = i\Omega \sum_{m=1}^{\infty} A_m W_m(z) \qquad \text{(F.49)}$$

At y=0, the solutions for Y are thus simply equal to 1. The orthogonality of the fluid modes is used to rewrite the above equation. When multiplied with another fluid mode

(Z_q), and integrated of the water depth, the following applies:

$$\int_{\Delta z}^{H} Z_p Z_q dz = \delta_{pq}\Delta_p \qquad\qquad \delta_{pq} = \begin{cases} 0, p \neq q \\ 1, p = q \end{cases} \tag{F.50}$$

In this, δ_{pq} is the dirac delta function and Δ_p is the solution of the integration, which is a constant for each $p = q$. equation (F.49) therewith becomes[10]:

$$-k_p \sum_{p=1}^{\infty} B_p \delta_{pq}\Delta_p = \Omega \sum_{m=1}^{\infty} A_m \int_0^H W_m(z) Z_q(z) dz \tag{F.51}$$

The integral on the right-hand side can be determined for each m and q and is renamed to Q_{mq}. Since the left-hand side of above equation is only non-zero when $p = q$, the equation reduces to:

$$B_p = -\frac{\Omega}{k_p \Delta_p} \sum_{m=1}^{\infty} A_m Q_{mp} \tag{F.52}$$

B_p is thus described in terms of the structural modal coefficients. The (dynamic) fluid pressures are described by:

$$p_f = -\rho_f \frac{\delta\Phi}{\delta t} = -i\Omega\rho_f \phi \tag{F.53}$$

The found solution for ϕ is substituted.

$$p_f(y = 0, z, t) = -i\Omega\rho_f \sum_{p=1}^{\infty} B_p Z_p(z) \tag{F.54}$$

When B_p is now replaced by the expression found in equation (F.52), the following expression for the fluid pressure is found:

$$p_f(y = 0, z) = -i\Omega\rho_f \sum_{p=1}^{\infty} \left(-\frac{\Omega}{k_p \Delta_p} \sum_{m=1}^{\infty} A_m Q_{mp}\right) Z_p(z) \tag{F.55}$$

$$p_f(y = 0, z) = i\Omega^2\rho_f \sum_{m=1}^{\infty} A_m \sum_{p=1}^{\infty} \frac{Q_{mp}}{k_p \Delta_p} Z_p(z) \tag{F.56}$$

F.5   Forced system of equations

The solutions for the fluid pressures and W(x), both described in terms of the modal coefficients A_m, are now substituted into the forced equation:

$$\sum_{m=1}^{\infty} A_m \left[EI\frac{d^4 W_m(z)}{dz^4} - \rho_b\Omega^2 W_m(z)\right] = F_f(z) - F_{ext}(\Omega, z) +$$

$$\sum_{m=1}^{\infty} A_m \left[[H(z - z_1) - H(z - z_2)] \cdot \left(\rho_p \cdot \Omega^2 - c_{pump} \cdot i\Omega\right) \cdot W_m(z) - k^* \cdot W_m(z)\right] \tag{F.57}$$

---

[10]Since their is no motion of the beam for z < 0, the integral on the right-hand side is zero for those coordinates and can be evaluated from z = 0 to z = H.

The structural modes were determined for the homogeneous equations and thus must satisfy to this:

$$EI\frac{d^4 W_m(z)}{dz^4} - \rho_b \omega_m^2 W_m(z) = 0 \tag{F.58}$$

In which ω_m^2 is the natural frequency corresponding to each structural eigenmode. The above equation is used to eliminate the differential equation from equation (F.57). Furthermore, the found expression for the fluid pressures is substituted:

$$\sum_{m=1}^{\infty} A_m \cdot \left[\rho_b \cdot (\omega_m^2 - \Omega^2) + k^*\right] \cdot W_m(z) = -F_{ext}(\Omega, z)$$

$$+ \sum_{m=1}^{\infty} A_m \cdot [H(z - z_1) - H(z - z_2)] \cdot \left(\rho_p \cdot \Omega^2 - c_{pump} \cdot i\Omega\right) \cdot W_m(z) \tag{F.59}$$

$$-i\Omega^2 \rho_f \sum_{m=1}^{\infty} A_m \sum_{p=1}^{\infty} \frac{1}{k_p \Delta_p} Q_{mp} Z_p(z)$$

The above equation is now multiplied by another structural mode W_n and integrated over the structure's height:

$$\sum_{m=1}^{\infty} A_m \cdot \left[\rho_b \cdot (\omega_m^2 - \Omega^2) + k^*\right] \cdot \int_0^{L_z} W_m(z) W_n(z) dz = - \int_0^{L_z} F_{ext}(\Omega, z) W_n(z) dz$$

$$+ \sum_{m=1}^{\infty} A_m \cdot \int_0^{L_z} [H(z - z_1) - H(z - z_2)] \cdot \left(\rho_p \cdot \Omega^2 - c_{pump} \cdot i\Omega\right) \cdot W_m(z) W_n(z) dz \tag{F.60}$$

$$+ i\Omega^2 \rho_f \sum_{m=1}^{\infty} A_m \sum_{p=1}^{\infty} \frac{Q_{mp}}{k_p \Delta_p} \int_0^{L_z} Z_p(z) W_n(z) dz$$

Similar to the orthogonality used with the fluid modes, the following integral can be evaluated as follows:

$$\int_0^{L_z} W_m(z) W_n(z) dz = \delta_{mn} \cdot \Gamma_n \tag{F.61}$$

The integral $\int_0^{L_z} Z_p(z) W_n(z) dz$ is renamed to Q_{pn}. The fluid contribution is denoted by Z_{nm}. The orthogonality of the structure modes only applies when the integral is evaluated over the full domain. The inertia force and damping of the pumps therefore also contains values for $m \neq n$.

The final system of equations therewith becomes:

$$\sum_{m=1}^{\infty} \left[\left(\rho_b \cdot (\omega_m^2 - \Omega^2) + k^*\right) \cdot \delta_{mn} \cdot \Gamma_n + Z_{N,mn} + Z_{S,mn} - I_{mn} + P_{mn}\right] \cdot A_n = F_n \tag{F.62}$$

Fluid impedance (north/south): $\qquad Z_{N,mn}$ or $Z_{S,mn} = i\Omega^2 \rho_f \sum_{p=1}^{\infty} \frac{Q_{mp} Q_{pn}}{k_p \Delta_p}$ (F.63)

Pump intertia: $\qquad I_{mn} = \rho_p \cdot \Omega^2 \cdot \int_{z_1}^{z_2} W_m(z) \cdot W_n(z) \, dz$ (F.64)

Pump damping: $\qquad P_n = c_{pump} \cdot i\Omega \cdot \int_{z_1}^{z_2} W_m(z) \cdot W_n(z) \, dz$ (F.65)

Modal force:
$$F_n = \int_0^{L_z} F_{ext}(z,\Omega) \cdot W_n(z)\, dz \tag{F.66}$$

And for completeness the two integrals that are part of the fluid impedance are repeated:

$$Q_{pn} = \int_0^H Z_p(z)W_n(z)dz \tag{F.67}$$

$$Q_{pm} = \int_0^H Z_p(z)W_m(z)dz \tag{F.68}$$

Hydrodynamic damping and mass

In the expression for the fluid impedance, the hydrodynamic mass and damping can be identified. It can be seen that the evanescent modes, $k_p = -k_{eva,p}$, result in an added mass. In case of the incompressible surface waves equations these are all modes except for the first fluid mode:

$$Z_{mn} = i\Omega^2 \sum_{m=1}^{\infty} A_m \sum_{p=2}^{\infty} \rho_f \frac{Q_{mp}Q_{pn}}{-k_{eva,p}i\,\Delta_p} = $$
$$-\Omega^2 \cdot \rho_f \sum_{m=1}^{\infty} A_m \sum_{p=2}^{\infty} \frac{Q_{mp}Q_{pn}}{k_{eva,p}\,\Delta_p} \tag{F.69}$$

As the mass of a structure M will result in an inertia force of $M \cdot \ddot{W} = -\Omega \cdot W$, the hydrodynamic mass of the incompressible wave system for a certain mode n can be considered ($p = 2, 3, .., \infty$):

$$M_{w_n} = \sum_{m=1}^{\infty} A_m \sum_{p=2}^{\infty} \tag{F.70}$$

As can be seen, this hydrodynamic mass is the sum of the hydrodynamic mass causes by all other modes on this particular mode n. The fluid thus couples all modes. This results in the non-diagonal fluid impedance matrix. The same applies to the hydrodynamic damping, which is found for the propagating mode (in case of the incompressible wave system $p = 1$):

$$Z_{mn} = i\Omega^2 \sum_{m=1}^{\infty} A_m \rho_f \frac{Q_{mp}Q_{pn}}{k_{prop} \cdot \Delta_p} = $$
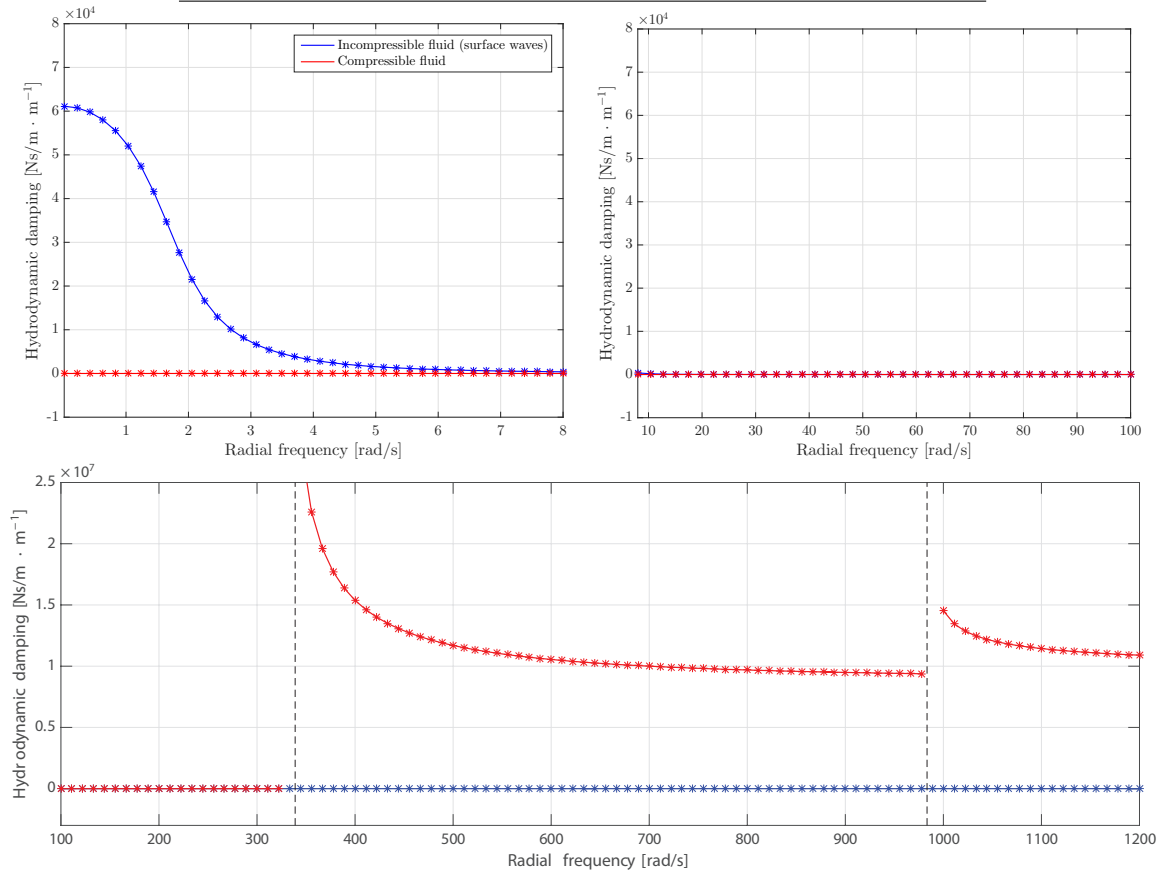$$i\Omega^2 \cdot \rho_f \frac{Q_{mp}Q_{pn}}{k_{prop} \cdot \Delta_p} \tag{F.71}$$

This contribution divided by $i\Omega$ can be considered the hydrodynamic damping:

$$C_{w_n} = \Omega \cdot \sum_{m=1}^{\infty} A_m \cdot \rho_f \frac{Q_{mp}Q_{pn}}{k_{prop} \cdot \Delta_p} \tag{F.72}$$

The coupled modal analysis method used, does not require however to explicitly describe these components.

F.6   Additional results

Hydrodynamic damping of the horizontally vibrating rigid gate

(a) Significant compressibility

Figure F.3: The total hydrodynamic damping compared for the compressible and incompressible system of equations for a water level of $h = 7.2$ m

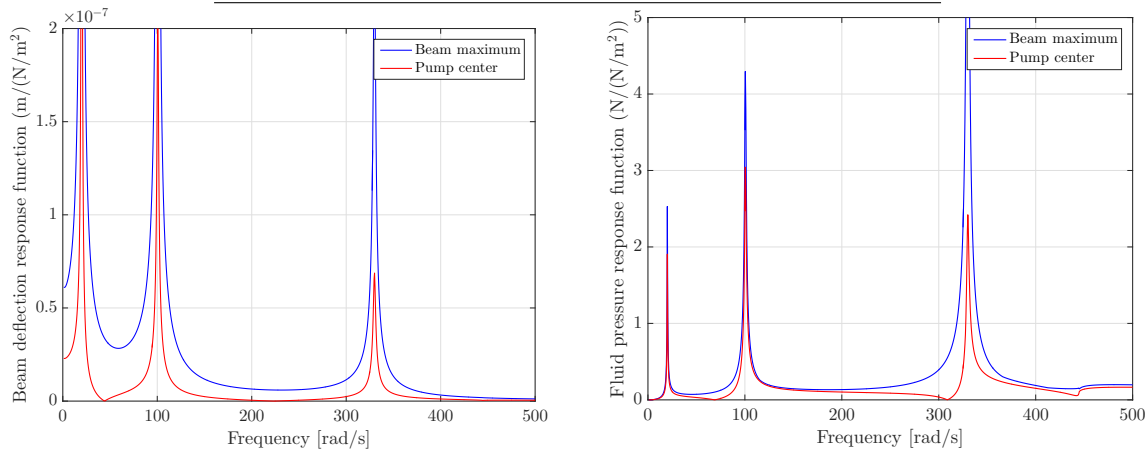## Response functions Den Oever for maximum water levels

Figure F.4: Maximum beam response of the beam and the pump's center to a unit distributed pump load at $h_S = 5.3$ and $h_N = 7.2$ metre

G | Analytical derivations and additional results plate model

In this appendix, the system of equations of the plate model is derived. This includes expressing the displacement of plate and fluid into a summation of eigenmodes. Through the interface condition, the fluid response at the plate's surface is expressed into modal coefficients of the plate. Subsequently, a system of analytical expressions is obtained for which the plate's vibration amplitudes can be solved. This method is the same as was elaborated in more detail for the beam system in section 5.1.

In section G.5 additional results of the plate model for the analysed Den Oever designs are given.

G.1 Structural modes

In section 6.3.1 the two dimensional plate shapes are described and evaluated. These are a product of modes in x- and z-direction:

$$W_{km}(x, z) = W_{x,k}(x) \cdot W_{z,m}(z) \tag{G.1}$$

The plate's equation of motion can not be separated into two directions directly and therefore a solution in x-direction was assumed based on the simply supported edges:

$$W_{x,k}(x) = sin(\beta_k x), \qquad \beta_k = \frac{k\pi}{L_x}, \text{ with: } k = 1, 2, .., \infty \tag{G.2}$$

When this solution is substituted in (6.3), and subsequently divided by $sin(\beta_k x)$, the following is obtained:

$$-\rho_s \omega_{km}^2 \cdot W_{z,m}(z) + D \cdot \beta_k^4 \cdot W_{z,m}(z) - 2D \cdot \beta_k^2 \cdot \frac{\partial^2 W_{z,m}(z)}{\partial z^2} + D \cdot \frac{\partial^4 W_{z,m}(z)}{\partial z^4} = 0 \leftrightarrow$$

$$D \cdot \frac{\partial^4 W_{z,m}(z)}{\partial z^4} - 2D \cdot \beta_k^2 \cdot \frac{\partial^2 W_{z,m}(z)}{\partial z^2} + \left[D \cdot \beta_k^4 - \rho_s \omega_{km}^2 \right] \cdot W_{z,m}(z) = 0 \tag{G.3}$$

For each mode k in x-direction, a homogeneous fourth order differential equation must thus be solved. An infinite number of modes m can be found for each differential equation. These modes are numerically evaluated with Matlab's *bvp4c* function. To do so, the differential equation (G.3) is written as a system of ordinary differential equations (with $z_1 = W_{z,m}$):

$$z_1' = z_2 \qquad z_2' = z_3 \qquad z_3' = z_4 \qquad z_4' = 2 \cdot \beta_k^2 \cdot z_3 + \left[\frac{1}{D} \cdot \rho_s \cdot \omega_{km}^2 - \beta_k^4 \right] \cdot z_1 \tag{G.4}$$

Since the natural frequency ω_{km} a fifth condition is necessary. The deflection at $z = L_z$ was set to 1 for this purpose. As an initial guess for each mode m, the shapes of the vertical beam modes derived in appendix F were used. The first four eigenmodes and corresponding eigenfrequencies evaluated numerically were shown in chapter 6, but are repeated in figure G.1 for the readers convenience. The total plate deflection is again an infinite summation of these modes.
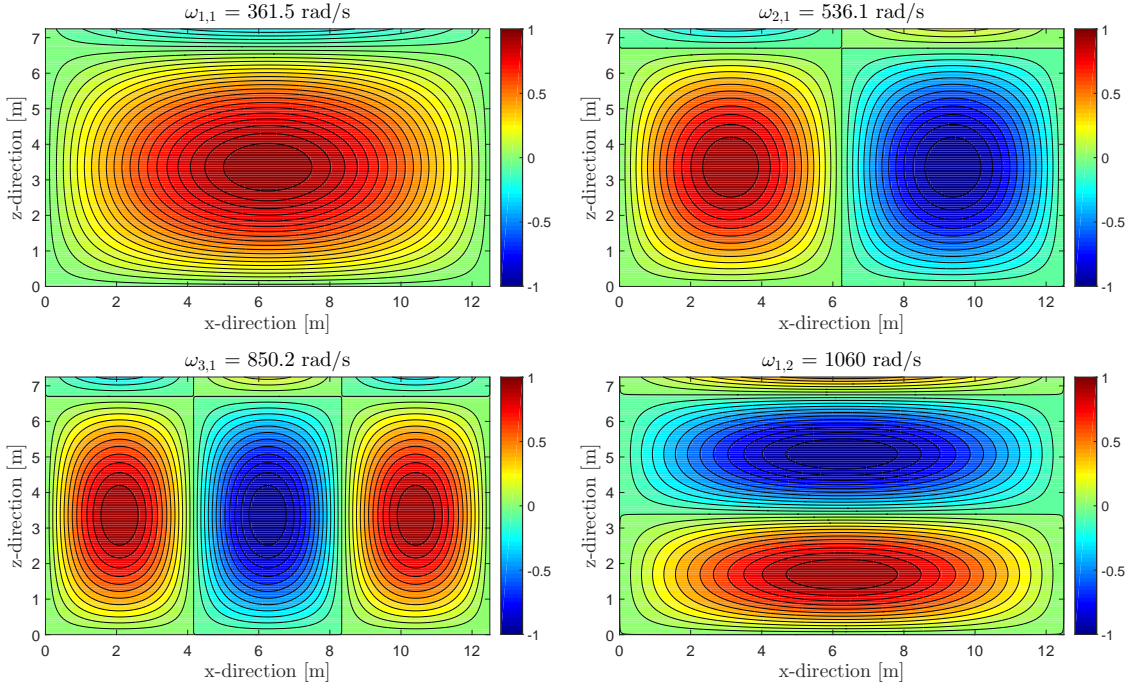

Figure G.1: The first four numerically evaluated eigenmodes of the plate (without pump weights) for the regular pump gate design. The deflection of each mode is normalised to a unit maximum.

G.2   Fluid modes

Separation of variables is again used to solve the partial differential equation. It is assumed the solution can be written as follows:

$$\tilde{\Phi}(x, y, z) = X(x) \cdot Y(y) \cdot Z(z) \tag{G.5}$$

When substituted in the equation of motion (6.8), this results in:

$$X(x)Y(y)\frac{d^2 Z(z)}{dz^2} + X(x)Z(z)\frac{d^2 Y(y)}{dy^2} + Y(y)Z(z)\frac{d^2 X(x)}{dx^2} + \frac{\Omega^2}{c_p^2} \cdot X(x) \cdot Y(y) \cdot Z(z) = 0 \tag{G.6}$$

$$\frac{1}{Z(z)}\frac{d^2 Z(z)}{\delta z^2} + \frac{1}{Y(y)}\frac{d^2 Y(y)}{dy^2} + \frac{1}{X(x)}\frac{d^2 X(x)}{dx^2} + \frac{\Omega^2}{c_p^2} = 0 \tag{G.7}$$

The latter expression can only be valid if each of these expressions is equal to a (separation) constant:

$$\frac{1}{Z(z)}\frac{d^2Z(z)}{dz^2} = -k_z^2 \qquad \frac{1}{Y(y)}\frac{d^2Y(y)}{dy^2} = -k_f^2 + k_z^2 + k_x^2 \qquad \frac{1}{X(x)}\frac{d^2X(x)}{dx^2} = -k_x^2 \qquad \text{(G.8)}$$

With $k_f^2 = \frac{\Omega^2}{c_p^2}$. When k_y is now defined as $k_y^2 = k_f^2 - k_z^2 - k_x^2$. The following three ordinary differential equations must now be solved for the boundary conditions.

$$\frac{d^2X(x)}{dx^2} + k_x^2 X(x) = 0 \qquad \text{(G.9)}$$

$$\frac{d^2Y(z)}{dy^2} + k_y^2 Y(y) = 0 \qquad \text{(G.10)}$$

$$\frac{d^2Z(z)}{dz^2} + k_z^2 Z(z) = 0 \qquad \text{(G.11)}$$

The boundary conditions for the z-direction are unchanged from those of the beam model. The following solution was obtained (see appendix F.3)

$$Z(z) = A \cdot \cos(k_z \cdot (z - \Delta z)) \qquad \text{(G.12)}$$

$$\Omega^2 = -gk_z \cdot \tan(k_z h) \qquad \text{(G.13)}$$

The expressions for X(x) is derived from substitution of the general solution into the boundary conditions.

$$X(x) = A\cos(k_x x) + B\sin(k_x x) \qquad \text{(G.14)}$$

$$\left.\frac{dX(x)}{dx}\right|_{x=\Delta x} = 0 \qquad \text{(G.15)}$$

$$\left.\frac{dX(x)}{dx}\right|_{x=L_x-\Delta x} = 0 \qquad \text{(G.16)}$$

Solving of this system is simplified by using a local coordinate system for the fluid $x' = x - \Delta x$, which is zero at one sluice wall and has a value of Lx', the sluice width, at the other. The first derivative of this general solution is then equal to:

$$\frac{dX(x')}{dx'} = -A\sin(k_x x') + B\cos(k_x x') \qquad \text{(G.17)}$$

The first boundary condition then results in B = 0. And the second in:

$$-A\sin(k_x L_x') = 0 \leftrightarrow \sin(k_x L_x') = 0 \leftrightarrow k_x = \frac{p\pi}{L_x'} \qquad \text{(G.18)}$$

The solution of X(x') is therefore:

$$X(x') = A_p\cos(k_{x,r}x')), \qquad k_{x,p} = \frac{p\pi}{Lx'} \qquad \text{with: } p = 1,2,..,\infty \qquad \text{(G.19)}$$

Substituting the expression for the original coordinate system, the following solution is obtained:

$$X(x) = A_r \cos(k_{x,p}(x - \Delta x)), \qquad k_{x,p} = \frac{r\pi}{Lx - 2\Delta x} \qquad \text{with: } p = 1, 2, .., \infty \qquad \text{(G.20)}$$

The solutions for the x- and z-direction thus resulted in two infinite series for the respective separation constants, which are named $k_{x,p}$ and $k_{z,r}$. From the definition of the constants, $k_{y,pr}$ is then expressed as follows:

$$k_{y,pr} = \pm\sqrt{k_f^2 - k_{x,p}^2 - k_{z,r}^2} = 0 \qquad \text{(G.21)}$$

Similar to the two-dimensional the solution for the y-direction, obeying the boundary condition at infinity, can be written as:

$$Y_p(y) = A_p \cdot e^{-ik_{y,pr}y} \qquad \text{(G.22)}$$

With:

$$Re(k_{y,pr}) \geq 0 \qquad \text{(G.23)}$$

$$Im(k_{y,pr}) \leq 0 \qquad \text{(G.24)}$$

Again, the real values for $k_{y,pr}$ correspond to a propagating wave and the imaginary to evanescent shapes. In contrast to the two-dimensional case, it is less clear in advance which values of k_z will lead to a real or imaginary $k_{y,pr}$.

The total solution for Φ is:

$$\tilde{\Phi}(x,y,z) = Z(z)X(x)Y(y) = \sum_{p=1}^{\infty}\sum_{r=1}^{\infty} B_{pr} \cos(k_{z,p} \cdot (z - \Delta z)) \cdot \cos(k_{x,r} \cdot (x - \Delta x)) \cdot e^{-ik_{pr}y}$$

$$\text{(G.25)}$$

G.3   Fluid response in terms of structural coefficients

The interface condition is now used to link the two systems and solve the forced solution:

$$\left.\frac{\partial \phi}{\partial y}\right|_{y=0} = \frac{\partial w}{\partial t} \qquad \text{(G.26)}$$

$$-ik_{pr}\sum_{p=1}^{\infty}\sum_{r=1}^{\infty} B_{pr}\Phi_{pr}(x,z) \cdot e^{-ik_{pr}y} = i\Omega \sum_{m=1}^{\infty}\sum_{k=1}^{\infty} A_{km}W_{mk}(x,z) \qquad \text{(G.27)}$$

The orthogonality of the fluid modes is used to rewrite the above equation. When multiplied with another fluid mode Φ_{qs}, and integrated of the water depth and sluice width, the

following applies:

$$\iint_{\Delta x,-\Delta z}^{L'_x,H} \Phi_{pr}(x,z) \cdot \Phi_{qs} \, dxdz = \delta_{pq}\delta_{rs}\Delta_{pr} \qquad \delta_{pq}\delta_{rs} = \begin{cases} 0, & \text{else} \\ 1, & \text{and}(p=q, r=s) \end{cases} \tag{G.28}$$

$$\tag{G.29}$$

In this, δ_{pq} and δ_{rs} are dirac delta functions and Δ_{pr} is the solution of the surface integration ($\iint$), which is constant for each $p=q$ and $r=s$. Equation (G.27) therewith becomes:

$$-k_{pr}\sum_{p=1}^{\infty}\sum_{r=1}^{\infty} B_{pr}\delta_{pqrs}\Delta_p\Delta_r \cdot e^{-ik_{pr}y} = \Omega \sum_{m=1}^{\infty}\sum_{k=1}^{\infty} A_{km} \iint_{\Delta x,0}^{L'_x,H} W_{mk}(x,z)\Phi_{pr}(x,z)dxdz \tag{G.30}$$

The integral on the right-hand side will be named Q_{kmpr}. Since the left-hand side of above equation is only non-zero when $p=q$ and $r=s$, the equation reduces to:

$$-k_{pr}B_{pr}\Delta_{pr} = \Omega \sum_{m=1}^{\infty}\sum_{k=1}^{\infty} A_{mk}Q_{kmpr} \tag{G.31}$$

B_{pr} is thus described in terms of the structural modal coefficients:

$$B_{pr} = -\frac{\Omega}{k_{pr}\Delta_{pr}} \sum_{m=1}^{\infty}\sum_{k=1}^{\infty} A_{mk}Q_{kmpr} \tag{G.32}$$

The (dynamic) fluid pressures are defined as:

$$p_f = -\rho\frac{\delta\Phi}{\delta t} = -i\Omega\rho\phi \tag{G.33}$$

The found solution for Φ is substituted.

$$p_f(y,z) = -i\Omega\rho_f \sum_{p=1}^{\infty}\sum_{r=1}^{\infty} B_{pr}\Phi_{pr}(x,z) \cdot e^{-ik_{y,pr}y} \tag{G.34}$$

And subsequently the found solution for B_{pr} is substituted:

$$p_f(x,y,z) = i\Omega^2\rho \sum_{m=1}^{\infty}\sum_{k=1}^{\infty} A_{mk} \sum_{p=1}^{\infty}\sum_{r=1}^{\infty} \frac{Q_{kmpr}}{k_{y,pr}\Delta_{pr}} \cdot \Phi_{pr}(x,z) \cdot e^{-ik_{y,pr}y} \tag{G.35}$$

At the gates' interface (y = 0), the pressures are thus described by:

$$p_f(x,y=0,z) = i\Omega^2\rho \sum_{m=1}^{\infty}\sum_{k=1}^{\infty} A_{mk} \sum_{p=1}^{\infty}\sum_{r=1}^{\infty} \frac{Q_{kmpr}}{k_{y,pr}\Delta_{pr}}\Phi_{pr}(x,z) \tag{G.36}$$

G.4   Forced system of equations

The solutions for the fluid pressures and W(x,z), both described in terms of the modal coefficients A_{km}, are now substituted into the forced equation:

$$
\sum_{k=1}^{\infty} \sum_{m=1}^{\infty} A_{km} \left[-\rho_s \Omega^2 \cdot W_{km}(x,z) + D \cdot \left[\frac{\partial^4 W_{km}(x,z)}{\partial x^4} + 2 \cdot \frac{\partial^4 W_{km}(x,z)}{\partial x^2 \partial y^2} + \frac{\partial^4 W_{km}(x,z)}{\partial z^4} \right] \right]
$$
$$
= \sum_{k=1}^{\infty} \sum_{m=1}^{\infty} A_{km} \left[\tilde{H}(x,z) \cdot \rho_p \Omega^2 \cdot W_{km}(x,z) \right] - F_{f_{N+S}}(x,z) - P(x,z) - F_{ext}(\Omega, x, z)
$$

(G.37)

The structural modes all satisfy the homogeneous structural equation of motion:

$$
-\rho_s \omega_{km}^2 \cdot W_{km}(x,z) + D \cdot \left[\frac{\partial^4 W_{km}(x,z)}{\partial x^4} + 2 \cdot \frac{\partial^4 W_{km}(x,z)}{\partial x^2 \partial y^2} + \frac{\partial^4 W_{km}(x,z)}{\partial z^4} \right] = 0 \quad \text{(G.38)}
$$

In which ω_{km}^2 is the natural frequency corresponding to each structural eigenmode. The above equation is used to eliminate the derivative terms from equation (G.37). Furthermore, the found expression for the fluid pressures is substituted:

$$
\sum_{k=1}^{\infty} \sum_{m=1}^{\infty} A_{km} \cdot \rho_s \cdot (\omega_{km}^2 - \Omega^2) \cdot W_{km}(x,z) = -P(z) - F_{ext}(\Omega, z)
$$
$$
+ \sum_{k=1}^{\infty} \sum_{m=1}^{\infty} A_{km} \cdot \tilde{H}(x,z) \cdot \rho_p \cdot \Omega^2 \cdot W_{km}(x,z)
$$
$$
- \left[i\Omega^2 \rho_f \sum_{k=1}^{\infty} \sum_{m=1}^{\infty} A_{km} \sum_{p=1}^{\infty} \sum_{r=1}^{\infty} \frac{Q_{kmpr}}{k_{y,pr} \Delta_{pr}} \Phi_{pr}(x,z) \right]_{N+S}
$$

(G.39)

The above equation is now multiplied by another structural mode W_{ln} and integrated over the structure's height and width:

$$
\sum_{k=1}^{\infty} \sum_{m=1}^{\infty} A_{km} \cdot \rho_s \cdot (\omega_{km}^2 - \Omega^2) \cdot \iint_{0,0}^{L_x, L_z} W_{km}(x,z) \cdot W_{ln}(x,z) \, dx dz =
$$
$$
- \iint_{0,0}^{L_x, L_z} P(x,z) \cdot W_{ln}(x,z) \, dx dz - \iint_{0,0}^{L_x, L_z} F_{ext}(\Omega, z) \cdot W_{ln}(x,z) \, dx dz
$$
$$
+ \sum_{k=1}^{\infty} \sum_{m=1}^{\infty} A_{km} \cdot \iint_{0,0}^{L_x, L_z} \tilde{H}(x,z) \cdot \rho_p \cdot \Omega^2 \cdot W_{km}(x,z) \cdot W_{ln}(x,z) \, dx dz
$$
$$
- \left[i\Omega^2 \rho_f \sum_{k=1}^{\infty} \sum_{m=1}^{\infty} A_{km} \sum_{p=1}^{\infty} \sum_{r=1}^{\infty} \frac{Q_{kmpr}}{k_{y,pr} \Delta_{pr}} \iint_{0,0}^{L_x, L_z} \Phi_{pr}(x,z) \cdot W_{ln}(x,z) \, dx dz \right]_{N+S}
$$

(G.40)

Similar to the orthogonality used with the fluid modes, the following integral can be evaluated as follows:

$$
\iint_{0,0}^{L_x, L_z} W_{km}(x,z) \cdot W_{ln}(x,z) \, dx dz = \delta_{kl} \delta_{mn} \cdot \Gamma_{ln}
$$

(G.41)

The integral $\iint_{0,0}^{L_x,L_z} \Phi_{pr}(x,z) \cdot W_{ln}(x,z) \; dxdz$ will be renamed to Q_{lnpr}. The total fluid contribution is denoted by Z_{klmn}. The orthogonality of the structure modes only applies when the integral is evaluated over the full domain. The inertia force caused by the pump weights therefore also contains values for $k \neq l$ and $m \neq n$. The final system of equations therewith becomes:

$$\sum_{k=1}^{\infty} \sum_{m=1}^{\infty} \left[\rho_s \cdot (\omega_{km}^2 - \Omega^2) \cdot \delta_{kl}\delta_{mn} \cdot \Gamma_{ln} + Z_{klmn} - I_{klmn} + P_{klmn} \right] \cdot A_{ln} = F_{ln} \qquad \text{(G.42)}$$

Fluid impedance (N/S): $\qquad Z_{N,kmln} \text{ or } Z_{S,kmln} = i\Omega^2 \rho_f \sum_{p=1}^{\infty} \dfrac{Q_{kmpr}Q_{lnpr}}{k_{y,pr}\Delta_p}$

Inertia pumps: $\qquad I_{klmn} = \rho_p \cdot \Omega^2 \cdot \displaystyle\iint_S \tilde{H}(x,z) \cdot W_{km}(x,z) \cdot W_{ln}(x,z) \; dxdz$

Pump damping: $\qquad P_{ln} = c_{pump} \cdot i\Omega \cdot \displaystyle\iint_S \tilde{H}(x,z) \cdot W_{km}(x,z) \cdot W_{ln}(x,z) \; dxdz$

Modal force: $\qquad F_{ln} = \displaystyle\iint_S F_{ext}(z,\Omega)W_{ln}(x,z) \; dxdz$

And for completeness the two integrals that are part of the fluid impedance are repeated:

$$Q_{lnpr} = \iint_{S_w} W_{km}(x,z) \cdot \Phi_{pr}(x,z) \; dxdz$$

$$Q_{kmpr} = \iint_{S_w} W_{ln}(x,z) \cdot \Phi_{pr}(x,z) \; dxdz$$

In which S is the total gate surface and S_w the wet surface of the gate.

G.5   Additional results

Regular pump gate design: fluid eigenmodes at the southern side of the gate for maximum water levels
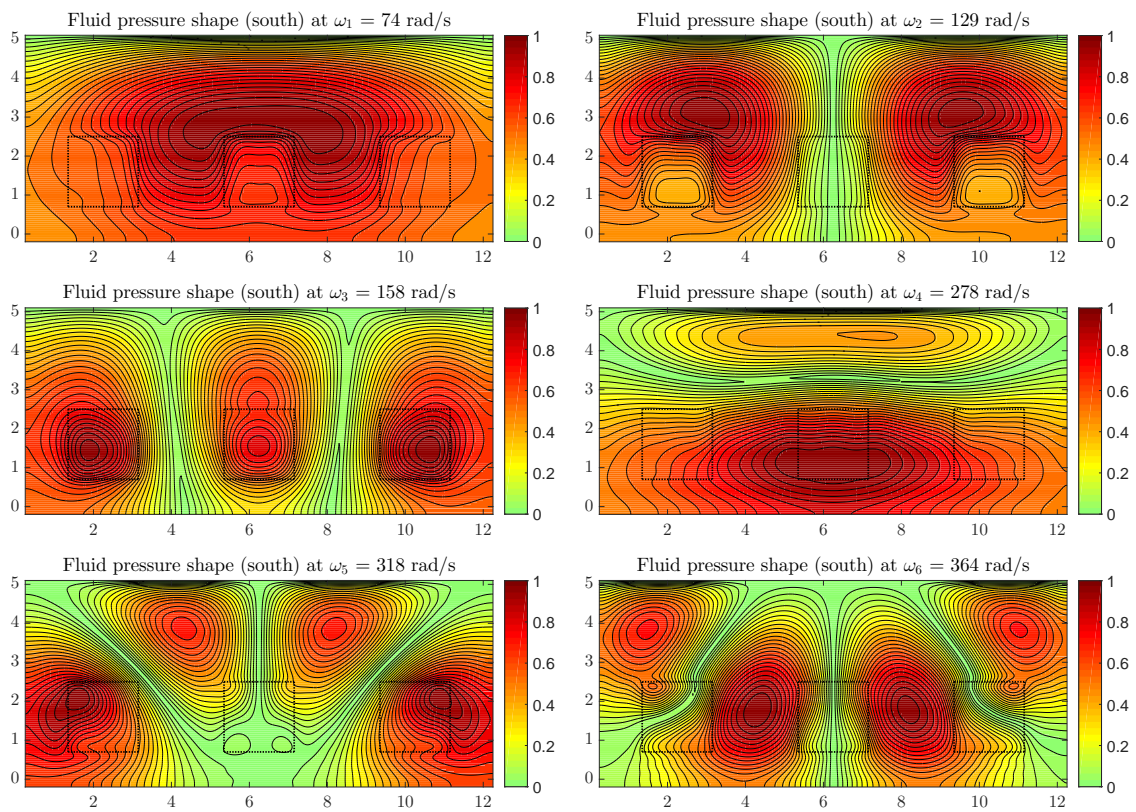

Figure G.2: The shapes of the fluid pressures at the southern gate's surface at the first six (approximate) eigenfrequencies of the structure-fluid system ($h_S = 5.3$ m, $h_N = 7.2$ m). The locations of the pumps, where the interface condition is not applied, are shown in black.
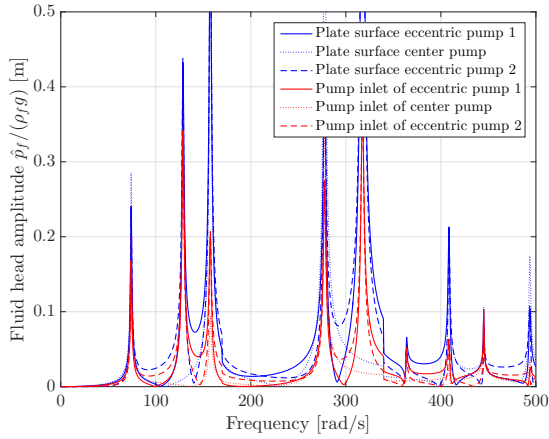
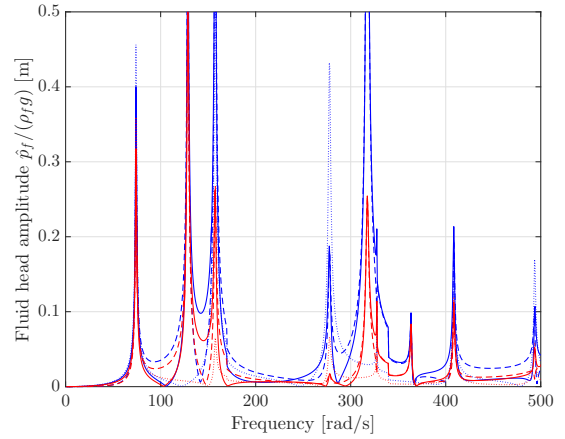Regular pump gate design: quantified fluid pressure response for maximum water levels
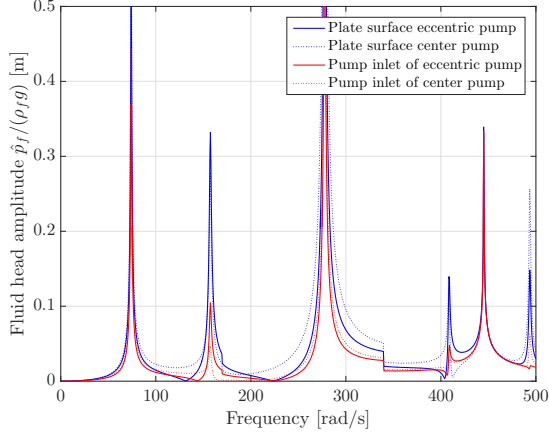
(a) Southern side of the gate, pump force in phase
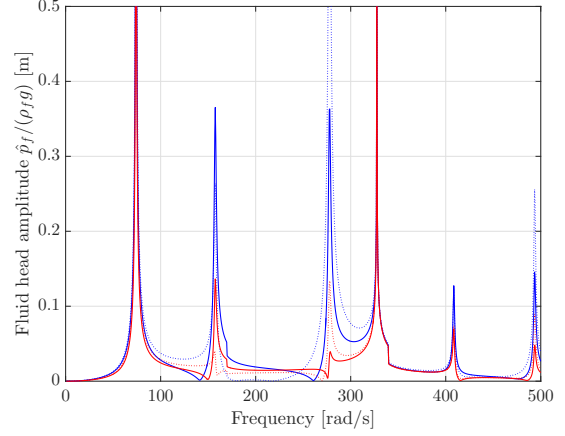
(b) Northern side of the gate, pump force in phase

(c) Southern side of the gate, eccentric pump force out of phase

(d) Northern side of the gate, eccentric pump force out of phase
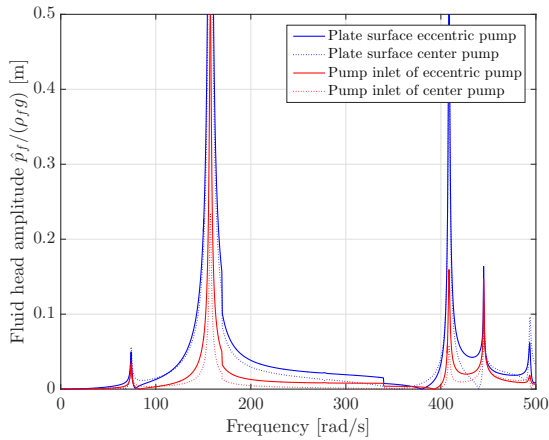
(e) Northern side of the gate, center pump force out of phase
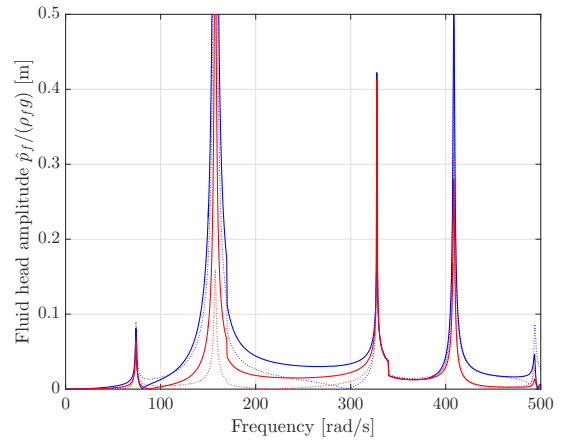
(f) Southern side of the gate, center pump force out of phase

Figure G.3: Pump fluid head amplitude at water levels $h_S = 5.3$ m and $h_N = 7.2$ m for the three pump phase combinations at both sides of the gate for the regular pump gate design, quantified for the pump force envelope.

179

Flood defence pump gate: deflection at maximum water levels
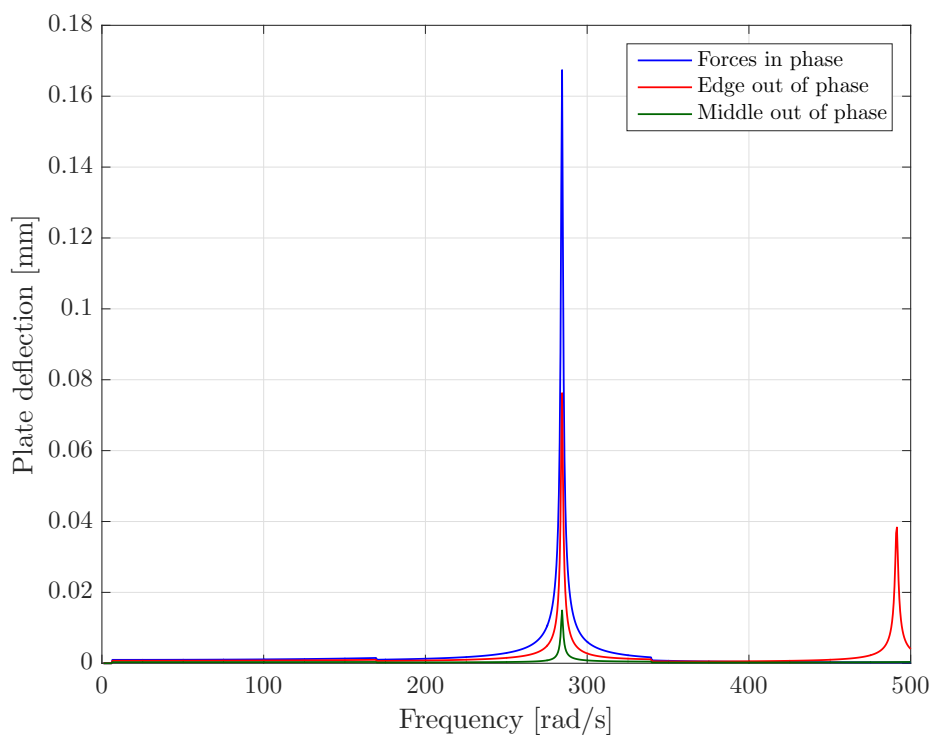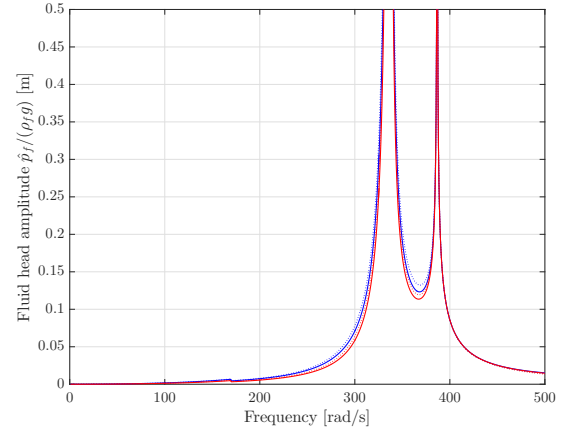

Figure G.4: Maximum gate deflection at maximum water levels ($h_N = 7.2$ m, $h_S = 5.3$ m) for the three pump phase possiblities, quantified for the pump force envelope.
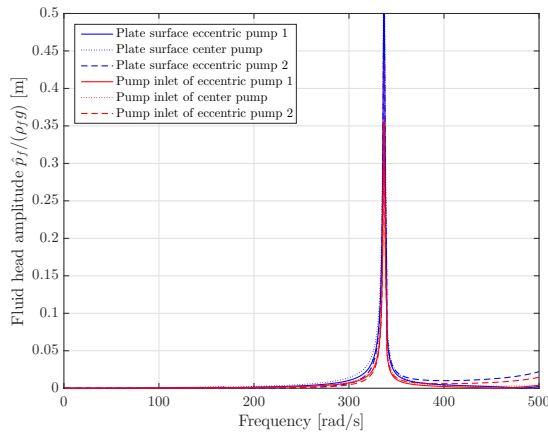
Flood defence pump gate: quantified fluid pressure response for cavitation-risk water levels
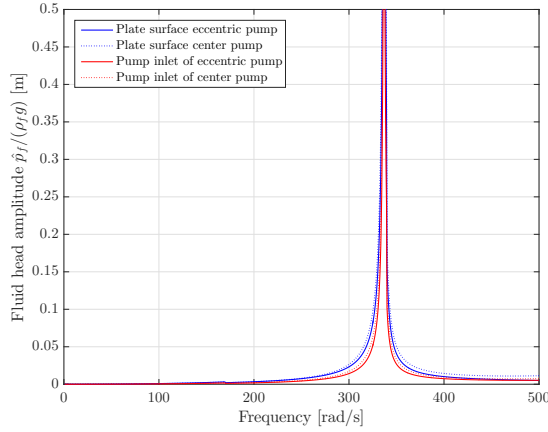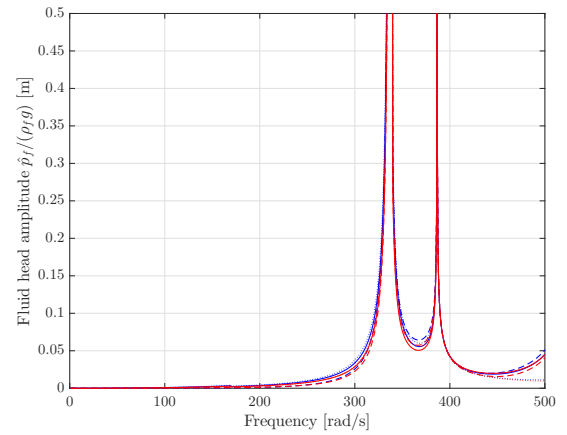

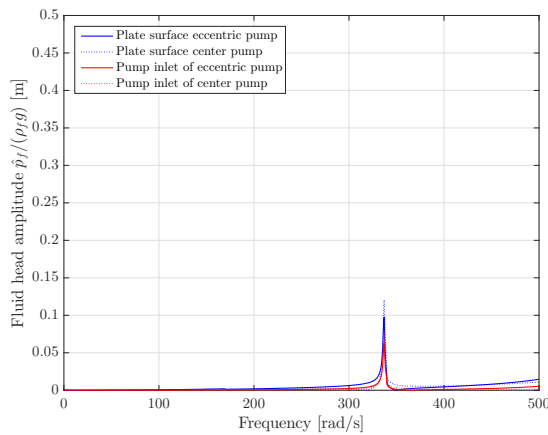(a) Southern side of the gate, pump force in phase

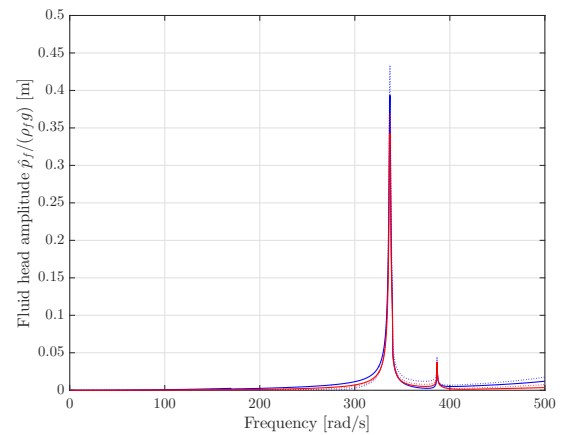(b) Northern side of the gate, pump force in phase

(c) Southern side of the gate, eccentric pump force out of phase

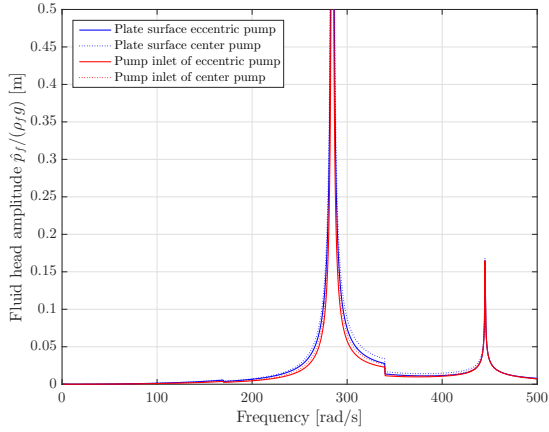(d) Northern side of the gate, eccentric pump force out of phase

(e) Northern side of the gate, center pump force out of phase

(f) Southern side of the gate, center pump force out of phase

Figure G.5: Pump fluid head amplitude at water levels $h_S = 4.1$ m and $h_N = 6.1$ m for the three pump phase combinations at both sides of the gate for the flood defence gate design, quantified for the pump force envelope.

Flood defence pump gate: quantified fluid pressure response for maximum water levels

(a) Southern side of the gate, pump force in phase

(b) Northern side of the gate, pump force in phase

(c) Southern side of the gate, eccentric pump force out of phase

(d) Northern side of the gate, eccentric pump force out of phase

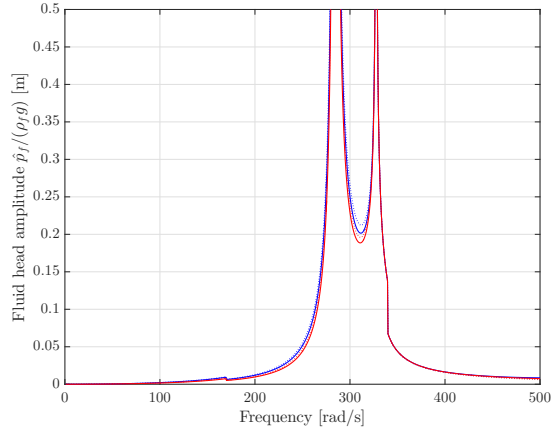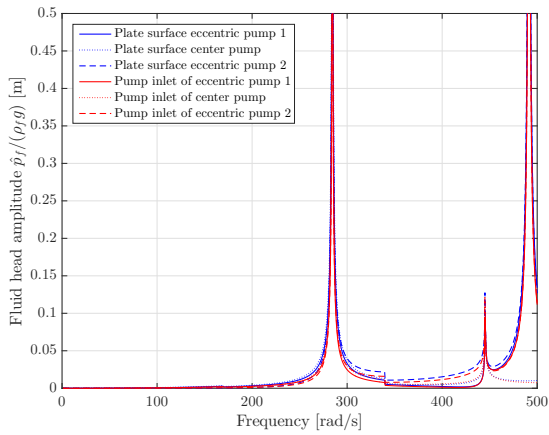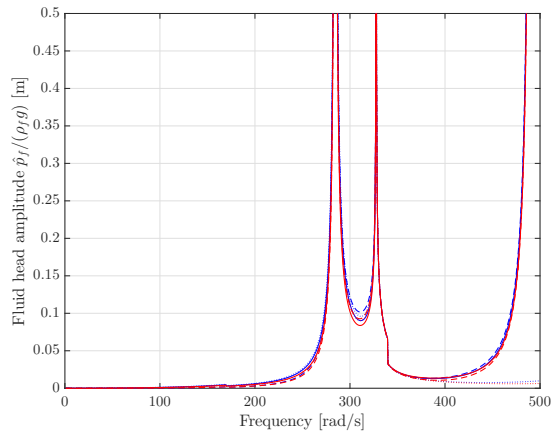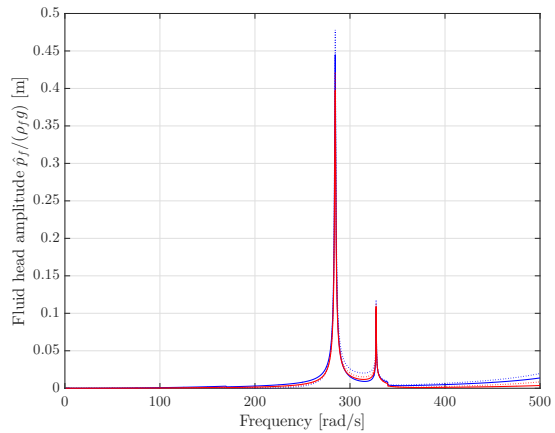(e) Northern side of the gate, center pump force out of phase

(f) Southern side of the gate, center pump force out of phase

Figure G.6: Pump fluid head amplitude at water levels $h_S = 5.3$ m and $h_N = 7.2$ m for the three pump phase combinations at both sides of the gate for the flood defence gate design, quantified for the pump force envelope.

H | Numeric fluid model: cell equations

In chapter 7 the hydrodynamic mass is investigated for the following four fluid model schematizations:

1. Closed gate (without pumps);
2. Closed gate with zero displacement/velocity at the location of the pumps;
3. Gate with openings and zero thickness
4. Gate with pump conduits of a certain length.

The amount and type of cell equations that must be evaluated for the numeric grid differs for each of these schematizations. These are worked out in this appendix. The general basis of these cell equations is elaborated and derived in section H.1. Schematizations 1 and 2 do not differ in model set-up, except for an input of zero velocity at the pump locations in case of the latter. These two schematizations are treated in section H.2. The cell equations for the other two schematizations are elaborated in section H.3 and H.4.

Note: in this appendix the axis system differs from what was used in the remainder of this thesis. In figure H.2 the axes are shown as are used in these derivations.

H.1   Numerical grid

As mentioned in section 7.1.2, a cubic grid is used dividing the domain into $N_x \cdot N_y \cdot N_z$ cells. The center of the outer cells have a distance of $\frac{1}{2}\Delta L$ to the boundary conditions, as can be seen in figure H.1, which shows the two dimensional example of the vibrating strip used by Kolkman [20]. In the example the domain is divided into $7*10$ cells, each represented by a point in figure H.1. The distance between the centers of neighboring cells is (evidently) equal to the cell width ΔL.

The cell equations are based on continuity. For the incompressible fluid, the sum of the discharges in every direction will be zero:

$$\Sigma \Delta q = \Delta q_L + \Delta q_R + \Delta q_U + \Delta q_D + \Delta q_F + \Delta q_B = 0 \tag{H.1}$$

in which: $\Delta q_{L/R/U/D/F/B}$ =   discharge over 'left/right/up/down/front/back' boundary of element

Using $\Delta q_L = V_L \, \Delta y \, \Delta z$ and the definition of the potential function in equation (4.14):

$$\Delta q_L = -\left(\frac{\delta \Phi}{\delta x}\right)_L \, \Delta y \, \Delta z \tag{H.2}$$
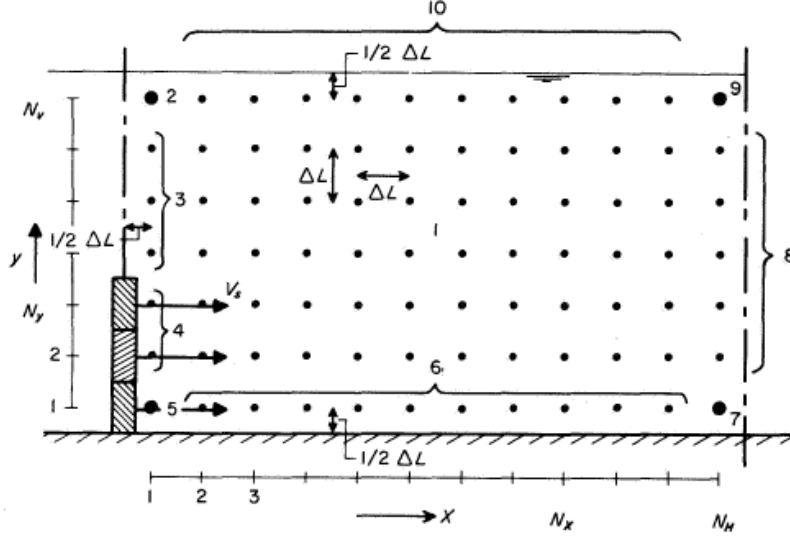
Figure H.1: Grid points at the center of each two dimensional cell for the vibrating strip example [20]

The same applies for the right boundary and the four other directions. Using the approximation $-\delta\Phi/\delta x = -\Delta\Phi/\Delta x = (\Phi_L - \Phi)/\Delta x$ and $\Delta x = \Delta y = \Delta z = \Delta L$, the following is obtained:

$$\Delta q_L = (\Phi_L - \Phi) \cdot \Delta L \tag{H.3}$$

In comparison to the two dimensional model used in Kolkman [20], a ΔL term remains in equation (H.3). Combining equations equation (H.1) and (H.3), the potential function for all inner elements is known:

$$\Phi = (\Phi_L + \Phi_R + \Phi_U + \Phi_D + \Phi_F + \Phi_B)/6; \tag{H.4}$$

In this equation, the ΔL term is voided due to the zero right hand side of equation (H.1). In a numerically more practical notation:

$$\Phi_{x,y,z} = (\Phi_{x-1,y,z} + \Phi_{x+1,y,z} + \Phi_{x,y+1,z} + \Phi_{x,y-1,z} + \Phi_{x,y,z-1} + \Phi_{x,y,z+1})/6; \tag{H.5}$$

All boundary elements have altered equations, with the corner elements again different from the rest. The example of figure H.1, but three dimensional, is used to present these equations for different boundary conditions. For the boundary elements at the left side above the thin strip, the boundary condition is at a distance of only $\frac{1}{2}\Delta L$. Therefore the discharge coming from the left side is:

$$\Delta q_L = 2 \cdot (\Phi_L - \Phi) \cdot \Delta L \tag{H.6}$$

The anti-symmetry or free surface boundary condition implies $\Phi_L = 0$, and thus $\Delta q_L = -2\Phi$. The equation of those cells therewith becomes:

$$\Phi_{x,y,z} = (\Phi_{x+1,y,z} + \Phi_{x,y+1,z} + \Phi_{x,y-1,z} + \Phi_{x,y,z-1} + \Phi_{x,y,z+1})/7; \tag{H.7}$$

The derivation for a right side, bottom, upper, front or back $\Phi = 0$ boundary condition, is equal.

At moving boundaries the discharge is known: $\Delta q_{gate_{y,z}} = V_s \cdot \Delta L^2$. In this case, dividing the ΔL term of equation (H.5) out of the equation has an effect on the q_{gate}-term. In case of the vibrating strip the cells in the middle of the strip (not at the edges), have the following cell equation:

$$\Phi_{x,y,z} = (\Delta q_{gate_{y,z}}/\Delta L + \Phi_{x+1,y,z} + \Phi_{x,y+1,z} + \Phi_{x,y-1,z} + \Phi_{x,y,z-1} + \Phi_{x,y,z+1})/5; \quad \text{(H.8)}$$

Other cell equations are treated in the following section based on the geometry of the pump gate used in the different model geometries.

H.2 Closed gate

For the reader's convenience, figure H.2 is repeated below. The cell equations of the 27 regions, coded as x_1-1 to x_1-9, x_{body}-1 to x_{body}-9 and x_{end}-1 to x_{end}-9, are elaborated below.
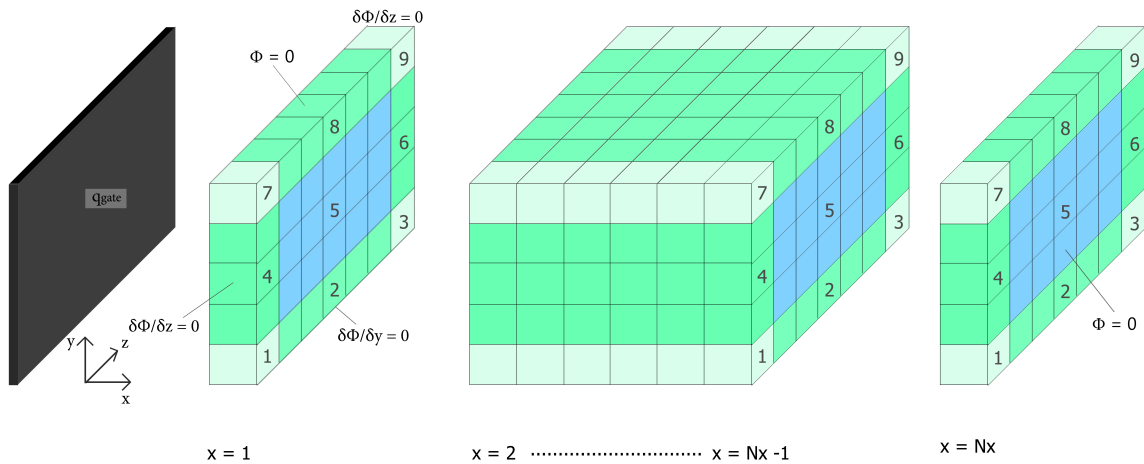
Figure H.2: Calculation grid of symmetric gate with regions of different cell equations (27 total)

The first 'slice' is that of the $x = 1$ coordinate. These are the cells adjacent to the gate, which is movement is defined by the matrix **q_gate** in y,z direction, of which each element is from now on denoted by $q_{y,z}$.

$(\mathbf{x_1 - 1})$ The lower left corner element must, besides the moving boundary condition $q(y, z)$, obey two other boundary conditions. In the z-direction it is adjacent to the closed sluice wall, which imposes the boundary conditions $\delta\Phi/\delta z = 0$. The sluice bottom imposes the same boundary conditions in y-direction: $\delta\Phi/\delta y = 0$.

These boundary conditions imply $q_F = 0$ and $q_D = 0$. The continuity equation (H.1) therewith becomes:

$$\Sigma \Delta q = q_{y,z} + \Delta q_R + \Delta q_U + \Delta q_B = 0 \tag{H.9}$$

With $\Delta q_{(R/U/D)} = (\Phi_{(R/U/D)} - \Phi) \cdot \Delta L$, the cell equation becomes:

$$\Phi_{x,y,z} = (q_{y,z}/\Delta L + \Phi_{x+1,y,z} + \Phi_{x,y+1,z} + \Phi_{x,y,z+1})/3 \tag{H.10}$$

$(\mathbf{x_1 - 2})$ The bottom elements have the gate and $\delta\Phi/\delta y = 0$ boundary conditions. The cell equation becomes:

$$\Phi_{x,y,z} = (q_{y,z} + \Phi_{x+1,y,z} + \Phi_{x,y+1,z} + \Phi_{x,y,z-1} + \Phi_{x,y,z+1})/4 \tag{H.11}$$

$(\mathbf{x_1 - 3})$ The lower right corner element is similar to the lower left one, except for q_B being q_F and thus $\Phi_{x,y,z+1} = \Phi_{x,y,z-1}$:

$$\Phi_{x,y,z} = (q_{y,z}/\Delta L + \Phi_{x+1,y,z} + \Phi_{x,y+1,z} + \Phi_{x,y,z-1})/3 \tag{H.12}$$

$(\mathbf{x_1 - 4})$ These cells have similar conditions as the bottom cells $(x_1 - 2)$, but the z-direction changes to the y-direction:

$$\Phi_{x,y,z} = (q_{y,z}/\Delta L + \Phi_{x+1,y,z} + \Phi_{x,y+1,z} + \Phi_{x,y-1,z} + \Phi_{x,y,z+1})/4 \tag{H.13}$$

$(\mathbf{x_1 - 5})$ The only difference with 'normal' continuity equation cells, is the moving boundary:

$$\Phi_{x,y,z} = (q_{y,z}/\Delta L + \Phi_{x+1,y,z} + \Phi_{x,y+1,z} + \Phi_{x,y-1,z} + \Phi_{x,y,z-1} + \Phi_{x,y,z+1})/5 \tag{H.14}$$

$(\mathbf{x_1 - 6})$ Opposite from $x_1 - 4$ in z-direction $(z + 1 = z - 1)$:

$$\Phi_{x,y,z} = (q_{y,z}/\Delta L + \Phi_{x+1,y,z} + \Phi_{x,y+1,z} + \Phi_{x,y-1,z} + \Phi_{x,y,z-1})/4 \tag{H.15}$$

$(\mathbf{x_1 - 7})$ The upper left element has three boundary conditions $\Phi_U = 0$, $\delta\Phi/\delta z = 0$, and q_{gate}. Similar to what was elaborated in chapter 7, due to the $\frac{1}{2}\Delta L$ distance between the cell center and the upper boundary conditions:

$$\Delta q_U = 2 \cdot (\Phi_U - \Phi) = 2 \cdot \Phi \tag{H.16}$$

And therefore:

$$\Phi_{x,y,z} = (q_{y,z}/\Delta L + \Phi_{x+1,y,z} + \Phi_{x,y-1,z} + \Phi_{x,y,z+1})/5 \tag{H.17}$$

$(\mathbf{x_1 - 8})$ Only the q_{gate} and $\Phi_U = 0$ conditions:

$$\Phi_{x,y,z} = (q_{y,z}/\Delta L + \Phi_{x+1,y,z} + \Phi_{x,y-1,z} + \Phi_{x,y,z-1} + \Phi_{x,y,z+1})/6 \tag{H.18}$$

($x_1 - 9$) Opposite from $x_1 - 7$ in z-direction ($z + 1 = z - 1$):

$$\Phi_{x,y,z} = (q_{y,z}/\Delta L + \Phi_{x+1,y,z} + \Phi_{x,y-1,z} + \Phi_{x,y,z-1})/5 \qquad \text{(H.19)}$$

The middle block of figure H.2, denoted by x_{body}, has to a great extend the same boundary conditions as the x_1 slice. The exception is the moving boundary, which is replaced by 'normal' adjacent cells. The q_L in the continuity equation is therefore no longer equal to q_{gate}, but instead:

$$\Delta q_L = (\Phi_L - \Phi) \cdot \Delta L \qquad \text{(H.20)}$$

The $q_{y,z}/\Delta L$ in each of the previous nine equations therefore changes to $\Phi_{x-1,y,z}$ and the value of the denominator in each equation increases by one.

$x_{body} - 1$ $\qquad \Phi_{x,y,z} = (\Phi_{x-1,y,z} + \Phi_{x+1,y,z} + \Phi_{x,y+1,z} + \Phi_{x,y,z+1})/4$ $\qquad$ (H.21)

$x_{body} - 2$ $\qquad \Phi_{x,y,z} = (\Phi_{x-1,y,z} + \Phi_{x+1,y,z} + \Phi_{x,y+1,z} + \Phi_{x,y,z-1} + \Phi_{x,y,z+1})/5$ $\quad$ (H.22)

$x_{body} - 3$ $\qquad \Phi_{x,y,z} = (\Phi_{x-1,y,z} + \Phi_{x+1,y,z} + \Phi_{x,y+1,z} + \Phi_{x,y,z-1})/4$ $\qquad$ (H.23)

$x_{body} - 4$ $\qquad \Phi_{x,y,z} = (\Phi_{x-1,y,z} + \Phi_{x+1,y,z} + \Phi_{x,y+1,z} + \Phi_{x,y-1,z} + \Phi_{x,y,z+1})/5$ $\quad$ (H.24)

$x_{body} - 5$ $\qquad \Phi_{x,y,z} = (\Phi_{x-1,y,z} + \Phi_{x+1,y,z} + \Phi_{x,y+1,z} + \Phi_{x,y-1,z} + \Phi_{x,y,z-1}$ $\qquad$ (H.25)
$$+ \, \Phi_{x,y,z+1})/6$$

$x_{body} - 6$ $\qquad \Phi_{x,y,z} = (\Phi_{x-1,y,z} + \Phi_{x+1,y,z} + \Phi_{x,y+1,z} + \Phi_{x,y-1,z} + \Phi_{x,y,z-1})/5$ $\quad$ (H.26)

$x_{body} - 7$ $\qquad \Phi_{x,y,z} = (\Phi_{x-1,y,z} + \Phi_{x+1,y,z} + \Phi_{x,y-1,z} + \Phi_{x,y,z+1})/6$ $\qquad$ (H.27)

$x_{body} - 8$ $\qquad \Phi_{x,y,z} = (\Phi_{x-1,y,z} + \Phi_{x+1,y,z} + \Phi_{x,y-1,z} + \Phi_{x,y,z-1} + \Phi_{x,y,z+1})/7$ $\quad$ (H.28)

$x_{body} - 9$ $\qquad \Phi_{x,y,z} = (\Phi_{x-1,y,z} + \Phi_{x+1,y,z} + \Phi_{x,y-1,z} + \Phi_{x,y,z-1})/6$ $\qquad$ (H.29)

The third block at x_{end} is again largely similar as the first and second blocks. In comparison to the middle block, it does not have a 'normal' cell at the right side of each element, but the $\Phi_R = 0$ condition. As is stated before, this condition leads to $\Delta q_R = 2 \cdot \Phi \cdot \Delta L$. Each $\Phi_{x+1,y,z}$ therefore is removed from above equations. The value of the denominator increases with one.

$x_{end} - 1$ $\qquad \Phi_{x,y,z} = (\Phi_{x-1,y,z} + \Phi_{x,y+1,z} + \Phi_{x,y,z+1})/5$ $\qquad$ (H.30)

$x_{end} - 2$ $\qquad \Phi_{x,y,z} = (\Phi_{x-1,y,z} + \Phi_{x,y+1,z} + \Phi_{x,y,z-1} + \Phi_{x,y,z+1})/6$ $\qquad$ (H.31)

$x_{end} - 3$ $\qquad \Phi_{x,y,z} = (\Phi_{x-1,y,z} + \Phi_{x,y+1,z} + \Phi_{x,y,z-1})/5$ $\qquad$ (H.32)

$x_{end} - 4$ $\qquad \Phi_{x,y,z} = (\Phi_{x-1,y,z} + \Phi_{x,y+1,z} + \Phi_{x,y-1,z} + \Phi_{x,y,z+1})/6$ $\qquad$ (H.33)

$x_{end} - 5$ $\qquad \Phi_{x,y,z} = (\Phi_{x-1,y,z} + \Phi_{x,y+1,z} + \Phi_{x,y-1,z} + \Phi_{x,y,z-1} + \Phi_{x,y,z+1})/7$ $\quad$ (H.34)

$x_{end} - 6$ $\qquad \Phi_{x,y,z} = (\Phi_{x-1,y,z} + \Phi_{x,y+1,z} + \Phi_{x,y-1,z} + \Phi_{x,y,z-1})/6$ $\qquad$ (H.35)

$x_{end} - 7$ $\qquad \Phi_{x,y,z} = (\Phi_{x-1,y,z} + \Phi_{x,y-1,z} + \Phi_{x,y,z+1})/7$ $\qquad$ (H.36)

$x_{end} - 8$ $\qquad \Phi_{x,y,z} = (\Phi_{x-1,y,z} + \Phi_{x,y-1,z} + \Phi_{x,y,z-1} + \Phi_{x,y,z+1})/8$ $\qquad$ (H.37)

$x_{end} - 9$ $\qquad \Phi_{x,y,z} = (\Phi_{x-1,y,z} + \Phi_{x,y-1,z} + \Phi_{x,y,z-1})/7$ $\qquad$ (H.38)

H.3   Pump openings

Compared to the geometry in previous section, only one type of cell equation is added at x_1. This is shown in figure H.3.
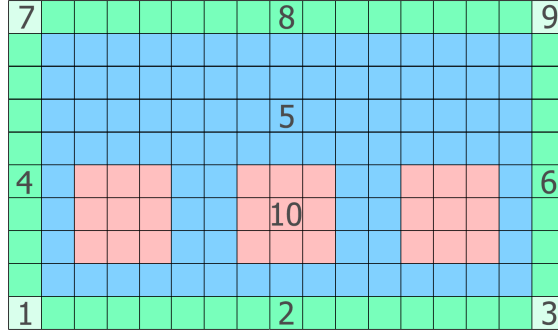

Figure H.3: Cell equations at x_1 for the gate with openings

In chapter 7 the gate was first considered anti-symmetric in order to reduce the required computational resources and give a quicker estimation of the change in added mass compared to the closed gate. In that case the cell equation is as follows:

$$\Phi_{x,y,z} = (\Phi_{x+1,y,z} + \Phi_{x,y+1,z} + \Phi_{x,y-1,z} + \Phi_{x,y,z-1} + \Phi_{x,y,z+1})/7 \qquad (\text{H.39})$$

When the potential is calculated for different water levels at both sides of the gate, and the situation is therefore no longer anti-symmetric, this equation becomes as follows:

$$\Phi_{N_{x,y,z}} = (\Phi_{S_{1,y,z}} + \Phi_{N_{x+1,y,z}} + \Phi_{N_{x,y+1,z}} + \Phi_{N_{x,y-1,z}} + \Phi_{N_{x,y,z-1}} + \Phi_{N_{x,y,z+1}})/6 \qquad (\text{H.40})$$

in which: $\Phi_{N_{x,y,z}}$ =   The potential at (x,y,z) at the northern side of the gate
$\Phi_{S_{x,y,z}}$ =   The potential at (x,y,z) at the southern side of the gate

The axes at both sides of the gate are mirrored in x-direction, with $x = 1$ at the gate $x = $ end at the sluice end. The y-axis and z-axis are equal.

H.4   Complete geometry

In this schematization the shape of the pump gate is still simplified to a plate. The length of the pumps is now taken into account by square conduits. The location of the pumps in the gate and the magnitude of their flow surface are expected to have the largest influence on the hydrodynamic mass, rather than their exact shape. The square shape of the conduits greatly eases the numerical evaluation. The plate thickness of the gate is 10 or 15 mm, depending on the design. This is negligible compared to the conduit length, which is expected to be about 3.5 metre (see chapter 2).

The conduits are schematized as infinitely thin as well, so they 'fit' in any of the previous grids. The cell equations adjacent to these conduits do however change. A 'new domain'

of cells with their own equations inside of the conduits is added. Furthermore, the body cells in previous cells are split into two parts: the smaller part where the pump conduits are present and the rest of the sluice length. The total number of cells, and therewith the computation time, does not increase. The number of cell equations does however. The different regions for x_1 are shown in figure H.4. In the conduits a new domain of equations, denoted by $c1$ to $c9$, is present.
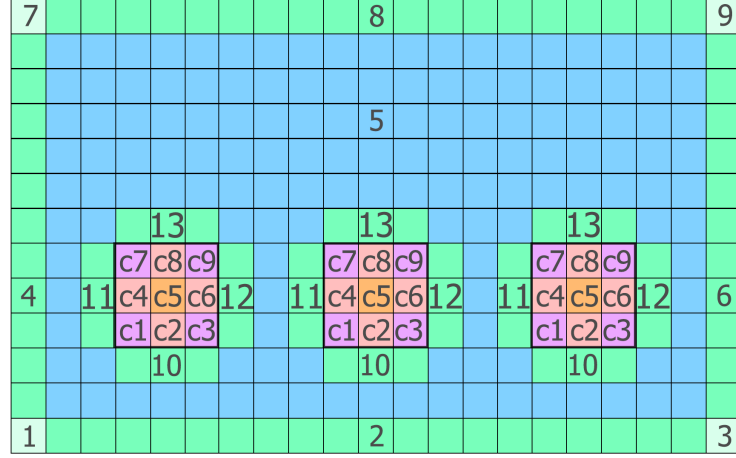

Figure H.4: Cell equations for the complete schematization at x_1. Cells in the conduits are not included. The gate, pump openings and grid are not drawn to scale.

Cell equations $x_1 - 1$ to $x_1 - 9$ remain equal to those stated for the closed gate. Cell equations $x_1 - 10$ to $x_1 - 13$ are added. Each of those cells is adjacent to the pump conduit, which is a closed boundary:

$$\frac{d\Phi}{dy} \text{ or } \frac{d\Phi}{dz} = 0 \tag{H.41}$$

The cell equations of these cells are therefore similar to those of the cells adjacent to the sluice walls and bottom ($x_1 - 2$, $x_1 - 4$, $x_1 - 6$). For clarity, $x_1 - 1$ to $x_1 - 9$ are repeated and completed with the remaining equations:

$x_1 - 1$ $\qquad \Phi_{x,y,z} = (q_{y,z}/\Delta L + \Phi_{x+1,y,z} + \Phi_{x,y+1,z} + \Phi_{x,y,z+1})/3$ $\qquad$ (H.42)

$x_1 - 2$ $\qquad \Phi_{x,y,z} = (q_{y,z}/\Delta L + \Phi_{x+1,y,z} + \Phi_{x,y+1,z} + \Phi_{x,y,z-1} + \Phi_{x,y,z+1})/4$ $\qquad$ (H.43)

$x_1 - 3$ $\qquad \Phi_{x,y,z} = (q_{y,z}/\Delta L + \Phi_{x+1,y,z} + \Phi_{x,y+1,z} + \Phi_{x,y,z-1})/3$ $\qquad$ (H.44)

$x_1 - 4$ $\qquad \Phi_{x,y,z} = (q_{y,z}/\Delta L + \Phi_{x+1,y,z} + \Phi_{x,y+1,z} + \Phi_{x,y-1,z} + \Phi_{x,y,z+1})/4$ $\qquad$ (H.45)

$x_1 - 5$ $\qquad \Phi_{x,y,z} = (q_{y,z}/\Delta L + \Phi_{x+1,y,z} + \Phi_{x,y+1,z} + \Phi_{x,y-1,z} + \Phi_{x,y,z-1}$ $\qquad$ (H.46)

$\qquad \qquad \qquad + \Phi_{x,y,z+1})/5$

$x_1 - 6$ $\qquad \Phi_{x,y,z} = (q_{y,z}/\Delta L + \Phi_{x+1,y,z} + \Phi_{x,y+1,z} + \Phi_{x,y-1,z} + \Phi_{x,y,z-1})/4$ $\qquad$ (H.47)

$x_1 - 7$ $\qquad \Phi_{x,y,z} = (q_{y,z}/\Delta L + \Phi_{x+1,y,z} + \Phi_{x,y-1,z} + \Phi_{x,y,z+1})/5$ $\qquad$ (H.48)

$x_1 - 8$ $\qquad \Phi_{x,y,z} = (q_{y,z}/\Delta L + \Phi_{x+1,y,z} + \Phi_{x,y-1,z} + \Phi_{x,y,z-1} + \Phi_{x,y,z+1})/6$ $\qquad$ (H.49)

$x_1 - 9$ $\qquad \Phi_{x,y,z} = (q_{y,z}/\Delta L + \Phi_{x+1,y,z} + \Phi_{x,y-1,z} + \Phi_{x,y,z-1})/5$ $\qquad$ (H.50)

$x_1 - 10$ $\qquad \Phi_{x,y,z} = (q_{y,z}/\Delta L + \Phi_{x+1,y,z} + \Phi_{x,y-1,z} + \Phi_{x,y,z-1} + \Phi_{x,y,z+1})/4$ $\qquad$ (H.51)

$x_1 - 11$ $\qquad \Phi_{x,y,z} = (q_{y,z}/\Delta L + \Phi_{x+1,y,z} + \Phi_{x,y+1,z} + \Phi_{x,y-1,z} + \Phi_{x,y,z-1})/4$ $\qquad$ (H.52)

$x_1 - 12$ $\quad\quad\quad \Phi_{x,y,z} = (q_{y,z}/\Delta L + \Phi_{x+1,y,z} + \Phi_{x,y+1,z} + \Phi_{x,y-1,z} + \Phi_{x,y,z+1})/4$ (H.53)

$x_1 - 13$ $\quad\quad\quad \Phi_{x,y,z} = (q_{y,z}/\Delta L + \Phi_{x+1,y,z} + \Phi_{x,y+1,z} + \Phi_{x,y,z-1} + \Phi_{x,y,z+1})/4$ (H.54)

For x_2 to $x_{(\text{end counduit})}$ the division is the same as given in figure H.4. These cells are denoted by $x_{body,c}$. The cell equations differ only slightly, i.e. $q_{y,z} = \Phi_{x-1,y,z}$ and the denominator is increased by 1. From $x_{(\text{end conduit}+1)}$ the cell equations remain unchanged to the x_{body} equations in previous sections.

$x_{body,c} - 1$ $\quad \Phi_{x,y,z} = (\Phi_{x-1,y,z} + \Phi_{x+1,y,z} + \Phi_{x,y+1,z} + \Phi_{x,y,z+1})/4$ (H.55)

$x_{body,c} - 2$ $\quad \Phi_{x,y,z} = (\Phi_{x-1,y,z} + \Phi_{x+1,y,z} + \Phi_{x,y+1,z} + \Phi_{x,y,z-1} + \Phi_{x,y,z+1})/5$ (H.56)

$x_{body,c} - 3$ $\quad \Phi_{x,y,z} = (\Phi_{x-1,y,z} + \Phi_{x+1,y,z} + \Phi_{x,y+1,z} + \Phi_{x,y,z-1})/4$ (H.57)

$x_{body,c} - 4$ $\quad \Phi_{x,y,z} = (\Phi_{x-1,y,z} + \Phi_{x+1,y,z} + \Phi_{x,y+1,z} + \Phi_{x,y-1,z} + \Phi_{x,y,z+1})/5$ (H.58)

$x_{body,c} - 5$ $\quad \Phi_{x,y,z} = (\Phi_{x-1,y,z} + \Phi_{x+1,y,z} + \Phi_{x,y+1,z} + \Phi_{x,y-1,z} + \Phi_{x,y,z-1}$ (H.59)
$\quad\quad\quad\quad\quad\quad + \Phi_{x,y,z+1})/6$

$x_{body,c} - 6$ $\quad \Phi_{x,y,z} = (\Phi_{x-1,y,z} + \Phi_{x+1,y,z} + \Phi_{x,y+1,z} + \Phi_{x,y-1,z} + \Phi_{x,y,z-1})/5$ (H.60)

$x_{body,c} - 7$ $\quad \Phi_{x,y,z} = (\Phi_{x-1,y,z} + \Phi_{x+1,y,z} + \Phi_{x,y-1,z} + \Phi_{x,y,z+1})/6$ (H.61)

$x_{body,c} - 8$ $\quad \Phi_{x,y,z} = (\Phi_{x-1,y,z} + \Phi_{x+1,y,z} + \Phi_{x,y-1,z} + \Phi_{x,y,z-1} + \Phi_{x,y,z+1})/7$ (H.62)

$x_{body,c} - 9$ $\quad \Phi_{x,y,z} = (\Phi_{x-1,y,z} + \Phi_{x+1,y,z} + \Phi_{x,y-1,z} + \Phi_{x,y,z-1})/6$ (H.63)

$x_{body,c} - 10$ $\quad \Phi_{x,y,z} = (\Phi_{x-1,y,z} + \Phi_{x+1,y,z} + \Phi_{x,y-1,z} + \Phi_{x,y,z-1} + \Phi_{x,y,z+1})/5$ (H.64)

$x_{body,c} - 11$ $\quad \Phi_{x,y,z} = (\Phi_{x-1,y,z} + \Phi_{x+1,y,z} + \Phi_{x,y+1,z} + \Phi_{x,y-1,z} + \Phi_{x,y,z-1})/5$ (H.65)

$x_{body,c} - 12$ $\quad \Phi_{x,y,z} = (\Phi_{x-1,y,z} + \Phi_{x+1,y,z} + \Phi_{x,y+1,z} + \Phi_{x,y-1,z} + \Phi_{x,y,z+1})/5$ (H.66)

$x_{body,c} - 13$ $\quad \Phi_{x,y,z} = (\Phi_{x-1,y,z} + \Phi_{x+1,y,z} + \Phi_{x,y+1,z} + \Phi_{x,y,z-1} + \Phi_{x,y,z+1})/5$ (H.67)

The cell equations $c1$ to $c9$ do not change for x_1, x_{body} and $x_{(\text{end conduit})}$ as there is not gate present in the conduits and the motion of the pumps is not included in this model. At x_1, the $\Phi_{x-1,y,z}$ term given in the equations is the potential at the other side of the gate, previously denoted by $\Phi_{S_{1,y,z}}$.

The equations for cells $c1$ to $c6$ are simply equal to those of $x_{body} - 1$ to $x_{body} - 6$. The equations for $c7$ to $c9$ or equal to those of $c1$ to $c3$, but with $\Phi(x, y + 1, z) = \Phi(x, y - 1, z)$:

$c1$ $\quad\quad\quad \Phi_{x,y,z} = (\Phi_{x-1,y,z} + \Phi_{x+1,y,z} + \Phi_{x,y+1,z} + \Phi_{x,y,z+1})/4$ (H.68)

$c2$ $\quad\quad\quad \Phi_{x,y,z} = (\Phi_{x-1,y,z} + \Phi_{x+1,y,z} + \Phi_{x,y+1,z} + \Phi_{x,y,z-1} + \Phi_{x,y,z+1})/5$ (H.69)

$c3$ $\quad\quad\quad \Phi_{x,y,z} = (\Phi_{x-1,y,z} + \Phi_{x+1,y,z} + \Phi_{x,y+1,z} + \Phi_{x,y,z-1})/4$ (H.70)

$c4$ $\quad\quad\quad \Phi_{x,y,z} = (\Phi_{x-1,y,z} + \Phi_{x+1,y,z} + \Phi_{x,y+1,z} + \Phi_{x,y-1,z} + \Phi_{x,y,z+1})/5$ (H.71)

$c5$ $\quad\quad\quad \Phi_{x,y,z} = (\Phi_{x-1,y,z} + \Phi_{x+1,y,z} + \Phi_{x,y+1,z} + \Phi_{x,y-1,z} + \Phi_{x,y,z-1}$ (H.72)
$\quad\quad\quad\quad\quad\quad + \Phi_{x,y,z+1})/6$

$c6$ $\quad\quad\quad \Phi_{x,y,z} = (\Phi_{x-1,y,z} + \Phi_{x+1,y,z} + \Phi_{x,y+1,z} + \Phi_{x,y-1,z} + \Phi_{x,y,z-1})/5$ (H.73)

$c7$ $\quad\quad\quad \Phi_{x,y,z} = (\Phi_{x-1,y,z} + \Phi_{x+1,y,z} + \Phi_{x,y-1,z} + \Phi_{x,y,z+1})/4$ (H.74)

$c8$ $\quad\quad\quad \Phi_{x,y,z} = (\Phi_{x-1,y,z} + \Phi_{x+1,y,z} + \Phi_{x,y-1,z} + \Phi_{x,y,z-1} + \Phi_{x,y,z+1})/5$ (H.75)

$c9$
$$\Phi_{x,y,z} = (\Phi_{x-1,y,z} + \Phi_{x+1,y,z} + \Phi_{x,y-1,z} + \Phi_{x,y,z-1})/4 \qquad \text{(H.76)}$$

As mentioned, the cell equations for $x > $ (end conduit) remain equal to those stated for the closed gate denoted by x_{body} and x_{end}, each containing nine different cell equations.